9 October 2009 | $10

Science

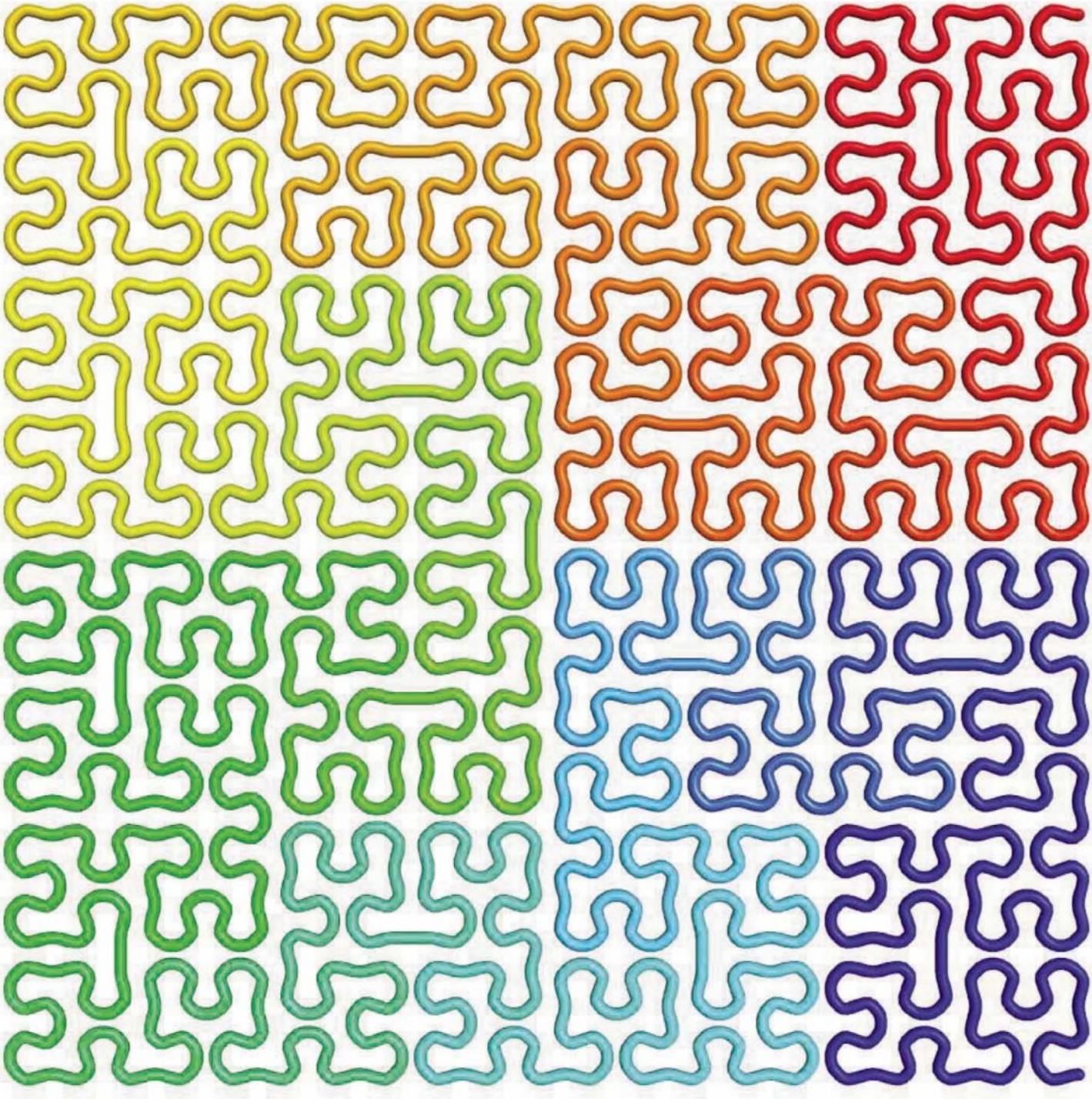

AAAS

High Efficiency Gene Transfer into Stem Cells

RetroNectin®

Recombinant Human Fibronectin Fragment

Use of RetroNectin®-based gene transduction protocols dramatically enhances the efficiency of retrovirus or lentivirus-mediated gene transfer **into mammalian cells. RetroNectin® is** a recombinant polypeptide consisting of three functional domains derived from the human **fibronectin. RetroNectin®'s enhancem**ent of gene transduction efficiency is hypothetically due to co-localization of retroviral particles and target cells **on the RetroNectin® molecule. Recent e**xperiments **demonstrate Retronectin®'s efficacy on s**tem cells.

- **Highly Efficient Retroviral or Lentiviral Gene Transfer** into Stem Cells*
- **No Polybrene Required** for Transduction
- **Facilitates development of innovative protocols** for proliferation of cells carrying a transferred gene, maintaining the function of the cells, and increasing transplant efficiency

* carrying VLA-4 and/or VLA-5 cell surface receptors

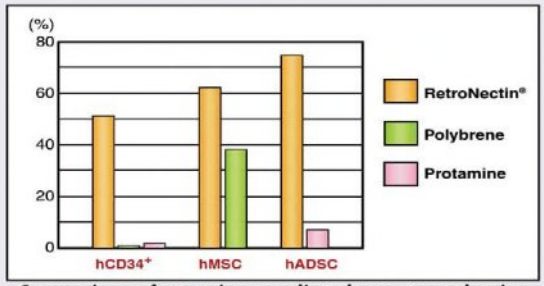

Comparison of retrovirus-mediated gene transduction efficiency in various methods into human stem cells.

RetroNectin® enables and enhances retrovirus-mediated gene transfer into stem cells which express lower levels of GALV envelope receptor, such as hCD34+ or hADSC

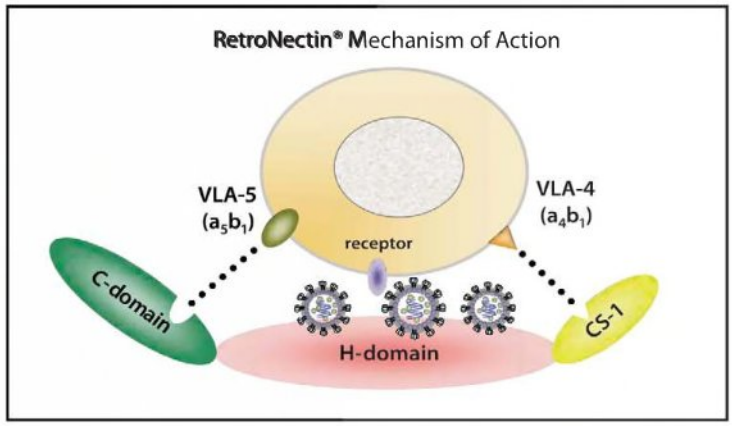

TaKaRa

For more information
www.takarabio.us

Japan:
Takara Bio Inc.
+81 77 543 7247
www.takara-bio.com

Europe:
Takara Bio Europe S.A.S.
+33 1 3904 6880
www.takara-bio.eu

USA:
Clontech Laboratories, Inc
A Takara Bio Company
888-251-6618
www.takara-bio.us

China:
Takara Biotechnology
(Dalian) Co., Ltd.
+86 411 8764 1681
www.takara.com.cn

Korea:
Takara Korea
Biomedical Inc.
+82 2 2081 2525
www.takara.co.kr

NATIONAL SCIENCE BOARD
2010 Honorary Awards
CALL FOR NOMINATIONS

Vannevar Bush Award

Honoring Exceptional Service to the Nation in Science and Technology

The Vannevar Bush Award honors truly exceptional lifelong leaders in science and technology who have made substantial contributions to the welfare of the Nation through public service activities in science, technology, and public policy. The award was established in 1980 in the memory of Vannevar Bush, who served as a science advisor to President Franklin Roosevelt.

Past recipients of the Vannevar Bush Award include such renowned leaders in science and technology as: Charles Townes, Harold Varmus, Maxine Singer, H. Guyford Stever, Phillip Abelson, Norman Ramsey, Linus Pauling, and James Killian.

Additional information and instructions for submitting nominations are available at:
http://www.nsf.gov/nsb/awards/bush.jsp

NSB Public Service Award

Honoring Service in Public Understanding of Science and Engineering

The National Science Board (NSB) Public Service Award honors individuals who and groups that have made substantial contributions to increasing public understanding of science and engineering in the United States. These contributions may be in a wide variety of areas that have the potential of contributing to public understanding of and appreciation for science and engineering.

Past recipients of the NSB Public Service Award include: NUMB3RS, the CBS television drama series; Ira Flatow, Host and Executive Producer of NPR's "Science Friday"; Alfred P. Sloan Foundation; Bill Nye The Science Guy; and NOVA, the PBS television series.

Additional information and instructions for submitting nominations are available at:
http://www.nsf.gov/nsb/awards/public.jsp

Contact: Jennifer Richards, jlrichar@nsf.gov, 703-292-4521 (p), 703-292-9008 (f)

Mailing Address: National Science Foundation, National Science Board,
4201 Wilson Blvd., Suite 1220, Arlington, VA 22230

Deadline for Nominations: November 4, 2009

The NSB is the 25-member policymaking body for the National Science Foundation (NSF) and advisory body to the President and Congress on science and engineering issues. Drawn from universities and industry, and representing a variety of science and engineering disciplines and geographic areas, NSB members are selected for their eminence in research, education, or public service, and records of distinguished service. For more on the NSB, visit: http://www.nsf.gov/nsb/about/index.jsp

GE Healthcare
Life Sciences

Interesting what a little imagination can do

Imagination has always inspired the scientific mind. At GE Healthcare Life Sciences, the same imagination inspires us to provide the most complete range of products and solutions available. Everything from innovative research system platforms, such as ÄKTA™, Biacore™ and IN Cell Analyzer, to everyday lab essentials from our Whatman™ and Amersham™ brands, to a full range of products for bioprocessing. Scientists around the world rely on these brands to deliver reproducible results, with the highest quality, that ultimately helps improve their productivity.

At GE Healthcare Life Sciences, our focus is on helping scientists achieve even more, faster. It's a commitment we have in our genes. And all this is backed by the service, support and investment for the future that being part of GE can bring.

Want to set your imagination free and do more? Why not talk with us today. Visit **www.gelifesciences.com**

I ÄKTA I Amersham I Biacore I IN Cell Analyzer I Whatman I GE Service I

imagination at work

First published September 2009
GE Healthcare Bio-Sciences AB, Björkgatan 30, 751 84 Uppsala, Sweden
GE15-09

EDITORIAL

NEWS OF THE WEEK

NEWS FOCUS

LETTERS

BOOKS *ET AL.*

POLICY FORUM

PERSPECTIVES

CONTENTS continued >>

page 218

page 232

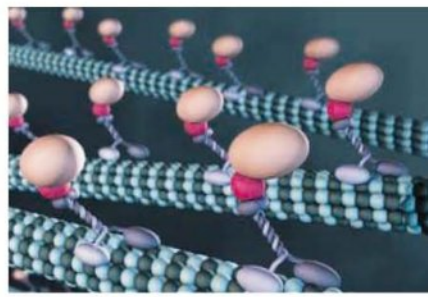

pages 238 & 298

COVER

First described by David Hilbert in 1891, the Hilbert curve is a one-dimensional fractal trajectory that densely fills higher-dimensional space without crossing itself. A new method for reconstructing the three-dimensional architecture of the human genome, described on page 289, reveals a polymer analog of Hilbert's curve at the megabase scale.

Image: Leonid A. Mirny and Erez Lieberman-Aiden

DEPARTMENTS

Epigenetics sample and assay technologies by QIAGEN

Trust in methylation analysis

Rely on QIAGEN epigenetics sample and assay technologies for:

- **DNA purification**
- **Bisulfite conversion**
- **Whole bisulfitome amplification**
- **Methylation-specific PCR**
- **Methylation detection and quantification with Pyrosequencing**

Making improvements in life possible — www.qiagen.com

QIAGEN®

Sample & Assay Technologies

BREVIA

RESEARCH ARTICLES

REPORTS

CONTENTS continued >>

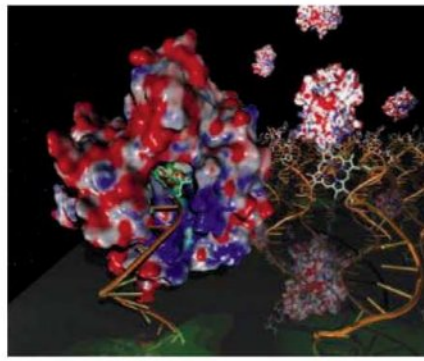

page 252

pages 243 & 278

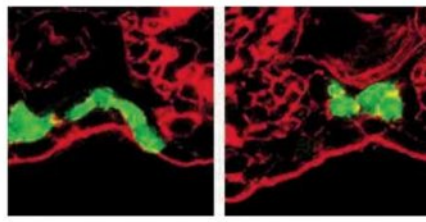

pages 242 & 294

MILLIPORE™

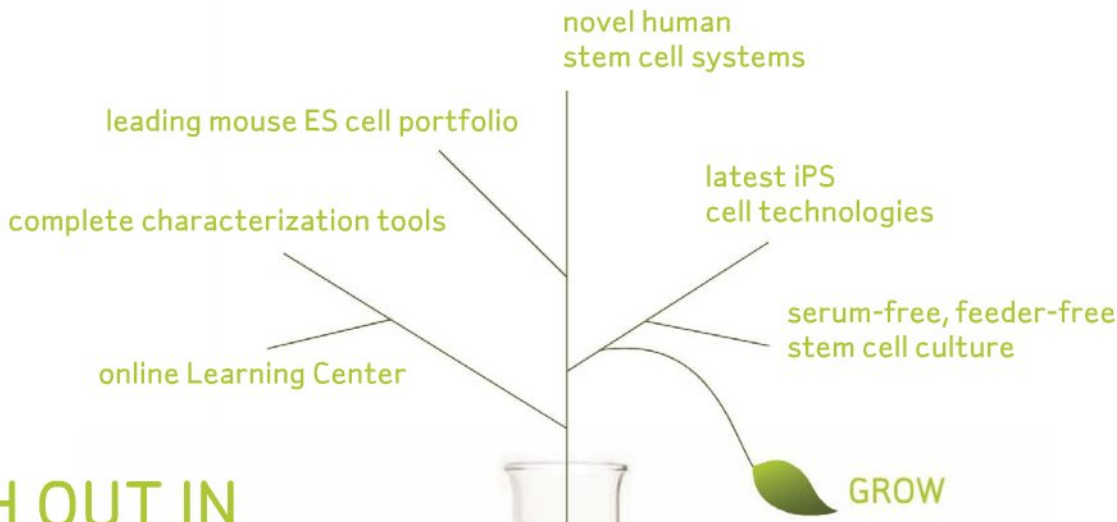

BRANCH OUT IN STEM CELL RESEARCH.

With Millipore as your partner, imagine what you'll discover.

With the right resources, stem cell research flourishes. Millipore is deeply committed to providing the tools, systems, education and online community that help turn goals into breakthroughs.

ADVANCING LIFE SCIENCE TOGETHER™
Research. Development. Production.

STEM CELL RESEARCH:
www.millipore.com/stemcells5

SCIENCEONLINE

SCIENCEXPRESS
www.sciencexpress.org

Genotype Analysis Identifies the Cause of the "Royal Disease"
E. I. Rogaev et al.

DNA from historical specimens reveals the mutation causing the hemophilia that afflicted the royal families of Europe.
10.1126/science.1180660

Detection of an Infectious Retrovirus, XMRV, in Blood Cells of Patients with Chronic Fatigue Syndrome
V. C. Lombardi et al.

Two-thirds of a sample of 101 U.S. patients with chronic fatigue syndrome harbor an infectious retrovirus in their blood cells.
10.1126/science.1179052

A New Virus for Old Diseases?
J. M. Coffin and J. P. Stoye
10.1126/science.1181349

Coupling of CO_2 and Ice Sheet Stability Over Major Climate Transitions of the Last 20 Million Years
A. K. Tripati et al.

Changes in global sea level and atmospheric carbon dioxide levels were similar during the past 20 million years.
10.1126/science.1178296

Microsecond Simulations of Spontaneous Methane Hydrate Nucleation and Growth
M. R. Walsh et al.

An extended simulation uncovers the intricate steps whereby methane can be trapped in ice.
10.1126/science.1174010

TECHNICALCOMMENTS

Comment on "The *Arabidopsis* Circadian Clock Incorporates a cADPR-Based Feedback Loop"
X. Xu et al.

full text at www.sciencemag.org/cgi/content/full/326/5950/230-b

Response to Comment on "The *Arabidopsis* Circadian Clock Incorporates a cADPR-Based Feedback Loop"
A. N. Dodd et al.

full text at www.sciencemag.org/cgi/content/full/326/5950/230-c

SCIENCENOW
www.sciencenow.org
Highlights From Our Daily News Coverage

Biosafety Bra, Beer Bottle Ballistics Win Ig Nobels
Read about the annual extravaganza of song, dance, and unbelievable science.

Buried Treasure Fills in Ancient Roman Puzzle
Forgotten coin stashes suggest Roman population dropped as the republic became an empire.

Helping Crops Shed Pesticides
Dousing plants with their own hormones helps them expel toxic chemicals.

SCIENCESIGNALING
www.sciencesignaling.org
The Signal Transduction Knowledge Environment

RESEARCH ARTICLE: Wingless Promotes Proliferative Growth in a Gradient-Independent Manner
L. A. Baena-Lopez et al.

Proliferation of cells in the *Drosophila* wing does not require a gradient of the morphogen Wingless.

RESEARCH ARTICLE: Coordinated Responses to Oxygen and Sugar Deficiency Allow Rice Seedlings to Tolerate Flooding
K.-W. Lee et al.

The protein kinase CIPK15 integrates the response to hypoxia with sugar signaling to allow submerged rice seedlings to grow.

PERSPECTIVE: Apoptosis—Calling Time on Apoptosome Activity
C. Adrain and S. J. Martin

Caspase-9 autoprocessing displaces active caspase-9 bound to the apoptosome, thereby limiting proteolytic activity.

PERSPECTIVE: Snapshots Form a Big Picture of Guanine Nucleotide Exchange
K. Rittinger

DOCK9 uses a unique mechanism to discriminate between GDP- and GTP-bound forms of Cdc42.

PODCAST
J.-P. Vincent and A. M. VanHook

Graded distribution of Wingless is not required for cell proliferation in the fly wing disc.

SCIENCECAREERS
www.sciencecareers.org/career_magazine
Free Career Resources for Scientists

SPECIAL RISK-TAKING ISSUE

Audacity, Part 2: A Blueprint for Audacious Science
A. Sasso

Breakthrough science needs passion, a supportive institution, and a suitable problem.

The Entrepreneurial Bug
A. Kotok

Academic scientists tell how they became driven to commercialize their science.

Making the Most of Opportunities and Challenges
R. Mejia

Neuroscientist Sam Pfaff went on to success after a falling out with his adviser.

SCIENCETRANSLATIONAL MEDICINE
www.sciencetranslationalmedicine.org
Integrating Medicine and Science

EDITORIAL: Space for the Cures
E. A. Zerhouni

Science launches a new journal for translational research.

COMMENTARY: Changing Models of Biomedical Research
W. F. Crowley Jr. and J. F. Gusella

Academic medical centers at the hub of a new style of research.

RESEARCH: Building Better Bones
D. Gesty-Palmer et al.

A biased agonist may promote bone growth more effectively.

PODCAST
This inaugural podcast features Advisory Board member Betsy Nabel on translational medicine and a discussion with several authors about osteoporosis drugs.

SCIENCEPODCAST
www.sciencemag.org/multimedia/podcast
Free Weekly Show

Download the 9 October *Science* Podcast to hear about personalized cancer treatments, persistent currents in nonsuperconductors, the organization of chromosomes, and more.

ORIGINSBLOG
blogs.sciencemag.org/origins
A History of Beginnings

SCIENCEINSIDER
blogs.sciencemag.org/scienceinsider
Science Policy News and Analysis

SCIENCE (ISSN 0036-8075) is published weekly on Friday, except the last week in December, by the American Association for the Advancement of Science, 1200 New York Avenue, NW, Washington, DC 20005. Periodicals Mail postage (publication No. 484460) paid at Washington, DC, and additional mailing offices. Domestic individual membership and subscription (51 issues): $146 ($74 allocated to subscription). Domestic institutional subscription (51 issues): $835; Foreign postage extra: Mexico, Caribbean (surface mail) $55; other countries (air assist delivery) $85. First class, airmail, student, and emeritus rates on request. Canadian rates with GST available upon request, GST #1254 88122. Publications Mail Agreement Number 1069624. **Printed in the U.S.A.**

Change of address: Allow 4 weeks, giving old and new addresses and 8-digit account number. **Postmaster:** Send change of address to AAAS, P.O. Box 96178, Washington, DC 20090–6178. **Single-copy sales:** $10.00 current issue, $15.00 back issue prepaid includes surface postage; bulk rates on request. The identification code for *Science* is 0036-8075. *Science* is indexed in the *Reader's Guide to Periodical Literature* and in several specialized indexes.

AAAS
ADVANCING SCIENCE, SERVING SOCIETY

GE Healthcare
Life Sciences

Inspired Ägain

Who better to draw inspiration for the new ÄKTA™ avant system than from customers using the 30,000 ÄKTA systems already in use around the world? Well, you spoke and we listened. The new ÄKTA avant is faster – enabling quicker insights. It minimizes the chance of error, even while working at higher speeds. And it allows for direct, reliable scalability. At GE Healthcare, our focus is on helping scientists achieve even more, faster. It's a commitment we have in our genes. And all this is backed by the service, support, and investment in the future that being part of GE can bring.

Want to know more? Why not talk with us today. Visit **www.gelifesciences.com/aktaavant**

I **ÄKTA** I Amersham I Biacore I IN Cell Analyzer I Whatman I GE Service I

imagination at work

The New ÄKTA avant

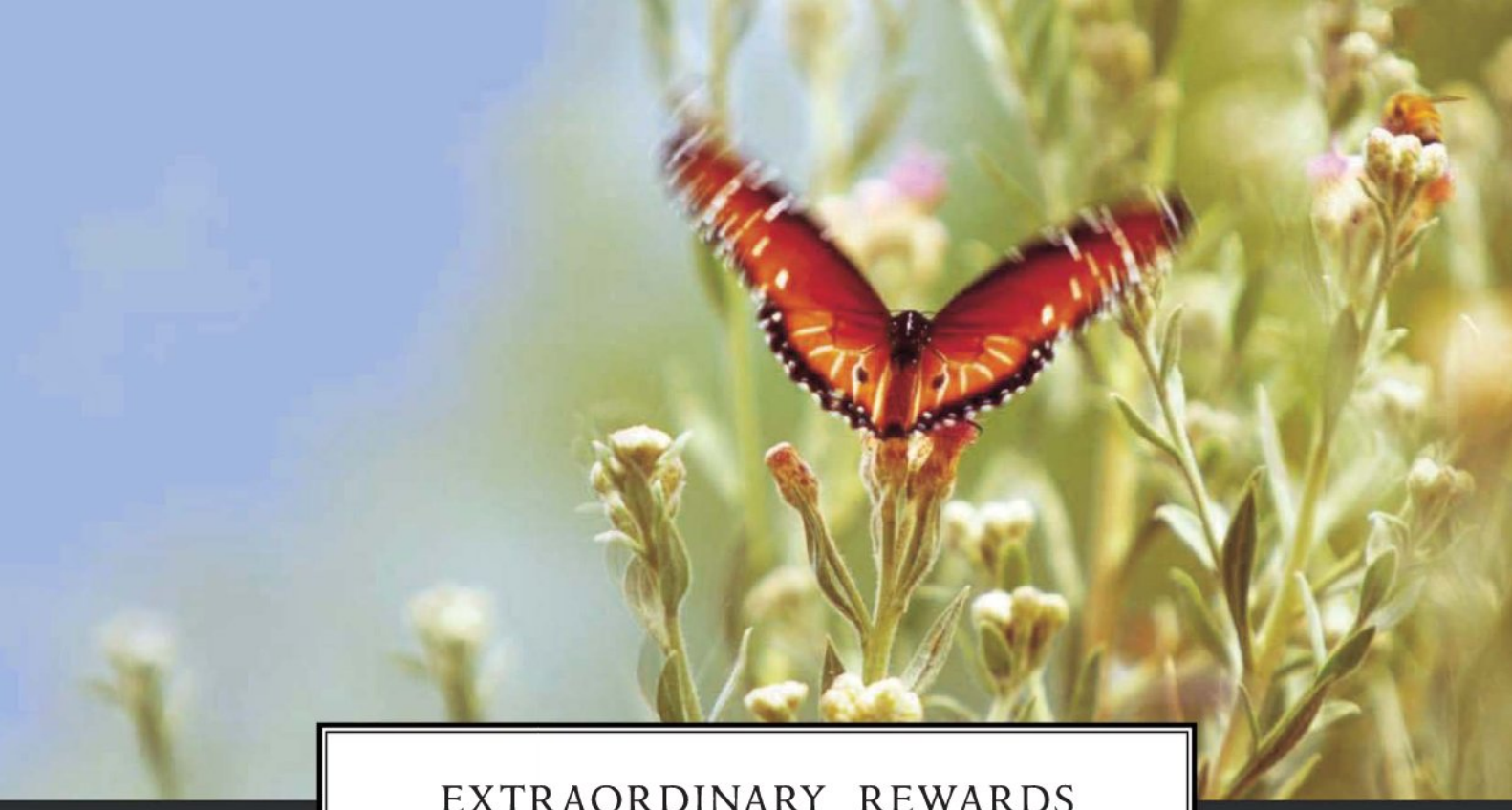

EXTRAORDINARY REWARDS

35th Anniversary Offers

As a trusted resource in the life science community, New England Biolabs would like to thank our customers for 35 years of support. Join us in celebrating our 35th anniversary by visiting www.neb.com to find 12 months of exciting offers, including significant product discounts and giveaways.

Look for the 35th Anniversary Offers icon on our website to learn about our monthly special offer.

www.neb.com

CELEBRATING 35 YEARS

NEW ENGLAND BioLabs® Inc.

enabling technologies in the life sciences

CLONING & MAPPING	DNA AMPLIFICATION & PCR	RNA ANALYSIS	PROTEIN EXPRESSION & ANALYSIS	GENE EXPRESSION & CELLULAR ANALYSIS

www.neb.com

EDITED BY STELLA HURTLEY

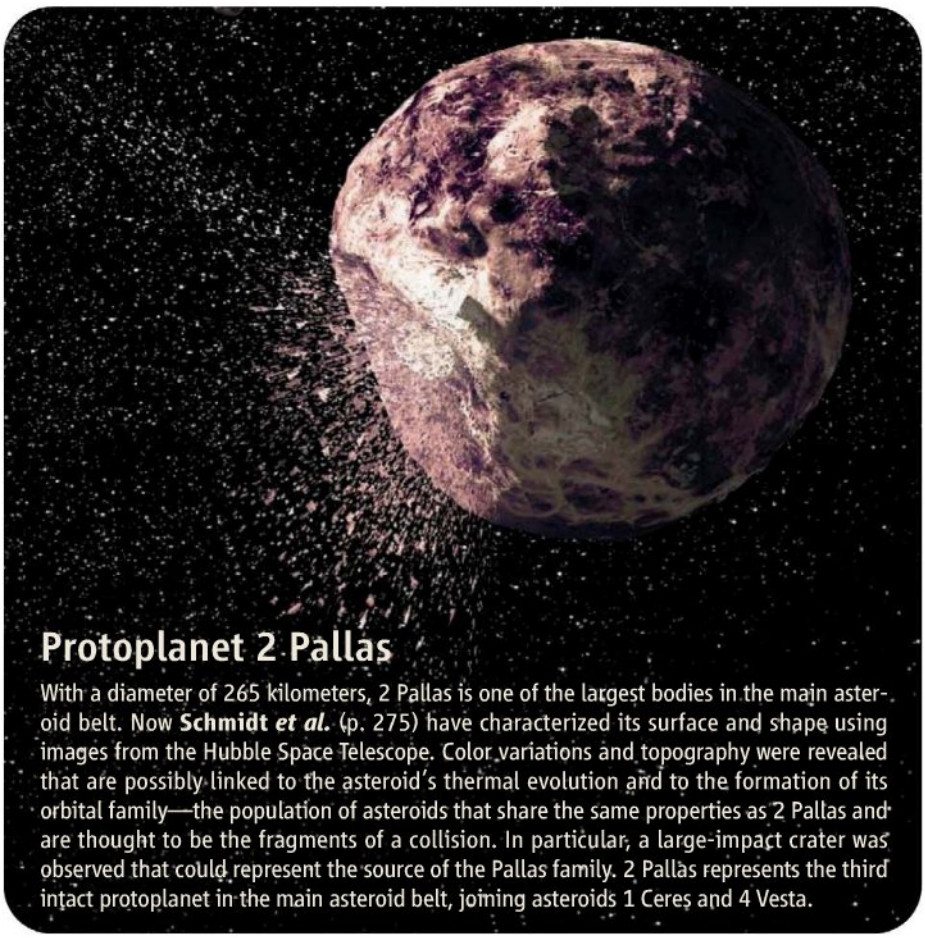

Protoplanet 2 Pallas

With a diameter of 265 kilometers, 2 Pallas is one of the largest bodies in the main asteroid belt. Now **Schmidt *et al.*** (p. 275) have characterized its surface and shape using images from the Hubble Space Telescope. Color variations and topography were revealed that are possibly linked to the asteroid's thermal evolution and to the formation of its orbital family—the population of asteroids that share the same properties as 2 Pallas and are thought to be the fragments of a collision. In particular, a large-impact crater was observed that could represent the source of the Pallas family. 2 Pallas represents the third intact protoplanet in the main asteroid belt, joining asteroids 1 Ceres and 4 Vesta.

Monsoon Cave Recordings

Rocky deposits in caves in central China record the changes over time in the Asian Monsoon through the oxygen isotopic composition of the minerals from which they are formed. These deposits can be precisely dated and provide an absolute time line for climate system changes. **Cheng *et al.*** (p. 248; see the Perspective by **Severinghaus**) present oxygen isotope data from speleothems collected from Sanbao Cave, China, for the three glacial terminations that occurred between 120,000 and 350,000 years ago. The data reveal variations in the amount of precipitation delivered by the Asian Monsoon over time. Comparison of the timing of these changes with corresponding changes in ice core and marine sedimentary records provides mechanistic insights into how variations in insolation affect ice sheets and ice age terminations.

Metabolite Arrays

Methods suitable for the biochemical analysis of multiple metabolic pathways in mixed samples are in short supply. **Beloqui *et al.*** (p. 252) report a method to sample the global metabolic state of an organism or mixture of organisms using an array of more than 1500 metabolites linked to a glass slide. The substrates are linked to the plate so that the reaction of an enzyme with one of the metabolites releases a fluorescent dye, which allows sensitive detection of the enzymatic activity. From a sample with small numbers of a mixture of bacteria, the authors were able to collect DNA, amplify it in a host bacterium, and measure its encoded metabolic activity with the array. Furthermore, by coating the substrates on nanoparticles with a specially designed linker, the authors could trap and purify enzymes that reacted with the immobilized substrate. The metabolite array may be useful in the characterization of environmental samples, in diagnostic procedures, and in enzyme discovery.

Extending Quantum Memory

Quantum information processing and communication relies on the ability to store, retrieve, and manipulate information stored in quantum memories. In most practical instances, however, the stored quantum information is fragile and susceptible to loss during readout. **Jiang *et al.*** (p. 267, published online 10 September) used a combination of quantum logic operations on the electronic spin of a nitrogen vacancy center in diamond to control its interactions with a nearby set of proximal nuclear spins of the carbon network. In this setup, the quantum memory of the electron spin could be made more robust. Extending the lifetime and allowing multiple readouts of the quantum memory should prove a useful technique for quantum information processing.

Ear, Ear

One defining feature of mammals, distinguishing them from other animals, is the separation of the middle ear from the jaw, which improves hearing sensitivity. **Ji *et al.*** (p. 278; see the Perspective by **Martin and Ruf**) describe an adult Mesozoic fossil mammal, in a lineage that led to both marsupials and placentals, in which the middle ear is still ossified to the jaw. Recent developmental studies have shown that the release of the ear is tied to multiple genes and signaling pathways during development. Together, these data suggest how gene patterning may have led to the early evolution of the mammalian ear.

Peeking at Pathogen Response Networks

Networks controlling gene expression serve as key decision-making circuits in cells, but the regulatory networks that control dynamic and specific gene expression responses to stimuli are often not well understood. This is particularly true for immune dendritic cells (DCs), which respond to pathogens by mounting elaborate transcriptional responses, and are centrally involved in infectious diseases, autoimmunity, and vaccines. **Amit *et al.*** (p. 257, published online 3 September) explored the transcriptional response of dendritic cells to specific classes of pathogens. The transcriptional subnetworks responsible for mammalian dendritic cell responses to different pathogens were identified, and the function of 100 regulators clarified.

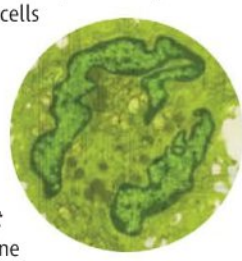

Quiet Clock

Many physiological processes have circadian rhythms driven by a biological clock in the suprachiasmatic nuclei (SCN) of the brain. Within the SCN, some neurons express the molecular components of the clock and others do not. Exactly how the clock mechanism is coupled to neuronal activity is not precisely understood. Investigation

Continued on page 203

CREDITS (TOP TO BOTTOM): B. E. SCHMIDT AND S. C. RADCLIFFE; SIGRID HART

Continued from page 201

of the electrophysiological properties of SCN neurons by **Belle *et al.*** (p. 281) found that, contrary to the conventionally expected rapid firing rate of the cells during the day, clock-containing cells tended not to fire, despite being in an electrically excited state. Modeling and experimental characterization of changes in channel activity revealed unexpected electrophysiological properties of the SCN cells requiring a reassessment of how the circadian clock regulates activity of SCN neurons.

Anti-HIV Antibodies

One of the top priorities for an HIV vaccine is the ability to elicit a broadly neutralizing antibody response, which should provide the best protection against infection. In the 25 years since the discovery of HIV, very few broadly neutralizing antibodies have been identified, and those that do exist were discovered nearly two decades ago. Using a high-throughput culture system, **Walker *et al.*** (p. 285; published online 3 September) now identify two additional broadly neutralizing antibodies isolated from a clade A HIV-infected African donor. These antibodies exhibit great potency and, in contrast to other known broadly neutralizing antibodies, are able to neutralize a wide range of viruses from many different clades. The antibodies recognize a motif in the trimerized viral envelope protein that is found in conserved regions of the variable loops of the gp120 subunit. Identification of this motif provides an intriguing new target for vaccine development.

Normally Persistent

In superconductors, currents are expected to flow persistently without dissipation. Quantum mechanics predicts that such persistent currents should also exist in normal mesoscopic metal rings. However, the predicted effect is small, which has made the detection of these currents difficult. **Bleszynski-Jayich *et al.*** (p. 272; see the Perspective by **Birge**) have developed a sensitive technique based on a nanomechanical resonator. An array of aluminum rings on the end of a resonator was fabricated to monitor the shift in frequency of the resonator as the rings were threaded with quanta of magnetic-field flux, setting up currents in the rings. In agreement with a theoretical scenario put forward over a decade ago, the results could be described with a model based on non-interacting electrons.

Chromosomal Mapping

The conformation of the genome in the nucleus and contacts between both proximal and distal loci influence gene expression. In order to map genomic contacts, **Lieberman-Aiden *et al.*** (p. 289, see the cover) developed a technique to allow the detection of all interactions between genomic loci in the eukaryotic nucleus followed by deep sequencing. This technology was used to map the organization of the human genome and to examine the spatial proximity of chromosomal loci at one megabase resolution. The map suggests that the genome is partitioned into two spatial compartments that are related to local chromatin state and whose remodeling correlates with changes in the chromatin state.

Making Split Decisions

Development of the vertebrate vasculature has been thought to involve just two mechanisms of blood vessel formation. **Herbert *et al.*** (p. 294; see the Perspective by **Benedito and Adams**) identified a third mechanism in zebrafish in which two distinct, unconnected vessels can be derived from a single precursor vessel. Several vascular endothelial growth factors and signaling pathways, including ephrin and notch signaling, coordinated the sorting and segregation of a mixture of arterial and venous-fated precursor cells into distinct arterial and venous vessels. These findings provide a mechanistic framework for how mixed populations of cells can coordinate their behavior to segregate and form distinct blood vessels.

Containing Neuronal Exuberance

In rats and mice, around the time of birth, neurons of the central nervous system switch from a growth mode and lose their ability to regenerate. Studying retinal ganglion cells of the rat, **Moore *et al.*** (p. 298; see the Perspective by **Subang and Richardson**) identified a gene, *Krüppel-like factor-4* (*KLF4*), that seems to contribute to the switch. The *KLF4* gene belongs to a family of related transcription factors that possess repressive or enhancing effects on axon growth. The combinatorial effect of this family of transcription factors before and after birth may fine-tune the ability of the neurons to extend axons.

CREDIT: BLESZYNSKI-JAYICH *ET AL.*

Eppendorf Consumables – it's Your sample

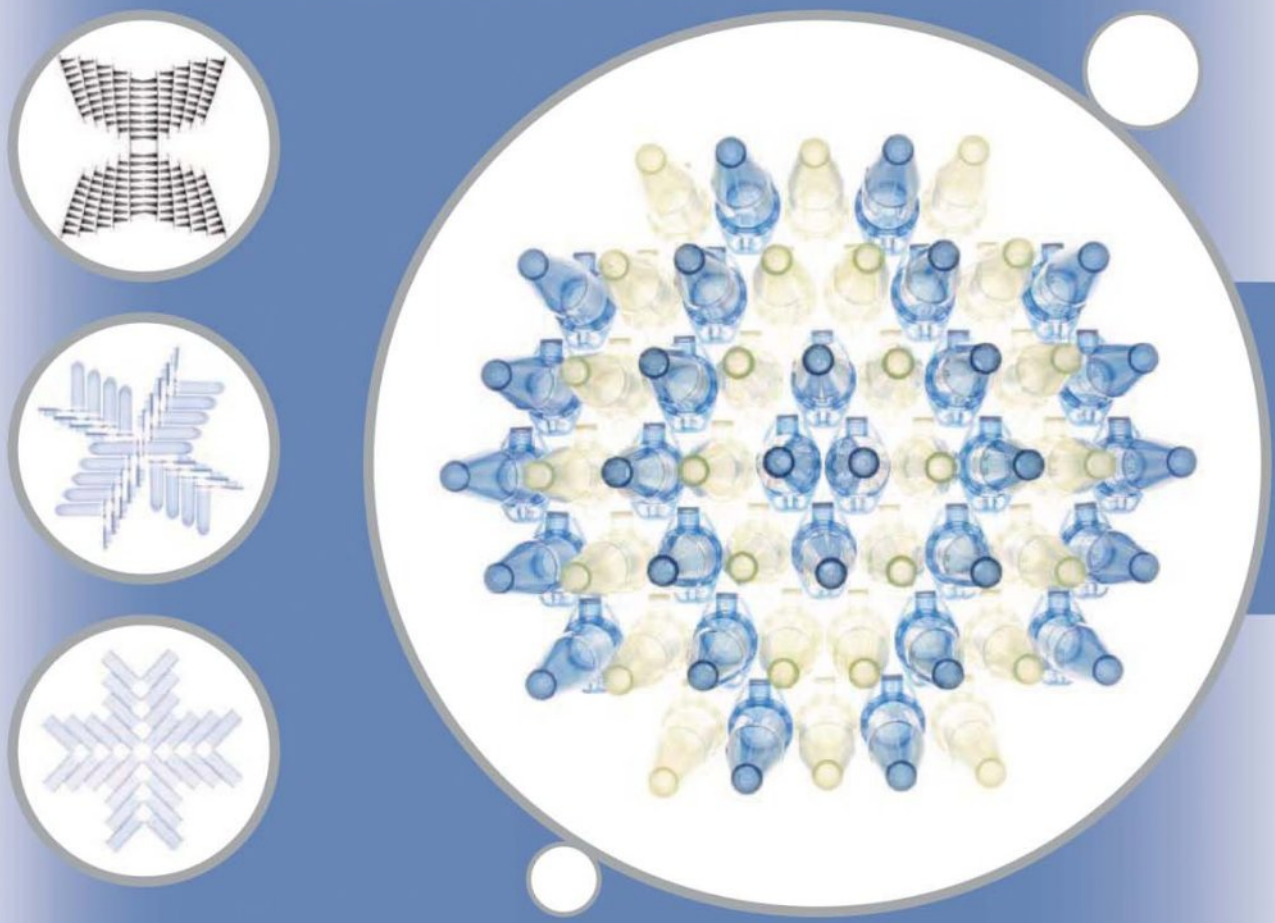

Make the best of it!

Top quality for your sample.

Each of your valuable samples deserves the best treatment. See for yourself how the original Eppendorf Tubes will save time and reduce costs.

Sample loss in tubes can be time consuming and expensive. Therefore, the close environment of each sample should be adapted to its specific quality and purity needs. This can involve a specific purity level or the absence of certain substances, but also stability, reliability, or geometry. Eppendorf Tubes are designed to cover all of the specific needs of your samples!

Eppendorf Safe-Lock Tubes

- Safe-Lock prevents accidental lid opening during incubation
- Precise sealing for lowest evaporation rates
- Large, frosted lid for easy labeling
- Exceptional centrifugation stability prevents tube breaking
- Hinged lid for easy, contamination-free opening
- Batch certified Eppendorf Biopur® or PCR clean quality

Learn more about Eppendorf consumables:
www.eppendorf.com/consumables

eppendorf

In touch with life

Your local distributor www.eppendorf.com/worldwide · **Application Support** E-Mail: support@eppendorf.com
Eppendorf AG · Hamburg · Germany · Tel: +49 40 538 01-0 · Eppendorf North America, Inc. · USA · Tel.: +1 800 645 3050

Bruce Alberts is Editor-in-Chief of *Science*.

The Art of Translation

THIS WEEK MARKS THE LAUNCH OF THE NEW AAAS JOURNAL *SCIENCE TRANSLATIONAL MEDICINE*. I am very pleased that we were able to recruit Elias A. Zerhouni, the distinguished former director of the U.S. National Institutes of Health, to be its chief scientific adviser, and Katrina L. Kelner, until recently the Deputy Editor for Biological Sciences at *Science*, to be its editor. As Zerhouni writes in his editorial, the goals of this journal, and of translational medicine more broadly, are to speed the rate at which the astounding recent advances in our basic understanding of biological mechanisms are exploited for preventing and treating human disease.*

Knowledge accumulates as science advances, and science and technology are generating new knowledge at an increasing pace. The acceleration becomes understandable once one recognizes that new knowledge is formed by creatively combining old knowledge in new ways, and that, for example, 100 pieces of knowledge can be combined in 100 times more ways than can 10 pieces of knowledge. The most striking innovations often come from combining knowledge across disparate domains, but only a tiny fraction of such combinations will be useful, making research strategies ever more critical as science proceeds. Great science therefore resembles great art in the sense that an outstanding scientist has carefully selected a "subject" (the unsolved problem to attack) and the "brushes and paints" (the research strategy and techniques), using them to skillfully create a pleasing original "painting" (a new explanation of some aspect of the natural world).

The opportunities and the challenges in translational medicine are enormous, and constant waves of innovation will be needed to meet them. New ideas and approaches are essential. Too often, information with the potential to improve human quality of life is available only through silo-like channels. For example, cardiologists who only attend specialized meetings and read the cardiology literature, but not the physics or computer science literature, can miss an important breakthrough that could advance their own research. To stimulate innovation, we must intentionally catalyze the mixing of scientists and clinicians from different disciplines, knowing that new approaches will emerge from their interactions. *Science Translational Medicine* strives to increase such mixing by keeping researchers informed about relevant advances across all disciplines.

When I was at the U.S. National Academies, we experimented with several types of scientific meetings that clearly demonstrated the power of transdisciplinary mixing. The simplest focused on developing new approaches to an important scientific challenge through a 2-day workshop involving no more than 30 scientists.

Traditionally, scientific meetings have been designed to bring together a large number of scientists who work on similar problems. For example, to discuss schizophrenia, the best scientists who study it would normally be invited to give back-to-back 30-minute talks about their most recent research over the course of 2 to 5 days. The schizophrenia workshop at the National Academies was very different. We invited only a few experts in schizophrenia, plus a larger group of leading scientists from a wide variety of fields, including cell biology, biochemistry, human genetics, and neuroscience. During the first half-day, the experts provided teaching sessions for those who knew little about schizophrenia, including overviews of the latest progress in understanding and treating the disease. The next day and a half was then devoted to brainstorming sessions, in which the non-experts attempted to bring their unique scientific perspectives to bear on a group effort to outline the most promising approaches for future research.

Exactly the same approach was used a few years later to scope out new approaches for developing antiviral treatments for smallpox. Both workshops were unusually stimulating and successful, generating important new ideas.† Analogously, it is our hope that *Science Translational Medicine*, by juxtaposing scientists and clinicians with very different backgrounds and approaches to disease, can speed the rate at which innovation increases human well-being.

– Bruce Alberts

10.1126/science.1182658

*E. A. Zerhouni, *Sci. Transl. Med.* **1**, 1ed1 (2009). †S. H. Barondes *et al.*, *Proc. Natl. Acad. Sci. U.S.A.* **94**, 1612 (1997); S. C. Harrison *et al.*, *Proc. Natl. Acad. Sci. U.S.A.* **101**, 11178 (2004).

CREDIT: (TOP) TOM KOCHEL

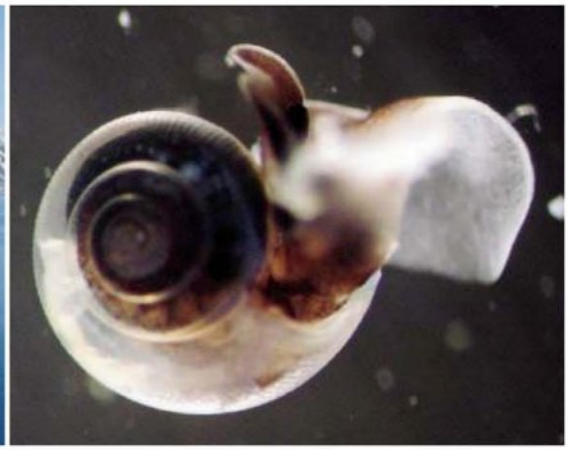

OCEAN SCIENCE

Dissolute Behavior Up North

Some species of sea butterfly have shells composed of aragonite, a metastable form of calcium carbonate. These pelagic mollusks are considered sentinels for environmental change; even though they can survive for a couple of days in water depleted of calcium carbonate, their shells already begin to show dissolution marks.

Comeau *et al.* have collected pteropods (*Limacina helicina*) from Kongsfjorden, Svalbard, to study their response to the acidification of polar waters that has been predicted will occur as atmospheric carbon dioxide increases, carbonate declines, and ice melts. They measured shell calcium flux by calcein staining and ^{45}Ca uptake, which revealed a 28% decrease in calcification as the pH dropped by 0.3 and aragonite saturation fell to 1.00, which is forecast to happen by the year 2100. Below this threshold, aragonite concentrations in seawater are too low to prevent the dissolution of shelled creatures—conditions that spell doom for more than just the sea butterflies. — CA

Biogeosciences **6**, 1877 (2009).

ASTRONOMY

Galactic Blowup

The deflection of light in the gravitational field of massive objects causes clusters of galaxies to act as cosmic lenses, magnifying and distorting the light of the galaxies that lie behind them. By analyzing Hubble Space Telescope archival images of the cluster MACS J1149.5+2223, Zitrin and Broadhurst have identified the most powerful gravitational lens yet: It magnifies a background spiral galaxy 200 times (summed over five multiple images). Distant galaxies normally appear as thin distorted arcs around the centers of clusters. In the case of this cluster, however, the lensed images of a background spiral galaxy are large and appear relatively undistorted, implying a nearly uniform mass distribution in the center of the cluster. The authors constructed a model of the mass distribution of the cluster to reproduce the lensed images they could readily identify, and they were then able to use it to predict the location of other images, ultimately identifying a total of 10 sets of multiple images of background galaxies. The refined model that reproduces all of these images is at odds with predictions made by simulations of the evolution of galaxies and associated large-scale distribution, thereby challenging our current theoretical models for the formation of structure in the universe. — MJC

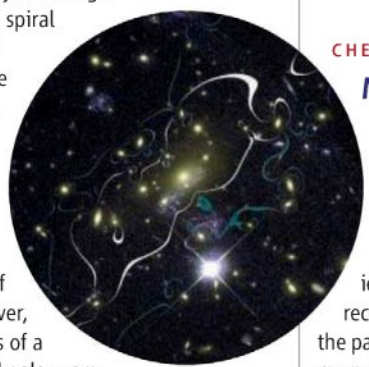

Astrophys. J. **703**, L132 (2009).

CHEMISTRY

Microwave-Safe Dishes

Numerous conveniences available in the chemistry laboratory (magnetic stirrers, for instance) have been slow to make their way into the kitchen. Chefs can still brag, though, that the ultimate kitchen convenience—the microwave oven—has only recently been widely exploited in the lab. Over the past decade, chemists have begun to explore more systematically the utility of intense microwave sources for accelerating organic reactions. The question remains, however, whether microwave technology is simply a means of achieving very rapid heating, or whether specific reaction pathways might be selectively enhanced through molecular absorption in this wavelength region. In part to address this question, Obermayer *et al.* fabricated a silicon carbide (SiC) reaction vessel, which absorbs microwaves far more efficiently than conventional Pyrex labware and thus transmits their energy to chemical reagents in conventional thermal fashion. On performing a diverse set of 18 organic reactions under microwave irradiation in both Pyrex and SiC, the authors observed no evidence of nonthermal chemistry. — JSY

Angew. Chem. Int. Ed. **48**, 10.1002/anie.200904185 (2009).

DEVELOPMENT

Pregnancy Can Be Stressful

When cells and tissues experience environmental stress, the endoplasmic reticulum (ER)—a membrane-bounded intracellular compartment—accumulates incorrectly folded proteins. The inositol requiring enzyme–1 (IRE1) mediates an unfolding protein response (UPR) that relieves ER stress by activating the expression of genes that participate in protein quality control.

Prior work has documented embryonic lethality in mice after inactivation of IRE1. Using in vivo imaging and knockout mice, Iwawaki *et al.* show

CREDITS (TOP TO BOTTOM): STEEVE COMEAU, CNRS-UPMC; ZITRIN *ET AL.*, *ASTROPHYS. J.* **703**, L132 (2009)

that IRE1 functions in the placenta after ER stress induction. In mice lacking IRE1, vascular endothelial growth factor–A was reduced and angiogenic defects were seen in the labyrinth layer of the placenta, consistent with diminished transport of oxygen and other nutrients. Therefore, IRE1 functions, at least in part, in extraembryonic tissues during early development. — BAP

Proc. Natl. Acad. Sci. U.S.A. **106**, 10.1073/pnas.0903775106 (2009).

BIOPHYSICS

Embedded Sensors

Drugs used in the treatment of fungal infections are often directed against the protective fungal cell wall (gray). Hence, a better understanding of how cell wall integrity is maintained under dynamic and stressful conditions has pharmaceutical implications. Proteins anchored in the underlying plasma membrane (orange) are thought to detect surface stress and to mediate adaptive responses, but the biophysics of stress sensing is unclear.

Dupres *et al.* have used atomic force microscopy (AFM) to characterize the response of the yeast plasma membrane protein Wsc1 to mechanical stress. Although the outer end of wild-type Wsc1 (red) is buried within the cell wall, adding a short extension (yellow) containing a histidine tag rendered the fusion protein accessible to a Ni^{2+}-derivatized AFM tip. Scanning the surfaces of live yeast cells and focusing on individual Wsc1 molecules revealed that they exhibited Hookean behavior with a spring constant of roughly 5 pN nm^{-1}. That is, lengthening of Wsc1 was linearly proportional to the force applied. This force-extension behavior required glycosylation (blue), which is expected to favor an extended and relatively stiff protein conformation and may be a key factor in the function of this nanospring. — LC

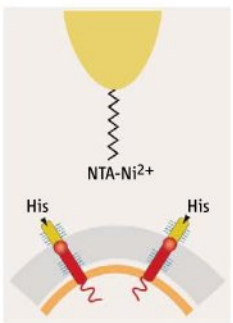

CREDIT: DUPRES *ET AL.*, *NAT. CHEM. BIOL.* **5**, 10.1038/NCHEMBIO.220 (2009)

Nat. Chem. Biol. **5**, 10.1038/nchembio.220 (2009).

EDUCATION

Enough Room for All

Debate about immigration and how it might strengthen or weaken a society often touches on education. Some opponents of immigration voice concerns that an influx of noncitizen foreigners may swamp school systems and labor markets with relatively uneducated newcomers, to the detriment of natives. Research has supported some fears of this sort, demonstrating, for example, that the enrollment of immigrants in some college programs may "crowd out" natives. But while such research has examined whether natives ultimately go to college and how well they fare once there, work by Neymotin examines important precursors: Do immigrants affect natives at key pre-college stages, as reflected by college entrance exam scores—obtained in the U.S. on the scholastic aptitude test (SAT)—and college application patterns? The 1990s brought one of the largest waves of immigration, with California and Texas representing two major gateways. The author analyzed questionnaires and SAT scores for every SAT-taking public school student in those two states during the years 1994 through 2001. These individual-level data were matched to information about the school, school district, and surrounding community gathered by the Department of Education and Census Bureau. Controlling for a wide range of variables and potential biases, the author concludes that immigration did not harm natives' test performance, nor diminish the probability of their applying to a top college or university. — BW

Econ. Educ. Rev. **28**, 538 (2009).

MATERIALS SCIENCE

A Penetrating Simulation

Simulating the diffusion of small molecules in a polymer melt is a difficult task on account of the multitude of length and time scales that must be accommodated, ranging from the fast motions of individual chain segments and pendant groups to the much slower fluctuations of the polymer backbones. Fritz *et al.* show that a hierarchical model can be used to calculate the diffusion coefficients and excess chemical potentials (solubilities) for ethylbenzene diffusion in atactic polystyrene melts. Diffusion coefficients were first obtained using molecular dynamics simulations of coarse-grained (CG) models, wherein each CG bead represented 5 to 10 atoms and the interactions between beads were guided by potentials derived from all-atom simulations, thus reducing the computational time by several orders of magnitude. By comparing the CG results with those from high-temperature, all-atom simulations, in which equilibration occurs quickly, the authors could extrapolate time scales to lower temperatures using a Volger-Fulcher relationship. The excess chemical potential was determined by thermodynamic integration of the work needed to perturb the system from state A to state B, thereby coupling the solute-polymer interactions. The authors believe that their methods can be applied for fast, quantitative calculations in the limiting case where penetrating molecules are similar in size to the polymer repeat unit. — MSL

Soft Matter **5**, 10.1039/b911713j (2009).

www.sciencemag.org

Science

1200 New York Avenue, NW
Washington, DC 20005
Editorial: 202-326-6550, FAX 202-289-7562
News: 202-326-6581, FAX 202-371-9227
Bateman House, 82-88 Hills Road
Cambridge, UK CB2 1LQ
+44 (0) 1223 326500, FAX +44 (0) 1223 326501

Subscription Services For change of address, missing issues, new orders and renewals, and payment questions: 866-434-AAAS (2227) or 202-326-6417, FAX 202-842-1065. Mailing addresses: AAAS, P.O. Box 96178, Washington, DC 20090-6178 or AAAS Member Services, 1200 New York Avenue, NW, Washington, DC 20005

Institutional Site Licenses please call 202-326-6755 for any questions or information

Reprints: Author Inquiries 800-635-7181
Commercial Inquiries 803-359-4578

Permissions 202-326-7074, FAX 202-682-0816

Member Benefits AAAS/Barnes&Noble.com bookstore www.aaas.org/bn; AAAS Online Store www.apisource.com/aaas/ code MKB6; AAAS Travels: Betchart Expeditions 800-252-4910; Apple Store www.apple.com/eppstore/aaas; Bank of America MasterCard 1-800-833-6262 priority code FAA3YU; Cold Spring Harbor Laboratory Press Publications www.cshlpress.com/affiliates/aaas.htm; GEICO Auto Insurance www.geico.com/landingpage/go51.htm?logo=17624; Hertz 800-654-2200 CDP#343457; Office Depot https://bsd.officedepot.com/portalLogin.do; Seabury & Smith Life Insurance 800-424-9883; Subaru VIP Program 202-326-6417; VIP Moving Services www.vipmayflower.com/domestic/index.html; Other Benefits: AAAS Member Services 202-326-6417 or www.aaasmember.org.

science_editors@aaas.org	(for general editorial queries)
science_letters@aaas.org	(for queries about letters)
science_reviews@aaas.org	(for returning manuscript reviews)
science_bookrevs@aaas.org	(for book review queries)

Published by the American Association for the Advancement of Science (AAAS), *Science* serves its readers as a forum for the presentation and discussion of important issues related to the advancement of science, including the presentation of minority or conflicting points of view, rather than by publishing only material on which a consensus has been reached. Accordingly, all articles published in *Science*—including editorials, news and comment, and book reviews—are signed and reflect the individual views of the authors and not official points of view adopted by AAAS or the institutions with which the authors are affiliated.

AAAS was founded in 1848 and incorporated in 1874. Its mission is to advance science, engineering, and innovation throughout the world for the benefit of all people. The goals of the association are to: enhance communication among scientists, engineers, and the public; promote and defend the integrity of science and its use; strengthen support for the science and technology enterprise; provide a voice for science on societal issues; promote the responsible use of science in public policy; strengthen and diversify the science and technology workforce; foster education in science and technology for everyone; increase public engagement with science and technology; and advance international cooperation in science.

Information for Authors
See pages 807 and 808 of the 6 February 2009 issue or access www.sciencemag.org/about/authors

It becomes you.

Introducing the 3500 Series Genetic Analyzer.

Get ready to make an amazing discovery: the new 8-capillary and 24-capillary 3500 Series Genetic Analyzers take DNA analysis to an entirely new level of performance. A level where your daily workflow seems like a natural extension of your own intuition. Where precise, quality-assured data inspires greater confidence. And where a new consumables design and intuitive software interface keep you current and in control.

Take a closer look, and you'll find the new 3500 and 3500xL Genetic Analyzers are like second nature. Which is our first priority when it's your data.

Discover the 3500 System at **www.appliedbiosystems.com/3500Series**

Easy-to-Use Consumables

Control at Your Fingertips

Quality-Assured Data

applied biosystems™

Meet your new lab partner.

The new Thermo Scientific NanoDrop 2000 and 2000c Spectrophotometers offer true micro-sample analysis, with sample size capability as low as 0.5 µl and a measurement time of less than five seconds. Either of these is the perfect instrument for all your quantitation needs—DNA, RNA, proteins and more. Providing full spectrum UV-Vis results, both instruments can analyze samples with concentrations greater than 15,000 ng/µl (dsDNA) without dilutions. Innovative software makes it easy to build your own methods, design reports and export data. And with both pedestal and cuvette capability, the NanoDrop™ 2000c is the one spectrophotometer that does it all.

Test-drive the NanoDrop 2000 or 2000c in your own lab!*

Visit **www.nanodrop.com** to schedule your test-drive. Try out an instrument and run your own samples. It's completely free.

*Available only in US and Canada

Thermo Scientific NanoDrop 2000c

The only spectrophotometer that combines micro-volume pedestal technology and cuvette capability

Moving science forward

Thermo SCIENTIFIC

Part of Thermo Fisher Scientific

Celebrating the Dugong

Nobody knows much about the religious life in Stone Age Arabia. Now, a 5500-year-old ritual mound in the Arabian Gulf gives a provocative clue: coastal dwellers venerated dugongs as mythic ancestors.

When paleontologists first came upon the 10-square-meter mound of bones in 1989 on the island of Akab 190 kilometers northeast of Abu Dhabi, they assumed it merely contained the remains of dozens of butchered dugongs. But when archaeologist Sophie Méry of the French national research agency, CNRS, and colleagues excavated the site, they discovered an intricately constructed monument. Akab's Neolithic fishers had first laid jawbones of dugongs—4-meter-long mammals related to the manatee—flat on the ground, wedged them in place with ribs, and drenched the assemblage with a red-ochre solution. On top they placed dugong skulls—all pointing toward the east—and bundles of ribs, as well as rare tubular stone beads and other ornaments.

"The discovery led us to various lines of questioning," says Méry, who has published the find in the latest issue of *Antiquity*. "Was it a sanctuary, a trophy, or a grave?" No similar site of this age has been discovered anywhere in the world. But, the authors note, aboriginal Australians built almost identical dugong bone mounds for hunting rituals beginning in the 14th century. Méry thinks similar rites took place on the Gulf coast 5000 years earlier. "The evidence," says Mark Beech, an archaeologist at Abu Dhabi Authority for Culture and Heritage, "looks very convincing."

A Matter of Scales

Growing numbers of farmed salmon in northern Europe are escaping and mingling with their tastier, sturdier cousins from the wild. Tracking this phenomenon is difficult because the two populations look alike.

But chemical signatures in fish scales may reveal a fish's origin, British salmon sleuths write in the *Marine Ecology Progress Series*. Fish scales accumulate tree-ring–like layers that reflect a fish's diet and the waters it has inhabited over the course of its lifetime. Pellet fish food contains slightly higher levels of manganese than is found in the diet of a wild fish. Clive Trueman of the National Oceanography Centre in Southampton and Elizabeth Adey of the Scottish Association for Marine Science in Oban, both in the United Kingdom, used a mass spectrometer to measure manganese levels in the scales of salmon from several Scottish farms and from the wild. They found that they "could easily distinguish between time a fish had spent at sea and in fresh water," Trueman says. By comparing the scale chemistry—cheaper than DNA analysis—ecologists can track the presence of intruders, the authors say, and determine where countermeasures are needed.

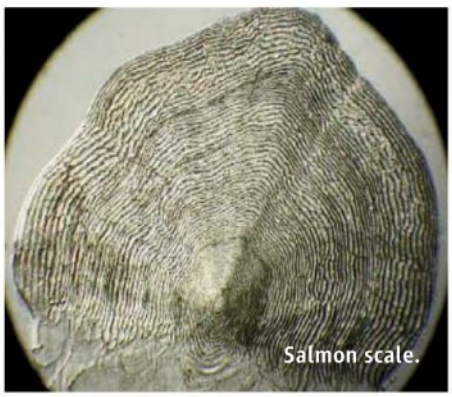

Salmon scale.

CREDITS (TOP TO BOTTOM): THOMAS ZAGORY/MAFUAE; REUTERS; REUTERS; CLIVE TRUEMAN/NATIONAL OCEANOGRAPHY CENTRE, SOUTHAMPTON

Iran Science Officials In Plagiarism Flap

Four scientific journals have retracted research articles by top Iranian government scientists, including the minister of science, after concluding that they include plagiarized material.

The flap started late last month when *Nature* reported that much of a 2009 article in the journal *Engineering with Computers* was copied verbatim from a 2002 article by South Korean researchers in the *Journal of Physics D: Applied Physics*. Both articles describe experiments involving tungsten alloy rods ricocheting off steel plates. The first author on the 2009 paper is Iran's science minister, Kamran Daneshjou, who wrote it with his former Ph.D. student Majid Shahravi, an engineer at the Iran University of Science and Technology (IUST) in Tehran. *Nature* subsequently reported plagiarism in two more articles by the same pair.

Iranian émigré scientists have expressed outrage and noted with irony that Daneshjou helped orchestrate the election—widely rejected as a fraud—of Iranian President Mahmoud Ahmadinejad. But some researchers in Iran are sticking up for Daneshjou and pointing the finger at his co-author. "After [Shahravi] has officially admitted his complete fault on this matter, he must be punished accordingly," says engineer Seyyed Hasheminejad of IUST.

Daneshjou.

In an interview with Iranian media, Shahravi denied any plagiarism, noting that articles by others had been cited in footnotes. Late last week, the plagiarism scandal had widened to include a 2006 paper co-authored by Iranian roads and transportation minister—and Ahmadinejad's former Ph.D. adviser—Hamid Behbahani.

Q&A with Francis Collins
214

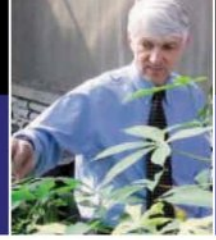

Revitalizing USDA research
216

PHYSIOLOGY NOBEL

U.S. Researchers Recognized for Work on Telomeres

An enzyme that keeps cells from premature death has won a bit of immortality for the scientists who discovered it.

This year's Nobel Prize in physiology or medicine recognizes the discovery of a key mechanism that cells use to protect their genetic information. Elizabeth Blackburn of the University of California, San Francisco; Carol Greider of Johns Hopkins University School of Medicine in Baltimore, Maryland; and Jack Szostak of Harvard Medical School in Boston will each receive one-third of the $1.4 million prize for their work describing telomeres, the repetitive DNA that caps the ends of chromosomes, and telomerase, the enzyme that makes the caps. The trio has long been considered top contenders for the prize. "I've been hoping for this for about 10 years. I'm thrilled," says Titia de Lange of Rockefeller University in New York City, who studies telomeres.

Interest in telomeres dates back to the 1930s and 1940s, when Nobel Laureates Barbara McClintock and Hermann J. Muller gathered indirect evidence that telomeres prevented chromosomes from attaching to each other. But later researchers never followed up because the specialized DNA was hard to isolate and study.

In the mid-1970s, Blackburn and Joseph Gall, now at the Carnegie Institution for Science in Baltimore, came up with a solution. Blackburn had just finished her Ph.D. under the direction of Fred Sanger at the University of Cambridge in the United Kingdom; she wanted to apply new sequencing approaches to telomeres. With Gall, she decided to study an unusual single-cell organism called *Tetrahymena*, which during its life cycle shatters its chromosomes into tens of thousands of pieces, each with telomeres. With abundant material, the duo discovered that the caps consisted of six-base segments that repeated 20 to 70 times.

Blackburn then teamed up with Szostak, who wanted to see if telomeres would work in yeast. Typically, when extra DNA is added to yeast cells, they break it down or reconfigure it. But when *Tetrahymena* telomeres were added to these pieces of DNA, their function was preserved. "It was really a shot in the dark," Blackburn recalls, because typically one organism's DNA didn't work in another organism. Yet in 1982, Blackburn and Szostak showed that yeast retained and copied extra genetic material containing *Tetrahymena* telomeres intact, suggesting this specialized DNA had an ancient function that predated when the ancestors of these two organisms went their separate ways.

Milestone. Blackburn (*left*), Greider, and Szostak share the prize—the first honoring two women—for work on telomeres (*stained yellow in inset*).

"It led to a better understanding of telomeres," says Thomas Cech of the University of Colorado, Boulder. Other experiments showed that yeast could extend the ends of inserted *Tetrahymena* telomeres by adding new DNA to the tips. Blackburn and Szostak suspected that an unknown enzyme was responsible.

In 1984, Greider, a Ph.D. student in Blackburn's lab, decided to see if Blackburn and Szostak's hunch was right. "It seemed like an exciting project that would potentially tell us something new about how telomeres would be maintained," Greider recalls. Because the enzyme that copies DNA doesn't travel all the way to the end of chromosomes during replication, researchers had wondered for decades why chromosomes didn't shrink with each cell division. A telomere-lengthening enzyme might explain the puzzle. In 1985, after a series of difficult experiments, Greider and Blackburn demonstrated that six-base segments of DNA were being added to existing telomeres—evidence that such an enzyme did exist. It took almost another year to purify it.

Telomerase proved quite complex. In 1987, Greider and Blackburn showed that it contained an RNA as well as a protein component, with the RNA serving as the template for adding the necessary bases to the end of the telomere. They pinned down the RNA by 1989, but the protein part took several more years to identify.

During the 1980s, telomere research "was a very obscure area," says Cech. These advances "were pretty exciting to the community, but it was a pretty small field." There were hints of a link to aging or cancer. For example, Szostak, working with mutant yeast that lacked the ability to maintain telomeres, discovered that telomeres shrank with each cell division until eventually the cell stopped dividing. "But it was not possible to rigorously test" these ideas, Cech says, until the catalytic protein was in hand in the mid-1990s.

At about that time, Szostak switched his focus to understanding the origin of life (*Science*, 9 January, p. 198). "Once it was pretty clear there would be biomedical applications and the questions would be taken care of, [I decided] it would be okay to go on to other things," he said at a press conference in Boston on Monday.

Telomerase is now thought of as a Dr. Jeckyll–Mr. Hyde molecule: good in one context, bad in another. Rapidly growing cells need active telomerase, but once cells have become specialized and cease dividing, telomerase gets turned off—or is supposed to be. Many types of cancer cells have overactive telomerase that allows them to con-

Personalizing cancer treatments
218

SLAC reinvents itself
221

tinue dividing when they shouldn't. "It's an almost universal oncology target," says Jerry Shay of the University of Texas Southwestern Medical Center in Dallas. Clinical trials are now under way to test whether a vaccine against telomerase could help fight certain kinds of cancer.

Not having enough telomerase is bad news, however. Deficient telomerase has been linked to a lung disease called pulmonary fibrosis and anemia caused by sporadic bone marrow failure. And a rare premature aging disease called dyskeratosis congenita is caused by a faulty telomere-maintenance system. No treatment is yet available, says Thomas Vulliamy of Queen Mary, University of London, who studies the disorder. "Sometimes we're a bit impatient. … I am sure that the understanding of telomeres will help us treat patients someday."

Other disease connections are being investigated. In 2004, Blackburn found a correlation between shorter telomeres and chronic stress. Other data show that shorter telomeres are associated with an increased risk or incidence of several common age-related diseases, such as heart disease. Telomeres "really do seem to reflect our status of health and our risk of disease," says Blackburn.

Shay is convinced that the prize will draw more people into telomere research and bring the clinical payoffs closer. But he says the field already has something to celebrate: Blackburn and Greider are the ninth and tenth women to be awarded the prize in physiology and medicine—the first time in history two women will share in the award.

–GRETCHEN VOGEL AND ELIZABETH PENNISI

PHYSICS NOBEL

Digital Imaging, Communication Advances Honored

Within seconds after the announcement of this year's Nobel Prize in physics, photos and videos of the winners were zinging across the globe via the Internet. Fittingly, the winners' discoveries made that instantaneous dissemination of information and images possible. Half the award goes to Charles Kao, an electrical engineer whose theoretical work lit the way to practical optical fibers for high-speed telecommunications. The other half honors physicists Willard Boyle and George Smith for inventing the first electronic chip that could capture an image.

Simply put, Kao figured out how to get light to travel far enough down a glass fiber to pass signals over great distances. Light tends to course down a microns-thick fiber instead of leaking out the side because it glances off the inside surface of the fiber and reflects back into the glass. The glass itself can absorb light, however, and until Kao's work in 1966, such absorption would soak up 99% of all the light passing through a 20-meter optical fiber.

Kao, who was born in Shanghai, China, and earned his Ph.D. in the United Kingdom, fingered iron impurities as the essential cause of the loss. Light can also bounce down a fiber in several different patterns or modes, and Kao, then at the Standard Telecommunication Laboratories in Harlow, U.K., correctly predicted that a very thin fiber that allowed the light to propagate in only one mode would be best for producing practical communications networks.

Kao, 75, "was the right choice because he was the one who brought to the attention of the community that it was possible to reduce the losses," says optical physicist Govind Agrawal of the University of Rochester in New York state. Still, Agrawal adds, "when I heard the news, my first thought was about the other people who could also have gotten it." In particular, he says, Donald Keck and colleagues at Corning Inc. in Corning, New York, were the first to produce the fibers Kao described theoretically.

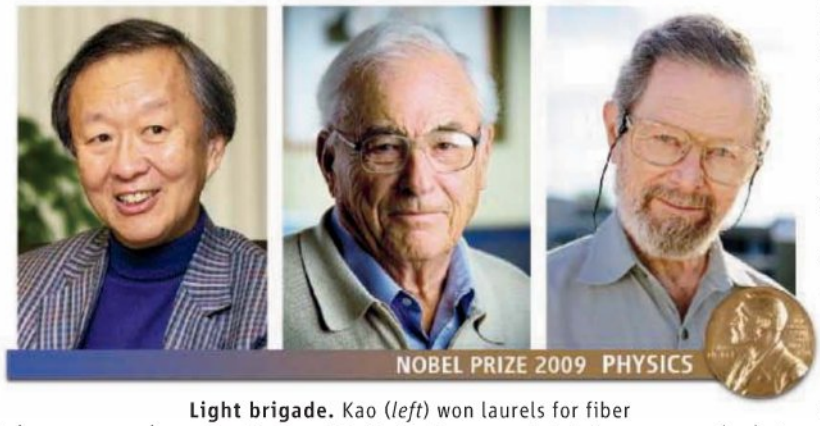

Light brigade. Kao (*left*) won laurels for fiber optics; Boyle and Smith, for charge-coupled devices.

Boyle, 85, and Smith, 79, invented the charge-coupled device (CCD), the first electronic chip capable of snapping a picture. It remains a key technology for medical imaging, astronomical telescopes, and digital cameras. Boyle and Smith "have enabled pretty much all of the modern imaging systems," says George T. C. Chiu, an engineer specializing in imaging at Purdue University in West Lafayette, Indiana. "The CCD has changed everything about how we gather information and images."

The CCD contains a silicon chip that is divided into cells or "pixels." When light hits a pixel, it excites an electric charge in the silicon, which then induces a charge in a tiny electrode on the chip's surface. The charge then quickly passes from electrode to electrode down a whole row of pixels—that's the "charge coupling"—and is read out at the edge of the chip.

Boyle, who was born in Canada and lives in Halifax, says he and Smith thought the device up in a couple of hours in 1969. "It was an October morning, and he came up to my office for some brainstorming. And pretty soon we had some sketches on the black board, and there it was." Smith says, "We complemented each other. We just seemed to click." The two worked at the famed Bell Labs in Murray Hill, New Jersey. Bell Labs can now claim a total of seven Nobel Prize-winning discoveries—a fact that Boyle says he finds more amazing than his own invention.

–ADRIAN CHO

CREDITS (LEFT TO RIGHT): REUTERS/LANDOV; NATIONAL ACADEMY OF ENGINEERING; JEFF ZELEVANSKY/REUTERS; © THE NOBEL FOUNDATION

Tutorial. President Obama hears from NIH Director Francis Collins (*left*) and cancer researcher Marston Linehan during a visit to NIH.

NEWSMAKER INTERVIEW

Francis Collins: Looking Beyond the Funding Deluge

U.S. National Institutes of Health (NIH) Director Francis Collins wound up his sixth week on the job with a splash last week, hosting a visit from President Barack Obama. On 30 September, the final day of the 2009 fiscal year, the president chose NIH as the place to highlight the first year of spending from his 2-year, $787 billion economic stimulus package. The $5 billion disbursed by NIH to more than 12,000 grants is "the single largest boost to biomedical research in history," Obama said.

Because $4 billion more has been committed for the second year of the new grants, NIH has effectively spent almost 90% of its $10.4 billion in stimulus funds, Collins told *Science* later that day. That includes nearly $100 million for autism, $750 million for heart disease research, and $175 million for The Cancer Genome Atlas. The process hasn't been easy, however. NIH staff and outside scientists have scrambled to review huge numbers of grant applications, including the Challenge Grants, a special competition that generated over 20,000 proposals requiring 15,000 reviewers.

Besides moving money out of the door in Collins's first weeks, NIH submitted its fiscal 2011 budget request to the White House. Collins has also been busy helping to find candidates to direct the National Cancer Institute, a presidentially appointed position; overseeing a review of the National Children's Study, which is facing cost overruns; and assessing the Roadmap, the now nearly $500 million pot of money for cross-institute projects created by previous director Elias Zerhouni.

The following are excerpts from a conversation with *Science*:

–JOCELYN KAISER

Q: Can you say anything about how NIH's 2011 budget is looking so far?

F.C.: There's going to be a lot of people making the case for why their particular part of the government is a uniquely wonderful investment. At the same time, we have an economy that continues to struggle, we have a deficit that is now grown to something like $9 trillion. The scientific community should not in any way imagine that this is going to be easy.

Q: So chances are there will be a plunge in success rates in 2011?

F.C.: It's likely to be a pretty tough year. It's not only because one has to worry about what that NIH base can be, but a large number of Challenge Grants that didn't get funded are going to come back as R01s [NIH's basic research grants]. So the number of applications is expected to be quite high.

Q: The Challenge Grants created a lot of work, and only 3% to 4% were funded. If you could go back and do it over again, would you rethink the Challenge Grant competition?

F.C.: I wasn't here then, but I don't hear that from others. I would say this is a great problem to have. What it showed was this pent-up demand that had been building over 5 years of flat budgets.

Q: Has Senator Charles Grassley (R–IA) uncovered a real problem with corruption in medicine?

F.C.: I think the vast, vast majority of scientists are honorable people. At the same time, if there are examples of people who have intentionally hidden financial benefits, that's a black eye for all of biomedical research and we need to get our house in order. So certainly NIH in December will be putting forward for the community to look at some ideas about how to tighten up the system of reporting. And at least for myself, I would think the Grassley proposal [for a public database of payments reported by companies] would be a good step forward.

Q: A recent report found that NIH is now awarding 19% of R01 grants to proposals that missed the "payline," or quality cutoff, largely to help new investigators. Is 19% too high?

F.C.: Isn't this an interesting discussion because certainly in the past the concern has been that NIH is not doing enough for new investigators. Now people are raising the issue: "Are we doing too much of this?" I don't think so. We're basically trying to give new investigators who already have a superb priority score but just missed the cut a chance to get started.

Q: What do you think of President Obama's proposal to double cancer research over 8 years?

F.C.: Obviously, the president has a particular interest in cancer because of experiences in his own family. Certainly, we would all agree that increasing the funding for cancer would be highly justified. At the same time, many people worry about a circumstance where one disease is picked out of the pile and made to sound like it is more important. And certainly from NIH's perspective, I think we would like to see the rising tide lift all the boats.

Q: The National Children's Study could cost double or more than the original estimate of $3 billion. Should the full study go forward?

F.C.: I'm certainly very much in favor of the science. We're going to take a very serious look at the study design, at what we've learned from the pilot projects. I think we have to figure out what we can afford to do.

VIROLOGY

Chronic Fatigue and Prostate Cancer: A Retroviral Connection?

As if chronic fatigue syndrome (CFS) hasn't caused enough brawls, a new study published online by *Science* (www.sciencemag.org/cgi/content/abstract/1179052) links the disease to a possibly contagious rodent retrovirus, XMRV, which has also been implicated in an aggressive form of prostate cancer. Related work by the authors also suggests that CFS might best be treated with AIDS drugs. Even the lead author, Judy Mikovits of the Whittemore Peterson Institute for Neuro-Immune Disease in Reno, Nevada, says she understands why linking CFS to a retrovirus and to prostate cancer has already drawn skepticism.

In 2006, an unrelated paper found an association between XMRV, which originated in mice, and a deadly prostate cancer exacerbated by a deficient enzyme. Mikovits and colleagues had seen the same deficiency in CFS cases. When they investigated further, the team discovered XMRV in the white blood cells of two-thirds of CFS patients but only 4% of control subjects. Intriguingly, Mikovits says XMRV does major damage in natural killer (NK) blood cells, which attack tumor cells and cells infected by viruses, and other studies suggest people with CFS suffer from high rates of cancer. Unpublished work, Mikovits adds, has found blood serum antibodies for XMRV in 95% of CFS patients.

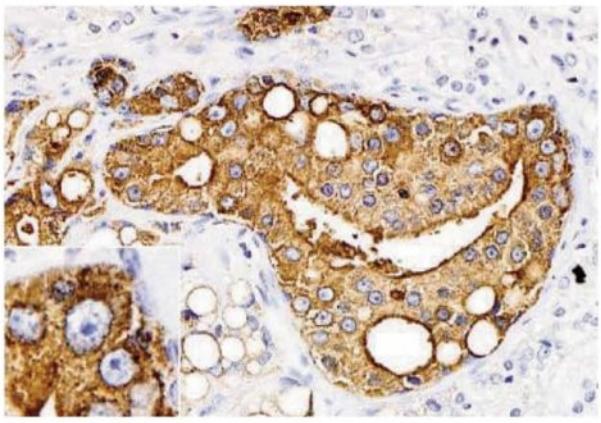

Controversial link. A study of chronic fatigue syndrome points to a retrovirus found in cancerous prostate cells (*magnified in inset*).

CREDITS (TOP TO BOTTOM): GEORGE DOYLE/STOCKBYTE; ROBERT SCHLABERG AND HARSH THAKER

All previous attempts to nail down a cause for CFS—including many links to viral infections—have foundered or been retracted, and many doctors remain doubtful that it's a coherent disease. Mikovits says her work "proves beyond a shadow of a doubt that CFS is a real disease." But some of her peers find the report of a viral link premature.

Joseph DeRisi, a molecular biologist at the University of California, San Francisco, who co-discovered XMRV, was not satisfied with details in the paper: He wanted to know more about the viral load in CFS patients and how the demographics of the control group matched that of CFS patients. And the Mikovits team didn't do enough to rule out contamination, he says. "One has to be very careful about making claims about such a sensitive and emotionally charged issue as CFS, where many claims have been made in the past." At the least, a double-blind study where a third-party lab searches for XMRV in CFS patients and in controls is vital, he says.

Other CFS specialists, including Jonathan Kerr at St. George's University of London, are convinced that the Mikovits team discovered something important. "The fact that the virus was actually grown from the blood cells of CFS patients strongly suggests some sort of role in the pathogenesis of the disease." But exactly what they discovered remains unclear, given that the group is not claiming to have identified a cause.

John Coffin, a molecular biologist at Tufts University in Boston, analyzed the Mikovits paper in a separate "Perspective" also published online by *Science* (www.sciencemag.org/cgi/content/abstract/1181349). Coffin was highly skeptical of the paper at first, but the team found enough independent lines of evidence for XMRV to convert him. "They will be celebrating in the clinics where these people [with CFS] are being treated," he now says.

Even if the finding of a link to XMRV holds up, treatment suggestions are bound to attract controversy. No one knows how easily XMRV spreads, although Mikovits says transmission can occur via bodily fluids, including saliva. Mikovits also says unpublished preclinical data hints that scientists can treat XMRV with AIDS drugs such as AZT, although AZT itself might prove too toxic. Kerr remained cautious about this: "With present public knowledge—what is described in this paper—further work would be necessary before antiretroviral drugs could be recommended." **–SAM KEAN**

ScienceNOW.org

From *Science*'s Online Daily News Site

2009 Ig Nobels Announced
Although the Nobel Prizes are grabbing the spotlight this week, last week belonged to the Ig Nobels, which honor the more humorous side of science. This year's winners include the inventor of a bra that can serve as a pair of emergency gas masks and a team that showed that compostable garbage can be reduced to less than 10% of its mass by fermenting it with bacteria derived from the feces of panda bears. http://bit.ly/EZ9U3

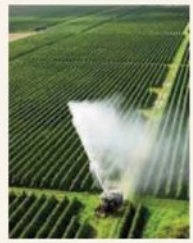

Helping Crops Shed Pesticides
Every year, 3 million tons of pesticides are sprayed on the world's food crops. The chemicals protect plants from voracious insects and pathogens, and they save billions of dollars in damages. Yet high doses of pesticides that accumulate in the body can cause cancer and other serious illnesses in humans. Now scientists may have found a way to help crops shed these toxicants long before they end up on dinner tables around the globe. http://bit.ly/xHNdm

Buried Treasure Solves Ancient Roman Puzzle
As civil wars erupted throughout the Roman Republic in the 1st century B.C.E., country dwellers may have fled to cities. Before they left, some people buried their valuables to hide them from looting armies. Now social scientists have studied these ancient stashes, called coin hoards, to answer a long-standing Roman mystery. http://bit.ly/4edUhG

The Fungus That Ate the World
Scientists claim that they have identified an ancient fungus that flourished about 250 million years ago, feeding on dead trees as it spread across the planet. Those remains could provide a crucial clue to the identity of what killed off much of Earth's plant and animal life at the time, although some researchers remain skeptical. http://bit.ly/1fZCbi

Read the full postings, comments, and more on **sciencenow.sciencemag.org**.

U.S. RESEARCH POLICY

Agricultural Science Gets More Money, New Faces

After decades of flat funding, agricultural research seems to have caught the attention of U.S. policymakers. Last week, Congress gave a 30% boost to the main competitive grants program of the U.S. Department of Agriculture (USDA), raising it to $262 million for 2010. Two new research chiefs at the department also hope to parlay an administrative reorganization into greater visibility for the field. Research advocates are cautiously upbeat that their labors are finally paying off. "There's fresh energy and optimism," says Thomas Van Arsdall of the National Coalition for Food and Agricultural Research in Fredericksburg, Virginia.

Many are expecting a lot from Rajiv Shah, the young and energetic deputy undersecretary for research who joined USDA in June from the Gates Foundation. Speaking with *Science* last week, Shah described his plans to shake up the massive department, which employs 2300 scientists and has a research budget of $2.8 billion. Lobbyists are also thrilled with this week's arrival of plant scientist Roger Beachy as head of the National Institute of Food and Agriculture (NIFA), the new home for USDA's extramural funding.

"Shah's a really smart guy. He's surrounding himself with smart people; he's got a big agenda and wants to do really big things," says Ferd Hoefner of the National Sustainable Agriculture Coalition in Washington, D.C. "He's got the personality and credibility to try to put that all together."

Advocates have been trying for years to raise the profile—and funding—of agricultural research. They applauded last year's passage of an agriculture bill that will provide $426 million over 4 years in new competitive research funding for bioenergy, organic farming, and vegetables and other so-called specialty crops (*Science*, 23 May 2008, p. 998). The bill also gives Shah the title of chief scientist as part of a broader move to improve how USDA manages research.

Shah, 36, was an unusual pick for the position. Not only is he far younger than previous undersecretaries, he's not a scientist. Trained as a physician and also holding a business degree, Shah worked on child immunization at the Gates Foundation before switching to agricultural development. Now he's applying those skills to a department whose research budget has remained essentially flat for decades. USDA is also seen by many as a bit player among federal science agencies, a status that was reinforced earlier this year when USDA received no research funds from the $787 billion American Recovery and Reinvestment Act while the National Institutes of Health (NIH), the National Science Foundation (NSF), and the Department of Energy's science programs each received billions. "I think that was the ultimate wake-up call," Shah says.

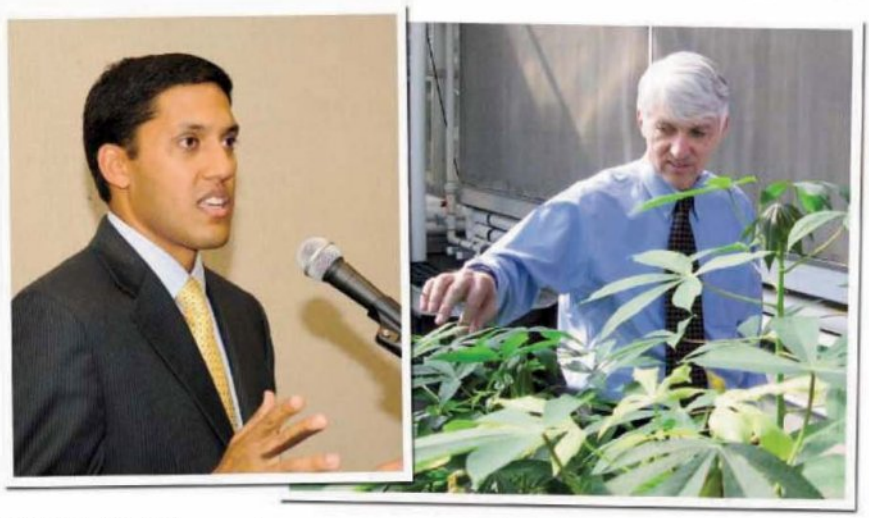

Seeding change. Rajiv Shah (*left*) and Roger Beachy hope to make USDA a bigger player in federal research.

Shah plans to raise the department's visibility by focusing research on five broad areas that align with Administration priorities: climate change, bioenergy, food safety, obesity, and overseas hunger. He wants to focus on core problems—such as the development of drought-tolerant crops and perennial grasses for biofuels—and leverage USDA's investments by partnering with other agencies. "Frankly, we've done too many discrete projects that are too small in scope." Similarly, Shah hopes to give out fewer but larger grants for work that fosters multidisciplinary collaborations. He plans to hold program managers accountable by asking them to set goals for two, five, and 10 years.

Extramural research is also being reorganized. In the farm bill, Congress directed USDA to convert its Cooperative State Research, Education, and Extension Service—which distributes extramural grants to individual scientists and so-called formula funding to land-grant universities—into NIFA and to appoint a distinguished scientist to head it.

Beachy, 65, qualifies by any measure. A member of the National Academy of Sciences, Beachy did important work on engineering virus resistance in plants and in 1998 became the founding president of the Donald Danforth Plant Science Center in St. Louis, Missouri. "My major goal is to improve the perception of the agency and gain the same level of respect as NSF and NIH," Beachy says. Karl Glasener, who directs science policy for the American Society of Agronomy, Crop Science Society of America, and Soil Science Society of America in Madison, says "Beachy's status as a star in the science community should help with image building."

One crucial measure of success, of course, will be the size of NIFA's budget. William Lesher, the director of Global Harvest Initiative in Washington, D.C., an agribusiness campaign to increase research on crop productivity, is optimistic that congressional appropriators will be receptive to requests from the Obama Administration to spend more. "If they propose larger budgets, it will really have a significant positive impact," Lesher says.

A coalition of research advocates, including Glasener and Hoefner, has been lobbying for a $300 million budget for competitive grants at USDA in fiscal year 2011. (The program is authorized at $700 million but received only $201 million in the 2009 fiscal year that ended last week.) Shah won't comment specifically on what the agency will request, a figure that is vetted by the White House before it's released in February as part of the president's overall budget submission to Congress. But he emphasizes that the Administration is serious about doing what it takes. "In order to get the breakthroughs we want, we have to invest at a certain level of scale and partner with others to do it well," he says. "That's what is coming."

–ERIK STOKSTAD

CREDITS: ALICE WELSH/USDA

CLIMATE CHANGE

Both of the World's Ice Sheets May Be Shrinking Faster and Faster

The two great ice sheets—Greenland's and Antarctica's—have had plenty of press lately, what with galloping glaciers and whole lakes of meltwater plunging into ice holes in minutes (*Science*, 18 April 2008, p. 301). Surveys of ice-sheet volume made from planes and satellites have quantified these losses, but those assessments have been spotty in time, space, or both. Shrinkage accelerated from the 1990s into the 2000s, but researchers couldn't be sure what would come next.

Now the latest analysis of the most comprehensive, essentially continuous monitoring of the ice sheets shows that the losses have not eased in the past few years. More ominously, losses from both Greenland and Antarctica appear to have accelerated during the past 7 years. If the acceleration out of the 1990s "was a hiccup, it was a big one, and it's getting bigger," says glaciologist Richard Alley of Pennsylvania State University, University Park, who was not involved in the work.

The results, in press at *Geophysical Research Letters*, are based on measurements by the Gravity Recovery and Climate Experiment (GRACE) satellite mission. Rather than measuring the volume of ice sheets every few years as most earlier surveys did, GRACE "weighs" them from month to month with a pair of spacecraft launched in March 2002 as a joint NASA and German Aerospace Center mission (*Science*, 14 August, p. 798). Flying in tandem 220 kilometers apart, the satellites can measure subtle variations in the pull of gravity as they pass over a large mass on the surface. By beaming microwaves from one to the other, they precisely gauge the changing distance between them as the added mass tugs first on the leading satellite and then on the trailing one. Changes in gravity from pass to pass reflect changes in the icy mass below.

The mass changes of Greenland and Antarctica during the past 7 years have all been negative, geophysicist Isabella Velicogna of NASA's Jet Propulsion Laboratory in Pasadena, California, concludes in the study. On Greenland, she calculates, the rate of ice mass loss doubled over the 7-year period, producing an acceleration of −30 cubic kilometers of water lost per year. On Antarctica, the loss rate more than doubled to produce a similar acceleration. Together, that would make for a 5% acceleration each year in the rise of sea level. Compounded year after year, "that is a big thing," says Velicogna. "We should be more concerned."

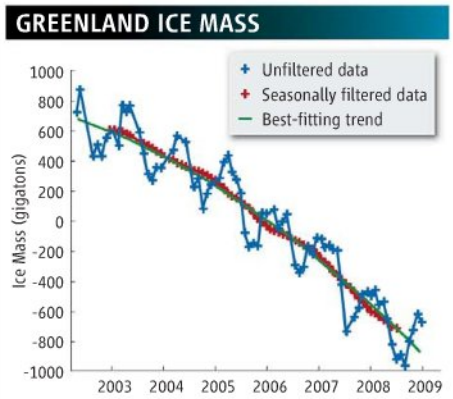

Bending down. The trend line of Greenland ice mass (green) curves downward with time, suggesting that losses have been accelerating.

The GRACE observations counter encouraging news from southeastern Greenland that the surging glaciers there had slowed (*Science*, 23 January, p. 458). The slowing was probably real, says Alley, but apparently the increasing losses from melting and accelerating glaciers elsewhere around Greenland at least made up for the slowing in the southeast. Whatever is driving ice loss—warmer oceans, warmer air, or both—is persisting, he says.

Glaciologist Waleed Abdalati of the University of Colorado, Boulder, says Velicogna's analysis "suggests—that's the key word—that there's been an acceleration in the period examined. We have to be careful to not overinterpret and speculate about the future." The record is too short to be extrapolated into the future, Abdalati says. And at least in Greenland, it was affected by the extreme warmth and resulting melting in 2007, a loss surge that might not be repeated in the next 7 years.

If bursts of ice loss do occur soon, GRACE may not be around to record it. Its two satellites will fall from orbit around 2013, dragged down after a decade of orbiting through Earth's outermost atmosphere. No replacement gravity mission is yet planned.

–RICHARD A. KERR

CREDIT: ADAPTED FROM ISABELLA VELICOGNA, *GEOPHYSICAL RESEARCH LETTERS*

*Science*Insider

From the *Science* Policy Blog

Scientists complain that the U.S. Army's claims of success with an **AIDS vaccine** tested in Thailand are undermined by an unrevealed second analysis. That result found a drop in vaccine efficacy and no statistical significance when it compared vaccinated and control groups that rigorously followed the protocol. http://bit.ly/lHVr8

A number of scientists are outraged over **a new program to use DNA and tissue samples** to determine the nationality of applicants for asylum by the U.K. Border Agency. After *Science*Insider revealed scientific condemnation of its plans to conduct DNA tests and isotope analyses to determine nationality (*Science*, 2 October, p. 30), the U.K. Border Agency this week changed its plans, saying such evidence would not yet be used in asylum decisions. http://bit.ly/2QxWBG

Energy Secretary Steven Chu tried to persuade Congress to fund eight **Energy Innovation Hubs** next year, but in a spending bill passed last week, Congress supported only three. http://bit.ly/2GPoDK

A controversy at the ***Proceedings of the National Academy of Sciences*** over the journal's standards for **peer review** took a new turn when it decided to postpone the publication of a controversial paper on butterflies that was already accepted and published online. http://bit.ly/zhJsk

A new study conducted by the National Football League suggested that playing professional American football increases the risk of **dementia**, increasing pressure on the sport to study the problem. http://bit.ly/wO8cd

Congress has given the U.S. Department of Energy's **Office of Science** a 2.7% boost in its 2010 budget, to $4.9 billion. The $131 million increase comes as the overall budget for the $27 billion agency was held relatively flat. http://bit.ly/fQLdN

For more science policy news, visit **blogs.sciencemag.org/scienceinsider**.

Looking for a Target On Every Tumor

Lethal threat. Even some advanced lung tumors have been slowed by focused drugs.

CREDIT: ANNE WESTON/WELLCOME IMAGES

Major cancer centers say they're getting ready to genotype every patient's tumor, hoping to match them with drugs specifically tailored to halt tumor growth

IN AUGUST 2007, KEVIN BRUMETT, AN athletic 29-year-old Massachusetts man, was stunned to find out why he was having severe back and stomach pain: He had advanced lung cancer. Brumett was young and had never smoked. Doctors at Beth Israel Deaconess Medical Center in Boston gave him standard chemotherapy, but the drugs became toxic over time, so they tried something new. They tested biopsies from his lung tumor for several mutations known to drive cell growth. "There was a small hope that if we found [the right sequence], there would be an approved drug or a clinical trial he would qualify for," says Daniel Costa, his oncologist at Beth Israel.

Brumett was lucky. His tumor cells had a fusion of two genes, *EML4* and *ALK*, recently found in a small fraction of patients with his type of cancer, non-small cell lung cancer, the most common form. A trial to test a drug targeted at *EML4-ALK* was just beginning at Beth Israel. A week after taking two pills daily to block the fusion gene's protein product, Brumett felt better. His nausea and fatigue were minimal, and the knifelike pain in his chest stopped.

Last summer on a patient message board, Brumett shared the good news that his tumor was shrinking. His advice: "I want every single patient who has been diagnosed with non-small cell lung cancer to tell your doctor that you want to have your tumors biopsied and tested for every type of genetic mutation they know of." That fall, Brumett told his story on local television and at events held by patient advocates.

Tumor genotyping is not part of standard treatment. But that is changing. A handful of major U.S. cancer centers are laying plans to analyze the tumors of every lung cancer patient who comes in the door and check for an array of mutations. The aim is to match patients with a drug that goes after the tumor's genetic weak spot. Two centers, Harvard's Massachusetts General Hospital (MGH) in Boston and Memorial Sloan-Kettering Cancer Center (MSKCC) in New York City, have already begun; they will add several other cancer types in the coming months. Proponents hope that comprehensive tumor genetic testing—aided by a major U.S. research effort to catalog mutations in tumors, called The Cancer Genome Atlas—will soon become a standard part of a patient's medical record. "The data are most useful if they're not squirreled away in a research lab," says medical oncologist Leif Ellisen of MGH.

Online
sciencemag.org
Podcast interview with author Jocelyn Kaiser.

But there are challenges. Even big cancer centers are still building the infrastructure needed to comprehensively genotype tumors. And testing is likely to help only a small fraction of cancer patients. Many tumors don't have any of the well-studied mutations. Only about 15% to 20% of all lung cancer patients have mutations that can be matched to targeted anticancer drugs, for example.

The grimmest reality, however, is that even when a match is found, the new targeted drugs have mainly slowed tumors, not stopped them in advanced lung cancer. After Brumett spent 8 months on the experimental drug, during which time he felt almost normal, his cancer developed resistance and began to spread. He died last May, 4 days after his wedding.

It's still early days for this technology, says Bert Vogelstein, a cancer biologist at Johns Hopkins University in Baltimore, Maryland. "I don't think there's any argument that, from a research perspective, these kinds of initiatives are great." But, he asks: "Is this something that's going to reduce suffering and death and prolong lives? I think it will, but it's still new."

Sharpshooters

Many agree with Vogelstein that tumor genotyping makes perfect sense as a tool for research. It's creating biobanks that make it easier to identify cancers that might be vulnerable to a new drug and will help attract companies to pay for trials aimed at the subset of patients most likely to benefit. That should speed treatments to the clinic, proponents say. "We simply cannot do another [large clinical] trial without having this kind of information," says John Niederhuber, director of the National Cancer Institute (NCI) in Bethesda, Maryland, a booster of the approach. Personalized treatment is exactly what NCI hopes will come out of The Cancer Genome Atlas, a huge sequencing initiative to find mutations in tumors. It is ramping up from a pilot phase and expects to tackle more than 20 cancer types in the next 5 years at a cost of $275 million the first 2 years.

The idea of giving a patient a drug tailored to the genetic makeup of his or her tumor goes back at least a decade. The most famous example is the leukemia drug Gleevec, which targets a genetic mistake, known as the Philadelphia chromosome, that leads to uncontrolled cell growth. Over 95% of chronic myeloid leukemia patients carry this glitch and most early-stage patients respond to the drug. Another example is the breast cancer drug Herceptin, a monoclonal antibody that blocks HER2, a protein on a cancer cell's surface that receives growth signals that trigger the cell to grow. The drug is given only to the 25% of breast cancer patients whose tumors have a mutation that overexpresses *HER2*. Its presence is determined by counting copies of the *HER2* gene or detecting protein levels.

The developers of Herceptin suspected from the start that only certain patients would benefit. But this became clear for other targeted drugs only after the drug was tested in a general population. Take Erbitux, a drug used since 2004 to treat colorectal cancer. It homes in on EGFR, a cell receptor in the same family as HER2. Retrospective studies showed that the tumor cells of patients with a mutated oncogene called *KRAS* can thwart EGFR-targeted drugs. Now the drug has been recommended only for the 60% of patients with tumors that have a normal version of the *KRAS* oncogene.

For lung cancer, a turning point came in 2004. Researchers at Harvard's Dana-Farber Cancer Institute and MGH, and at MSKCC, were exploring why Iressa, another drug that targets EGFR, didn't seem to help most patients but dramatically shrank lung tumors in about 10% of patients. They realized that these "responders," more often Asian and nonsmokers, had certain mutations in *EGFR* that made the tumors more vulnerable (*Science*, 30 April 2004, p. 658).

The initial poor showing led the U.S. Food and Drug Administration to sideline Iressa in the United States. But a new trial in Asia published this year clearly showed that for patients with the EGFR mutations, the rate of disease progression was slower in those who were on Iressa than it was in those on chemotherapy. The drug has now been approved in Europe for targeted use in patients with the *EFGR* mutations that make the cells vulnerable, and the manufacturer, AstraZeneca, is seeking approval for similar use in the United States. The Asia trial convinced even the skeptics that *EGFR* mutations should guide treatment decisions, says cancer biologist William Pao, who left MSKCC for the Vanderbilt-Ingram Cancer Center in Nashville this year.

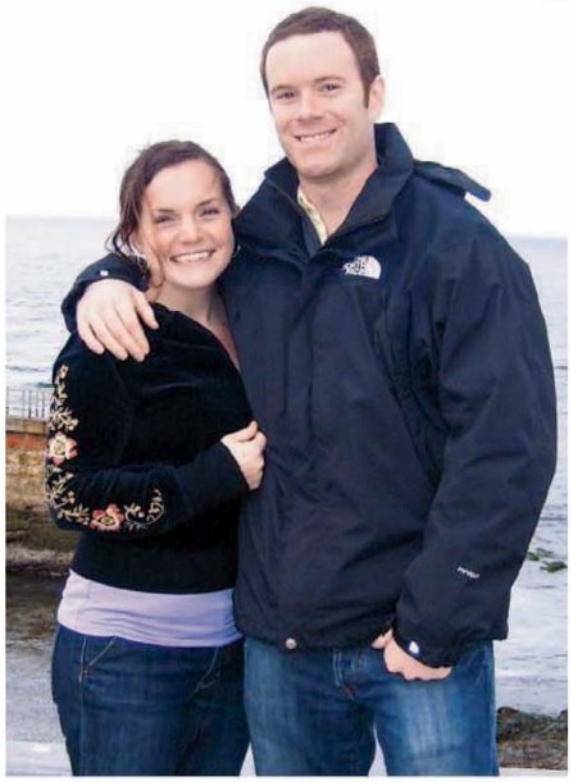

Good match. A new drug aimed at a mutation in his lung tumor made life almost normal for several months for Kevin Brumett (shown last December with fiancée Stephanie Fellingham).

CREDIT: STEPHANIE BRUMETT

The list of mutations that affect lung cancer patients' response to drugs, meanwhile, has continued to grow. Some *EGFR* mutations that crop up after treatment with EGFR-targeted drugs confer resistance to these agents. Patients with mutated *KRAS* don't respond, the same pattern seen in colon cancer. In addition, *ALK-EML4* and rarer mutations in genes such as *BRAF*, *MEK-1*, and *ERBB2*, make some patients' tumors susceptible to other kinds of targeted drugs (see graph, p. 220).

More targets

As the picture of gene-drug interactions fills in, researchers at some cancer centers have decided to make genetic profiling of lung tumors part of routine care. In January, MSKCC began to test all patients with lung adenocarcinomas, the main type of non-small cell lung cancer, for the *EML4-ALK* fusion gene and for 40 mutations in seven other genes. MSKCC is also testing colorectal cancers and will add melanoma and thyroid cancers next year. The data will go into a research database so that even if no drug is available for that patient now, oncologists can find patients with specific mutations for clinical trials months from now. This is the only way to find enough patients to test drugs targeting rare mutations, says molecular pathologist Marc Ladanyi of MSKCC. "Otherwise, it would take years," he says.

MGH began testing nearly all lung adenocarcinoma patients this spring for 113 mutations in 13 genes known to be involved in cancer. It aims to test most cancer types, including gastrointestinal and breast cancers, by the end of next year. Other cancer centers are jumping on board, including Dana-Farber, Duke Comprehensive, Vanderbilt-Ingram, MD Anderson, and Fox-Chase in Philadelphia. In the United Kingdom, Royal Marsden hospital has begun routinely testing some cancer patients to find subjects for early (phase I) clinical trials, says Marsden's Johann de Bono.

Genotyping is a good way to categorize tumors for clinical decisions—more robust than using tumor gene expression data to fingerprint a tumor, Vogelstein says. He and others argue that gene-expression analysis hasn't been as strongly validated. "Because DNA mutations are easy to assess and have a proven track record of response prediction, it makes good sense to start there," agrees Charles Sawyers of MSKCC, who helped develop Gleevec.

Researchers acknowledge that a broad screening effort to genotype tumors won't help most patients just yet. That's because relatively few targeted drugs have been developed, and many of the mutations isolated so far tend to rule out drugs, not rule them in. Take adenocarcinomas: A sizable portion of these tumors—at least 33%—don't have any of the known driver mutations that might be susceptible to attack, according to a literature review by Ladanyi and others. That observation is also emerging from large-scale tumor-sequencing projects such as The Cancer Genome Atlas. Still, it's worth developing new tools if they work against these tumors, Pao says. For a major threat like lung cancer, which kills 16,000 Americans a year, even if a drug helps only 1% or 2% of patients, that's a lot of people.

Gearing up

Cancer centers that hope to expand tumor genotyping still have a lot of kinks to work out. Logistics are the first challenge. "It sounds easy, but it requires top-down" organization, Pao says. Many pathology departments don't have a well-developed molecular diagnostics lab—so cancer centers are building them. Tissue banks are essential; centers that invested earlier in well-organized biobanks are at an advantage.

Because the genetic changes of interest include DNA rearrangements and deletions as well as mutations, these labs can't use just a single technology to detect them. And they must be able to produce results quickly after a sample is taken, within 2 weeks, so that oncologists can use them in time to make treatment decisions. Some cancer centers use standalone clinical assays to test for a few genes; others are buying genotyping systems to detect larger numbers of mutations, then adding tests to find other genetic changes. MGH's assay is "really labor intensive," says Ellisen: Technicians extract DNA from the tumor, amplify it, test for 60 loci, then perform further tests. On the plus side, once the technology is set up, it will be easy to incorporate new mutations being turned up by the cancer genome projects.

It's not yet clear how much a typical tumor test will cost or how much will be covered by insurance. Testing is often done today as part of a research project. MGH puts the actual cost of a typical tumor genetic analysis at about $2000. (That may sound like a lot, but it's no more than a magnetic resonance imaging scan, Ellisen points out.) Ladanyi says MSKCC's assay will likely cost $500 to $1000. Insurers might be willing to cover that if it's done by a certified lab and costs no more than what they now pay—usually under $1000—for standard clinical tests for *KRAS* and *EGFR*, he notes.

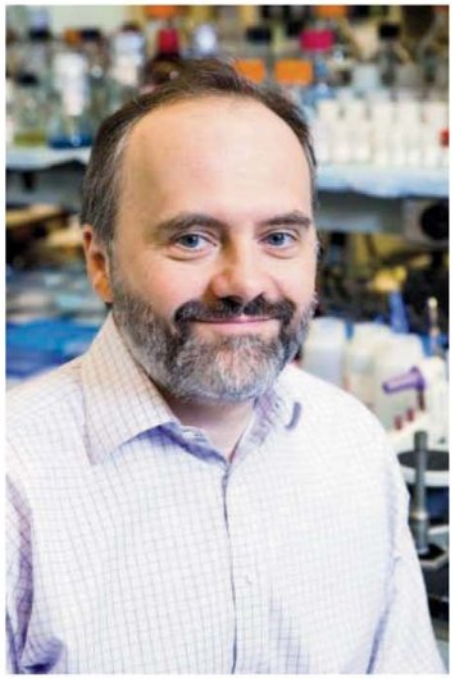

Personal touch. Memorial Sloan-Kettering's Marc Ladanyi and others want to use tumor genetic profiling to match lung cancer patients with the best drug.

Looming over the field is the question of how owners of key intellectual property—such as Genzyme, Harvard, and MSKCC, which hold or have licensed patents for *EGFR* testing for lung cancer—will handle the patent issues. Academic cancer centers could run into legal trouble if they test for these mutations on their own instead of using commercial labs that offer the tests. And the drugs are expensive. A year's supply of Herceptin—the standard treatment—costs about $60,000.

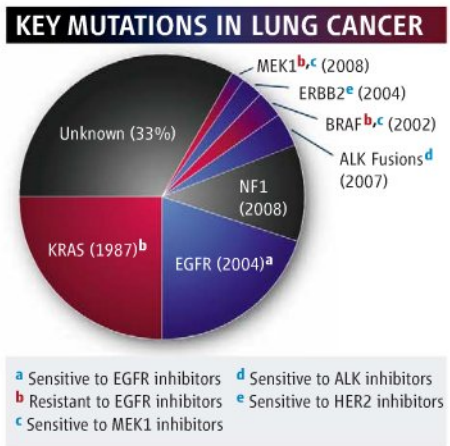

Points of attack. Several mutations found in lung adenocarcinomas, a common type of lung cancer, make them vulnerable to molecularly targeted drugs.

Pao and others organized a "nuts and bolts" meeting of five cancer centers last November to discuss the logistics, technologies, and data-management issues of genotyping lung tumors. One objective is to pool patients for joint trials of drugs and test them in combinations, the most promising strategy for avoiding drug resistance. Finding enough patients to get statistically significant results for a rare cancer subset "will require a type of collaboration never seen before," says Roy Herbst of MD Anderson in Houston, Texas, who heads a prototype for this kind of lung cancer trial. In a boost for such efforts, the National Institutes of Health last month awarded $5 million in Recovery Act money to a consortium of 13 institutions that will test out tumor genotyping techniques on 1000 lung cancer patients.

Even with a system up and running smoothly, another hurdle is getting busy doctors to take an interest in the tests, says Joseph Nevins of Duke University in Durham, North Carolina, who is working on using gene-expression signatures to guide chemotherapy. They will have to go to the trouble of collecting tissue samples and getting patients' written agreement to have their genetic data used for research. "Maybe the samples will sit in somebody's freezer for 5 years and nothing will be done with them."

Indeed, one tough issue raised by tumor genotyping is how to weigh the merits of a procedure that is expensive, likely to become more complex, and rarely provides a cure—but will be intensely sought after by patients and their families. Even when the new gene-targeted drugs work, they may offer just what they gave Kevin Brumett: a few good months. In January, after a period of relatively good health—"We took vacations, we went to weddings," says his widow, Stephanie—Brumett went to the emergency room with a headache and learned that his cancer had metastasized to his brain. Although his doctors didn't seem that surprised, "for us, it came out of the blue," says Stephanie.

She expects to carry on her husband's efforts with advocacy groups to encourage patients to be tested for genetic mutations and volunteer for research. "He felt so strongly about it. It was a miracle drug, and he helped a lot of other patients get on the trial." And with more work, researchers hope to find ways to get around drug resistance. If that happens, knowing the genetic fingerprint of a patient's lung tumor will not only make life with cancer more bearable for a while but also turn this killer into a manageable disease.

–JOCELYN KAISER

CREDITS (TOP TO BOTTOM): ROBERT A. LISAK; (SOURCE): MARC LADANYI AND WILLIAM PAO

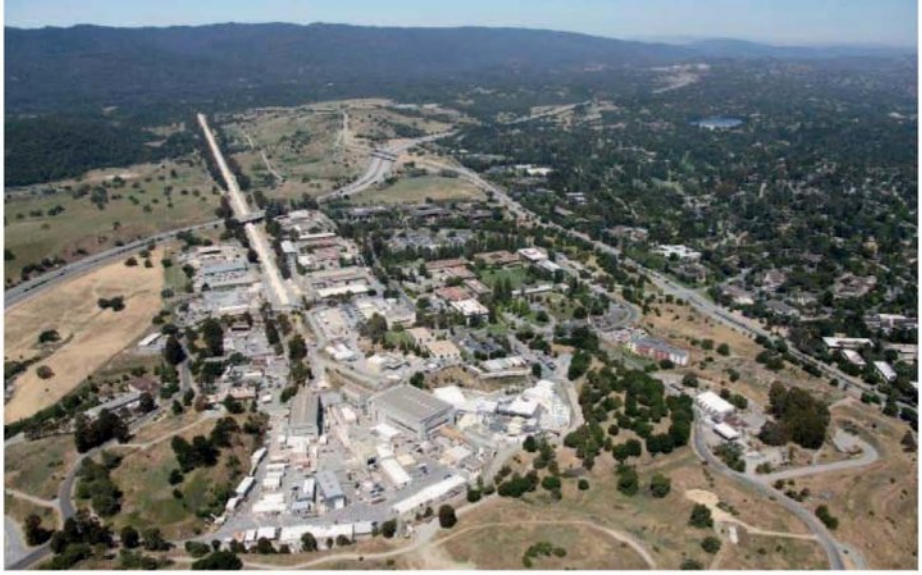

NATIONAL LABS

For a Famous Physics Laboratory, A Quick and Painful Rebirth

Renowned for particle physics experiments, SLAC National Accelerator Laboratory has reinvented itself as a multipurpose lab featuring the world's first x-ray laser

MENLO PARK, CALIFORNIA—When the pipe exploded, it packed the wallop of two sticks of dynamite. The 13 September 2007 mishap could have maimed or killed technicians here at SLAC National Accelerator Laboratory. It certainly jolted Persis Drell, the particle physicist who had become acting director of the famed lab just 4 days earlier.

The blast resulted from the kind of mistake anyone might make: Welders cutting into a steel water pipe ignited fumes from epoxy used to attach a plastic extension the day before. But Drell was already in a tricky position. Renowned as a center for particle physics, SLAC had begun a wrenching shift to a broader mission emphasizing x-ray studies for fields such as materials science and structural biology. The lab was also under fire from its owner, the U.S. Department of Energy (DOE), for management deficiencies and safety lapses, including a nearly fatal electrical accident in 2004. The blast was another boulder in a rockslide falling on the lab. Yet, Drell says, "I joke, the explosion was the best thing that ever happened to us."

The blast proved that things had to change, Drell says. She feared that if the lab had another accident like the one in 2004, DOE might shut it down for good—a fear that Paul Golan, manager of DOE's site office at the lab, calls "not unreasonable." So Drell and Golan began meeting every morning to plan how to head off incidents like the explosion. Although only the acting director, Drell also began rearranging management at the lab, which is operated by Stanford University in neighboring Palo Alto, California. In December 2007 she became director, tasked with guiding SLAC through its scientific and managerial metamorphosis. "It's hard for me to imagine that you could make a transition more quickly," she says. "It's been a bit brutal."

Like a butterfly cracking its chrysalis, SLAC has shed its former self. On 7 April 2008, physicists turned off the lab's last particle smasher. On 10 April 2009, they turned on its new flagship facility, the world's first x-ray laser. Dubbed the Linac Coherent Light Source (LCLS), the laser shines a billion times brighter than any previous x-ray source. First experiments with it began last week, and with the shift in science come equally dramatic changes in the management and culture of the storied lab.

Forward! Director Persis Drell has pushed SLAC through its speedy transformation.

SLAC officials are rearranging everything, including the furniture—particle physicists' offices in the lab's main building are being converted into labs to support the LCLS. Even some of the lab's most eminent particle physicists say the changes are necessary. "Labs like SLAC are institutions for the long term, and they have to evolve," says Burton Richter, a former SLAC director and one of the lab's three Nobel laureates.

But other particle physicists fault Drell for not fighting to keep their last collider, called PEP-II, running or pushing for another project to replace it. They say that whereas past directors fought for the lab's autonomy, Drell has embraced DOE's micromanagement. "It seems to me that we're largely being run out of Washington," says SLAC veteran Martin Breidenbach. "There's little evidence of pushing back."

One sharp corner

DOE's nine other science labs have faced changes in their missions as well, particularly as particle physics facilities have shut down. In 1979, DOE closed down a proton accelerator known as the Zero Gradient Synchrotron at Argonne National Laboratory in Illinois after a higher energy machine turned on 40 kilometers away at Fermi National Accelerator Laboratory (Fermilab) in Batavia. Not long after, Argonne disbanded its 400-member accelerator physics division, recalls Ronald Martin, who was then division director.

The lab went without a major accelerator until 1988, when it won DOE approval for an x-ray source based on a circular accelerator called a synchrotron, in which the particles radiate as they circulate. The $812 million Advanced Photon Source revved up in 1995 and is Argonne's largest facility. "Without that, it would have been a terrible disaster" for the lab, Martin says.

Similarly, in 1983, DOE canceled the half-built ISABELLE proton collider at Brookhaven National Laboratory in Upton, New York, to shift resources to an even bigger atom smasher, the Superconducting Super Collider (which, ironically, was canceled during construction 10 years later).

CREDITS (TOP TO BOTTOM): SLAC; BRADLEY R. PLUMMER/SLAC

"We had 300 or 400 hundred people working on ISABELLE, and we had to let most of them go," recalls Nicholas Samios, a particle physicist who was Brookhaven's director at the time. Brookhaven waited until 1990 to get the go-ahead for a different collider to smash heavy atomic nuclei for studies in nuclear physics, the $616 million Relativistic Heavy Ion Collider, which has been running since 2000.

In contrast, SLAC has not had to languish without a major facility. LCLS construction started in 2006, 2 years before SLAC's last particle collider shut down. However, SLAC is also facing a more dramatic transformation. Both Argonne and Brookhaven were already multipurpose labs at which particle physics accounted for only a fraction of the research. In contrast, since its founding 47 years ago, SLAC has focused almost exclusively on particle physics, making its shift far more drastic. "If you bet all your money on one thing and all of a sudden that one thing doesn't have a future, then you have a problem," Samios says.

Fortunately for SLAC physicists, the key to their future in x-ray physics already lay before them: the 3-kilometer-long linear particle accelerator, or linac, that has been the backbone of the particle physics program since the lab's inception.

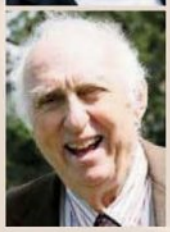

Nobel Prize-winning SLAC-kers

Richard Taylor—cited with two others, discovered that protons contain particles called quarks

Burton Richter—cited with one other, discovered the hypothesized charm quark

Martin Perl—discovered the tau lepton, a massive cousin of the electron.

Stanford University biochemist Roger Kornberg did prize-winning work at SLAC's synchrotron x-ray source. SLAC's BaBar experiment confirmed the prize-winning prediction of Japanese particle theorists Makoto Kobayashi and Toshihide Maskawa.

The light at the end of the tunnel

Lining one side of a broad tunnel and gleaming beneath the overhead lights, the LCLS looks powerful. On their waist-high mounts, 33 magnets called undulators lie connected end to end, each a cylinder 3.4 meters long and 30 centimeters in diameter. A beam of high-energy electrons from the linac enters one end of the chain; a laser beam of x-rays emerges from the other. The LCLS is an x-ray source unlike any before, scientists say. It's also a nifty trick done without mirrors.

A conventional laser consists of two mirrors, one of which lets some light through. Between them sits a material that emits photons, such as a crystal that fluoresces when zapped with electricity. The photons bounce between the mirrors, and as they pass through the material, they stimulate the atoms in it to emit more light. That feedback creates a torrent of photons moving in synchrony that emerges through the imperfect mirror as the laser beam.

Mirrors for x-rays don't exist, however, so the LCLS works in a different way. Each undulator consists of two rows of 224 small magnets, one above and one below the pipe that carries the electrons. Neighboring magnets point in opposite directions, and their fields cause electrons passing down the pipe to wiggle from side to side and radiate x-rays. The x-rays also whiz down the beam pipe, and they push the electrons into tiny bunches. "Now each bunch radiates as if it were a single electron with an enormous electric charge," which greatly amplifies the x-rays, says John Galayda, the SLAC accelerator physicist who directed LCLS construction.

The 90-micrometer-wide electron beam must overlap with the nearly-as-narrow x-ray beam through the entire 130-meter row of undulators, a challenge that led some researchers to question whether the LCLS would ever work. On 10 April, Galayda's team put all doubts to rest, producing the world's first x-ray laser beam after less than 2 hours of trying. "It was a really, really nice experience," Galayda says with a wide smile.

SLAC isn't a newcomer to x-ray science. Since 1973, the lab has run a relatively small synchrotron x-ray source, one of the first. But the LCLS may put the lab on the top of the heap. It could enable researchers to make "movies" of chemical reactions in progress, determine the structure of proteins from a sample of one molecule, or probe matter under conditions found at the center of planets.

The LCLS cranks out x-rays with a wavelength of 0.15 nanometers—short enough to probe the atomic-scale structure of materials—in pulses lasting only 2 millionths of a nanosecond. Such short pulses should allow experimenters to snap the x-ray equivalent of stop-action photos of chemical reactions as they occur, says Joachim Stöhr, an x-ray physicist and associate director for the LCLS at SLAC. "That's one big aspect of the LCLS," he says. "It couples the atomic scale with the ultrafast."

The LCLS has already attracted far more proposals for experiments than it can accommodate and is drawing top researchers. "I came here for the LCLS," says Philip Bucksbaum, an atomic physicist at SLAC and expert in ultrafast lasers who arrived in 2006 from the University of Michigan, Ann Arbor. "It's a chance in about 10 lifetimes."

The outsider from within

The LCLS wasn't always so attractive to scientists. The idea was dreamed up in 1992 by Claudio Pellegrini of the University of California, Los Angeles. He and SLAC's Herman Winick proposed a $100 million demonstration project that would work at slightly longer wavelengths. "All through the 1990s, it was just a curiosity," Winick says. "DOE didn't really want to hear about it because they were busy with the [synchrotron] sources."

Even as plans evolved for shorter wavelengths, x-ray scientists remained wary. "Many of us weren't quite sure what we would do with such a machine," Stöhr says. Various independent reviews convinced DOE that the LCLS was worth pursuing—although it insisted on a larger, potentially expandable facility, raising the cost to $420 million.

Drell's predecessor, Jonathan Dorfan, targeted the LCLS as the lab's next major facility, but some SLAC scientists were reluctant to get involved in the project. From 1999 until 2008, most lab researchers focused on running an electron-positron collider called PEP-II and the accompanying BaBar particle detector, which measured particles called B mesons to probe the asymmetry between matter and antimatter. Some people had to be ordered to work on the new project, says Tor Raubenheimer, director of accelerator research at the lab.

At the same time, DOE wanted SLAC to improve its outmoded management structure and practices. Drell made it her mission to push the hesitant lab down the path ahead of it.

CREDIT: DIANA ROGERS/SLAC

In a flash. SLAC's John Galayda directed construction of the world's first x-ray laser. The machine came on in less than 2 hours and immediately met or exceeded its design goals.

CREDIT: BRADLEY R. PLUMMER/SLAC

SLAC had traditionally promoted from within, choosing managers from among its scientists. Drell hired outside experts in management for positions such as chief operating officer and director of environment, safety, and health. SLAC needed the perspective of newcomers with more professional management experience, she says.

Drell herself hardly fits that description, however. The daughter of Sidney Drell, a prominent particle theorist at SLAC, she had been a professor at Cornell University when she joined SLAC in 2002 as director of research. It was her first foray into management at a national lab. "Granted, she didn't have all the experience, but she had all the right instincts," says William Madia, Stanford's vice president for SLAC, who has been director of two national labs himself.

Drell reorganized the lab to try to break down barriers between the particle physics and x-ray science sides of the lab, for example, by pulling all accelerator work into its own division. She instituted protocols that in 2 years reduced SLAC's accident rate, which had been twice the industrial average, by 67%. (She also formed a committee to rename the lab when DOE and Stanford got into a spat over rights to the old name, Stanford Linear Accelerator Center.)

Drell says she's committed to doing what's best for the scientific community as whole, even if it means taking a hit at home. In December 2007, last-minute cuts to the federal budget forced the lab to lay off 100 of its then-1600 staff. Drell simply made the cuts. In contrast, officials at Fermilab delayed similar layoffs until the U.S. Congress came to the rescue with extra money. The crisis forced DOE to scuttle the PEP-II collider 6 months early, another decision Drell did not fight, to keep Fermilab's larger Tevatron Collider running. "DOE's Office of High Energy Physics had to make some tough decisions, and I supported those decisions," Drell says.

That rankled many physicists, who thought Drell should have already been fighting to push back PEP-II's scheduled shutdown by a couple years. "I thought Persis should say to the DOE, 'Straighten out our particle physics program, or I'm going to resign,'" says Martin Perl, another of SLAC's Nobelists.

Now that SLAC has started to come through its transition, however, some critics have begun to warm to Drell's vision and style. Perl says he now realizes that lab directors no longer have the kind of power they used to and that what Drell did was best for SLAC. "A few months ago I apologized to her," he says. "I was wrong."

Dreams deferred

SLAC has not given up on particle physics, although it has expanded its conception of the field to include astrophysics. For example, SLAC researchers helped build the main instrument for the Fermi Gamma-ray Space Telescope, launched in June, and run the operations center that processes its data. Some SLAC physicists are joining in experiments at Europe's Large Hadron Collider (LHC) near Geneva, Switzerland, which should start smashing protons this winter. Some are still analyzing data from BaBar.

That's a far cry from physicists' ambitions of just a few years ago. Throughout the 1990s, SLAC researchers developed plans for a linear collider 30 kilometers long and based on the same basic technology as its linac. Dorfan says they hoped that, by about 2010, SLAC would lead a global effort to build the machine, which would complement the LHC. In 2004, however, the particle-physics community opted for a different technology being developed primarily in Germany. In 2007, DOE lost enthusiasm for the whole project, when physicists estimated the cost at well over $7 billion.

Some physicists say that SLAC could do more to maintain an accelerator-based particle physics program. The PEP-II collider could be upgraded to boost its collision rate, an option SLAC shelved to push for the linear collider, says lab veteran David Leith. In fact, researchers in Italy would like to rebuild the machine at the University of Rome Tor Vergata. "I'm working very hard to have this as part of the lab's program," Leith says, "but it doesn't seem to fit into the new direction." Without such a project for researchers to work on, SLAC's expertise in electron accelerators—its *raison d'être*—will likely wither, Leith says.

Others say that in the transition to a multipurpose lab, SLAC has lost the cohesive culture that made it such a stimulating place to work. Michael Huffer, who worked on the BaBar particle detector, says SLAC's ethos reflected the values of its founding director, Wolfgang Panofsky: Everyone from the scientists to the custodians should have a say, there should be little hierarchy, and the lab should maintain its independence.

Now the lab is more bureaucratic, and DOE takes a bigger role in its inner workings, Huffer says. DOE site officials now roam the site to talk directly to employees, he says, something he doubts Panofsky or Richter would have tolerated on the grounds that Stanford alone ran the lab. "Management has to worry that the things that made SLAC attractive to people are the things that aren't here anymore," Huffer says. "If you kill that culture, you kill the golden goose."

Still, most scientists are adjusting. Christopher O'Grady also worked on BaBar and says he would have been happy if SLAC's particle physics experiments had continued. But even as it became clear that they wouldn't, O'Grady says, he was becoming intrigued by something else entirely: the basic science needed to address the world's energy problem.

So O'Grady, 45, signed on to work on LCLS experiments, which are likely to be more relevant to the issue. "Just this morning I was in a meeting with the catalyst guys, and it was pretty challenging because I don't know what's going on," he says. O'Grady says he has no regrets, though. "I decided in the eighth grade that I wanted to do high-energy physics, and that's what I did. This is the first time in my life that I've ever wanted to do something else." At SLAC, now is the time to make a change. **–ADRIAN CHO**

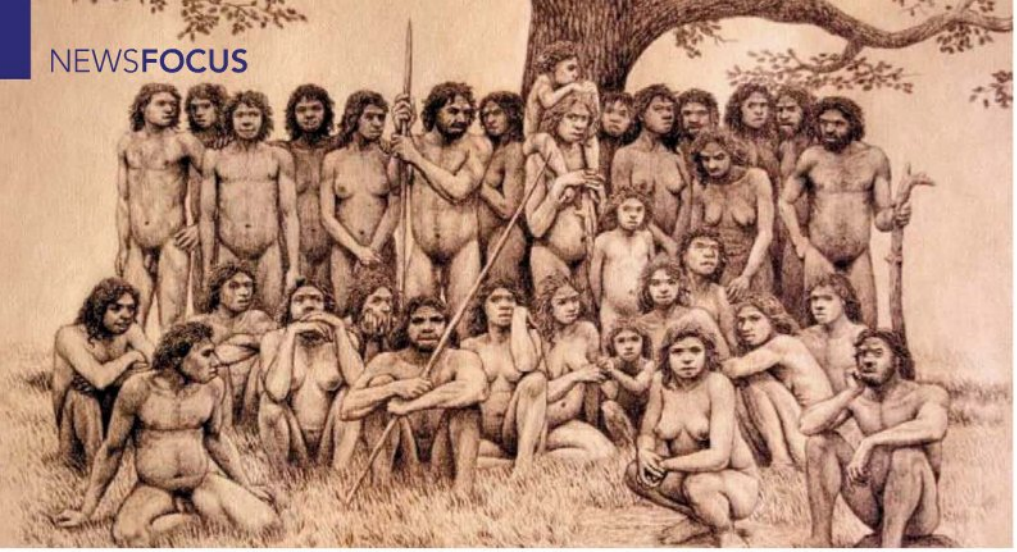

Who were they? Scientists aren't sure how to classify early humans fossilized at Sima de los Huesos.

PALEOANTHROPOLOGY

New Work May Complicate History Of Neandertals and *H. sapiens*

Bones in a Spanish cave and stone tools in Asia spark controversial new ideas about human evolution and migration

GIBRALTAR—In 1848, quarry workers on this peninsula at the southernmost tip of Spain unearthed the first known Neandertal skull. Sixteen years later, two friends of Charles Darwin's brought the skull to him at his sister-in-law's home in London. History does not record Darwin's thoughts as he stared at the massive skull's thick brow ridges and jutting face. Indeed, Darwin made no mention at all of human evolution in his 1859 book *On the Origin of Species*, and he acknowledged the Neandertals only fleetingly in 1871's *The Descent of Man*. Yet the nearly 100 scientists who gathered here last month* to ponder the latest research on Neandertals and other ancient humans were happy to embrace him as their intellectual godfather.

"Charles Darwin was the man who did more than anyone else to crystallize the idea that life had changed over time and that, by implication, humankind had extinct relatives who could be found in the fossil record," Ian Tattersall, a paleoanthropologist at the American Museum of Natural History in New York City, told attendees of the meeting in one of many talks that began by paying homage to the great man. And although Darwin may have understood the big picture, unraveling the many twists and turns that human evolution has taken over millions of years remains very much a work in progress. Among the critical questions under debate at the meeting: What were the evolutionary origins of the Neandertals, and how early did their close cousins, *Homo sapiens*, begin their highly successful colonization of the globe?

What's in a name?

Neandertals, identifiable by their unique skull shapes and stocky bodies, show up in the fossil record of Europe and western Asia at least 130,000 years ago. Recent sequencing of ancient Neandertal DNA suggests that their common ancestor with modern humans lived a bit less than 500,000 years ago, quite likely in Africa (*Science*, 13 February, p. 870). Some researchers call this common ancestor *H. heidelbergensis*, although they disagree about which fossils to group in that species. In his talk at Gibraltar, Tattersall argued that the real evolutionary picture might be much more complicated.

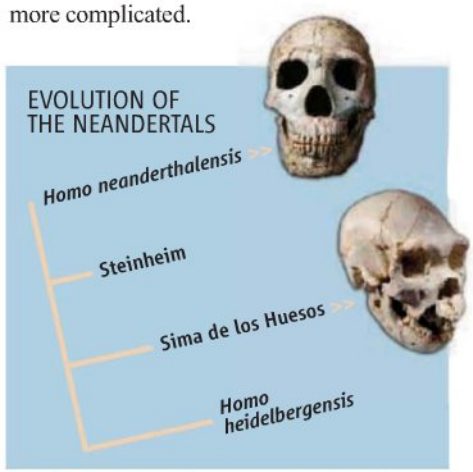

Family branches. Two or more hominin lineages may have lived in Europe at the same time.

Many anthropologists detect "incipient" Neandertal features, including an increased forward projection of the face and the beginnings of a characteristic depression at the back of the skull, in European hominins dated at half a million years ago or less. In 1988, anthropologist Jean-Jacques Hublin, now at the Max Planck Institute for Evolutionary Anthropology in Leipzig, Germany, proposed that those unusual features had accumulated slowly over time. Later, Hublin and colleagues argued that Neandertals had evolved in four stages, beginning with fossils usually assigned to *H. heidelbergensis* (although Hublin prefers to call them *H. rhodesiensis*, after a skull found in Zambia).

Tattersall agreed that some fossils—including the 225,000-year-old Steinheim skull found near Stuttgart, Germany, and a 400,000-year-old skull from Swanscombe, England—might fit Hublin's "accretion model." But others, he said, emphatically do not. The big stumbling block is one of the most spectacular fossil finds in the history of paleoanthropology: the discovery since the mid-1990s of thousands of bones from some 28 hominin individuals at the cave site of Sima de los Huesos in northern Spain (*Science*, 2 March 2001, p. 1722). The published finds include four hominin skulls with both Neandertal-like and non-Neandertal features. And the team working at the site, co-led by anthropologist Juan Luis Arsuaga of the Complutense University of Madrid, has assigned its fossils to *H. heidelbergensis*.

The Sima fossils were first dated to about 350,000 years ago. But more recent uranium-series dating, led by geochronologist James Bischoff of the U.S. Geological Survey in Menlo Park, California, suggests that they are at least 530,000 years old. That would make them as old as or older than "classic" *H. heidelbergensis* fossils from southern France, Greece, and other places—fossils that the Sima skulls don't much resemble, Tattersall insisted. Tattersall concludes that two or more hominin lineages must have existed side by side in Europe for several hundred thousand years before *H. sapiens* arrived from Africa. One line led to the Neandertals and may have included the Sima fossils; another, rightly called *H. heidelbergensis*, went extinct while the Neandertals lived on until at least 30,000 years ago.

Tattersall then looked at Arsuaga, who was sitting in the audience waiting to speak next: "My central plea is to the colleagues who assigned the Sima de los Huesos fossils

*Human Evolution 150 Years After Darwin, Gibraltar, 16–20 September 2009.

CREDITS (TOP TO BOTTOM): MAURICIO ANTON; IRA BLOCK/GETTY IMAGES; D. FINNIN/AMNH

to *H. heidelbergensis*. They are clearly not Neandertals, but not being a Neandertal does not make them *H. heidelbergensis*. They need another name."

A hush fell over the room as Tattersall sat down and Arsuaga got up to speak. To nearly everyone's surprise, Arsuaga agreed that the Sima de los Huesos skulls looked nothing like other *H. heidelbergensis* specimens. Nor, he said, do 13 other skulls his team had recently excavated there. "We have always said that we put the Sima hominins under the *H. heidelbergensis* umbrella for convenience, for practical reasons," Arsuaga said, adding that his team agrees with Tattersall that the accretion scenario is not likely. But he resisted Tattersall's call to rename the Sima fossils, at least until the remaining 13 skulls are published in coming months.

Chris Stringer, a paleoanthropologist at the Natural History Museum in London whose early research led to the recognition of *H. heidelbergensis* as a formal species, says a lot is riding on the new 530,000-year minimum date for the Sima fossils. If the dating is right, Stringer says, "it would be evident that an early form of Neandertal was [in Europe] alongside of *H. heidelbergensis*." But he argues that the dating is at the limit of the uranium-series technique and also contradicts other molecular and fossil evidence suggesting that the Neandertal line split off somewhat after 500,000 years ago. Bischoff defends his methodology, however, saying that the date is a "conservative" estimate and that the Sima hominins could be even older than 530,000 years but not younger.

Hublin, who was not at the meeting, stands by accretion and sees no need to find a new name for the Sima fossils. He told *Science* that all of the hominins under discussion "have Neandertal features to some degree" that become more pronounced over time. The best solution, Hublin says, would be to scrap the species name *H. heidelbergensis* and lump all of these fossils, including those from Sima, together as *H. neanderthalensis*.

But Tattersall insists that names do matter, even if more of them are required to classify the fossil record. "Species have an independent existence in nature," he says. "They are the basic actors in the evolutionary play, and if you don't know who the cast is, you will never understand the plot."

Out of Africa and into Asia

While the Neandertals were sorting out their family relations in Eurasia, our own species, *H. sapiens*, was emerging in Africa, probably from *H. heidelbergensis* or *H. rhodesiensis* ancestors. The first recognizably modern human fossils show up in Ethiopia about 200,000 years ago. Yet many experts have concluded, from genetic and other evidence, that modern humans did not leave Africa and begin to colonize the globe until about 50,000 years ago. The exception is the Levant, where modern humans apparently lived alongside Neandertals between about 130,000 and 75,000 years ago, as part of what some scientists have called a "failed dispersal."

In recent years, however, some researchers have seen evidence for earlier dispersals, especially into southern Asia. In 2007, for example, a team led by archaeologist Michael Petraglia, now at the University of Oxford in the United Kingdom, published evidence that hominins making sophisticated stone tools were established in south India by 74,000 years ago (*Science*, 6 July 2007, p. 114). The team found the tools at several archaeological sites in India's Kurnool District, above and below ash layers from a well-dated eruption of Mount Toba in Indonesia, one of Earth's most cataclysmic volcanic events. Although no human fossils were found, the team concluded that the tools bore striking similarities to Middle Stone Age tools made by modern humans in Africa and suggested that *H. sapiens* might have made the Indian artifacts as well.

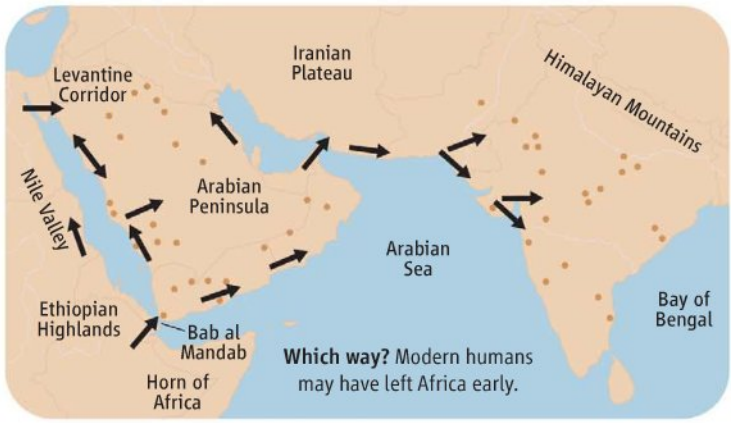

SOURCE: MICHAEL PETRAGLIA

In a talk at Gibraltar, Petraglia argued that new work by his team and others in both India and the Arabian Peninsula strongly supports an earlier modern human dispersal out of Africa. At the site of Shi`bat Dihya 1 in Yemen, a French-led team recently reported finding stone tools dated by optically stimulated luminescence to between 70,000 and 80,000 years ago. Slightly older dates have emerged from work by a German-led team at Jebel Faya 1 in the United Arab Emirates. Meanwhile, at new sites in the Kurnool District and India's Middle Son valley, Petraglia and colleagues have uncovered thousands more stone tools below and above the 74,000-year-old Toba ash layer.

Some of the Indian and Arabian tools resemble those of the African Middle Stone Age; others are typical of so-called Middle Paleolithic tools that Neandertals made in Europe and that both Neandertals and modern humans made in the Levant. Because Neandertals are not known in south Asia, and other "archaic" hominins such as *H. heidelbergensis* and *H. erectus* are assumed to have been extinct by 80,000 years ago, Petraglia argued that modern humans are the most likely toolmakers.

If so, Petraglia said, the "failed dispersal" in the Levant might not have been such a bust after all. Modern humans might have continued on to south Asia and ultimately Australia, where they show up at least 40,000 years ago. Other possibilities include additional dispersals from Africa, possibly via the narrow Bab al Mandab strait between Arabia and the Horn of Africa.

To some researchers at the meeting, such scenarios make perfect sense. "This is the most parsimonious explanation," says paleoanthropologist David Begun of the University of Toronto in Canada. "Who else could it be if not *Homo sapiens*?" And Robin Dennell, an archaeologist at the University of Sheffield in the United Kingdom, notes that there were no climatic or geographical barriers to keep modern humans out of south Asia. "Once they were in the Levant and Arabia, there was nothing stopping them."

But not everyone was ready to jump on the early-dispersal bandwagon. "Mike is giving himself the benefit of the doubt," says John Shea, an archaeologist at Stony Brook University in New York state. "The morphology of the tools doesn't tell you who made them, unless you have some other sort of proof." Archaeologist Curtis Marean of Arizona State University, Tempe, agrees: "I am skeptical of the idea that modern humans made Middle Paleolithic tools any further east than the Levant, because we have not found modern human fossils with [those tools] further east than that." Petraglia has provided a "plausible hypothesis," Marean says. But to prove it, he and others say, Petraglia's team needs to find modern human fossils.

And that, Petraglia told attendees at the meeting, is just what he and his co-workers are now looking for. **–MICHAEL BALTER**

Expand!

Sigma Stemline™ Stem Cell Media

SIGMA Life Science

Quality and performance you can count on every time!

Sigma-Aldrich has developed the Stemline™ Platform that includes media optimized for the expansion and maturation of various adult stem cell types. The optimized formulations and proven consistent results have made Sigma-Aldrich Stemline media a must-have for the challenge of stem cell expansion and maturation in blood and bone's marrow samples.

- Serum-free media or serum-free basal formulation
- Optimized for maximized expansion of hematopoietic, neural, and mesenchymal stem cells
- Tested extensively with consistent quality and performance

Stemline Media for Expansion of:

- Hematopoietic Stem Cell
- Mesenchymal Stem Cell
- T-Cell
- Neural Stem Cell
- Dendritic cell
- Keratinocyte

Visit ***sigma-aldrich.com/stembio*** to view our broad portfolio of reagents, supplements, 3D matrices, antibodies, and cytokines!

Our Innovation, Your Research — Shaping the Future of Life Science

sigma-aldrich.com

SIGMA-ALDRICH®

LETTERS

edited by Jennifer Sills

Life-Long Learning for Physicians

IN THEIR EDITORIAL ("SCIENCE FOR FUTURE PHYSICIANS," 5 JUNE, p. 1241), S. Long and R. Alpern emphasized that graduate medical education must keep pace with advancing technology. Practicing physicians and surgeons responsible for current patient care also need continual education in state-of-the-art biomedical and biotechnology research.

A recent review of the recertification results for the American Board of Surgery demonstrated that examinees who were about 30 years out of training were less successful in their examinations than those closer to their time of training (*1*). The up-to-date scientific knowledge of such a group can be fundamentally improved by mandatory scientific training sessions throughout their professional careers.

The ever-expanding knowledge in medicine and the ever-changing technology in treatments requires practitioners to constantly educate themselves in their specific fields. Current methods to address this include Continuing Medical Education (CME) exercises with Maintenance of Certification (MoC). Along with the modification of the Medical College Admissions Test, substantial resources should be diverted to scientific education and skills training for specialists. This will ultimately result in improved patient care.

KAMRAN AHMED* AND HUTAN ASHRAFIAN

Department of Biosurgery and Surgical Technology, Imperial College London, London W2 1NY, UK.

*To whom correspondence should be addressed. E-mail: k.ahmed@imperial.ac.uk

Reference

1. J. Buyske, *Arch. Surg.* **144**, 101 (2009).

Make Room for Computing

ALTHOUGH P. PEVZNER AND R. SHAMIR, AS WELL as the Bio2010 project, are right about the importance of computational, mathematical, and modeling skills for the next generation of biologists ("Computing has changed biology—biology education must catch up," Education Forum, 31 July, p. 541), they ignore the realities of the modern biology curriculum and student learning. Specifically, it is unlikely that a single course can achieve the goal they desire.

Computational and modeling mastery is not a trivial topic to append to a curriculum. Moreover, there is no surplus of student credit hours to absorb the courses needed. To introduce new topics in a pedagogically realistic manner, departments will have to restructure currently required courses. This will involve redesigning base biology courses to emphasize the relevance and application of modeling and computational skills, particularly given the observation that many biology students are actively mathphobic. Developing true expertise will require student credit hours. Where will they come from? One possibility is to redirect credit hours associated with medical school admission (but largely irrelevant to most biologists). Whatever the source, it is clear that programs need to reconsider where our limited resources are currently being spent. We cannot afford to waste the students' time on irrelevant or ineffectual courses.

MICHAEL W. KLYMKOWSKY

Molecular, Cellular, and Developmental Biology and CU Teach STEM Education Certification Program, University of Colorado, Boulder, CO 80309, USA. E-mail: michael.klymkowsky@colorado.edu

News Story on Italy's MIT Disappoints

WE WERE SURPRISED BY THE TONE AND CONTENT of the News of the Week story by L. Margottini about the new Italian Institute of Technology (IIT) ("Italy's MIT grows, and so does controversy," 19 June, p. 1502).

The remark that international competition was ignored in recruiting IIT scientists is patently false. IIT, at its inception in 2005, set up international competitions for both senior and junior investigators. These positions were advertised widely in scientific journals, including *Science* and *Nature*. As a result of this international search, four of the six appointed IIT research directors come from abroad, and among junior appointments, one-third are Italians returning from abroad, one-third are Italians already residing in Italy, and one-third are foreigners.

Also untrue is Margottini's reported concern that IIT's scientific roster includes big names who do not do the bulk of their work at IIT. Recently appointed senior scientists might continue working at a previous institution for some time while their laboratory space at IIT is refurbished and equipment is ordered. However, after this setup period they do their work onsite.

Margottini's story is largely based on a report written by Mario Rasetti and Elio Raviola, who visited the institute on 6 June 2007, barely 11 months after the first directors were selected, and before any labs were operational. The IIT laboratories started in a 25,000-m^2 facility that was first made avail-

able in January 2006. As such, Rasetti and Raviola's report was documenting a work in progress and was designed to monitor the early stages of the Institute's development. Their report reflects problems typical of the birth of new institutions. Nonetheless, the report was regarded, on balance, as positive, and IIT was indeed given continued support.

The News story does not mention the substantial progress achieved by IIT in the past 2 years. After the review by Rasetti and Raviola, an independent international advisory board made an onsite evaluation of IIT in December 2008 and a general assessment in May 2009; both gave IIT a ringing endorsement. The May 2009 report concludes that "[i]n general, both the accomplishments of the past three years and the future plans seem excellent" (R. Horvitz, Nobel Laureate), and that "[t]he IIT initiative has been remarkably successful…the quality of the new members is very high and would be competitive in all highly developed countries" (P. Greengard, Nobel Laureate) (*1*).

Like all major scientific endeavors, IIT has had some growing pains, but we believe it has a very bright future. The best evidence is something that Margottini overlooks in her article: Scores of excellent young Italian and foreign researchers have returned to Italy or come to Italy for the first time to work at IIT.

ROBERTO CINGOLANI[1]* AND EMILIO BIZZI[2]

[1]Italian Institute of Technology, 16163 Genova, Italy. [2]McGovern Institute for Brain Research, Massachusetts Institute of Technology, Cambridge, MA 02139, USA.

*To whom correspondence should be addressed. E-mail: roberto.cingolani@unile.it

Reference

1. E. Bizzi *et al.*, "Evaluation report of Technical and Scientific Committee of the IIT-Foundation" (9 May 2009).

Response

THE NEWS STORY NOTED BOTH IIT'S SUCcesses, including positive committee reviews, and criticisms from several sources, on ongoing issues such as conflict of interests, lack of industrial partners, and management structure. While Cingolani and Bizzi may consider Raviola and Rasetti's report "positive," Rasetti's comments suggest otherwise, and Cingolani acknowledges that IIT was never given the full report; Italy's Treasury Department has not made it public despite requests. Finally, the more recent "independent" assessments cited in the letter are from IIT's ongoing advisory committee that, according to IIT, "collaborates with the President, the Scientific Director and the Executive Committee" on setting budgets and research agendas. The article does not assert that the IIT is a failure, but concludes rather that the young institute remains controversial within Italy. **LAURA MARGOTTINI**

Conflicting Data About Dyslexia's Cause

J. D. E. GABRIELI ("DYSLEXIA: A NEW SYNERGY between education and cognitive neuroscience," Review, 17 July, p. 280) mentions that dyslexia could be the result of a deficit in the magnocellular part of the visual system. He cites only a few corroborating studies and provides no counterexamples. In doing so, he risks leaving the reader with the impression that the support for a magnocellular deficit in dyslexia is solid.

However, the data are conflicting and do not point unequivocally to a magnocellular

deficit (*1*). For example, an extensive review of data from tests of contrast sensitivity (which is arguably the most direct and best-established psychophysical test of magnocellular activity) found that many studies have detected no evidence for such impairments (*2*). Indeed, the review found that there are more studies with results inconsistent with a magnocellular deficiency than studies whose data are consistent with such deficits. Studies of visually evoked potentials provide another example; one study (*3*) found support for magnocellular deficits, whereas two studies (*4*, *5*) were unable to replicate these findings. Gabrieli seeks to link magnocellular deficits to impaired processing of rapidly changing visual stimuli. One review (*6*) has shown that many tests are poorly suited to assess temporal processing and that the better tests have yielded results that conflict or provide little support for an impairment.

JOHN R. SKOYLES* AND BERNT C. SKOTTUN

Centre for Mathematics and Physics in the Life Sciences and Experimental Biology (CoMPLEX), University College London, London WC1E 6BT, UK.

*To whom correspondence should be addressed. E-mail: j.skoyles@ucl.ac.uk

References

1. G. T. Lueder *et al.*, *Pediatrics* **124**, 837 (2009).
2. B. C. Skottun, *Vision Res.* **40**, 111 (2000).
3. M. S. Livingstone, G. D. Rosen, F. W. Drislane, A. M. Galaburda, *Proc. Natl. Acad. Sci. U.S.A.* **88**, 7943 (1991).
4. J. D. Victor, M. M. Conte, L. Burton, R. D. Nass, *Visual Neurosci.* **10**, 939 (1993).
5. S. Johannes, C. L. Kussmaul, T. F. Munthe, G. R. Mangun, *Neuropsychologia* **34**, 1123 (1996).
6. B. C. Skottun, J. R. Skoyles, *J. Clin. Exp. Neuropsychol.* **30**, 666 (2008).

Letters to the Editor

Letters (~300 words) discuss material published in *Science* in the previous 3 months or issues of general interest. They can be submitted through the Web (www.submit2science.org) or by regular mail (1200 New York Ave., NW, Washington, DC 20005, USA). Letters are not acknowledged upon receipt, nor are authors generally consulted before publication. Whether published in full or in part, letters are subject to editing for clarity and space.

Heretical DNA Sequences?

WHEN "GENOMIC CLUES TO DNA TREASURE sometimes lead nowhere" (D. Monroe, News Focus, 10 July, p. 142), the apparent impasse should indeed stimulate more subtle interpretation. Exceptions to the "conservation equals function" rule for sequence evolution are "heretical" only when mutations are expected to occur at random and to be rejected by selection in functional sequences while accumulating unchecked elsewhere. However, that simplistic view is untenable (*1*). Intragenomic, site-specific mutation rates vary across orders of magnitude. Sequences critical for adaptation may well have higher-than-average mutation rates, leading to rapid divergence even among closely related species.

For example, Riley and Krieger (*2*, *3*) recently described a set of simple sequence repeats (SSRs) that have been retained over deep evolutionary time even though neither the repeating motif nor the number of repeats is conserved. SSRs are mutation-prone stretches, once dismissed as meaningless stutters, that turn up within many functional domains. Earlier this year, *Science* reported experimental confirmation (*4*) of a decades-old prediction (*5*) that SSRs' high mutation rates could promote efficient evolutionary adaptation. The SSRs

discovered by Riley and Krieger are flanked by highly conserved upstream sequences within the untranslated regions of 22 genes, all but one of which have neurodevelopmental roles. These SSRs display recurring patterns of motif replacement across a wide range of vertebrates. Some function is evidently being preserved in the repetitive (and hypermutable) nature of these sites, one which can persist through, or perhaps even exploit, the accumulation of sequence-transforming mutations.

Genome treasure-hunters should expect the unexpected; additional gems surely remain buried within nonconserved sequences.

DAVID G. KING AND YECHEZKEL KASHI*

Departments of Anatomy and Zoology, Southern Illinois University, Carbondale, IL 62901, USA. Department of Biotechnology and Food Engineering, The Technion—Israel Institute of Technology, Haifa 32000, Israel.

*To whom correspondence should be addressed. E-mail: kashi@tx.technion.ac.il

References

1. D. King, Y. Kashi, *Nat. Rev. Genet.* **8**, 10.1038/nrg2158-c1 (2007).
2. D. E. Riley, J. N. Krieger, *Gene* **429**, 74 (2009).
3. D. E. Riley, J. N. Krieger, *Gene* **429**, 80 (2009).
4. M. Vinces *et al.*, *Science* **324**, 1213 (2009).
5. E. N. Trifonov, *Bull. Math. Biol.* **51**, 417 (1989).

CORRECTIONS AND CLARIFICATIONS

Reviews: "Strategic reading, ontologies, and the future of scientific publishing" by A. H. Renear and C. L. Palmer (14 August, p. 828). There was an error in the key of Fig. 1. The label for the blue line should read "Total MEDLINE abstracts × 10^{-2}" instead of "Total MEDLINE abstracts." The figure has been corrected in the HTML version of the article online.

Letters: "Open access: Increased citations not guaranteed" by P. M. Davis (17 July, p. 266). The page number in reference 3 was incorrect. The correct reference is: P. M. Davis *et al.*, *BMJ* **337**, a568 (2008).

TECHNICAL COMMENT ABSTRACTS

COMMENT ON "The *Arabidopsis* Circadian Clock Incorporates a cADPR-Based Feedback Loop"

Xiaodong Xu, Richard Graeff, Qiguang Xie, Karen L. Gamble, Tetsuya Mori, Carl Hirschie Johnson

Dodd *et al.* (Reports, 14 December 2007, p. 1789) reported that the *Arabidopsis* circadian clock incorporates the signaling molecule cyclic adenosine diphosphate ribose (cADPR). In contrast, we found that there is no rhythm of cADPR levels nor are there any significant effects on the rhythm by cADPR overexpression, thus raising questions about the conclusions of Dodd *et al.*

Full text at www.sciencemag.org/cgi/content/full/326/5950/230-b

RESPONSE TO COMMENT ON "The *Arabidopsis* Circadian Clock Incorporates a cADPR-Based Feedback Loop"

Antony N. Dodd, Michael J. Gardner, Carlos T. Hotta, Katharine E. Hubbard, Neil Dalchau, Fiona C. Robertson, John Love, Dale Sanders, Alex A. R. Webb

Xu *et al.* were unable to measure circadian oscillations of cyclic adenosine diphosphate ribose (cADPR). Their experiments showing very low concentrations of cADPR lack appropriate controls, which suggests that technical limitations might explain their negative result. Xu *et al.* also report that chemically induced ADP ribosyl cyclase did not alter clock function, which exactly replicates our findings.

Full text at www.sciencemag.org/cgi/content/full/326/5950/230-c

MATHEMATICS

Two Doors and a Goat

Donald O. Granberg

> You are shown three identical doors. Behind one of them is a car. The other two conceal goats. You are asked to choose, but not open, one of the doors. After doing so, Monty, who knows where the car is, opens one of the two remaining doors. He always opens a door he knows to be incorrect, and randomly chooses which door to open when he has more than one option (which happens on those occasions when your initial choice conceals the car). After opening an incorrect door, Monty gives you the option of either switching to the other unopened door or sticking with your original choice. You then receive whatever is behind the door you choose. What should you do?

The Monty Hall Problem
The Remarkable Story of Math's Most Contentious Brain Teaser

by Jason Rosenhouse

Oxford University Press, Oxford, 2009. 208 pp. $24.95, £13.99. ISBN 9780195367898.

This, according to Jason Rosenhouse in *The Monty Hall Problem*, is the "canonical version" of "classical Monty." Scientists and mathematicians approach such problems with a dual purpose. They seek to find or devise rational solutions, and they observe how people actually behave. Rosenhouse (a mathematician at James Madison University, Virginia) seems more interested in the former but is not unconcerned with the latter. He sees himself as "a chronicler of all things related to the Monty Hall problem."

The author does a masterful job of tracing the problem back to its origin. Of greatest relevance is the "three prisoners" problem first published by Martin Gardner in 1959 (*1*). Three convicts, A, B, and C, are scheduled to be executed. The governor decides that one of them is to be pardoned and tells the warden his identity but asks the warden to keep it a secret. However, A prevails upon the warden to tell A the name of one of the other two who will be executed. The warden tells A that B is to be executed. A is encouraged, thinking that his chance of being pardoned has increased from 1/3 to 1/2. Is he justified in thinking that his chance of being pardoned had actually increased?

Rosenhouse claims that this "is the Monty Hall problem in all but name.... or at least of something formally equivalent to it." This raises the question of what constitutes the essence of the dilemma. I contend that lies in Monty's offering the contestant the opportunity to change a choice in light of new information. It is the second-stage decision to switch or stick that is so excruciating, engaging, and entertaining. If I'm right about this, primary credit for introducing the Monty Hall dilemma to academia goes to Steve Selvin and his two brief letters in *The American Statistician* (*2*, *3*).

One difficulty with word problems is their ambiguity. Rosenhouse does a superb job of reducing, if not eliminating, this source of endless argumentation with his canonical version.

Rosenhouse is adamant that one must "stipulate" that random selection is used by Monty when the contestant's initial guess is correct. But is there any more plausible alternative? Are there other stipulations that are of equal importance, e.g., Monty's honesty? Would it be better to say, "After opening an incorrect door, Monty gives every contestant the option of switching to the other unopened door or sticking with their original choice?"

In any event, most people conclude that both of the contestant's options offer the same probability of success, 0.50. In fact, this "classical Monty" yields probabilities of 1/3 for sticking and 2/3 for switching. Rosenhouse discusses proofs of that answer, various ways of expanding the original problem, and some empirical studies that have used Monty's problem.

He gives considerable coverage to a series of four columns by Marilyn vos Savant that appeared in *Parade* (a Sunday newspaper supplement with a very large circulation) in 1990–1991. The first posed the Monty Hall problem and provided vos Savant's answer: switch, because that offers a 2/3 probability of winning. That column, and its successors, evoked a huge response, generating far more mail than any other column she had written.

Most of the response was critical, even harsh. However, in the four columns she made only two, seemingly minor mistakes: Where she wrote "nine out of 10 readers completely disagree with my reply," "nine out of 10 letter writers" would have been more accurate.

And, in her initial response to her critics, she showed confusion over the concepts of odds and probability, writing, "The winning odds of 1/3 can't go up to 1/2" where (judging from what she wrote elsewhere) she intended to say "odds of 1:2 can't go up to 1:1." For some reason, when Rosenhouse presents this section from her second column he corrects "odds" to "chances" and makes other small changes in the wording without marking them. Elsewhere he repeats part of the same section without altering the original wording. In her 1996 book (*4*), vos Savant corrected the errors herself. And Rosenhouse's discussion of "*L'Affaire* Parade" has an error of its own: Presenting three complaints that vos Savant included in her first follow-up column, he claims the correspondents "were all mathematicians." Two were not. All were Ph.D.s, but that is more than a subtle difference.

Rosenhouse briefly mentions a couple of comparable problems in which the contestant's best choice is to stick with her initial pick. For example, start with three doors hiding two cars and one goat.

To stick or to switch?

The chapter "Bayesian Monty" examines several variations: What if the host does not know the location of the car and randomly chooses a door other than that chosen by the contestant? And if Monty is not reliable? Or if the car is not placed randomly?

Rosenhouse devotes an entire chapter to "progressive Monty." Here there are more than three doors. The contestant and the host take turns, with the contestant picking but not opening a door and the host opening one other door until two doors remain. The contestant then makes a final decision. After discussing a published solution to the four-door case (*5*), Rosenhouse provides an exhaustive

The reviewer is at the Department of Sociology, University of Missouri, Columbia, MO 65211–6100, USA. E-mail: granbergd@missouri.edu

proof that this "switch at the last moment" strategy is optimal.

Subsequent chapters explore some cognitive and philosophical aspects of the Monty Hall problem. An appendix lists the 15 variations of the problem that Rosenhouse discusses. Not all of them make a whole lot of sense.

The nonmathematician deserves to be warned that *The Monty Hall Problem*'s contents are highly mathematical. What would one expect from a math whiz? (My rough count came to 318 equations.) Yet the first 60 pages are quite accessible, as is the material from page 155 on. And I liked Rosenhouse's sense of humor. My favorite is his comparison of people's reactions when learning of the Monty Hall problem to the stages of grief: denial, anger, bargaining, depression, and, finally, acceptance.

The Monty Hall Problem is much more comprehensive and wide-ranging than the many articles on the subject that have dribbled out. Those, of necessity, are more sharply focused. Rosenhouse offers readers much to think about concerning the perplexing question of whether to stick or switch.

References

1. M. Gardner, *Sci. Am.* **201**, 174 (1959).
2. S. Selvin, *Am. Stat.* **29**, 67 (1975).
3. S. Selvin, *Am. Stat.* **29**, 134 (1975).
4. M. vos Savant, *The Power of Logical Thinking* (St. Martin's, New York, 1996).
5. V. V. Bapeswara Rao, M. B. Rao, *Math. Sci.* **17**, 89 (1992).

10.1126/science.1177947

ANTHROPOLOGY

Sex, War (and Ecology)

Hillard Kaplan

Sex and War offers a compelling discussion of the biological roots of human warfare. Building on arguments developed in Richard Wrangham's book *Demonic Males* (*1*), Malcolm Potts (a population biologist at the University of California, Berkeley, School of Public Health) and coauthor Thomas Hayden (a science writer) explore the phylogenetic origins of human warfare. They argue that group aggression by males is a fundamental feature of human evolutionary history, whose roots are well developed in our closest living relative, the chimpanzee.

The reviewer is at the Department of Anthropology, University of New Mexico, Albuquerque, NM 87131, USA. E-mail: hkaplan@unm.edu

The book begins with Potts's own experiences in 1972, attending to (and providing abortions for) women who had been raped and abused during the war in Bangladesh. He recounts the cruelty enacted by groups of men, united in an armed struggle for power, on thousands of women. He then presents the book's main thesis: such acts of violence are far from isolated incidents and modern aberrations due to extreme conditions—rather they are the norm for our species. What Potts calls "behavioral propensities to engage in male coalitional violence" are products of a long evolutionary history, in which males who engaged in such behavior produced more genetic descendants than males without such propensities. He further argues that coalitional violence by groups of males evolved at least as far back as the common ancestor before the chimpanzee-human divergence and is a direct manifestation of sexual selection on male-male competition. Such behavioral propensities did not evolve in females of either species.

The term "behavioral propensity" is used throughout the book to highlight the idea that a propensity can be controlled by cultural and social means. Propensities to form coalitions among males against other males are in some sense genetically programmed into chimpanzee and human psychology, but there are also norms for culturally appropriate behavior as well as social institutions that can serve to counteract those propensities. In fact, the solution to decreasing violence and warfare in modern times comes from the recognition that our biological heritage has produced very different behavioral propensities in human males and females.

Sex and War
How Biology Explains Warfare and Terrorism and Offers a Path to a Safer World

by Malcolm Potts and Thomas Hayden

BenBella, Dallas, 2008. 463 pp. $24.95, C$29. ISBN 9781933771571.

By empowering women to be leaders in cultural, social, and political spheres, the violent propensities of men can be restrained, and perhaps men can learn to be less violent themselves. According to Potts and his wife Martha Campbell (a health policy specialist who coauthored the prescriptive section of the book), empowering women will also have indirect and long-term effects on reducing violence. Empowerment of women also implies that they have control over their reproduction, and as a consequence they will elect to have smaller families than their husbands or mates would want them to have. This population reduction, in turn, will have impacts on the environment, population pressure, and other factors that promote violence and conflict.

Throughout *Sex and War*, a good deal of scholarship is in evidence. The authors provide a detailed treatment of intergroup violence among chimpanzee males and the way it serves to secure good territories for females to reside in, and hence secures sexual access to more females with better chances for reproductive success. They also consider bonobos (formerly referred to as pygmy chimpanzees), the sister species to the chimpanzee, whose male members do not appear to engage in coalitional violence regularly. Confronting such evidence, Potts argues that bonobos branched off from the chimpanzee lineage and that violent behavior by males was subsequently lost in this species, after the chimpanzee-human split. The authors also cite abundant archaeological evidence supporting their view that large-scale violence by males has a long history and prehistory in our species.

This review benefits from an "Author Meets Critic" session dedicated to the discussion of the *Sex and War* at the April 2009 Population Association of America meetings (*2*). Session chair Kenneth Wachter, a mathematical demographer, praised the prescriptive section of the book for "laying the groundwork for a renewed alliance between feminism and population action," based on a principled understanding of the common biological roots that link male coercive control over women's reproduction and violent conflict. His comments drew on the population policies that grew out of the World Population Conference in Cairo, which placed the major focus on women's empowerment as the means to effective population control. He argued that those policies were based more on alliance of convenience than on principle and, as a result, diverted attention away from population growth.

Joseph Rodgers, a behavioral geneticist, raised the issue of intrapopulation genetic variance, which is not addressed in the book. Behavioral genetics research on violence tends to yield fairly high heritabilities (about 50%), which suggests that a substantial amount of genetic variance exists in such behavioral propensities within populations of human males. Rodgers pointed out that if the tendency to form violent coalitions had been under constant positive selection in human history, we should find that the genetic variance would have been selected out of the population and heritabilities should approach zero. An adequate theory will have to account for the maintenance of such variability.

Population scientist John Haaga critiqued the book in terms of the nature-nurture dualism inherent in its argument. He pointed out that mainstream thinking among biologists has moved away from such dualism to a more nuanced understanding of gene-environment interactions—from epigenetic programming of gene activity to adaptive contingent behavioral responses to environmental variation.

My own comments build on each of these themes. There are four extant great ape species. Each has a different social system, with chimpanzees being the only species to regularly evidence multimale violent coalitions. There are important ecological differences among the species in diet and female behavior that affect the value of multimale territorial coalitions. For example, female gorillas, presumably because they eat more leaves than do other great apes, tend to group together. This social pattern allows one male to become dominant and exclude all other adult males from the group. Sexual selection on gorilla males may have favored violence, but it has not led to male coalitions. Similarly, there are no human groups that have been documented to have a mating system similar to that of chimpanzees. In chimpanzees, each female, when she is in estrous, generally mates with every male in her group. Males join forces to defend their territory, which subsumes the range of multiple females, and each male will have access to all those females—albeit dominant males tend to monopolize matings on the peak fertility days during estrous. Marriage is a universal human behavior, and it is defined by cultural and legal rules proscribing sex outside of marriage, particularly by women.

The Sabine Women. Jacques-Louis David (1796–1799).

As Potts discusses in detail, all available evidence suggests that intergroup violence, practiced primarily by males, does have a long evolutionary history in our species. However, the intensity and nature of that violence is highly variable. I argue that this variability is patterned, just as the differences between ape species can be explained by variation in the social and ecological conditions in which they live. The most fundamental traits characterizing our species (large brains, verbal language, marriage and kinship reckoning, and intense cooperation and exchange) all apparently evolved during our hunting and gathering past, which characterized the bulk of our evolutionary history.

The hunting and gathering adaptation, especially in its mobile form, does not appear to promote large-scale warfare, not only because groups are small, but because incentives are largely absent. Monogamy is the most common marital form (probably because women depend on men's meat contribution and it is difficult to support two wives), so there is less incentive for bride-capture warfare. There can be territorial conflicts, but nothing in comparison to the conflicts that occur over precious lands when agricultural becomes the dominant way of life.

The scope for warfare has changed considerably as human economic systems have changed. Once people settle and the value of land varies from place to place, large-scale warfare becomes a persistent feature of human behavior, almost exclusively practiced among men. The riches to be had from control over productive river valleys (such as the Tigris, Euphrates, and Nile) not only led to large-scale warfare but also to extreme differences in power and status, harems, and rape of women during and after war. Interestingly, these characteristics of early "civilizations" were independently "invented" with very similar results across the continents of the world from China to the Americas. [For a more comprehensive treatment of these issues, see (*3*).]

I would modify the authors' prescription for lowering violence and warfare in modern societies. Rather than simple cultural control over our predispositions toward male coalitional violence, an understanding of the conditions that promote violence and conflict and changing the incentives may be more effective. With respect to the specific emphasis on shifting policy toward the empowerment of women and increasing their role in the political arena, it is important to keep in mind one of Potts's fundamental points. That is that it is mostly men who engage in violent coalitions—so we must understand their incentives. Men with poor economic prospects have been the soldiers and have commonly engaged in other violent and risky endeavors for much of human history (*4*). The growing number of unemployed men in the developing world and in some urban areas in developed nations promotes gang violence, recruitment into violent extremism, and single-parent families. My concern is that in the context of changing world economic systems, men with low levels of completed education are particularly disadvantaged in the modern labor markets, especially in the developing world. I hypothesize that if they were educated and could find good jobs, most of those men would become fathers and family men with little time for violence. Public investments should not ignore men.

Sex and War integrates information from multiple disciplines into a captivating read. It challenges us to ask deep questions about why the pattern of coalitional violence is so widespread in our species and why it is almost exclusively men who are involved. The fact the chimpanzees engage in warlike behavior involving male coalitions is also striking. We still lack a definitive understanding of group-level violence and its variation in different societies and during different historical periods. But I agree with Potts that such an understanding will likely require a joint theory of our biology and social history.

References

1. R. W. Wrangham, D. Peterson, *Demonic Males: Apes and the Origins of Human Violence* (Houghton Mifflin, Boston, 1996).
2. http://paa2009.princeton.edu/sessionViewer.aspx?sessionId=805
3. H. Kaplan, P. Hooper, M. Gurven, *Philos. Trans. R. Soc. London Ser. B* **364**, 3289 (2009).
4. J. Boone, *Am. Anthropol.* **88**, 859 (1986).

10.1126/science.1176071

MEGASCIENCE

'Omics Data Sharing

Dawn Field,[1]*†‡ Susanna-Assunta Sansone,[1,2]† Amanda Collis,[3]† Tim Booth,[1] Peter Dukes,[4] Susan K. Gregurick,[5] Karen Kennedy,[6] Patrik Kolar,[7] Eugene Kolker,[8] Mary Maxon,[9] Siân Millard,[10] Alexis-Michel Mugabushaka,[11] Nicola Perrin,[12] Jacques E. Remacle,[7] Karin Remington,[13] Philippe Rocca-Serra,[12] Chris F. Taylor,[12] Mark Thorley,[14] Bela Tiwari,[1] John Wilbanks[15]

Development of high-throughput genomic and postgenomic technologies has caused a change in approaches to data handling and processing (*1*). One biological sample might be used to generate many kinds of "big" data in parallel, such as genome sequence (genomics), patterns of gene and protein expression (transcriptomics and proteomics), and metabolite concentrations and fluxes (metabolomics). Extensive computer manipulations are required for even basic analyses of such data; the challenges mount further when two or more studies' outputs must be compared or integrated.

Grassroots movements (*2*–*5*), efforts including the Science Commons, which is initiating an open-access data protocol (*6*), as well as top-down (funder-led) efforts (see table, page 235), have led to a range of policies for data management and sharing. A recent European Science Foundation consultation exercise confirmed a lack of explicit, well-documented data-sharing policies for most funding agencies in European countries (*7*). If we are to avoid squandering the immediate and extended value of big data, a focused strategy will be pivotal.

Early policies were driven by the need to manage long-term data sets (those accrued over 30 or more years), such as those in the social and environmental sciences. More recently, policies have emerged in response to increased funding for high-throughput approaches in major 'omics fields. The European Commission has invited the member states to develop policies to implement access, dissemination, and preservation for scientific knowledge and data (*8*).

Beyond public and private funding agencies, regulatory agencies such as the U.S. Food and Drug Administration (FDA) (*9*), European Medicines Agency (EMEA) (*10*), and U.S. Environmental Protection Agency (EPA) (*11*) are also working to define guidelines to facilitate electronic submission of traditional and 'omics data types. These, as well as industry guidelines, are beyond the scope of this document, but much could be learned from an exchange of ideas and practices (*12*).

The policies listed here share common principles. They aim to protect cumulative data outputs. All recognize data as a public good and data sharing as a way to accelerate subsequent exploitation. On a practical level, all acknowledge the right of first use for data providers and the right to appropriate accreditation. Likewise, these policies have been generated through the same basic process (table S1) (*13*).

Despite these commonalities, there is still room for heterogeneity, as expected, given the different types of communities served by each funder and the data types they generate. Care must be taken, though, that these differences do not impede seamless interoperability. The path a funding agency takes in supporting its data policy largely reflects the relative emphasis placed on managing versus sharing data. A focus on managing is often accompanied by an institutional infrastructure. Such centralization provides economy of scale, institutional memory, and reusable capability, but it also incurs a substantial direct cost that may compete with research funding (*14*). The UK Natural Environment Research Council (NERC) sustains a system of national data centers and has invested in the NERC Environmental Bioinformatics Centre (NEBC) to cover 'omics data (*15*, *16*). Similarly, the UK Economic and Social Research Council provides a central data service for social scientists (*17*). Policies that focus on sharing tend to place more responsibility on researchers. For example, the UK Biotechnology and Biological Sciences Research Council (BBSRC) is supporting its data-sharing policy through funds that allow researchers to develop their own solutions from the bottom up.

Massive-scale raw data must be highly structured to be useful to downstream users. Standardized solutions are increasingly available for describing, formatting, submitting, and exchanging data (*18*, *19*). These reporting standards include minimum information checklists, ontologies, and file formats. Minimum information checklists are simple, structured documents that reflect the consensus view of a community on the information to report about particular kinds of biological studies or instrument-based assays. Ontologies provide terms needed to describe the minimal information requirements. File formats define a shared syntax to transmit and exchange standardized information.

There are now an escalating number of community-developed checklists, ontologies, and file-format projects, a positive sign of community engagement. But this proliferation brings with it new sociological and technological challenges—creating interoperability and avoiding unnecessary overlaps and duplication of efforts. These projects largely focus on a particular technology or a specific biological knowledge domain (e.g., ontologies for anatomy, gene functions, or the environment) and are by nature fragmented and not designed to be interoperable. A range of activities are fostering harmonization and consolidation of these standards for checklists (*5*), ontologies (*4*), and representation of information in electronic formats (*2*, *3*).

Many large coordinative initiatives (*20*–*23*) are working to address the problem of archiving and integrating data. The ELIXIR project (*22*) aims to construct and operate a common, sustainable bioinformatics research infrastructure to support the life sciences across Europe. The Infrastructure for Spatial Information in the European Community (INSPIRE) directive requires that Europe binds together its geospatial data into portals (*23*). Widely useful are initiatives like the Digital Curation Centre (DCC), which tracks data standards, documents best practice, and has published a data life-cycle model to underpin long-term data-preservation policies (*24*).

Achieving Adherence

Community adherence would be automatic if guidelines aligned with prevailing scientific culture and (emergent) practice. However, there is often a gulf or even outright resistance (*25*, *26*).

Policies that stipulate public data release, especially of prepublication data, raise researchers' concerns about loss of intellectual ownership—for example, by compromising

Data sharing, and the good annotation practices it depends on, must become part of the fabric of daily research for researchers and funders.

[1]U.K. Natural Environment Research Council (NERC), Environmental Bioinformatics Centre. [2]European Molecular Biology Laboratory (EMBL) Outstation, The European Bioinformatics Institute (EBI). [3]U.K. Biotechnology and Biological Sciences Research Council. [4]U.K. Medical Research Council. [5]U.S. Department of Energy. [6]Genome Canada and Wellcome Trust Sanger Institute. [7]Unit for Genomics and Systems Biology, European Commission. [8]Seattle Childrens Hospital. [9]Marine Microbiology Initiative, Gordon and Betty Moore Foundation. [10]U.K. Economic and Social Research Council. [11]European Science Foundation. [12]The Wellcome Trust. [13]U.S. National Institute of General Medical Science, NIH. [14]NERC. [15]Science Commons.

*Full author affiliations are available on *Science* Online. †These authors contributed equally to this article. ‡Author for correspondence. E-mail: dfield@ceh.ac.uk

Funding body	Country	Year	Policy information
Economic and Social Research Council (ESRC)	UK	(1994) 2000	www.esrcsocietytoday.ac.uk/ESRCInfoCentre/Images/DataPolicy2000_tcm6-12051.pdf
Natural Environment Research Council (NERC)	UK	(1996) 2008	www.nerc.ac.uk/research/sites/data/policy.asp
National Science Foundation (NSF)	US	2001	www.nsf.gov/pubs/2001/gc101/gc101rev1.pdf
National Institute of Health (NIH)	US	2003	http://grants.nih.gov/grants/policy/data_sharing/
Gordon and Betty Moore Foundation (GBMF)	US	(2005) 2008	www.moore.org/docs/GBMF_Data%20Sharing%20Philosophy%20and%20Plan.pdf
Genome Canada	Canada	(2005) 2008	www.genomecanada.ca/medias/PDF/EN/DataReleaseandResourceSharingPolicy.pdf
Medical Research Council Data Sharing and Preservation Policy (MRC)	UK	2006	www.mrc.ac.uk/Ourresearch/Ethicsresearchguidance/Datasharinginitiative/Policy/index.htm
Biotechnology and Biological Sciences Research Council (BBSRC)	UK	2007	www.bbsrc.ac.uk/publications/policy/data_sharing_policy.html
Wellcome Trust	UK	2007	www.wellcome.ac.uk/About-us/Policy/Policy-and-position-statements/WTX035043.htm
Department of Energy (DOE)	US	2008	http://genomicsgtl.energy.gov/datasharing
European Commission	Europe	NA	Issued Communication calling for uniform policies across Member Nations http://ec.europa.eu/research/science-society/document_library/pdf_06/communication-022007_en.pdf
European Science Foundation	Europe	NA	Researchers are expected to follow the policies of the national agencies that directly provide research funding.

Examples of data policies from major funding agencies in the United States and United Kingdom. Funders are listed by the first year in which they made their policy public (in parentheses if a newer version of the policy exists). The NSF document is the Grant General Award document, rather than a formal policy. The DOE example is a program-level policy, as an agency-level policy does not yet exist. NA, not applicable.

chances to publish, to commercialize aspects of funded work, or to collaborate with industry. Public release of 'omics data has also been complicated by the increasing use of human subjects (*27*) in medical-related studies and the resulting ethical issues. Funding agencies must allay fears that data could be reused without permission or due recognition by clarifying the agency's expectations. There is currently no large-scale infrastructure ready to support data citations, but interest in this issue is growing (*28*).

Researchers may be limited in their ability to comply by inadequate resourcing; time-inefficient data management at the local or community level; or a lack of tools, databases or informatics expertise. Researchers must now incorporate the cost of this type of essential work into research grants effectively and consistently, and an expert pool of scientists with the requisite skills must be developed, as well as a community of biocurators (*29*, *30*). Mechanisms for crediting data generators when their data sets are published or reused would help justify making the data public in the mind of the researcher, especially if funding decisions took into account prior good practice.

Collecting, holding, and disseminating electronic data are substantial undertakings, if considered at the global level. If policies are to be successful, information superhighway infrastructure must be built. This must involve the creation and adoption of appropriate standards that enable electronic data to be shuttled around, tools for doing the actual task, and world-class database infrastructure to hold the collective submissions. Journals, for example, will only require compliance with reporting standards when appropriate standards-compliant software tools and public repositories become available (*31*). An exemplar project already exists, the Investigation/Study/Assay (ISA) Infrastructure, which is developing standards to enable freely available tools that encompass several 'omics technologies and facilitate curation and reporting at the community level (*3*, *32*). Lack of funding for these activities has already been highlighted (*33*, *34*), and new ways of balancing streams of funding for the generation of novel data versus the protection of existing data must be found.

The Future

We recommend that a single, brief, high-level consensus guideline serve as a template for policy documents at the funder, community, and project levels. At its heart should be the public and timely release of data. It should be based on the principle that funders and the research community must work together to develop best practice. On enforcement of policy, we suggest that, in addition to mandating the inclusion of data-sharing plans in grant applications, deposition of supporting (or ideally, all) data in appropriate databases be the rule within a specified time period in accordance with international standards. This would uphold and extend the model of "accession number for publication" that has worked well for DNA sequence data (*27*). "Appropriate" databases, by definition, should be secure, should be publicly accessible, and ought to have a long-term funding horizon. This allows reviewers to focus on the science, while creating a simple way to check compliance via a URL. When funders do not have a suitable database or repository to endorse, they should attempt to find or fund one (*14*).

We created the BioSharing Web site to centralize and to give a higher profile to bioscience data policies and standards (*35*). It offers a focal point for stakeholders in data policy (i) by providing a "one-stop shop" for those seeking data policy documents and information (including information about the standards and technologies that support them) and (ii) by encouraging exchange of ideas and policy components among funders, and between funders and potential fundees. For example, a recent post covers the "Toronto" (*36*) and "Rome" data-sharing meetings (*37*) that aimed to build upon the highly influential Bermuda Principles (*38*) and the Fort Lauderdale report (*39*). Ideally, this hub could spark the formation of a BioSharing Consortium that would work at the global level to build essential linkages between funders and awardees and among the main research groups.

References and Notes

1. Big Data special issue. *Nature* **455**, 1 (2008).

2. A. R. Jones *et al.*, *Nat. Biotechnol.* **25**, 1127 (2007).
3. S. A. Sansone *et al.*, *OMICS* **12**, 143 (2008).
4. B. Smith *et al.*, *Nat. Biotechnol.* **25**, 1251 (2007).
5. C. F. Taylor *et al.*, *Nat. Biotechnol.* **26**, 889 (2008).
6. "Protocol for implementing open access data," http://sciencecommons.org/projects/publishing/open-access-data-protocol.
7. European Science Foundation (ESF), *Shared Responsibilities in Sharing Research Data: Policies and Partnerships*, Report of an ESF–Deutsch Forschungsgemeinschaft workshop, Padua, Italy, 21 September 2007 (ESF, Strasbourg, France, 2008).
8. European Commission (EC), "On scientific information in the digital age: Access, dissemination and preservation"; http://ec.europa.eu/research/science-society/document_library/pdf_06/communication-022007_en.pdf
9. FDA, "Genomic data submission"; www.fda.gov/Drugs/ScienceResearch/ResearchAreas/Pharmacogenetics/ucm083641.htm.
10. EMEA, *Guideline on Pharmacogenetics Briefing Meetings*; www.emea.europa.eu/pdfs/human/pharmacogenetics/2022704en.pdf.
11. EPA, *Potential Implications of Genomics for Regulatory and Risk Assessment Applications at EPA*; www.epa.gov/osa/genomics.htm.
12. "Pistoia vision," www.pistoiaalliance.org/.
13. Organisation for Economic Co-operation and Development, *OECD Principles and Guidelines for Access to Research Data from Public Funding* (OECD, Paris, 2007); www.oecd.org/dataoecd/9/61/38500813.pdf.
14. B. Tiwari, D. Field, J. Snape, *Nature* **439**, 912 (2006).
15. D. Field, B. Tiwari, J. Snape, *PLoS Biol.* **3**, e297 (2005).
16. D. Field *et al.*, *Nat. Biotechnol.* **24**, 801 (2006).
17. Economic and Social Data Service, www.esds.ac.uk/.
18. D. Field, S. A. Sansone, *OMICS* **10**, 84 (2006).
19. Standardizing data. *Nat. Cell Biol.* **10**, 1123 (2008).
20. Cancer Biomedical Informatics Grid, (caBIG), National Cancer Institute, NIH; http://cabig.cancer.gov.
21. Biomedical Informatics Research Network, www.nbirn.net/.
22. ELIXIR, http://www.elixir-europe.org.
23. EC, "INSPIRE Directive," http://inspire.jrc.ec.europa.eu/index.cfm.
24. DCC, www.dcc.ac.uk/.
25. C. Thomas, *Science* **324**, 1632 (2009).
26. S. Wiley, *Scientist* **23**, 33 (2009).
27. E. Pennisi, *Science* **324**, 1000 (2009).
28. Earth System Science Data, www.earth-system-science-data.net/.
29. D. Howe *et al.*, *Nature* **455**, 47 (2008).
30. International Society for Biocuration, www.biocurator.org.
31. H. Barsnes *et al.*, *Nat. Biotechnol.* **27**, 598 (2009).
32. Investigation/Study/Assay (ISA) Infrastructure for Managing Experimental Metadata, http://isatab.sf.net.
33. C. Brooksbank, J. Quackenbush, *OMICS* **10**, 94 (2006).
34. Z. Merali, J. Giles, *Nature* **435**, 1010 (2005).
35. Biosharing, http://biosharing.org/.
36. Toronto International Data Release Workshop Authors, *Nature* **461**, 168 (2009).
37. P. N. Schofield *et al.*, *Nature* **461**, 171 (2009).
38. "Summary of principles agreed at the First International Strategy Meeting on Human Genome Sequencing, Bermuda, 25 to 28 February 1996 (Human Genome Organisation, Singapore, 1996); available at www.ornl.gov/sci/techresources/Human_Genome/research/bermuda.shtml.
39. Sharing Data from Large-Scale Biological Research Projects, *A System of Tripartite Responsibility*, Fort Lauderdale, FL, 14 and 15 January 2003 (Wellcome Trust, 2003); available at www.wellcome.ac.uk/stellent/groups/corporatesite/@policy_communications/documents/web_document/wtd003207.pdf.

Supporting Online Material

www.sciencemag.org/cgi/content/full/326/5950/234/DC1

10.1126/science.1180598

GENOMICS

Genome Project Standards in a New Era of Sequencing

More detailed sequence standards that keep up with revolutionary sequencing technologies will aid the research community in evaluating data.

P. S. G. Chain,[1,2,3]*†§ D. V. Grafham,[4]†§ R. S. Fulton, [5]† M. G. FitzGerald,[6]† J. Hostetler,[7]† D. Muzny,[8]† J. Ali,[9] B. Birren,[6] D. C. Bruce,[1,10] C. Buhay,[8] J. R. Cole,[3] Y. Ding,[8] S. Dugan,[8] D. Field,[11] G. M. Garrity,[3] R. Gibbs,[8] T. Graves,[5] C. S. Han,[1,10] S. H. Harrison,[3]* S. Highlander,[8] P. Hugenholtz, [1] H. M. Khouri,[12] C. D. Kodira,[6]* E. Kolker,[13,14] N. C. Kyrpides,[1] D. Lang,[12] A. Lapidus,[1] S. A. Malfatti,[12] V. Markowitz,[15] T. Metha,[6] K. E. Nelson,[7] J. Parkhill,[4] S. Pitluck,[1] X. Qin,[8] T. D. Read,[16] J. Schmutz,[17] S. Sozhamannan,[18] P. Sterk,[11] R. L. Strausberg,[7] G. Sutton,[7] N. R. Thomson,[4] J. M. Tiedje,[3] G. Weinstock,[5] A. Wollam,[5] Genomic Standards Consortium Human Microbiome Project Jumpstart Consortium,‡ J. C. Detter[10]†‡

For over a decade, genome sequences have adhered to only two standards that are relied on for purposes of sequence analysis by interested third parties (*1*, *2*). However, ongoing developments in revolutionary sequencing technologies have resulted in a redefinition of traditional whole-genome sequencing that requires reevaluation of such standards. With commercially available 454 pyrosequencing (followed by Illumina, SOLiD, and now Helicos), there has been an explosion of genomes sequenced under the moniker "draft"; however, these can be very poor quality genomes (due to inherent errors in the sequencing technologies, and the inability of assembly programs to fully address these errors). Further, one can only infer that such draft genomes may be of poor quality by navigating through the databases to find the number and type of reads deposited in sequence trace repositories (and not all genomes have this available), or to identify the number of contigs or genome fragments deposited to the database. The difficulty in assessing the quality of such deposited genomes has created some havoc for genome analysis pipelines and has contributed to many wasted hours. Exponential leaps in raw sequencing capability and greatly reduced prices have further skewed the time- and cost-ratios of draft data generation versus the painstaking process of improving and finishing a genome. The result is an ever-widening gap between drafted and finished genomes that only promises to continue (see the figure, page 236); hence, there is an urgent need to distinguish good from poor data sets.

The sequencing institutes and consortia whom we represent believe that a new set of standards is required for genome sequences. The following represents community-defined categories of standards that better reflect the quality of the genome sequence, based on our understanding of the technologies, available assemblers, and efforts to improve upon drafted genomes. Due to the increasingly rapid pace of genomics, we avoided rigid numerical thresholds in our definitions to take into account products achieved by any combination of technology, chemistry, assembler, or improvement and/or finishing process.

Standard Draft: minimally or unfiltered data, from any number of different sequencing platforms, that are assembled into contigs. This is the minimum standard for a submission to the public databases. Sequence of this quality will likely harbor many regions of poor quality and can be relatively incomplete. It may not always be possible to remove contaminating sequence data. Despite its shortcomings, Standard Draft is the least expensive to produce and still possesses useful information.

High-Quality Draft: overall coverage representing at least 90% of the genome or target region. Efforts should be made to exclude contaminating sequences. This is still a draft assembly with little or no manual review of the product. Sequence errors and misassem-

[1]U.S. Department of Energy Joint Genome Institute. [2]Lawrence Livermore National Laboratory. [3]Michigan State University. [4]The Sanger Institute. [5]Washington University School of Medicine. [6]The Broad Institute. [7]J. Craig Venter Institute. [8]Baylor College of Medicine. [9]Ontario Institute for Cancer Research. [10]Los Alamos National Laboratory. [11]Natural Environmental Research Council Centre for Ecology and Hydrology. [12]National Center for Biotechnology Information. [13]Seattle Children's Hospital and Research Institute. [14]University of Washington School of Medicine. [15]Lawrence Berkeley National Laboratory. [16]Emory GRA (Georgia Research Alliance) Genomics Center. [17]HudsonAlpha Institute. [18]Naval Medical Research Center.

*Full affiliations are available on *Science* Online. †Finishing in the Future Working Group members. ‡These authors contributed equally to organizing this work. §Authors for correspondence. E-mail: pchain@lanl.gov (P.S.G.C.); dg1@sanger.ac.uk (D.V.G.)

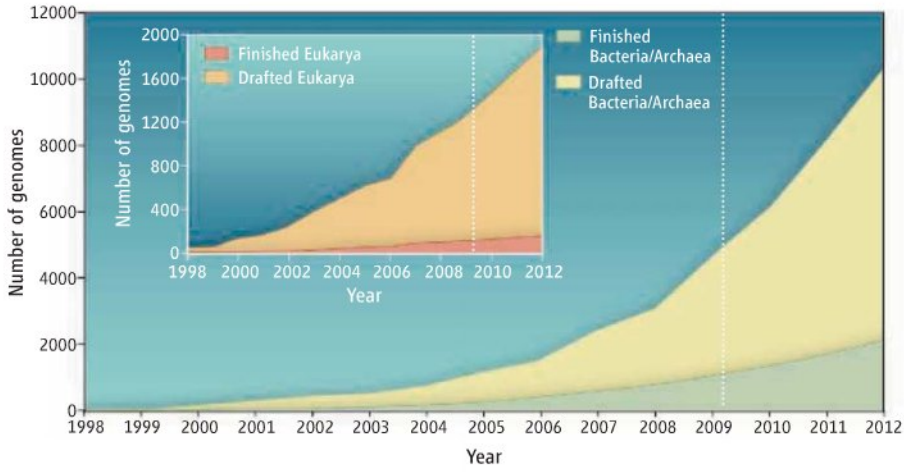

Trends in generation of drafted and finished genomes. A conservative estimate of future projects is shaded in light blue. Data were derived from (*6*, *7*).

blies are possible, with no implied order and orientation to contigs. This is appropriate for general assessment of gene content.

Improved High-Quality Draft: additional work has been performed beyond the initial shotgun sequencing and High-Quality Draft assembly, by using either manual or automated methods. This should contain no discernable misassemblies and should have undergone some form of gap resolution to reduce the number of contigs and supercontigs (or scaffolds). Undetectable misassemblies are still possible, particularly in repetitive regions. Low-quality regions and potential base errors may also be present. This standard is normally adequate for comparison with other genomes.

Annotation-Directed Improvement: may overlap with the previous standards, but the term emphasizes the verification and correction of anomalies within coding regions, such as frameshifts, and stop codons. It will most often be used in cases involving complex genomes where improvement beyond this category fails to outweigh the associated costs. Gene models (gene calls, including intron-exon determination for eukaryotes) and annotation of the genomic content should fully support the biology of the organism and the scientific questions being investigated. Exceptions to this gene-specific finishing standard should be noted in the submission. Repeat regions at this level are not resolved, so errors in those regions are much more likely. This standard is useful for gene comparisons, alternative splicing analysis, and pathway reconstruction.

Noncontiguous Finished: describes high-quality assemblies that have been subject to automated and manual improvement, and where closure approaches have been successful for almost all gaps, misassemblies, and low-quality regions. Attempts have been made to resolve all gap and sequence uncertainties, and only those recalcitrant to resolution remain (with notations in the genome submission as to the nature of the uncertainty). This product is thus of "Finished" quality with the only exception being repetitive or intractable gaps, along with heterochromatic sequence for eukaryotic applications. Thus, it is appropriate for most analyses. For nearly all higher organisms, this is the grade previously called "Finished."

Finished: refers to the current gold standard; genome sequences with less than 1 error per 100,000 base pairs and where each replicon is assembled into a single contiguous sequence with a minimal number of possible exceptions commented in the submission record. All sequences are complete and have been reviewed and edited, all known misassemblies have been resolved, and repetitive sequences have been ordered and correctly assembled. Remaining exceptions to highly accurate sequence within the euchromatin are commented in the submission. The Finished product is appropriate for all types of detailed analyses and acts as a high-quality reference genome for comparative purposes. Some microbial genome sequences where multiple platforms have been used for the same genome have exceeded this standard, and it is believed that no bases are incorrect except for natural, low-level biological variation.

Intermediate standards often overlap, and although we do not advocate any one standard, we recommend that the target standard be based on the needs and goals of each project. There may be cases where select regions will be targeted for improvement and more than one standard may apply (such regionally improved sequences should be identified). This approach is most often used for eukaryotic whole-genome sequencing projects, where the cost of complete finishing remains prohibitive, and allows improvement to be directed at euchromatic sequence, because heterochromatic sequence remains largely recalcitrant to available approaches. Legacy eukaryotic tiling path standards will remain in use for a time.

Here, we have attempted to capture in a technology-independent fashion the types of whole-genome sequencing projects that are beginning to populate databases, and we have defined a set of standards that accommodate a growing list of alternative genome products that have been obtained via less conventional means, such as environmental (metagenomic) or single-cell sequencing. Ongoing discussions with genome database repositories have been met with enthusiasm, and the implementation of these standards as a requirement for genome submissions is expected. To aid in adoption of this classification of sequence finishing standards, we have added this classification to the Sequence Ontology (*3*) where it can now be used to comply with the Genomic Standards Consortium's (GSC) "Minimum Information about a Genome Sequence" standard (*4*) "sequencing status" descriptor. Furthermore, the efforts described here recently have been adopted under the umbrella of the GSC (*5*). This common currency in defining the products of genome projects enables better management of expectations and allows users of genomic data to assess the quality of the deposited available sequences and decide whether these meet their needs.

References and Notes

1. International standards for sequence fidelity, established at the Second International Strategy Meeting on Human Genome Sequencing in Bermuda in 1997 (27 February to 2 March). "Finished" quality standards, commonly known as the Bermuda standards, defined finished sequence as a contiguous sequence with less than one error per 10,000 bases. Almost everything else was "draft."
2. R. W. Blakesley *et al.*, *Genome Res.* **14**, 2235 (2004).
3. K. Eilbeck *et al.*, *Genome Biol.* **6**, R44 (2005).
4. D. Field *et al.*, *Nat. Biotechnol.* **26**, 541 (2008).
5. Genomic Standards Consortium, http://gensc.org.
6. GOLD, Genomes OnLine Database, www.genomesonline.org.
7. K. Liolios *et al.*, *Nucleic Acids Res.* **36**, D475 (2008).
8. For Joint Genome Institute members, work was performed under the auspices of the U.S. Department of Energy Office of Science, Biological and Environmental Research Program; by the University of California, Lawrence Berkeley National Laboratory, contract no. DE-AC02-05CH11231; Lawrence Livermore National Laboratory contract no. DE-AC52-07NA27344; and Los Alamos National Laboratory, contract no. DE-AC02-06NA25396. Naval Medical Research Center work was supported by grant TMTI0068_07_NM_T from the Joint Science and Technology Office for Chemical and Biological Defense, Defense Threat Reduction Agency Initiative to T.D.R.

Supporting Online Material
www.sciencemag.org/cgi/content/full/326/5950/236/DC1

10.1126/science.1180614

NEUROSCIENCE

Nuclear Power for Axonal Growth

A transcription factor involved in oncogenesis and stem cell biology also controls neuronal axon outgrowth.

M. C. Subang[1] and P. M. Richardson[2]

Mammalian neurons exhibit a propensity for axonal growth during development and, to a varying degree, after axonal injury. In general, this growth is unnecessary for most of a neuron's lifetime. In rat retinal ganglion cells and other neurons of the mammalian central nervous system, the potential for axonal growth diminishes sharply around the time of birth. On page 298 of this issue, Moore *et al.* (*1*) show that the regenerative capacity of certain central nervous system neurons is suppressed by Krüppel-like factor–4 (KLF4), thus increasing the repertoire of transcription factors that regulate axonal growth. Information on intrinsic axonal growth programs is relevant not only to understanding nervous system development, but also to the long-standing hope of repairing the adult nervous system.

In a survey of more than 100 neuronal genes whose expression in rat retinal ganglion cells changes around birth, *Klf4* was found to be the most potent inhibitor of axonal outgrowth in rat embryonic hippocampal neurons in culture. Overexpression of *Klf4* reduced axonal length and branching in retinal ganglion cells and cortical neurons also. Conversely, targeted deletion of the *Klf4* gene in mouse retinal ganglion cells resulted in an increased number and length of neurites. The absence of *Klf4* also enhanced regeneration of axons after injury to the optic nerve. If increased endogenous KLF4 activity underlies perinatal loss of axonal growth capacity in retinal ganglion cells, then posttranslational modification of the transcription factor may be involved because expression of its encoding messenger RNA is only modestly increased. Alternatively, or additionally, other KLF family members, in particular, KLF9, may contribute to suppressing axon growth through redundant function (*2*).

KLF4 is one of a quartet of transcription factors sufficient to transform fibroblasts into pluripotent stem cells (*3*). Analysis of KLF4-deficient mice reveals that it is necessary for terminal differentiation of the epidermis and intestinal epithelium (*4*). The transcription factor is a tumor suppressor in human gut tumors, but may be oncogenic in other cancers. The latter activity reflects antiapoptotic properties of KLF4 through its suppression of the tumor suppressor gene *p53*. A functional link between KLF4 and p53 (also a transcription factor) is evident in the generation of pluripotent stem cells, where inactivation of p53 can substitute for overexpression of KLF4 (*5*). Moore *et al.* now add neuron growth to the functions of KLF4.

Motility and extension of the growth cone are ultimately mediated by remodeling of the actin and microtubule cytoskeleton. Extrinsic factors such as the extracellular matrix and diffusible growth factors act through cell surface receptors to activate signaling cascades that converge on actin and tubulin remodeling proteins. How can changes in transcriptional activity in the nucleus modify responsiveness to extracellular cues at the remote growth cone? The likely answer is through increased synthesis of molecules with rate-limiting function in growth cone signaling pathways, or of proteins that transport such molecules in axons (see the figure). Collapsin response mediator protein–2 (CMRP-2) fulfills both functions (*6*): It pro-

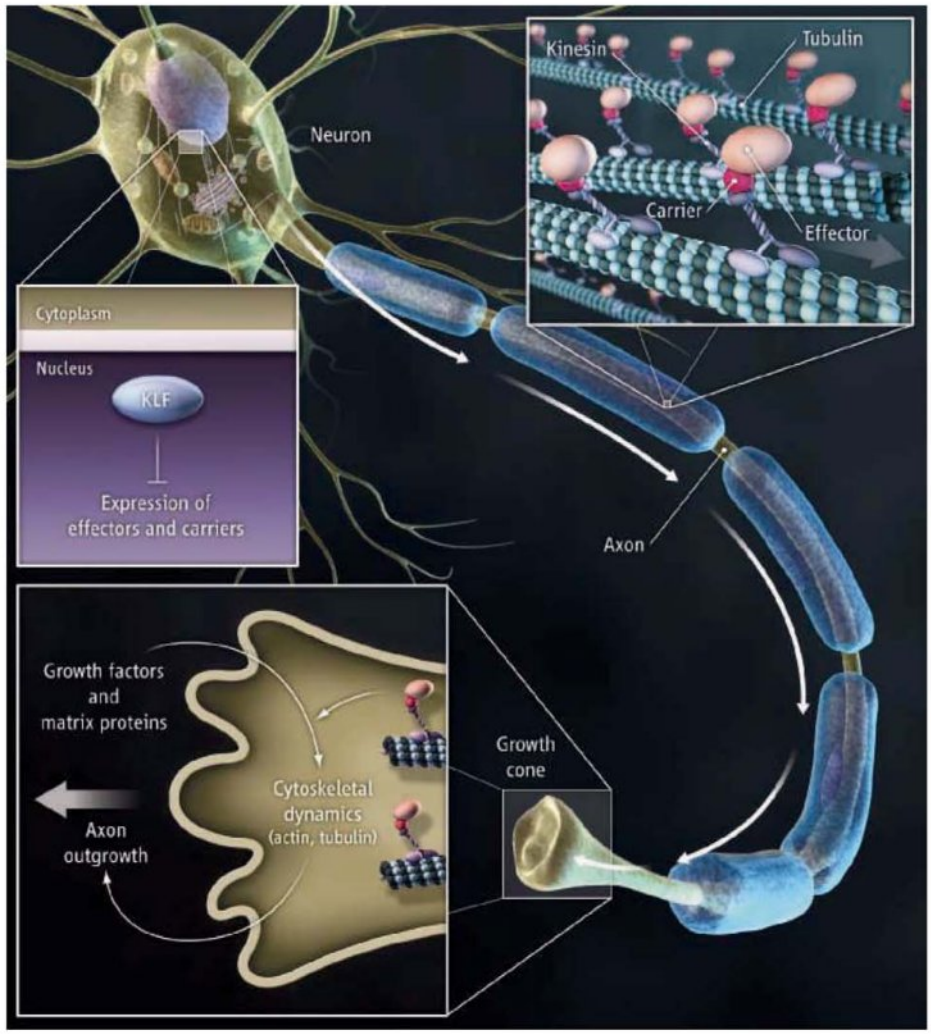

Remote control. In the nucleus of a mammalian neuron, KLF4 could suppress transcription of genes that encode proteins that modify the actin and microtubule cytoskeleton in the growth cone or that transport such growth-enhancing proteins.

CREDIT: C. BICKEL/SCIENCE

[1]Bone and Joint Research, Barts and the London School of Medicine, Charterhouse Square, London EC1M 6BQ, UK. E-mail: m.c.subang@qmul.ac.uk [2]Neurosurgery, Barts and the London Hospitals, Whitechapel, London E1 1BB, UK. E-mail: p.richardson@qmul.ac.uk

motes microtubule assembly and acts as a linker between a cargo (SRA1-WAVE1) and a molecular motor protein (kinesin) for microtubule-based axonal transport to the growth cone. The SRA1-WAVE complex generates free actin filaments that promote axonal extension. However, relations between transcription factors and growth-effecting molecules such as CMRP2 remain to be established. Although the same basic mechanisms of actin and tubulin remodeling likely underlie all forms of axonal growth, neurons may use different molecular strategies to modify the remodeling mechanisms. For example, primary sensory neurons use signaling pathways specifically activated by neurotrophins and neuropoietic cytokines to activate axonal growth capacity during development and regeneration, respectively (*7*). Because of such complexity, the copious information on axon initiation by embryonic neurons (*8*) must be extrapolated cautiously to the regrowth of a severed axon of an adult neuron over centimeters.

KLF4 and KLF9 are unusual among transcription factors in having a suppressive rather than stimulatory influence on intrinsic axonal growth capacity. On the other hand, at least seven neuronal transcription factors are necessary and/or sufficient for axonal growth (*9*). Two from the growth-enhancing group, signal transducer and activator of transcription 3 (STAT3) (*10*) and p53 (*11*), have been functionally linked to KLF4. Although STAT3 induces transcription of KLF4 (*12*) and both transcription factors promote a pluripotent cell phenotype, STAT3 and KLF4 have opposite actions on axonal growth capacity, albeit in different neurons. Because KLF4 blocks expression of the *p53* gene (*13*), suppression of *p53* is a candidate mechanism by which KLF4 suppresses axonal growth. However, p53 also contributes to the death of axotomized retinal ganglion cells (*14*). Obviously, a transcription factor may participate in multiple biological functions, and biological function results from the action of multiple transcription factors.

The challenge to reengineer axonal growth propensity in adult neurons by gene or small-molecule therapy remains daunting, but less so if a dormant growth program can be derepressed by silencing of one or a few transcription factors.

References

1. D. L. Moore *et al.*, *Science* **326**, 298 (2009).
2. J. Jiang *et al.*, *Nat. Cell Biol.* **10**, 353 (2008).
3. K. Takahashi *et al.*, *Cell* **131**, 861 (2007).
4. M. O. Nandan, V. W. Yang, *Histol. Histopathol.* **24**, 1343 (2009).
5. T. Kawamura *et al.*, *Nature* **460**, 1140 (2009).
6. Y. Kawano *et al.*, *Mol. Cell. Biol.* **25**, 9920 (2005).
7. R. Y. Liu, W. D. Snider, *J. Neurosci.* **21**, RC164 (2001).
8. N. Arimura, K. Kaibuchi, *Nat. Rev. Neurosci.* **8**, 194 (2007).
9. H. Zou, C. Ho, K. Wong, M. Tessier-Lavigne, *J. Neurosci.* **29**, 7116 (2009).
10. T. Miao *et al.*, *J. Neurosci.* **26**, 9512 (2006).
11. A. Tedeschi, S. Di Giovanni, *EMBO Rep.* **10**, 576 (2009).
12. P. Y. Bourillot *et al.*, *Stem Cells* **27**, 1760 (2009).
13. B. D. Rowland, R. Bernards, D. S. Peeper, *Nat. Cell Biol.* **7**, 1074 (2005).
14. K. K. Park *et al.*, *Science* **322**, 963 (2008).

10.1126/science.1181038

GENETICS

Life After GWA Studies

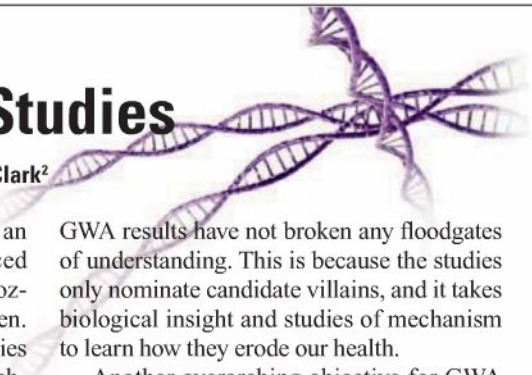

Emmanouil T. Dermitzakis[1] and Andrew G. Clark[2]

Genome-wide association findings should be integrated into a wider scope of information, including biological processes and environments.

In the Hollywood movie *GATACCA*, an infant's genome sequence is produced in seconds and the probabilities of dozens of chronic disorders roll off the screen. Although real-world progress in technologies for DNA sequencing seems to be approaching the science fiction version of genomics, the ability to predict an individual's risk of chronic disease based on DNA sequence is lagging behind. How do we bridge this gap? Or is it time to reconsider the goal of accurately predicting individual risk?

The explosion of genome-wide association (GWA) studies has expanded the set of candidate genes and genomic regions for future study (*1*). Examples include underscoring the role of immunity in macular degeneration (*2*), and shifting the emphasis in type 2 diabetes risk from genetic factors affecting insulin resistance to those that influence insulin production (*3*). But progress in chronic disease etiology has been slow, and GWA results have not broken any floodgates of understanding. This is because the studies only nominate candidate villains, and it takes biological insight and studies of mechanism to learn how they erode our health.

Another overarching objective for GWA studies—to facilitate prediction of the likelihood of future disease—has taken a rockier road. The challenge is highlighted by the most striking general result that pervades all GWA studies—the magnitude of genetic effects is uniformly very small. Even for a trait with strong familial clustering, the strongest associations explain little of the genetic variance for the trait. For example, the heritability of stature is 80%, yet the top 20 candidate genetic variants identified in GWA analyses explain only 3% of the variance (*4*, *5*). Possible reasons include missing low-frequency alleles, genetic heterogeneity of the trait, genotype-environment interaction, and epistasis (*6*). And the possible roles of epigenetic variation in mediating phenotypic differences also cannot be ignored. The lesson is that we do not yet fully grasp the genetic architecture of complex disorders in humans, and we will not be able to make accurate individual predictions of risk until we do.

Predicting individual risk of complex traits is a tall challenge, in part because of the context-dependent way that the genotype manifests its effects on disease risk. Moreover, any prediction of risk must somehow integrate over possible environments. Investment analysts apply Monte Carlo simulations to project the future value of investment accounts, sampling over many possible future economic scenarios. The future of gene-based diagnostics, at least for complex disorders, might similarly have to incorporate many possible environmental and other insults into their predictions of individual risk. It might be possible to represent a projected "norm of reaction" as the distribution of possible phenotypic outcomes of a particular genotype, but it is nearly impossible to know how useful such a prediction could be. For many complex traits, the range of predictions with and without the genetic data may differ very little. But for others, the genetic information may impose constraints that would have useful predictive value.

Opportunities for improved accuracy in predicting disease risk appear especially bleak when one considers that individual prediction of complex traits in model organisms, such as the fly *Drosophila melanogaster*, is not much

[1]Department of Genetic Medicine and Development, University of Geneva Medical School, 1 Rue Michel-Servet, Geneva 1211, Switzerland. E-mail: emmanouil.dermitzakis@unige.ch [2]Department of Molecular Biology and Genetics, Cornell University, Ithaca, NY 14853, USA. E-mail: ac347@cornell.edu

CREDIT: C. BICKEL/SCIENCE

better than in humans. Precise effects of specific genetic variants on bristle number in flies have been mapped to several genes, and yet those same variants within a natural population have little bearing on bristle counts (*7*). Prediction of individual phenotypes is practiced in plant and animal breeding, where the genetic dimensionality is radically reduced. Modeling and prediction of complex phenotypes of inbred lines in the laboratory can be quite accurate, and yet when the same genes and phenotypes are projected into a free-living population, individual prediction entails too many additional variables and accuracy suffers.

So what comes next in complex disease research? The technology for identifying genetic differences is racing forward, with the 1000 Genomes Project (*8*) and efforts to accurately characterize copy number variation. The notion that whole-genome sequencing will become routine medical practice no longer seems so futuristic. But the biggest opportunity for making serious progress in understanding chronic disease risk lies in developing a deeper "biological awareness" into genomic approaches to the study of complex disorders. We tend to talk about pathways and processes as if they are discrete compartments of biology. But genes and their products contribute to a network of interactions that differ radically among tissues. Even our inference of gene regulatory networks suffers from being confined to a narrow biological context. A "candidate-tissue approach" still limits attention to a subset of tissues based on incomplete information and tenuous assumptions, and like candidate gene studies, there is no guarantee that these guesses are correct.

Though we have developed sophisticated statistical tools to analyze and identify genetic variants in the context of whole-organism phenotypes and to detect associations of effects that are far apart (in terms of molecular interactions), we have been unable to bridge the gap between the genetic lesion, or the biochemical effect, and the phenotype except in a few cases (*9*). A major breakthrough will be to predict and interpret the effect of mutational and biochemical changes in human cells and understand how this signal is transmitted spatially (among tissues) and temporally (spanning development) (*10*). Manipulation of induced pluripotent stem cells (*11*) may allow the analysis of diverse cell types from a number of individuals to examine the effects of genotypes in different biological contexts.

To date, GWA studies have relied on a rather unlikely model for the genetics of complex traits—that common DNA sequence variations (known as single-nucleotide polymorphisms) with widespread (but marginal) effects will predominate. This was a sensible place to start, but perhaps it should not be surprising that common variants provide little help in predicting risk. With the arrival of data for ever rarer variants in large, well-designed cohort samples, we should now decide how much emphasis to place on individual prediction, and ask how we can improve the currently unsatisfying record. Large cohort studies should provide information on candidate genes and on combinations of factors that influence groups that are at risk, even if accurate individual risk prediction is never achieved. An attainable public health goal that deserves emphasis is to identify, for each individual, life-style choices that pose particularly elevated risk of chronic disease.

References

1. www.genome.gov/26525384
2. R. J. Klein *et al.*, *Science* **308**, 385 (2005).
3. E. Zeggini *et al.*, *Nat. Genet.* **40**, 638 (2008).
4. M. N. Weedon *et al.*, *Nat. Genet.* **40**, 575 (2008).
5. G. Lettre *et al.*, *Nat. Genet.* **40**, 584 (2008).
6. T. A. Manolio *et al.*, *Nature* **461**, 747 (2009).
7. S. J. Macdonald, T. Pastinen, A. D. Long, *Genetics* **171**, 1741 (2005).
8. www.1000genomes.org
9. E. E. Schadt, *Nature* **461**, 218 (2009).
10. E. T. Dermitzakis, *Nat. Genet.* **40**, 492 (2008).
11. A. Meissner, M. Wernig, R. Jaenisch, *Nat. Biotechnol.* **25**, 1177 (2007).

10.1126/science.1182009

ATMOSPHERIC SCIENCE

Monsoons and Meltdowns

Jeffrey P. Severinghaus

A counterintuitive connection between ice-sheet melting and weak monsoons helps to explain ice age cycles.

What do periods of weak low-latitude rainfall have to do with the meltdown of great ice sheets? On page 248 of this issue, Cheng *et al.* (*1*) show that this counterintuitive association contains a hot clue about the much-debated causes of the ice age cycles that end every 100,000 years or so in a collapse of the great Northern Hemisphere ice sheets (a glacial termination). Understanding this collapse is relevant to human affairs both past and future, because the collapse typically causes a subsequent period of unusual climatic stability and warmth (an interglacial period), exemplified by the past 11,700 years of relatively stable climate in which human agriculture and civilization have flourished (*2*). Further, the future stability of ice sheets is an urgent question facing society today (*3*).

Scripps Institution of Oceanography, University of California San Diego, La Jolla, CA 92093–0244, USA. E-mail: jseveringhaus@ucsd.edu

The melting ice sheets inject so much low-density fresh water into the North Atlantic that they weaken or entirely shut down the normal sinking of dense water that fuels the ocean circulation (the meridional overturning circulation, or MOC). The loss of this circulation allows sea ice to cover the North Atlantic in winter, preventing ocean heat from warming the air and leading to extremely cold winters in Europe and Eurasia, which seem to weaken the following summer's monsoon in Asia (see the figure). The exact mechanism that links cold winters to weak monsoons is still debated, but could be simply that the more extensive spring snow cover and cold, wet soils slow the heating of the land surface that is the main driver of the monsoon. These cold winters do not, however, prevent continued summer melting of the ice sheets, because ice survival is relatively insensitive to winter temperature (*4*).

The occurrence of weak monsoons may thus provide an indirect time marker of ice-sheet meltdowns. As a record of past monsoon strength, Cheng *et al.* use the ratio of oxygen isotopes in the calcium carbonate of stalagmites (cave deposits precipitated from groundwater seepage) from the Asian monsoon region. Stalagmites are the most accurately dated paleoclimate records on the relevant 100,000-year time scale, with errors of mere decades (*5*).

The breakthrough of Cheng *et al.* is that they have achieved unprecedented dating precision, and correlate the monsoon record with ice core and marine records, providing all three with an accurate time scale for the past four ice age terminations. They can thus compare the precise timing of meltdowns with potential causes, such as the amount of sunshine (insolation) that fell on the northern ice sheets in the melting season from June to August, or the concentration of atmospheric CO_2 known from trapped air bubbles in ice cores.

The authors find that the last four meltdowns began when northern sunshine was

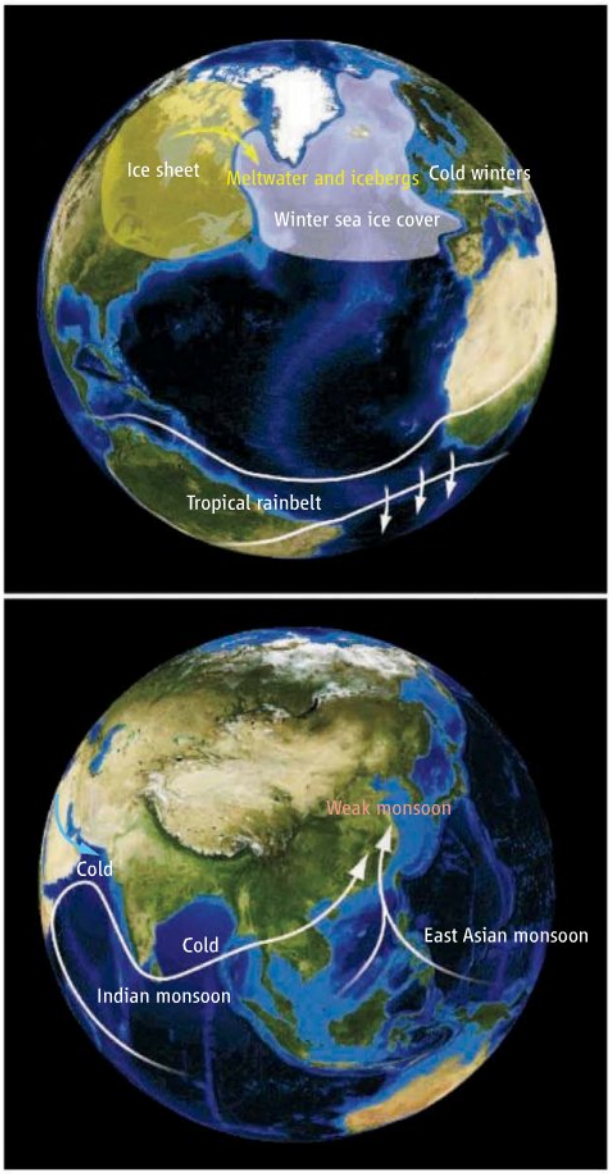

How meltwater from the North American ice sheet may cause weak Asian monsoons. Meltwater runoff into the North Atlantic prevents sinking of water around Greenland, because fresh water has a lower density than salt water. This leads to a collapse of the Atlantic Meridional Overturning Circulation (MOC), in turn further freshening the surface North Atlantic as a result of loss of northward transport of salt by the MOC. This fresh surface layer enhances winter sea ice formation because its low density prevents deep convection, restricting surface access to the enormous heat reservoir represented by the deep ocean. Widespread sea ice cover in turn causes extremely cold winter air temperatures downwind of the North Atlantic due to the insulating effect of sea ice. A southward-shifted atmospheric jet brings cold air into the Mideast and Indian Ocean region. Cooling of the Asian landmass and the North Indian Ocean in winter then weakens and delays the onset of the following summer's monsoon.

intensifying, in accordance with the classical Milankovitch or astronomical theory of the ice ages (*6*). By linking their cave chronology with ice cores via the spike of atmospheric methane (*7*) that accompanies abrupt increases in monsoon intensity, the authors further show that meltdowns occur hand in hand with rising CO_2. They also link the timing of their weak monsoons to Heinrich events, which are pulses of icebergs recorded in marine sediment cores as layers of ice-rafted debris. This allows them to place the sediment core records on an accurate time scale, which is important because the classical indicator of sea level (oxygen isotopes in calcium carbonate shells) is borne by sediment cores. Their finding that sea levels rose in synchrony with CO_2 during glacial terminations clears up an old confusion that came from the use of the oxygen isotopes of atmospheric O_2 as an indicator of sea level, now known to be unreliable (*8*).

These are impressive accomplishments by themselves, but the hot clue that Cheng *et al.* provide is that most of the meltdown and sea-level rise occurs during periods of weak monsoons, when the MOC is shut down and CO_2 is rising. Is there something about an "off" MOC that helps to destroy an ice sheet? Cheng *et al.*'s timing data provide support for the hypothesis (*9*, *10*) that an "off" MOC forces CO_2 out of the Southern Ocean, warming the globe by its greenhouse effect, which in turn causes more melting of the ice sheets, ensuring that the MOC stays in its "off" position in a positive-feedback loop.

In this view, the distinguishing characteristic of glacial terminations—in contrast to other periods of high Northern Hemisphere sunshine that do not trigger a termination—is a huge ice sheet that can provide sufficient meltwater to keep the MOC in its "off" position for some critical duration, allowing a large enough CO_2 rise to fatally damage the ice sheet. This critical duration entails the crossing of some threshold, beyond which the ice sheet has too low an altitude and thus cannot survive, because the air temperature increases with falling altitude. An alternative hypothesis is that massive ice sheets are inherently vulnerable and cannot survive the combined onslaught of Milankovitch and CO_2; the two hypotheses are not mutually exclusive and may both operate.

In either case, the answer to the question "Why do terminations recur roughly every 100,000 years?"—attributed to Raymo (*11*)—is that terminations require an existing massive ice sheet, and that Earth's orbit becomes nearly circular every ~100,000 years, eliminating periods of intense sunshine and thereby permitting the gradual accumulation of a massive ice sheet. An interesting exception cited by Cheng *et al.* is the anomalously weak sunshine 229,000 years ago that apparently allowed accumulation of a massive ice sheet within a short time, causing a termination that does not fit neatly into the 100,000-year paradigm.

Cheng *et al.* thus confirm the astronomical theory of the ice ages, but with a twist: The shutoff of the MOC and its associated southward shift of tropical rain belts, warming of the Southern Hemisphere (termed the "bipolar seesaw"), and rise in atmospheric CO_2 plays an integral role in the meltdown of the great ice sheets. Using monsoons to improve dating precision across the whole suite of paleodata, Cheng *et al.* show the way to the first coherent narrative that truly explains terminations and the inseparable question of what causes ice age cycles (*12*).

References and Notes

1. H. Cheng *et al.*, *Science* **326**, 248 (2009).
2. B. F. Byrd, *J. Archaeol. Res.* **13**, 231 (2005).
3. R. B. Alley, P. U. Clark, P. Huybrechts, I. Joughin, *Science* **310**, 456 (2005).
4. G. H. Denton, R. B. Alley, G. C. Comer, W. S. Broecker, *Quat. Sci. Rev.* **24**, 1159 (2005).
5. C.-H. Cheng *et al.*, *Geochim. Cosmochim. Acta* **72**, 1598 (2008).
6. J. D. Hays, J. Imbrie, N. J. Shackleton, *Science* **194**, 1121 (1976).
7. K. Kawamura *et al.*, *Nature* **448**, 912 (2007).
8. J. P. Severinghaus, R. Beaudette, M. A. Headley, K. Taylor, E. J. Brook, *Science* **324**, 1431 (2009).
9. D. Paillard, *Rev. Geophys.* **39**, 325 (2001).
10. G. H. Denton *et al.*, *Pages News* **14**, 14D16 (2006).
11. M. E. Raymo, *Paleoceanography* **12**, 577 (1997).
12. This article neglects the role of the tilt of Earth's axis in causing terminations. Every ~400,000 years, Earth's orbit becomes really circular. At these times, the meltdowns occur when Earth's tilt is at a maximum, because the higher the tilt, the higher the Sun is in the sky in the polar regions during summer; the trigger of the meltdown is then not a minimal Earth-Sun distance, but rather a maximal tilt of Earth's axis. Milankovitch combined the effects of tilt and Earth-Sun distance by plotting June insolation (sunshine intensity) at 65°N versus time when discussing the causes of the ice ages.

10.1126/science.1179941

DEVELOPMENT

Aorta's Cardinal Secret

Rui Benedito and Ralf H. Adams

An unexpected process for forming arteries and veins that involves cell segregation is discovered in zebrafish.

In vertebrates, blood vessels form a tree-like, tubular network consisting of arteries, capillaries, and veins. In development, tissue repair, or cancer, the vasculature expands by angiogenesis, the growth and reorganization of existing vessels. By contrast, the earliest vascular structures in the embryo and the two major axial blood vessels (dorsal aorta and cardinal vein) are thought to be generated by the direct assembly of endothelial precursor cells (vasculogenesis) (*1*, *2*). However, on page 294 of this issue (*3*), Herbert *et al.* challenge this dogma by showing that cardinal vein formation is very different from what was previously thought.

Zebrafish (*Danio rerio*) is the shooting star among model organisms for vascular morphogenesis, because it is highly accessible to genetic and live imaging approaches (*2*). This enabled Herbert *et al.* to observe that early embryos initially contain only a single axial trunk vessel in the location of the aorta. They propose it to be a common precursor vessel that gives rise to a distinct dorsal aorta and cardinal vein, which can be unambiguously identified by positions and molecular markers. The process involves ventral sprouting from the precursor vessel and the migration of venous-fated endothelial cells (see the figure). Thus, the cardinal vein is formed not by vasculogenesis but by arterial-venous cell segregation, which could be considered a specialized form of angiogenesis or a new mode of vessel growth.

What are the molecular signals controlling the separation of cells within the common precursor vessel? Herbert *et al.* investigated several known regulators of vascular growth and arterial-venous differentiation. VEGF-C, a member of the vascular endothelial growth factor family, its cellular receptor Flt4/VEGFR3, and the p110α catalytic subunit of the enzyme phosphoinositide 3-kinase—all of which promote endothelial cell motility (*4*, *5*)—are required for the ventral migration of venous-fated cells and cardinal vein formation. Conversely, VEGF-A, its receptor Kdrl/VEGFR2, and downstream signaling by the enzyme phospholipase C–γ1 (PLCγ1) restrict this process. Suppressing the latter molecular signals leads to excessive ventral migration of endothelial cells, loss of the aorta, and assembly of a large vessel in the venous position. Signaling triggered by VEGF-A also promotes the expression of activating ligands for the cell surface receptor Notch. Consistent with its role in arterial-venous differentiation (*6*), Notch promotes dorsal aorta formation and prevents excessive ventral sprouting.

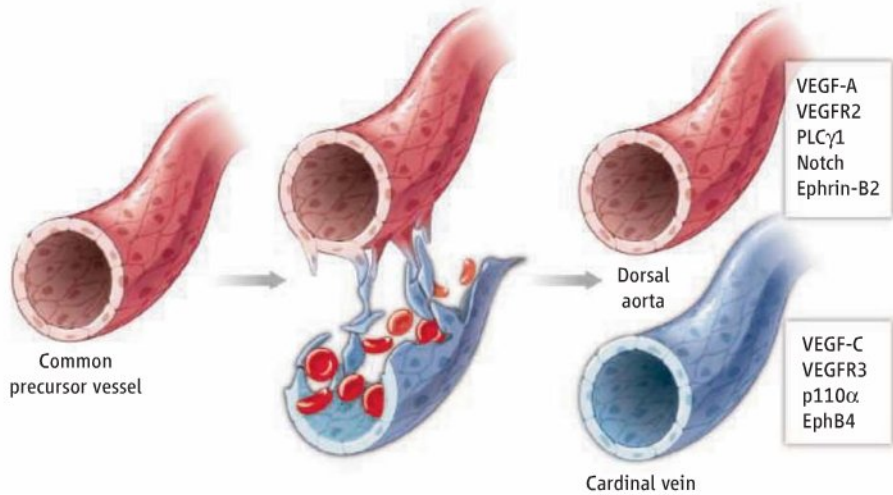

Blood vessel growth. In zebrafish, the segregation of endothelial cells within a common progenitor vessel gives rise to a dorsal aorta and cardinal vein. The process is controlled by the indicated signaling molecules.

These results suggest that extensive sorting processes separate cells with distinct arterial and venous fates within the common precursor vessel. Ephrin ligands and their cognate Eph receptors control tissue patterning in many biological settings by preventing or resolving cell mixing. In the vasculature, ephrin-B2 expression in arterial cells increases in response to Notch, whereas expression of the cognate EphB4 receptor is strongest in veins and repressed by Notch (*6*). Herbert *et al.* show that ephrin-B2–expressing endothelial cells have limited ability to migrate ventrally, whereas those expressing EphB4 preferentially contribute to the cardinal vein. These findings further delineate a molecular framework for the arterial-venous segregation process.

Although we know very little about the conversion of endothelial cell cords and sprouts into perfused, blood-transporting vessels, it is commonly assumed that blood flow plays a critical role (*7*). Surprisingly, Herbert *et al.* find that distinct processes control lumen formation in the dorsal aorta and cardinal vein. Whereas the aortic lumen forms by hollowing of the axial endothelial cell cord (*8*), hematopoietic cells seem to be important for the cardinal vein. Erythrocytes accumulate beneath the common precursor vessel and move toward the newly forming cardinal vein. They are engulfed by venous endothelial cells and carried away by the circulation after a continuous lumen is established. Thus, lumenization of the cardinal vein relies on blood cells but precedes blood flow. This somewhat resembles another primitive, embryonic vascular structure: Precursor endothelial cells (angioblasts) enclose hematopoietic cells in embryonic blood islands, which subsequently fuse, form an early vascular plexus, and release blood into the circulation (*1*).

Could this same principle of arterial-venous segregation apply to mammals? In the mouse, Notch signaling controls the diameter of arteries and veins (*9*). Moreover, dorsal artery and cardinal vein calibers are reciprocally balanced by Notch, ephrin-B2, and EphB4, and conspicuous connections occur transiently in the anterior part of these two major vessels (*10*, *11*). These observations suggest putative similarities between mouse and zebrafish, but formal proof for a conserved arterial-venous segregation process is lacking. An interesting parallel is the development of a second endothelial tubular network—the lymphatic vasculature—later in mouse embryogenesis. It is initiated by differentiation of the first lymphatic endothelial cells within the cardinal vein (*4*). The segregation of these cells from their neighbors, and their migration and assembly into lymph sacs (which depends on VEGF-C and its receptor VEGFR3), recapitulates aspects of the arterial-venous segregation in zebrafish and hints at shared principles.

Department of Tissue Morphogenesis, Max Planck Institute for Molecular Biomedicine, 48149 Münster, Germany, and Faculty of Medicine, University of Münster, 48149 Münster, Germany. E-mail: ralf.adams@mpi-muenster.mpg.de

Herbert *et al*. provide a first glimpse of an exciting new concept in vascular biology, thus raising many questions. Whether or not other vessels form in the same fashion will need to be determined. It's also not yet clear whether angioblasts have a fixed arterial or venous fate (*12*) or reprogram in the precursor vessel in response to local cues. If arterial-venous segregation occurs in mammals, we need to consider that distortion of the normal balance during development could be a cause of human cardiovascular malformations.

References

1. I. Flamme *et al*., *J. Cell. Physiol.* **173**, 206 (1997).
2. N. D. Lawson, B. M. Weinstein, *Nat. Rev. Genet.* **3**, 674 (2002).
3. S. P. Herbert *et al*., *Science* **326**, 294 (2009).
4. K. Alitalo *et al*., *Nature* **438**, 946 (2005).
5. M. Graupera *et al*., *Nature* **453**, 662 (2008).
6. F. J. Lin, M. J. Tsai, S. Y. Tsai, *EMBO Rep.* **8**, 920 (2007).
7. M. L. Iruela-Arispe, G. E. Davis, *Dev. Cell* **16**, 222 (2009).
8. L. H. Parker *et al*., *Nature* **428**, 754 (2004).
9. T. R. Carlson *et al*., *Proc. Natl. Acad. Sci. U.S.A.* **102**, 9884 (2005).
10. R. Benedito *et al*., *BMC Dev. Biol.* **8**, 117 (2008).
11. Y. H. Kim *et al*., *Development* **135**, 3755 (2008).
12. T. P. Zhong, S. Childs, J. P. Leu, M. C. Fishman, *Nature* **414**, 216 (2001).

10.1126/science.1181033

PALEONTOLOGY

On the Mammalian Ear

Thomas Martin and Irina Ruf

Embryonic development played a key role in the evolution of the mammalian ear.

During their development, embryos of many species repeat evolutionary stages of their ancestors (*1*). For example, in human embryos gill pouches are formed during early developmental stages. Developmental heterochrony—that is, the differing timing of developmental processes during embryonic growth—can lead to a premature fixation of ancestral character states and the retention of embryonic patterns in the adult. This process is believed to be an important driving force for evolution (*2*, *3*). One of the key innovations in mammalian history is the evolution of the mammalian ear, leading to the most efficient hearing among vertebrates. On page 278 of this issue, Ji *et al*. (*4*) use an analysis of the Early Cretaceous mammal *Maotherium* to show how heterochrony routed the evolution of the definitive mammalian middle ear (DMME).

Maotherium belongs to the crown group of mammals, represented by the living mammals (egg-laying monotremes, marsupials, and placental mammals) and their last common ancestor, as well as its extinct descendants. The new fossil clearly shows that although *Maotherium* was a crown mammal, it lacked one of the key features characterizing all living mammals: the DMME, in which the middle ear bones are separated from the mandible. The more primitive Early Cretaceous eutriconodont mammals *Yanoconodon* and *Repenomamus* also lacked the DMME (*5*, *6*). Given that there is convincing fossil evidence that the DMME was present in the last common ancestor of crown mammals, a reversal to a more ancestral stage must have occurred in *Maotherium* and in eutriconodonts, with the middle ear attached to the lower jaw by ossified Meckel's cartilage. This premature ossification was caused by heterochronic processes during early ontogeny (early lifetime) (see the figure).

In nonmammalian vertebrates, the middle ear bones are attached via Meckel's cartilage to the inner side of the mandibular bone. In the course of evolution, the middle ear bones of mammals became detached from the mandible by resorption of the cartilaginous connection. There is an ongoing debate concerning whether the DMME evolved once and is one of the strongest shared derived characters of living mammals, or whether it was acquired independently in monotremes and therians (marsupials and placental mammals) as well as in several extinct groups (*5*–*9*).

Maotherium adds important new evidence to that discussion. Apparently, the DMME even evolved independently in crown mammals that are situated well above the split of the monotremes in the mammalian tree. Although it is a crown mammal, *Maotherium* lacks this derived key character (as does the closely related *Zhangheotherium*). The explanation of this obvious paradox is that heterochrony during early development caused a reversal to a more primitive character state of the middle ear in adult *Maotherium*. In more derived spalacotheroids (*Maotherium*'s allies), the DMME later evolved again, independently from the DMME of other crown mammals.

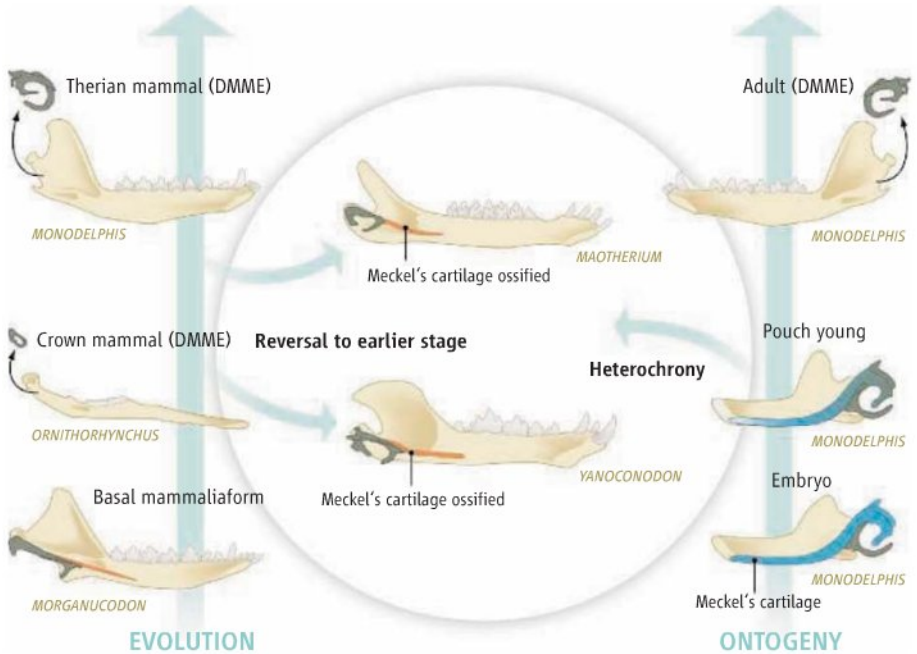

Development drives evolution. (Left) The predecessor of the crown mammals, *Morganucodon*, lacks the DMME (definitive mammalian middle ear), but the DMME is present in basal crown mammals (such as the monotreme *Ornithorhynchus*) and in therian mammals, such as the marsupial *Monodelphis*. **(Right)** In *Monodelphis*, the middle ear bones are attached to the mandible via Meckel's cartilage in early embryonic stages, but subsequent resorption of this connection enables detachment of middle ear bones in the adult. **(Middle)** In the Early Cretaceous crown mammals *Yanoconodon* and *Maotherium*, Meckel's cartilage was prematurely ossified during early ontogeny, preventing detachment of the middle ear bones in the adult. Cartilaginous middle ear structures and Meckel's cartilage are shown in blue; ossified stages are red (ossified Meckel's cartilage) and gray (middle ear ossicles). The figure is not to scale.

CREDIT: ADAPTED FROM DOROTHEA KRANZ/STEINMANN-INSTITUT, UNIVERSITÄT BONN

Steinmann-Institut für Geologie, Mineralogie und Paläontologie, Universität Bonn, Nussallee 8, 53115 Bonn, Germany. E-mail: tmartin@uni-bonn.de

It is well known from embryological studies of living mammals that the process of detachment of the middle ear bones is repeated during early ontogeny (*10*, *11*). In recent decades, evolutionary developmental biology studies have elucidated the driving forces for this process. The partial resorption of Meckel's cartilage and disconnection of the middle ear ossicles from the mandible in modern mammals are controlled by complex regulatory networks; mutant mouse studies have shown that changes in these networks can alter the timing of resorption and ossification, causing morphological transformations such as the permanent connection of middle ear ossicles and mandible (*12*–*14*). From an evolutionary biologist's viewpoint, the "reevolution" of an ancestral character state appears unlikely, but in the case of *Maotherium*'s DMME, a simple temporal change causing premature ossification of Meckel's cartilage during embryo development fixed the ancestral condition in the adult.

The approach of Ji *et al*. exemplifies recent studies that have combined paleontology and developmental biology to gain deep insight into evolutionary processes (*15*). These studies have shown that mammalian evolution was much more complex than had been thought a few years ago. Developmental processes played a central role in evolutionary changes in mammals, as recently shown for patterns of rodent teeth (*16*). The middle ear and mandible of *Maotherium* demonstrate that besides orderly evolution from primitive to derived characters, reversals to more primitive conditions are also to be expected. In the case of the DMME, the labile phase with multiple reversals appears to have ended with the evolution of the coiled cochlea in the inner ear of more derived ancestors of therian mammals (marsupials and placentals) (*17*).

References

1. E. Haeckel, *Generelle Morphologie der Organismen* (Georg Reimer, Berlin, 1866).
2. S. J. Gould, *Ontogeny and Phylogeny* (Belknap, Cambridge, MA, 1977).
3. M. L. McKinney, K. J. McNamara, *Heterochrony: The Evolution of Ontogeny* (Plenum, New York, 1991).
4. Q. Ji, Z.-X. Luo, X. Zhang, C.-X. Yuan, L. Xu, *Science* **326**, 278 (2009).
5. J. Meng, Y. Hu, Y. Wang, C. Li, *Zool. J. Linn. Soc. London* **138**, 431 (2003).
6. Z.-X. Luo, P. Chen, G. Li, M. Chen, *Nature* **446**, 288 (2007).
7. G. Fleischer, *Adv. Anat. Embryol. Cell Biol.* **55**, 3 (1978).
8. T. H. Rich, J. A. Hopson, A. M. Musser, T. F. Flannery, P. Vickers-Rich, *Science* **307**, 910 (2005).
9. T. Rowe *et al.*, *Proc. Natl. Acad. Sci. U.S.A.* **105**, 1238 (2008).
10. C. Reichert, *Müllers Arch. Anat. Physiol. Wiss. Med.* **1837**, 120 (1837).
11. E. Gaupp, *Archiv Anat. Entwickl.* **1912**, 1 (1913).
12. Y. Ito *et al.*, *Dev. Dyn.* **224**, 69 (2002).
13. A. S. Tucker *et al.*, *Development* **131**, 1235 (2004).
14. K. Oka *et al.*, *Dev. Biol.* **303**, 391 (2007).
15. B. K. Hall, *Palaeontology* **45**, 647 (2002).
16. K. D. Kavanagh *et al.*, *Nature* **449**, 427 (2007).
17. I. Ruf *et al.*, *J. Anat.* **214**, 679 (2009).

10.1126/science.1181131

PHYSICS

Sensing a Small But Persistent Current

A magnetic field can create tiny currents that flow continuously in an ordinary metal ring, despite its electrical resistance.

Norman O. Birge

The idea that a normal, nonsuperconducting metal ring can sustain a persistent current—one that flows forever without dissipating energy—seems preposterous. Metal wires have an electrical resistance, and currents passing through resistors dissipate energy. Besides, time-reversal symmetry should forbid a current choosing one direction over the other around the ring.

The latter argument is indeed correct. The persistent current exists only in the presence of a magnetic field piercing the ring, which breaks time-reversal symmetry. All physical properties of a metal ring vary periodically with the magnetic flux through the ring (*1*), with period equal to the magnetic flux quantum, $\Phi_0 = h/e$, where h is Planck's constant and e is the charge of an electron. Among those properties is the ring's persistent current (*2*), and this current exists even in realistic metal rings containing atomic defects, grain boundaries, and other kinds of static disorder (*3*). The current is extremely small and notoriously difficult to measure. Two recent studies, one by Bluhm *et al*. (*4*) and one by Bleszynski-Jayich *et al*. on page 272 of this issue (*5*), report new ways to measure persistent currents. These studies help resolve some of the discrepancies that have arisen in previous studies spanning nearly 20 years.

Several factors conspire to render detection of the persistent currents extremely difficult. The current flows only around a closed ring, so the effect is lost if a device like an ammeter is put into the circuit to measure it directly. The very small magnetic moment produced by the current must be measured instead. Theory predicts that the magnitude of the persistent current is roughly equal to the charge of a single electron divided by the time it takes an electron to diffuse around the ring. Experimentalists have kept this time small by using rings with diameters ranging from half a micrometer to a few micrometers. The persistent current diminishes rapidly as the temperature is raised, so temperatures are kept near 1 K. The sign of the persistent current in a real sample depends on the details of the disorder (the defects that scatter electrons and create resistance), and varies randomly from ring to ring, so many rings must be used as samples to get a good estimate of the typical current. Finally, spurious magnetic moments that can arise from contamination on the surface of the sample can easily swamp the magnetic moment created by the persistent current.

The first two persistent-current experiments used very different strategies. In 1990, Lévy and co-workers measured an array of 10 million copper rings; their strategy was to add together many small signals to create a much larger, measurable signal (*6*). However, because the persistent current in each ring has a random sign, the total signal was proportional only to the square root of the number of rings (*7*).

It turns out that there is a second kind of persistent current, whose period is half of the magnetic flux quantum, $\Phi_0/2 = h/2e$. The "$h/2e$" persistent currents are normally much smaller than the "h/e" persistent currents, but they have the same sign in every ring, so the total signal is proportional to the number of rings. Lévy *et al*. did indeed observe the $h/2e$ persistent current, but both the magnitude and the sign of their results disagreed with the theoretical predictions of that time (*8*, *9*). A possible resolution of that discrepancy has been proposed recently (*10*).

In 1991, Webb and co-workers measured the persistent current in three individual

Department of Physics, Michigan State University, East Lansing, MI 48824, USA. E-mail: birge@pa.msu.edu

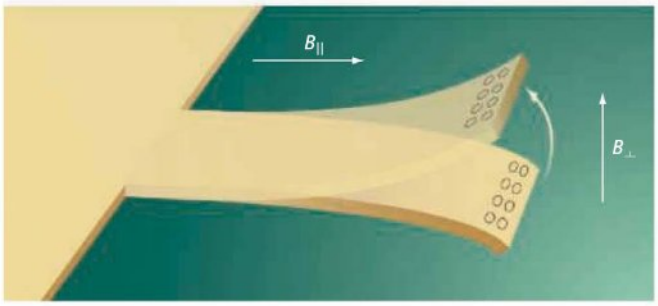

A ring cycle of currents. Persistent currents flow through an ordinary metal ring penetrated by a magnetic field. Bleszynski-Jayich *et al*. fabricated either a single ring or an array of rings near the tip of a nanomechanical cantilever that serves as an oscillator (the rings vary in diameter from 0.6 to 1.6 μm, while the cantilevers are 450 μm long and 40 to 80 μm wide). The magnetic field perpendicular to the plane of the rings, $B_{\perp}$, produces magnetic flux through the rings, which causes the persistent currents to appear. The interaction of the persistent current with the magnetic field parallel to the plane, $B_{||}$, causes a torque on the cantilever, which changes its oscillation frequency slightly. The vibration amplitude is highly exaggerated in the figure.

gold rings (*11*). They observed a persistent current with flux periodicity of h/e, but with a magnitude at least 30 times greater than predicted by theory. Later experiments by Webb's group on an array of 30 rings gave results closer to the theoretical prediction (*12*), but still left several questions unanswered. Experiments on semiconducting rings (*13*) have given results in closer agreement with theory.

The field received a huge boost in the past year from two experiments. Bluhm *et al*. used a scanning microscope to measure the persistent currents in 33 gold rings, one ring at a time (*4*). Magnetic fields were detected with superconducting quantum interference devices, or SQUIDs. The ability of the microscope to spatially scan over the sample led to several improvements over previous measurements, including a better understanding of the background signals and better statistics from measuring many individual rings. Nevertheless, the small magnitude of the signals required 12 hours of signal averaging to obtain each data point. The observed h/e-periodic persistent currents varied randomly in sign from ring to ring, as expected, and had an overall magnitude in good agreement with theory.

Bleszynski-Jayich *et al*. used a much different technology to improve the measurement sensitivity and enable measurements in high magnetic fields. They adapted methods from nanoelectromechanical systems. Specifically, they fabricated the rings on the ends of ultrasmall mechanical cantilevers, as shown schematically in the figure. The cantilevers oscillate at a frequency determined by their stiffness and mass, and this oscillation frequency can be measured with extremely high precision.

When the cantilevers are placed in a large magnetic field, the interaction of the persistent current with the field leads to a very small torque on the cantilever, which in turn changes its oscillation frequency ever so slightly. Using this technique, Bleszynski-Jayich *et al*. achieved a sensitivity about 100 times greater than the SQUID-based measurements. The large magnetic field suppressed any background signal caused by contamination from impurity spins, and the large range of field enabled the experimentalists to obtain a statistical sampling of the persistent current in a single ring. They measured the h/e persistent currents in a single ring and in arrays containing 242, 990, and 1680 rings.

The total signal is proportional to the square root of the number of rings, confirming the randomness of the sign discussed above. Both the overall magnitude of the persistent current and its temperature dependence agree extremely well with theory (*14*). The $h/2e$ persistent currents, however, are not visible in this experiment because of the presence of the large magnetic field.

It is safe to say that the h/e persistent currents in isolated metal rings are now well understood. So where do we go from here? Bleszynski-Jayich *et al*. propose coupling small rings to more complicated circuits, to see how the latter influence the former. The $h/2e$ puzzle remains, at least until the recent hypothesis (*10*) can be checked experimentally.

References and Notes

1. N. Byers, C. N. Yang, *Phys. Rev. Lett.* **7**, 46 (1961).
2. M. Büttiker, Y. Imry, R. Landauer, *Phys. Lett.* **96A**, 365 (1983).
3. H.-F. Cheung, E. K. Riedel, Y. Gefen, *Phys. Rev. Lett.* **62**, 587 (1989).
4. H. Bluhm *et al*., *Phys. Rev. Lett.* **102**, 136802 (2009).
5. A. C. Bleszynski-Jayich *et al*., *Science* **326**, 272 (2009).
6. L. P. Lévy, G. Dolan, J. Dunsmuir, H. Bouchiat, *Phys. Rev. Lett.* **64**, 2074 (1990).
7. The square-root behavior is well known in many areas of science, most notably in the context of particle diffusion. Imagine a drunken sailor taking a series of steps in random directions. After taking N steps, his distance from his starting point is typically equal to the square-root of N times his step size.
8. V. Ambegaokar, U. Eckern, *Phys. Rev. Lett.* **65**, 381 (1990).
9. V. Ambegaokar, U. Eckern, *Phys. Rev. Lett.* **67**, 3192 (1991).
10. H. Bary-Soroker, O. Entin-Wohlman, Y. Imry, *Phys. Rev. Lett.* **101**, 057001 (2008).
11. V. Chandrasekhar *et al*., *Phys. Rev. Lett.* **67**, 3578 (1991).
12. E. M. Q. Jariwala, P. Mohanty, M. B. Ketchen, R. A. Webb, *Phys. Rev. Lett.* **86**, 1594 (2001).
13. D. Mailly, C. Chapelier, A. Benoit, *Phys. Rev. Lett.* **70**, 2020 (1993).
14. E. K. Riedel, F. von Oppen, *Phys. Rev. B* **47**, 15449 (1993).
15. I thank K. Moler for helpful suggestions.

10.1126/science.1180577

CHEMISTRY

Energy Flow Under Control

Victor S. Batista

Laser pulses can be shaped to control energy transfer at the molecular scale in light-harvesting systems.

Controlling energy transfer at the molecular scale has been a long-standing goal since the development of high-power lasers in the 1960s. Appreciable advances toward this goal have been made with demonstrations of laser-controlled energy flow in natural and artificial light-harvesting antennas (*1*, *2*). Based on closed-loop control experiments (*3*, *4*), these techniques can efficiently shape femtosecond laser pulses to control and optimize a variety of molecular processes. However, the details of the resulting control mechanisms are difficult to extract from a cursory examination of the shaped pulses. On page 263 of this issue, Kuroda *et al*. (*5*) report an important contribution toward understanding shaped laser pulses that control energy transfer at the molecular scale. The reported insights on the control mechanism are valuable to understand laser control, in general, in a variety of molecular systems with common relaxation processes.

The goal of Kuroda *et al*. was to elucidate how to optimize the flow of energy in donor-acceptor dendrimer aggregates in liquids, as monitored by the radiative fluorescence of

Department of Chemistry, Yale University, New Haven, CT 06520–8107, USA. E-mail: victor.batista@yale.edu

the acceptor energy trap (see the figure, top panel). These extended π-conjugated structures, attached to a central ring that is tethered to the acceptor perylene moiety, function as biomimetic light-harvesting systems by absorbing ultraviolet-visible light and transferring the captured energy to the perylene trap. Such a mechanism mimics the primary steps of natural photosynthesis, where solar energy is harvested by multichromophoric aggregates and then funneled to an energy trap where reactions are initiated.

The laser control reported by Kuroda *et al.* reveals fundamental aspects of energy flow mechanisms that might be common to a variety of branched dendrimers. In most para-conjugated dendrimers (i.e., linear chains), the optically excited charged carriers are thought to move coherently and become fully delocalized across the molecular aggregate. In contrast, meta-substitutions (i.e., branched chains) are thought to decouple the constituent linear segments (*6*). Therefore, coherent and incoherent energy transfer pathways usually compete (*6*, *7*).

To optimize energy transfer, Kuroda *et al.* designed laser pulses by using closed-loop optimal control experiments. Pulses shaped by maximization of the trap fluorescence were compared to those obtained by maximization of the dendrimer absorption. An important finding was that the optimum pulse was essentially a double pulse. The initial spike component was followed by a weaker subpulse, delayed by ~70 fs. From the analysis of such pulses, a "pump-pump" control mechanism was proposed (see the figure, bottom panel) in which the first pulse component pumps the absorption according to a nonresonant two-photon excitation, while the delayed subpulse promotes the system from the first excited state to a second excited state resonantly accessed through a one-photon transition. Such a mechanism controls (enhances) the trap fluorescence yield as the excitation to the second excited state detours the system away from detrimental nonradiative pathways. This control scheme can be placed alongside other double-pulse control scenarios, including the "pump-dump" method (*8*), in which the second transition dumps the system to a lower energy state instead of pumping it up to a higher energy level.

To support the proposed mechanism, Kuroda *et al.* performed several auxiliary experiments, including a pump-probe measurement where the dendrimer was resonantly excited with an ultrafast ~400-nm pump pulse (equivalent to the two-photon excitation at 800 nm) and probed with another pulse at 800 nm. Such a bichromatic double-pulse experiment demonstrated that a delayed femtosecond pulse, applied soon after the first excitation, could indeed pump the system to a second excited state, as in the proposed "pump-pump" scenario.

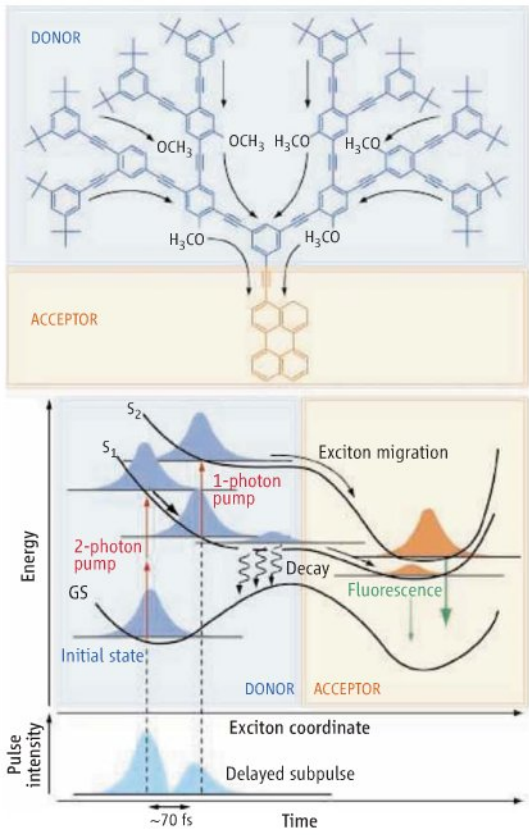

Energy migration under control. Kuroda *et al.* (**top**) achieved laser control of energy migration in a donor-acceptor dendrimer antenna. The "pump-pump" control mechanism (**bottom**) involves a two-photon excitation to a first excited state (S_1), immediately followed by a one-photon transition to a second excited state (S_2), detouring the system away from nonradiative decay pathways.

The "pump-pump" laser control can also be compared to double-pulse coherent control schemes, including femtosecond pulse versions of the bichromatic coherent control method (*9*, *10*) and the bichirped coherent control scenario (*11*) (where the chirp gives the time-dependence of the pulse instantaneous frequency). In these methods, the second pulse is usually applied simultaneously with the first pulse (rather than delayed) to create a second excitation in the first excited state that could interfere with the one generated by the first pulse. Control is achieved by changing the relative phases between the two pulses (without pumping or dumping into higher or lower energy states). While the dynamics remains coherent, the manipulation of the pulse phase affects the interference phenomena and therefore the motion of the resulting excitation. Whether the flow of energy transfer in dendrimers can be manipulated by these coherent control methods remains an open question that should be further investigated. In liquids, coherent control is typically compromised by decoherence unless the dynamical processes of interest are ultrafast. Otherwise, chromophore-solvent interactions randomize the quantum phases very quickly, rendering coherent control techniques ineffective. At later times, coherent control is ruled out by decoherence, and the dynamics can only be controlled by manipulating the laser intensity profile.

The success reported by Kuroda *et al.* (*5*) in achieving "pump-pump" laser control of excitations in dendrimer antennas and the similarities between the characterized control mechanism and other double-pulse laser control scenarios should motivate further experimental and theoretical work. Much remains unknown about the coherent and incoherent aspects of energy migration in light-harvesting systems, including the potential role that quantum interferences might play during the early time relaxation (*12*). Many of these fundamental aspects could be learned from understanding laser control of energy flow at the molecular scale, where branching ratios between coherent and incoherent relaxation pathways could be controlled either by affecting quantum interferences or by driving auxiliary transitions through the manipulation of laser intensities.

References

1. J. Savolainen *et al.*, *Proc. Natl. Acad. Sci. U.S.A.* **105**, 7641 (2008).
2. J. L. Herek *et al.*, *Nature* **417**, 533 (2002).
3. A. Assion *et al.*, *Science* **282**, 919 (1998).
4. R. J. Levis, G. Menkir, H. Rabitz, *Science* **292**, 709 (2001).
5. D. G. Kuroda *et al.*, *Science* **326**, 263 (2009).
6. S. Tretiak, V. Chernyak, S. Mukamel, *J. Phys. Chem.* **102**, 3310 (1998).
7. E. Atas, Z. Peng, V. D. Kleiman, *J. Phys. Chem. B* **109**, 13553 (2005).
8. D. J. Tannor, S. A. Rice, *J. Chem. Phys.* **83**, 5013 (1985).
9. P. Brumer, M. Shapiro, *Chem. Phys. Lett.* **126**, 541 (1986).
10. V. S. Batista, P. Brumer, *Phys. Rev. Lett.* **89**, 143201 (2002).
11. S. C. Flores, V. S. Batista, *J. Phys. Chem. B* **108**, 6745 (2004).
12. G. S. Engel *et al.*, *Nature* **446**, 782 (2007).

10.1126/science.1179694

Reconstituting Bacterial RNA Repair and Modification in Vitro

Chio Mui Chan,[1]* Chun Zhou,[1]* Raven H. Huang[1,2]†

All small RNAs in plants and a subset of small RNAs in animals are 2′-O-methylated at their 3′-terminal nucleotides, carried out by plant and animal Hen1 (*1*–*4*), respectively. Hen1 homologs (~460–amino acid protein) are also found in a subset of bacteria species, but the biological function is unknown (*5*). We found that, in the operon containing bacterial Hen1, there is a second conserved gene encoding a ~850–amino acid protein immediately downstream of Hen1. The latter protein from *Clostridium thermocellum*, named *Cth*pnkp, has been shown to possess kinase, phosphatase, and adenylyltransferase activities, a hallmark of RNA repair (*6*). However, *Cth*pnkp alone was not able to complete the RNA repair despite its three enzymatic activities described above (*7*). We show here that the bacterial Pnkp and Hen1 from *Anabaena variabilis* form a stable heterotetramer in vitro (*8*) (fig. S1) and that *Av*Pnkp/*Av*Hen1 heterotetramer not only repairs tRNAs cleaved by ribotoxins but also adds a methyl group at the cleavage site during repair, which substantially enhances the repair outcome.

To test RNA repair, we cleaved *Escherichia coli* $tRNA^{Asp}$ and $tRNA^{Arg}$ with ribotoxins colicin E5 and colicin D (*9*, *10*) (fig. S2) and carried out RNA repair experiments (Fig. 1A). *Av*Pnkp or *Av*Hen1 alone did not repair the cleaved $tRNA^{Asp}$ (Fig. 1A, lanes 3 and 4), but *Av*Pnkp/*Av*Hen1 heterotetramer was able to produce full-length $tRNA^{Asp}$ (Fig. 1A, lane 5). Despite the substantial difference in the location of the cleavage site (fig. S2), $tRNA^{Arg}$ cleaved by colicin D was also efficiently repaired by *Av*Pnkp/*Av*Hen1 heterotetramer (Fig. 1A, lane 10). Thus, bacterial Pnkp/Hen1 heterotetramer constitutes an RNA repair system, and the RNA repair requires both proteins.

To provide direct evidence of the involvement of methylation during RNA repair, we carried out methylation assays of unlabeled $tRNA^{Asp}$ (full-length and cleaved) in the presence of ^{14}C-AdoMet (Fig. 1B). In addition to the expected 2′-O-methylation at the 3′-terminal nucleotide of the full-length and cleaved $tRNA^{Asp}$, Pnkp/Hen1 heterotetramer methylated the 5′ half of cleaved $tRNA^{Asp}$ in the absence of adenosine triphosphate (ATP) (Fig. 1B, lane 4). Addition of ATP resulted in an almost quantitative shift of the methylated product from the 5′-half to the full-length $tRNA^{Asp}$ (Fig. 1B, lane 5). These results, combined with other complementary experiments (*8*) (fig. S4), demonstrate that a methyl group was incorporated into the original cleavage site of repaired tRNAs. Although methylation increases the efficiency of RNA repair, it is not a requirement (*8*) (fig. S3).

The biological effect of methylation was tested through recutting of repaired $tRNA^{Asp}$ by colicin E5 (Fig. 1C). While cleavage of the original $tRNA^{Asp}$ by colicin E5 proceeded very quickly (Fig. 1C, left half of gel), the repaired $tRNA^{Asp}$ resisted cleavage (Fig. 1C, right half of gel). Prolonged incubation of the original $tRNA^{Asp}$ with colicin E5 (40 min) resulted in almost complete cleavage (94%), whereas 65% of the repaired $tRNA^{Asp}$ remained intact with the same period of incubation. The repaired $tRNA^{Arg}$ also resisted cleavage by colicin D (fig. S4G, right half of gel). Therefore, methylation at the cleavage site during RNA repair protects the repaired tRNAs from recutting by ribotoxins.

The data presented here, together with biochemical studies on *Cth*Pnkp by Shuman and coworkers (*6*, *7*), allowed us to provide functional assignments of bacterial Pnkp and Hen1 (Fig. 1D). The kinase, phosphatase, and methyltransferase activities are contributed from individual protein (Fig. 1D, colored cyan, magenta, and orange). On the other hand, the ligase activity (Fig. 1D, colored green) requires both Pnkp and Hen1, and the contribution from Hen1 is from the N terminus (*8*).

We do not yet know the in vivo bona fide RNA substrate(s) of bacterial Pnkp/Hen1 heterotetramer. Nevertheless, judged by the efficient repair of the cleaved tRNAs reported here, the probability of a cleaved tRNA as the natural substrate of bacterial Pnkp/Hen1 heterotetramer is high (*8*). Furthermore, the fact that Hen1 from both eukaryotes and bacteria catalyze the same chemical reaction, but play distinct biological roles, raises an intriguing question in terms of the possible evolutionary origin of Hen1, which requires further investigation.

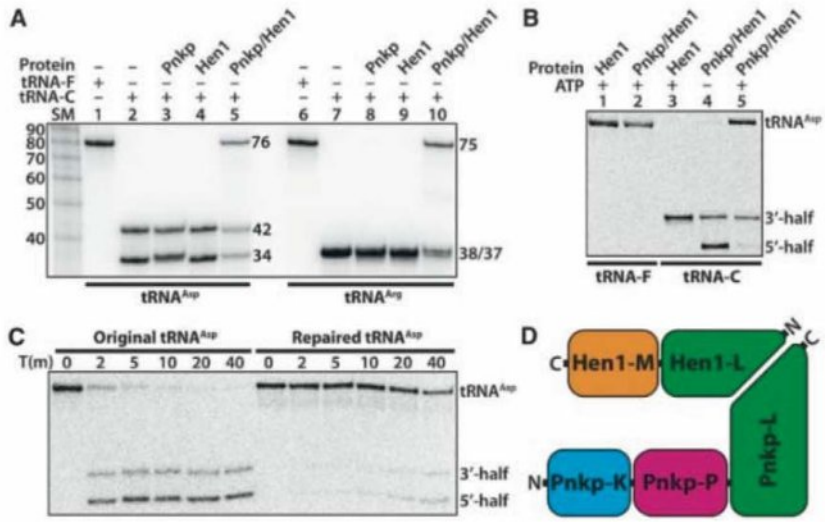

Fig. 1. (**A**) Repair of $tRNA^{Asp}$ cleaved by colicin E5 and $tRNA^{Arg}$ cleaved by colicin D. tRNA-F indicates full-length tRNA; tRNA-C, cleaved tRNA; SM, RNA size markers (in numbers of nucleotides). (**B**) Methylation of $tRNA^{Asp}$. Because $tRNA^{Asp}$ was unlabeled and ^{14}C-AdoMet was the methyl donor, only the methylated RNAs could be observed. (**C**) Time-dependent cleavage of the original and repaired $tRNA^{Asp}$ by colicin E5. T(m), reaction time in minutes. (**D**) Schematic representation of proposed enzymatic functions of bacterial Pnkp/Hen1 complex involved in RNA repair and modification.

References and Notes

1. B. Yu *et al.*, *Science* **307**, 932 (2005).
2. V. V. Vagin *et al.*, *Science* **313**, 320 (2006); published online 28 June 2006 (10.1126/science.1129333).
3. M. D. Horwich *et al.*, *Curr. Biol.* **17**, 1265 (2007).
4. K. Saito *et al.*, *Genes Dev.* **21**, 1603 (2007).
5. K. L. Tkaczuk, A. Obarska, J. M. Bujnicki, *BMC Evol. Biol.* **6**, 6 (2006).
6. A. Martins, S. Shuman, *RNA* **11**, 1271 (2005).
7. N. Keppetipola, J. Nandakumar, S. Shuman, *Nucleic Acids Res.* **35**, 3624 (2007).
8. Materials and methods are available as supporting material on *Science* Online.
9. T. Ogawa *et al.*, *Science* **283**, 2097 (1999).
10. K. Tomita, T. Ogawa, T. Uozumi, K. Watanabe, H. Masaki, *Proc. Natl. Acad. Sci. U.S.A.* **97**, 8278 (2000).

11. We thank C. Wraight, D. Shapiro, and C. Vanderpool for critical reading of the manuscript; T. Thiel (University of Missouri St. Louis) and C. Hayes (University of California Santa Barbara) for materials; and X. Chen (University of California Riverside) for inspiration. Supported by NSF grant MCB-0920966.

Supporting Online Material

www.sciencemag.org/cgi/content/full/326/5950/247/DC1
Materials and Methods
Figs. S1 to S4
References

21 July 2009; accepted 28 August 2009
10.1126/science.1179480

[1]Department of Biochemistry, University of Illinois at Urbana-Champaign, Urbana, IL 61801, USA. [2]Center for Biophysics and Computational Biology, University of Illinois at Urbana-Champaign, Urbana, IL 61801, USA.

*These authors contributed equally to this work.
†To whom correspondence should be addressed. E-mail: huang@uiuc.edu

Ice Age Terminations

Hai Cheng,[1] R. Lawrence Edwards,[1]* Wallace S. Broecker,[2] George H. Denton,[3] Xinggong Kong,[4] Yongjin Wang,[4] Rong Zhang,[5] Xianfeng Wang[1]

^{230}Th-dated oxygen isotope records of stalagmites from Sanbao Cave, China, characterize Asian Monsoon (AM) precipitation through the ends of the third- and fourthmost recent ice ages. As a result, AM records for the past four glacial terminations can now be precisely correlated with those from ice cores and marine sediments, establishing the timing and sequence of major events. In all four cases, observations are consistent with a classic Northern Hemisphere summer insolation intensity trigger for an initial retreat of northern ice sheets. Meltwater and icebergs entering the North Atlantic alter oceanic and atmospheric circulation and associated fluxes of heat and carbon, causing increases in atmospheric CO_2 and Antarctic temperatures that drive the termination in the Southern Hemisphere. Increasing CO_2 and summer insolation drive recession of northern ice sheets, with probable positive feedbacks between sea level and CO_2.

The "sawtooth" character of late Quaternary ice-age cycles, with gradual buildup and rapid collapse of ice sheets, has been known since Emiliani's pioneering oxygen isotope ($\delta^{18}O$) measurements on marine sediments (*1*). Explanations of the rapid collapses, dubbed "terminations" (*2*), have long been sought. The ice-age cycles have been linked to changes in Earth's orbital geometry (the Milankovitch or Astronomical theory) through spectral analysis of marine oxygen-isotope records (*3*), which demonstrate power in the ice-age record at the same three spectral periods as orbitally driven changes in insolation. However, explaining the 100 thousand-year (ky)–recurrence period of ice ages has proved to be problematic because although the 100-ky cycle dominates the ice-volume power spectrum, it is small in the insolation spectrum. In order to understand what factors control ice age cycles, we must know the extent to which terminations are systematically linked to insolation and how any such linkage can produce a nonlinear response by the climate system at the end of ice ages.

Answering such questions depends on establishing the precise timing of a number of terminations relative to changes in insolation. Recent improvements in the precision and accuracy of ^{230}Th dating techniques have substantially increased our ability to determine absolute ages for $CaCO_3$ (*4*) and thus allow us to establish the exact timing of climate events preserved in some types of cave deposits. For the last glacial period, it has been shown that times of unusually high $\delta^{18}O$ in speleothems from Chinese caves correlate with Heinrich events (*5*) recorded in North Atlantic marine sediments (*6*, *7*). Because portions of each of the last four terminations coincide with a major Heinrich event (*8*), we can establish the timing of marine oxygen-isotope terminations by correlating North Atlantic ice-rafted debris (IRD) to radiometrically dated oxygen-isotope cave records from China (*6*).

Variations in atmospheric methane concentration, as revealed in ice cores, correlate with changes in $\delta^{18}O$ in speleothems from Chinese caves (*6*, *7*) for the major climate events of the last glacial period. The last two terminations also were accompanied by abrupt $\delta^{18}O$ shifts that correlate with sharp methane changes (*6*, *7*). Here, we show that the two next-oldest terminations [Termination III (T-III) and IV (T-IV)] also have corresponding shifts in methane and cave $\delta^{18}O$. Thus, we are able to determine the timing of events recorded in Antarctic ice cores by correlating them to the radiometrically dated cave record (*6*, *9*). Using the cave-marine and cave–ice-core correlations, we ascertained for each of the last four terminations the timings of the marine termination, the CO_2 rise, the Antarctic temperature rise, the shift in the $\delta^{18}O$ of atmospheric O_2, and the lowering of dust flux to Antarctica. We then compared the timing of these changes to the known variations in insolation.

We have previously reported AM data for T-I (*7*, *10*) and T-II (*6*, *9*). Here, we confirm the T-II data at yet higher resolution (Fig. 1) and present data for T-III and T-IV. In all cases, we correlate the monsoon signature both to marine and to ice-core records. By comparing and contrasting the character and sequence of events in all four terminations, we make plausible inferences regarding processes that cause terminations.

The highest-resolution data for T-III and T-IV are from Sanbao Cave, which augment the existing record (*11*). We also present Sanbao data for T-II and for the precession cycle after T-III, which includes an interval of time that we call T-IIIA [the shift from Marine Isotope Stage (MIS) 7.4 to 7.3]. Finally, we report data from two stalagmites from nearby Linzhu Cave, which corroborate the Sanbao data.

Chinese caves and the oxygen-isotopic composition of cave calcite. Sanbao (SB) and Linzhu (LZ) caves are located in Hubei province, central China, on the northern slope of Mountain Shennongjia, near the southern edge of the Chinese Loess Plateau (110°26'E, 31°40'N, elevation 1900 m and 110°19'E, 31°31'N, elevation 780 m, respectively) (fig. S1). The area is currently affected by the summer AM, with a mean annual precipitation of 1900 to 2000 mm and mean annual temperature between 8 and 9°C. During summer (June through September), the inland flow of warm/humid air from the tropical Indo-Pacific penetrates to the northern slope of Mountain Shennongjia, delivering about 80% of the total annual precipitation.

We obtained precise ages (±100 years for T-II, ±800 years for T-III, and ±1500 years for T-IV) using a recently developed ^{230}Th dating technique (fig. S2 and table S1) (*4*). Subsamples for oxygen-isotope measurements (table S2) had temporal spacings of 20 to 70 years.

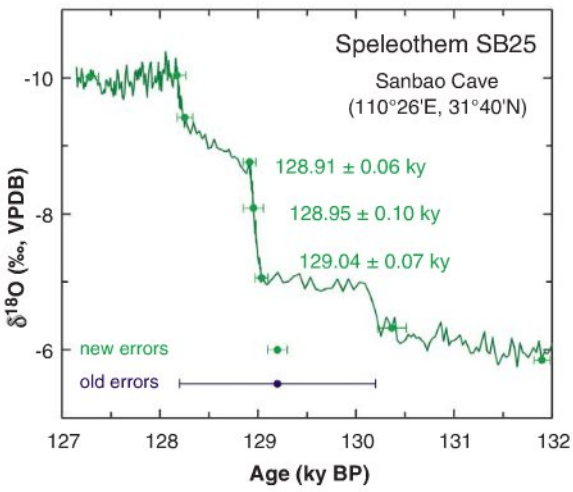

Fig. 1. The $\delta^{18}O$ time series showing the abrupt shift in the AM during T-II, as recorded in Sanbao Cave. This feature was previously observed in Dongge Cave (*9*) and Hulu Cave (*6*), as well as Sanbao Cave (*11*); however, the new dating methods applied here constrain the age of this feature to lie within a century of 129.0 ky B.P. This date agrees with previous dates; however, the errors reported here are about an order of magnitude smaller than those reported in the earlier studies.

[1]Department of Geology and Geophysics, University of Minnesota, Minneapolis, MN 55455, USA. [2]Lamont-Doherty Earth Observatory of Columbia University, 61 Route 9W, Post Office Box 1000, Palisades, NY 10964–1000, USA. [3]Department of Earth Sciences, Bryand Global Sciences Center, Climate Change Institute, University of Maine, Orono, ME 04469, USA. [4]College of Geography Science, Nanjing Normal University, Nanjing 210097, China. [5]National Oceanic and Atmospheric Administration (NOAA)/Geophysical Fluid Dynamics Laboratory, Princeton, NJ 08540, USA.

*To whom correspondence should be addressed. E-mail: edwar001@umn.edu

On the basis of the replication test (Figs. 2, 3, and 4 and fig. S3) (*12*) and other lines of reasoning (*4*), most of the variability in our records results from changes in the $\delta^{18}O$ of precipitation. We interpret these changes following the original reasoning of Wang *et al.* [(*7*); see also (*6*, *9*)], who noted that (i) most precipitation in southeastern China is summer monsoon rainfall, with distinctly lower $\delta^{18}O$ than precipitation during the rest of the year, and (ii) the effect of mean summer temperature or precipitation on mean summer $\delta^{18}O$ is small, as is the case for winter. Thus, neither the temperature-$\delta^{18}O$ relationship, commonly used to interpret ice-core data, nor the interpretation based on the "amount effect" (*13*) is justified, as confirmed by Johnson and Ingram (*14*). Instead, Wang *et al.* (*7*) suggested that a changing ratio of low-$\delta^{18}O$ (summer monsoon) rainfall to high-$\delta^{18}O$ (rest of the year) rainfall could explain the cave isotopic data. Because the low-$\delta^{18}O$ rainfall has a distant tropical Indo-Pacific source (*6*) and the high-$\delta^{18}O$ precipitation probably has a more local oceanic source, the Wang *et al.* interpretation invokes varying proportions of rainfall from these two sources to explain the data. To the extent that the ratio of low- to high-$\delta^{18}O$ precipitation correlates with the absolute amount of low-$\delta^{18}O$ (summer monsoon) precipitation, we can view the cave record as a measure of the amount of summer monsoon precipitation or "summer monsoon intensity." Because cave records from sites across southern Asia have similar signatures (*6*, *9*, *11*, *15*–*17*), the $\delta^{18}O$ variations probably result from broad changes in atmospheric circulation, which shift moisture sources and rainfall patterns across the whole southern Asia region. A simple example would be a change in the fraction of the year dominated by the summer monsoon circulation pattern. Such a process could easily account for the large observed range in cave $\delta^{18}O$, in view of the fact that the modern seasonal range is even larger.

Correlations with North Atlantic climate. Chinese cave $\delta^{18}O$ records (*6*, *7*, *9*–*11*, *17*) have clear correlations with (i) summer insolation (Fig. 4) and (ii) North Atlantic climate. The most striking of these links (*7*) are the close correspondence between the monsoon and the Greenland stadial-interstadial sequences (*18*) and the tie between high cave $\delta^{18}O$ and Heinrich events (*19*). The link to Heinrich events suggests that the monsoon responds to the breakup of the Laurentide Ice Sheet. This is supported by T-I and T-II cave records (Fig. 2), for which the monsoon generally follows summer insolation, with the distinct exception of "gouges" (times of weak monsoon) that correlate broadly to Heinrich stadial I (H-I) and to the Younger Dryas (during T-I) and to H-11 (during T-II). We interpret these gouges as times when the monsoon deviated from a simple insolation response because of cold anomalies generated by ice-sheet disintegration and the resulting influx of meltwater and icebergs to the North Atlantic. The influx could trigger an anomaly by reducing meridional overturning circulation (MOC) and associated northward surface-ocean transport of heat (*20*, *21*).

Sea-ice formation would amplify the anomaly (*22*), particularly during winter, causing pronounced seasonality in the North Atlantic region (*23*, *24*). Extensive winter sea ice cover would seal off the escape of heat to the atmosphere, causing winter temperatures to plunge, generating a climate akin to that of Siberia today. This winter anomaly would probably advect eastward into the northern Indian Ocean and Eurasia, affecting the summer monsoon (*25*, *26*), as observed in the Chinese cave records. Alternately, the monsoon may respond through shifts in both Hadley and Walker circulation triggered by the anomaly (*27*). The sea-ice mechanism and associated seasonality may help to explain an apparent paradox in our scenario. How can the northern ice sheets retreat at times when the North Atlantic is cold? The answer may be that the cold anomaly is largely a winter phenomenon. The glaciers would melt during the relatively warm summers but would not be strongly affected by the unusually cold winters (*23*).

Denton *et al.* (*28*) provided an overview of the main events (including the early stages of the termination itself) that took place at about the time of H-1 [17.5 to 14.5 ky before the present (B.P.)] and termed it the "Mystery Interval" (MI). Cheng *et al.* (*6*) subsequently identified an

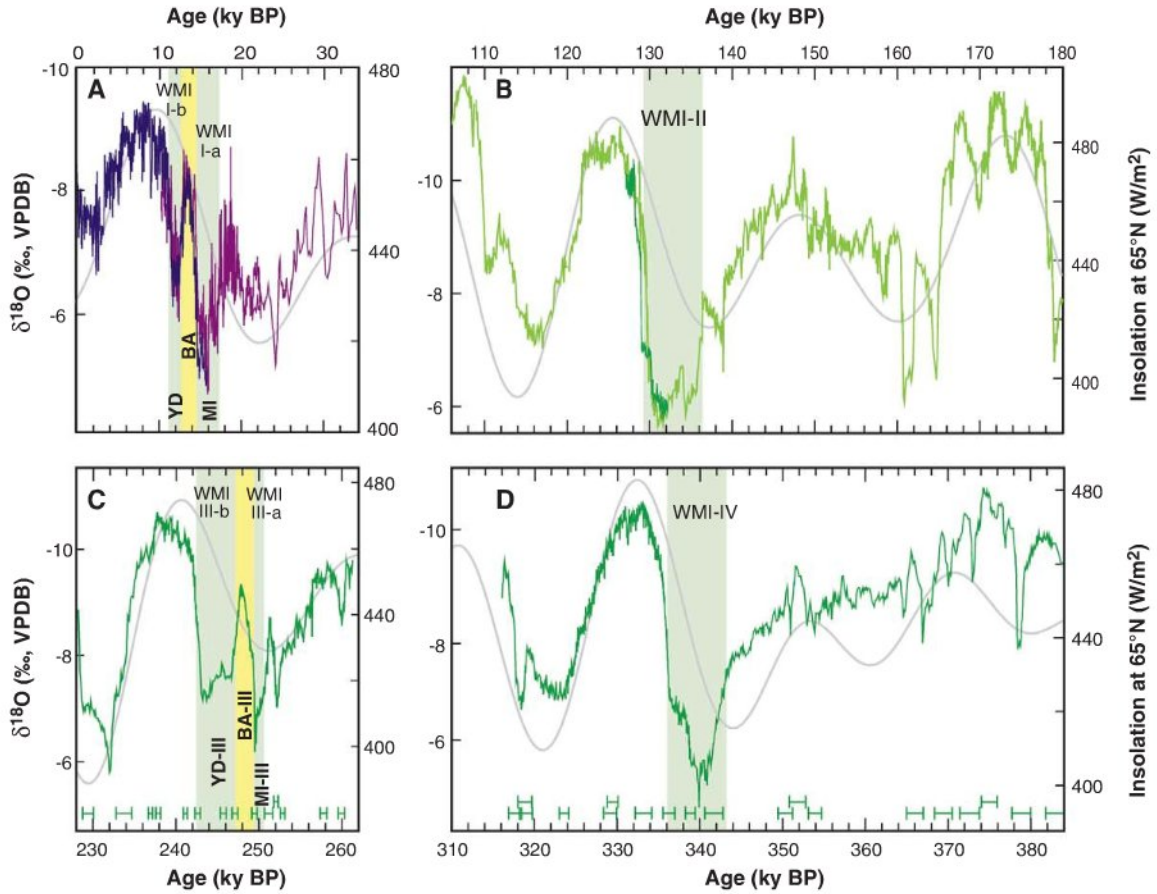

Fig. 2. The $\delta^{18}O$ time series over the past four glacial terminations from (**A**) Hulu and Dongge caves (*7*, *10*), (**B**) Sanbao Cave [light green (*11*) and dark green SB25 (this study)], and (**C** and **D**) Sanbao Cave [sample SB61 (this study)]. Error bars indicate ^{230}Th dates and 2σ errors. $\delta^{18}O$ increases downward. 21 July insolation at 65°N (*29*) is in gray. Light green bars depict the WMIs. Similarities between T-I and T-III and between T-II and T-IV are apparent. Analogous to the MI, BA (yellow bar), and YD events during T-I, we identify similar events during T-III: MI-III, BA-III (yellow bar), and YD-III. The light green bars WMI-Ia and WMI-Ib (YD); WMI-II, WMI-IIIa, and WMI-IIIb (YD-III); and WMI-IV indicate WMIs.

analogous MI during T-II (MI-II, 136 to 129 ky B.P.), which includes most of the termination and corresponds to the H-11 stadial in the North Atlantic. They termed the monsoon during this time the "Weak Monsoon Interval" (WMI-II). T-I and T-II monsoons have similar total lengths of weak monsoons (T-I, 4600 years for the combined duration of MI-I and the YD; T-II, 6000 years). In both cases, the WMI or the pair of WMIs ended with an abrupt shift to low $\delta^{18}O$, which was maintained for about 10 ky during the subsequent interglacial period. However, the weak monsoon of T-I is interrupted by an interstadial [the Bølling-Allerød (BA)] lasting 1800 years, whereas the weak monsoon of T-II is punctuated by an interstadial (at 134 ky B.P.) no more than several hundred years in length (Fig. 2).

Our data show that WMIs occurred during T-III and T-IV (Fig. 2), too. The monsoon during T-III has a signature similar to that of T-I, with two WMIs. WMI-IIIa lasted about 2000 years from 251 to 249 ky B.P. WMI-IIIb lasted about 4500 years from 247 to 242.5 ky B.P. Thus, the total duration of T-III WMIs was 6500 years. As in T-I, the WMIs of T-III are separated by a long interstadial that lasted ~2000 years from 249 to 247 ky B.P. By analogy to the BA, we term this long interstadial the Bølling-Allerød-III (BA-III) and the subsequent WMI the Younger Dryas-III (YD-III). The monsoon signature during T-IV has a simpler structure, with one long WMI (WMI-IV) lasting about 7000 years from 343 to 336 ky B.P. and ending with an abrupt shift as in the other terminations. The monsoon during T-IV is close in structure to that during T-II, although we see no evidence for even a short interstadial punctuating WMI-IV. In sum, the monsoon during each of the last four terminations features one or two WMIs with total lengths of several millennia. The WMI (or WMIs) begins when boreal summer insolation intensity (*29*) is low but increasing (Fig. 2). The remainder of the WMI (or WMIs) coincides with the rising limb of the boreal insolation curve (Fig. 2). If the WMIs represent the response to North Atlantic cold anomalies from ice-sheet disintegration, these observations suggest that classic Milankovitch boreal summer insolation rise acting on northern ice sheets is one of the drivers of terminations.

Further support for this idea comes from IRD/Heinrich stadial records from North Atlantic sediments (*8*). The Ocean Drilling Program (ODP) 980 core has maxima in IRD (*8*) at about the time of each of our WMIs (Fig. 2). Indeed, for T-III, we observe two IRD peaks, which correspond to WMI-IIIa and WMI-IIIb, and even a third smaller IRD peak that corresponds to an earlier weak monsoon episode (at 252 ky B.P.). By correlating the IRD peaks to the dated WMIs, we established the timing of each termination as recorded by benthic $\delta^{18}O$ values. We observe that (i) the benthic $\delta^{18}O$ values begin decreasing at the beginning of the first WMI in each termination and (ii) much of each benthic marine termination takes place during the WMIs. These observations substantiate the view that the WMIs represent the response of the monsoon to a North Atlantic cold anomaly caused by disintegrating ice sheets and amplified through sea-ice formation.

Northern Hemisphere summer insolation. As with the WMIs, each marine termination begins when boreal summer insolation intensity is low but rising, with much of the remainder taking place during the rising limb of the insolation curve (Fig. 3). The first observation suggests that the termination is initially triggered by rising insolation, whereas the second observation suggests that rising insolation plays a role in driving the termination to completion. There is a lack of a clear lag between insolation rise and ice-sheet response. Thus, a several-thousand-year lag, commonly assumed in astronomical tuning of marine oxygen-isotope records (*30*), does not seem to occur during terminations. This apparent sensitivity is a point that is relevant for projecting the future behavior of today's glaciers (*31*, *32*) in a higher-CO_2 world.

If insolation is the trigger, why do terminations not occur every time that insolation rises from a low value (Fig. 4)? An additional necessary condition could be the presence of a massive, isostatically compensated ice sheet (*33*–*35*) whose collapse was triggered by a rise in summer insolation intensity. All other factors being equal, isostatic compensation would lower the ice-sheet

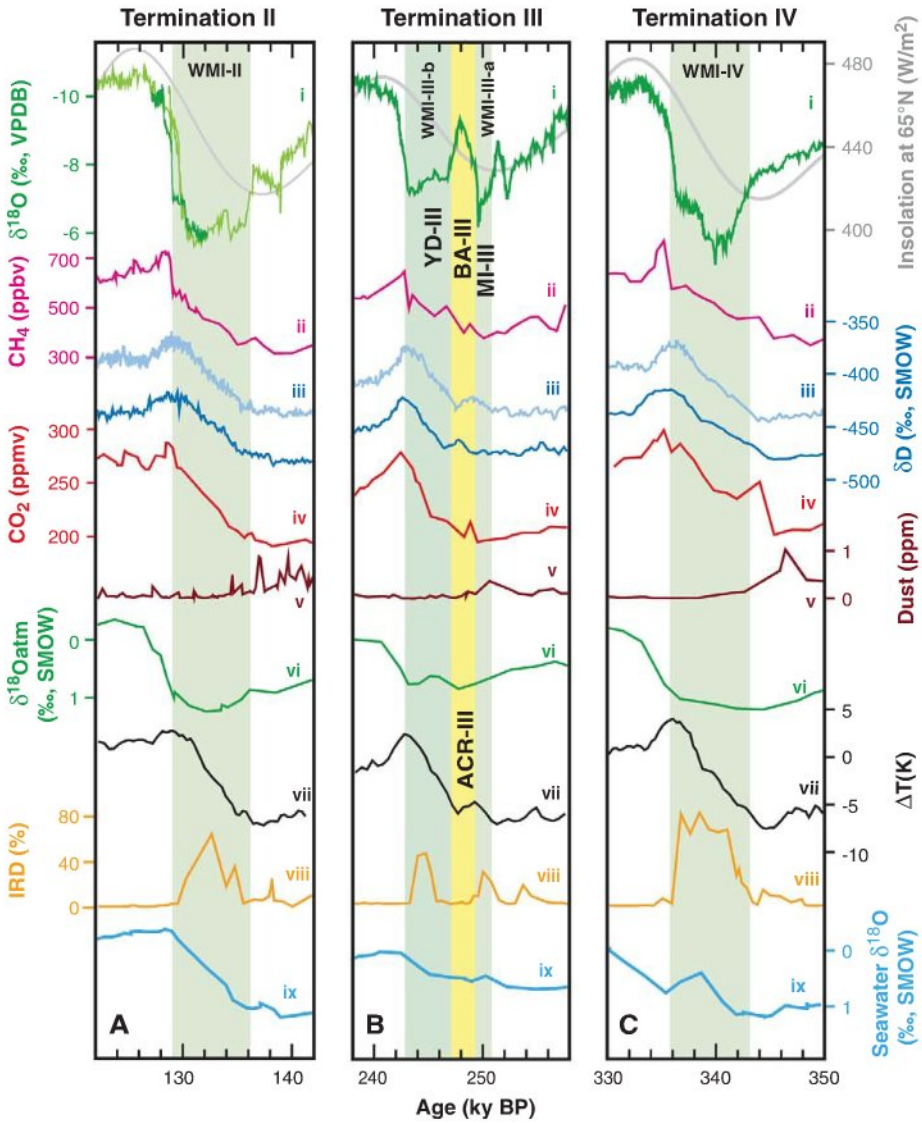

Fig. 3. Events during (**A**) T- II, (**B**) T-III, and (**C**) T-IV. (i) Sanbao $\delta^{18}O$, colors and sources as in Fig. 2. Light green bars indicate WMIs; yellow bars indicate the YD-III and BA-III/ACR-III. 21 July insolation at 65°N is plotted in gray (*29*). Antarctic records of (ii) CH_4 (*36*), (iii) δD [dark blue, Vostok (*36*), light blue EPICA/Dome C (*39*)], (iv) CO_2 (*36*), (v) dust (*36*), (vi) $\delta^{18}O$ of O_2 (*36*), and (vii) Vostok temperature deviation (*40*). North Atlantic sediment (ODP 980) records (*8*) of (viii) IRD and (ix) benthic $\delta^{18}O$ are also shown. All records are plotted on their original time scales but shifted so that the abrupt methane shifts correlate with the abrupt cave $\delta^{18}O$ shifts and the marine IRD peaks correlate with the high-$\delta^{18}O$ cave excursions. The Antarctic records with O_2/N_2 chronologies were shifted no more than 2.2 ky, within quoted errors.

surface, thereby increasing both the average surface temperature and the area of the ice sheet grounded below sea level. Both of these responses would predispose an ice sheet to collapse.

The amount and rate of insolation rise may also be important controls on ice sheets. All four terminations occur when the magnitudes of insolation rise (Fig. 4B), along with the maximum in the rate of insolation rise (Fig. 4C), are average or above average in value, which may be critical in driving the termination to completion. Supporting this idea is the observation that the two terminations (T-I and T-III) interrupted by interstadials (BA and BA-III) are associated with relatively low insolation shifts and rates of insolation change. In contrast, the uninterrupted (T-IV) and minimally interrupted (T-II) terminations are associated with high shifts and rates. Additional observations also support this view. The lowest insolation value in the last 400 ky is at 229 ky B.P., and the highest is at 218 ky B.P., with the highest magnitude and rate of rise occurring between these times (Fig. 4, B and C). The highest $\delta^{18}O$ values (corresponding to the weakest monsoon) in the Sanbao record is between 227 to 229 ky B.P. (Fig. 4 and fig. S5), corresponding to the beginning of the insolation rise. On the basis of its correlation to an IRD peak in ODP 980 (*8*), we observe that this event takes place during the early portion of the transition from MIS 7.4 to MIS 7.3. Moreover (as described below for the main terminations), by correlating the cave and the Antarctic ice-core records, we observe relationships similar to those of the main terminations for CO_2 and Antarctic temperature. We view this set of events as an extra termination (T-IIIA) that takes place one precession cycle after T-III, which is probably the result of unusually low insolation that rapidly generates a large ice sheet, followed by unusually high insolation that triggers collapse.

Correlations with Antarctic ice cores. As with T-I and T-II (*6*), abrupt monsoon changes during T-III and T-IV were probably contemporaneous with methane shifts observed in Antarctic cores. We applied this correlation (Fig. 3) to the Vostok (*36*), Fuji Dome (*37*), and European Project for Ice Coring in Antarctica (EPICA)/Dome C (*38*, *39*) cores. Ages based on this correlation of the cave chronologies agree within the uncertainties with ages for those cores with O_2/N_2 chronologies [Vostok (*40*) and Fuji Dome (*37*)]. We can now add CO_2, Antarctic temperature/hydrogen isotope ratio (δD), Antarctic dust, and $\delta^{18}O$ of O_2 to the marine and cave records, all on the cave chronology. For each termination, Antarctic temperature rise takes place during the WMI (or WMIs), broadly paralleling the benthic marine termination and the rising limb of the insolation curve. As in T-I, the rise in temperature during T-III reverses at about the same time as BA-III, a feature we term ACR-III.

For each termination, the CO_2 rise also broadly parallels the marine termination and the insolation rise. The idea of a CO_2 rise synchronous with the marine termination differs from some earlier work, which suggested that the marine termination lagged the CO_2 rise by several millennia (*41*) on the basis of an observed lag in $\delta^{18}O$ of atmospheric O_2 relative to CO_2 (Fig. 3). The basis for the earlier argument is the known link between $\delta^{18}O$ of O_2 and $\delta^{18}O$ of seawater. It is now known that there is also a strong correlation between the $\delta^{18}O$ of O_2 and Chinese cave $\delta^{18}O$ (*11*, *42*). This link is reinforced by the observed similarity between $\delta^{18}O$ of O_2 and Sanbao cave $\delta^{18}O$ for T-II through T-IV (Fig. 3). On the basis of these relationships, we argue that the main shift in $\delta^{18}O$ of O_2 during each of the last four terminations results from the abrupt change in the hydrologic cycle, which we observe as the abrupt shift in cave $\delta^{18}O$ that marks the end of the last WMI in each termination. Because of the ~1 ky residence time of O_2 in the atmosphere (*43*), the change in $\delta^{18}O$ of O_2 is more gradual than the cave $\delta^{18}O$ shift and appears slightly lagged. Ironically, in this view, the change in the $\delta^{18}O$ of O_2 is related to the termination but, rather than tracking the termination directly, is delayed by the termination itself until the end of the last WMI. The observation that termination and CO_2 rise are broadly synchronous is important because CO_2 can be considered one of the drivers of the termination (along with boreal summer insolation rise). Mechanisms involving positive feedbacks between sea-level and atmospheric CO_2 should now be reconsidered.

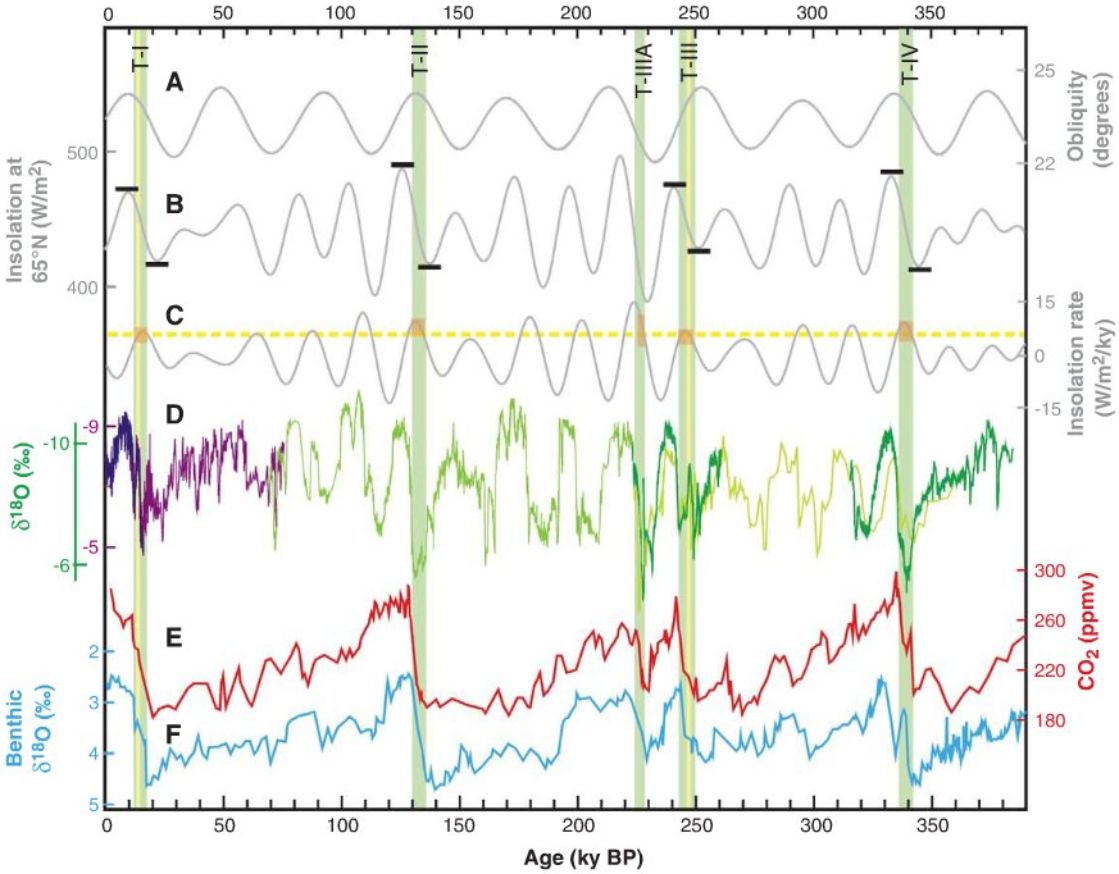

Fig. 4. (**A**) Obliquity (*29*) and (**B**) 21 July insolation at 65°N (*29*). Black bars highlight the highest and lowest insolation value bounding each major termination. (**C**) Rate of change of 21 July insolation at 65°N (*29*). Red shading indicates the timing of the WMIs. The yellow dashed line indicates the lowest maximum for the four terminations. (**D**) $\delta^{18}O$ from Hulu (purple) (*7*), Dongge Caves (dark blue) (*10*), Sanbao Cave [light green (*11*), dark green (this study)], and Linzhu Cave [yellow-green (this study)]. (**E**) Vostok CO_2 record (*36*) on a time scale created by interpolating linearly between methane-cave correlation points on each of the four terminations and T-IIIA. (**F**) Benthic $\delta^{18}O$ values for ODP 980 (*8*) on a time scale created by interpolating linearly between IRD-cave correlation points on each of the four terminations and T-IIIA. Light green and yellow vertical bars are the same as in Fig. 2.

Termination mechanisms. On the basis of our data, we envision that rising insolation triggers the initial disintegration of a massive, isostatically compensated ice sheet, which in turn triggers a slowing of MOC and hence a lowering of surface-ocean heat flux to the North Atlantic. Along with sea-ice formation, this collapse generates a cold anomaly in the North Atlantic, which weakens the AM through atmospheric teleconnections (*26*, *27*) and also moves the Intertropical Convergence Zone (ITCZ) to the south (*44*–*46*). Antarctic temperature increase could result from CO_2 rise, from the bipolar seesaw mechanism (*20*, *47*–*51*), and from southward shifts in atmospheric circulation patterns (*52*).

A number of mechanistic ties between this set of events and CO_2 rise seem plausible. First, simple southward movement of climatic zones [observed for ITCZ (*45*) and southern Brazil (*52*)] could include a southward shift in the westerlies (*53*), resulting in enhanced wind-driven upwelling in the ocean around Antarctica, promoting ventilation of respired CO_2, atmospheric CO_2 rise, and observed productivity peaks (*54*). Second, warming from the bipolar seesaw mechanism could melt sea ice in the Southern Ocean, also promoting CO_2 ventilation (*55*). Third, warming associated with southerly shifts in climate zones could reduce Patagonian glaciation, lowering the flux of dust and iron from Patagonia to the Southern Ocean, reducing the efficiency of the biological pump (*56*). There are limits (imposed by bounds on the glacial-interglacial change in the carbonate compensation depth) on the extent to which alkalinity-based mechanisms can contribute to the CO_2 rise (*57*, *58*). However, within these limits, it is plausible that alkalinity-based mechanisms may contribute. Given the broad synchrony between terminations and CO_2 rise, alkalinity-based feedbacks between sea level and atmospheric CO_2, such as the coral reef hypothesis (*59*), may well contribute once the sea level begins to rise. Archer *et al.* (*57*) argued that no single mechanism could explain the full glacial-interglacial range in CO_2. Here, we present a scenario in which CO_2 rise could be caused by a set of mechanisms all ultimately linked to the rise in boreal summer insolation. Both rising insolation and rising CO_2 (*60*–*62*), generated with multiple positive feedbacks, drove the termination.

References and Notes

1. C. Emiliani, *J. Geol.* **63**, 538 (1955).
2. W. S. Broecker, J. van Donk, *Rev. Geophys. Space Phys.* **8**, 169 (1970).
3. J. D. Hays, J. Imbrie, N. J. Shackleton, *Science* **194**, 1121 (1976).
4. Materials and methods are available as supporting material on *Science* Online.
5. H. Heinrich, *Quat. Res.* **29**, 142 (1988).
6. H. Cheng *et al.*, *Geology* **34**, 217 (2006).
7. Y. J. Wang *et al.*, *Science* **294**, 2345 (2001).
8. J. F. McManus, D. W. Oppo, J. L. Cullen, *Science* **283**, 971 (1999).
9. M. J. Kelly *et al.*, *Palaeogeogr. Palaeoclimatol. Palaeoecol.* **236**, 20 (2006).
10. C. A. Dykoski *et al.*, *Earth Planet. Sci. Lett.* **233**, 71 (2005).
11. Y. J. Wang *et al.*, *Nature* **451**, 1090 (2008).
12. C. H. Hendy, *Geochim. Cosmochim. Acta* **35**, 801 (1971).
13. W. Dansgaard, *Tellus* **16**, 436 (1964).
14. K. R. Johnson, B. L. Ingram, *Earth Planet. Sci. Lett.* **220**, 365 (2004).
15. D. Fleitmann *et al.*, *Quat. Sci. Rev.* **26**, 170 (2007).
16. A. Sinha *et al.*, *Geology* **33**, 813 (2005).
17. C. Hu *et al.*, *Earth Planet. Sci. Lett.* **266**, 221 (2008).
18. R. B. Alley *et al.*, *Nature* **362**, 527 (1993).
19. G. Bond *et al.*, *Nature* **365**, 143 (1993).
20. W. S. Broecker, D. M. Peteet, D. Rind, *Nature* **315**, 21 (1985).
21. J. F. McManus, R. Francois, J. M. Gherardi, L. D. Keigwin, S. Brown-Leger, *Nature* **428**, 834 (2004).
22. J. C. H. Chiang, M. Biasutti, D. S. Battisti, *Paleoceanography* **18**, 1094 10.1029/2003PA000916 (2003).
23. G. H. Denton, R. B. Alley, G. C. Comer, W. S. Broecker, *Quat. Sci. Rev.* **24**, 1159 (2005).
24. W. S. Broecker, *Global Planet. Change* **54**, 211 (2006).
25. H. F. Blanford, *Proc. R. Soc. London* **37**, 3 (1884).
26. T. P. Barnett, L. Dümenil, U. Schlese, E. Roeckner, *Science* **239**, 504 (1988).
27. R. Zhang, T. L. Delworth, *J. Clim.* **18**, 1853 (2005).
28. G. H. Denton, W. S. Broecker, R. B. Alley, *Pages News* **14**, 14 (2006).
29. A. L. Berger, *Quat. Res.* **9**, 139 (1978).
30. J. Imbrie *et al.*, in *Milankovitch and Climate, Part I*, A. Berger, J. Imbrie, J. Hays, G. Kukla, B. Saltzman, Eds. (Reidel, Norwell, MA, 1984), pp. 269–305.
31. L. G. Thompson *et al.*, *Science* **298**, 589 (2002).
32. R. B. Alley, P. U. Clark, P. Huybrechts, I. Joughin, *Science* **310**, 456 (2005).
33. G. E. Birchfield, W. S. Broecker, *Paleoceanography* **5**, 835 (1990).
34. W. R. Peltier, *Science* **265**, 195 (1994).
35. M. E. Raymo, *Paleoceanography* **12**, 577 (1997).
36. J. R. Petit *et al.*, *Nature* **399**, 429 (1999).
37. K. Kawamura *et al.*, *Nature* **448**, 912 (2007).
38. L. Loulergue *et al.*, *Nature* **453**, 383 (2008).
39. J. Jouzel *et al.*, *Science* **317**, 793 (2007).
40. M. Suwa, M. Bender, *Quat. Sci. Rev.* **27**, 1093 (2008).
41. N. J. Shackleton, *Science* **289**, 1897 (2000).
42. J. P. Severinghaus *et al.*, *Science* **324**, 1431 (2009).
43. M. Bender, T. Sowers, L. Labeyrie, *Global Biogeochem. Cycles* **8**, 363 (1994).
44. L. C. Peterson, G. H. Haug, K. A. Hughen, U. Röhl, *Science* **290**, 1947 (2000).
45. X. F. Wang *et al.*, *Nature* **432**, 740 (2004).
46. J. C. H. Chiang, C. M. Bitz, *Clim. Dyn.* **25**, 477 (2005).
47. T. J. Crowley, *Paleoceanography* **7**, 489 (1992).
48. T. F. Stocker, D. G. Wright, L. A. Mysak, *J. Clim.* **5**, 773 (1992).
49. W. S. Broecker, *Paleoceanography* **13**, 119 (1998).
50. T. Blunier, E.J. Brook, *Science* **291**, 109 (2001).
51. T. F. Stocker, S. J. Johnsen, *Paleoceanography* **18**, 1087 (2003).
52. X. F. Wang *et al.*, *Geophys. Res. Lett.* **34**, L23701 10.1029/2007GL031149 (2007).
53. J. R. Toggweiler, J. L. Russell, S. R. Carson, *Paleoceanography* **21**, 2005 (2006).
54. R. F. Anderson *et al.*, *Science* **323**, 1443 (2009).
55. R. F. Keeling, B. B. Stephens, *Paleoceanography* **16**, 112 (2001).
56. J. H. Martin, S. E. Fitzwater, *Nature* **331**, 341 (1988).
57. D. Archer, A. Winguth, D. Lea, N. Mahowald, *Rev. Geophys.* **38**, 159 (2000).
58. D. M. Sigman, E. A. Boyle, *Nature* **407**, 859 (2000).
59. B. N. Opdyke, J. C. G. Walker, *Geology* **20**, 733 (1992).
60. D. Paillard, *Rev. Geophys.* **39**, 325 (2001).
61. J. P. Severinghaus, *Nature* **457**, 1093 (2009).
62. P. U. Clark, A. M. McCabe, A. C. Mix, A. J. Weaver, *Science* **304**, 1141 (2004).

63. We thank the late Gary Comer for his generous support and J. Severinghaus, V. Masson-Delmotte, and P. Clark for valuable suggestions. This work was supported by U.S. NSF grant 0502535, Gary Comer Science and Education Foundation grant CC8, NOAA grants to G.H.D., and National Natural Science Foundation of China grants 40631003 and 40771009.

Supporting Online Material

www.sciencemag.org/cgi/content/full/326/5950/248/DC1
Materials and Methods
SOM Text
Figs. S1 to S5
Tables S1 and S2
References

17 June 2009; accepted 14 September 2009
10.1126/science.1177840

Reactome Array: Forging a Link Between Metabolome and Genome

Ana Beloqui,[1]* María-Eugenia Guazzaroni,[1]* Florencio Pazos,[2] José M. Vieites,[1] Marta Godoy,[2] Olga V. Golyshina,[3] Tatyana N. Chernikova,[3] Agnes Waliczek,[3] Rafael Silva-Rocha,[2] Yamal Al-ramahi,[1] Violetta La Cono,[4] Carmen Mendez,[5] José A. Salas,[5] Roberto Solano,[2] Michail M. Yakimov,[4] Kenneth N. Timmis,[3,6] Peter N. Golyshin,[3,7,8]†‡ Manuel Ferrer[1]†‡

We describe a sensitive metabolite array for genome sequence–independent functional analysis of metabolic phenotypes and networks, the reactomes, of cell populations and communities. The array includes 1676 dye-linked substrate compounds collectively representing central metabolic pathways of all forms of life. Application of cell extracts to the array leads to specific binding of enzymes to cognate substrates, transformation to products, and concomitant activation of the dye signals. Proof of principle was shown by reconstruction of the metabolic maps of model bacteria. Utility of the array for unsequenced organisms was demonstrated by reconstruction of the global metabolisms of three microbial communities derived from acidic volcanic pool, deep-sea brine lake, and hydrocarbon-polluted seawater. Enzymes of interest are captured on nanoparticles coated with cognate metabolites, sequenced, and their functions unequivocally established.

Functional genomics has greatly accelerated research on the genomic basis of life processes in health and disease and provided a quantum advance in our understanding of such processes, their regulation, and underlying mechanisms (*1*). Functional assignments and metabolic network reconstructions have generally depended on both the genome sequence of the organism(s) in question and bioinformatic analyses based on homology to known genes and proteins

(*2*–*6*). However, many genes in databases have questionable annotations or are not annotated at all (*7*–*9*), which hinders effective exploitation of the rapidly growing volume of genome sequence data. Metabolomics provides new insights into the metabolic state of a cell under a given set of environmental parameters, or in response to a parameter change, independently of a genome sequence, although problems of metabolite identification and quantification exist (*10*–*12*). Functionally associating the metabolic profile obtained with the enzymes and pathways responsible still depends heavily on sequenced-based metabolic reconstructions. There is thus a need for a new method to causally link metabolites with cognate enzymes, which, in addition to delivering global descriptions of metabolic responses to given environmental conditions, simultaneously provides annotation of the enzymes featured. The "reactome array" we describe here forges this link between genome and metabolome and provides a global metabolic phenotype of a cell extract derived from a clonal population of cells or a mixture of cell types, as is found in clone libraries, tissues, or multicellular organisms. The array constitutes a generic tool for metabolic phenotyping of cells and annotation of proteins and has applications in diverse aspects of biology and medicine.

The reactome array. We synthesized 1676 metabolites—known from the Kyoto Encyclopedia of Genes and Genomes (KEGG) database (*13*) to collectively represent central metabolic pathways in all organisms—and 807 other substrate molecules (*14*). We coupled these to the dye Cy3 and to a linker molecule used to immobilize the compounds on glass slides to produce the array (fig. S1). The compounds printed on the array are characterized by two key features (Fig. 1). One is that the Cy3 dye component of the compound as synthesized is inactive, as a result of intramolecular resonance quenching. Productive catalytic action of an enzyme on the substrate results in the release of the reaction product and the dye, thereby relieving the quenching such that the dye becomes activated and gives a fluorescent signal (movie S1). The arrayed metabolites (~0.7 fmol/spot; $P < 0.011$, $N = 9$) provided detections down to absolute concentrations of 5.7 ng protein/ml ($P < 0.043$, $N = 12$) (fig. S2). Even at the lowest enzyme concentrations, no signal interference by proteins or other substances in cell lysates down to a target:total protein ratio of $1{:}10^6$ (total concentration, 100 μg/ml) was detected (fig. S2). Such sensitivity is sufficient for activity determination of enzymes in many types of sample, including clinical samples. Nonproductive interactions of proteins with the metabolites—binding without chemical change—do not release either the substrate or the dye and thus do not relieve dye quenching. The reactome array contained a total number of 2483 metabolites (tables S1 and S2) that collectively serve as substrates in all metabolic pathways figuring in the KEGG and PubMed databases and the University of Minnesota Biocatalysis/Biodegradation Database.

The nature of the linker molecule, a Co(II) complex containing a poly(A) tail, is such that productive reaction of an enzyme with the substrate leads to release of both histidine "tags" anchored to the Co(II), thereby exposing an active cobalt cation which ligates and immobilizes the enzyme on the array spot (Fig. 1 and fig. S1). This feature is exploited to capture for characterization enzymes determined from the array as being of interest. In this case, individual compounds are attached via their linkers to gold nanoparticles (Fig. 2A), which serve as high-capacity capture probes for cognate enzymes (a concentration of 9×10^{10} particles/ml of diameter ~2.9 ± 0.8 nm, corresponds to a surface area of ~141 ± 3 cm^2/ml that displays 62.5 pmol of substrate with a binding capacity of 3 to 18 pmol protein per ml). Nanoparticles are mixed with the cell lysate to allow enzyme reaction with the substrate; this in turn results in its selective capture by the nanoparticle, which is readily recovered. The captured protein is then released in essentially pure form for characterization by imidazole treatment of the nanoparticle (*14*).

The reactomes of *Pseudomonas putida* and *Streptomyces coelicolor*. To validate the reactome array, we used it to determine the metabolic profiles of cultures of the bacteria *P. putida* strain KT2440 (Pp) and *S. coelicolor* strain M145 (Sc). The genomes of both organisms have been sequenced and, according to current annotations, of the 1676 KEGG metabolites printed in the array, 595 should be metabolized by Pp and 598 by Sc, whereas 1081 and 1033, respectively, should not (*13*). The reactome profiles are displayed in fig. S3. The fluorescence signal (table S3; $P < 0.0255$, $N = 9$) was used as the score for the receiver operating characteristic (ROC) analysis (*15*), based on the assumption of a positive relationship between spot intensity in the array and metabolism of the compound by Pp or Sc extracts (figs. S4 and S5). Over an optimal value of 1.0, the score obtained of 0.74 ($P = 1.73e^{-71}$) and 0.85 ($P = 5.77e^{-172}$), for Pp and Sc, respectively, indicates that the array readily discriminates compounds metabolized by extracts of both organisms from those that are not. These values are reasonably high, given that the composition of the array is based on the assumption that the reactions carried out by Pp and Sc are those annotated in KEGG, and that this is obviously not true, because the reactome array has revealed the existence of reactions not annotated in KEGG.

Reactome-based (re)annotations. At present, the rate of generation of genomic sequence data

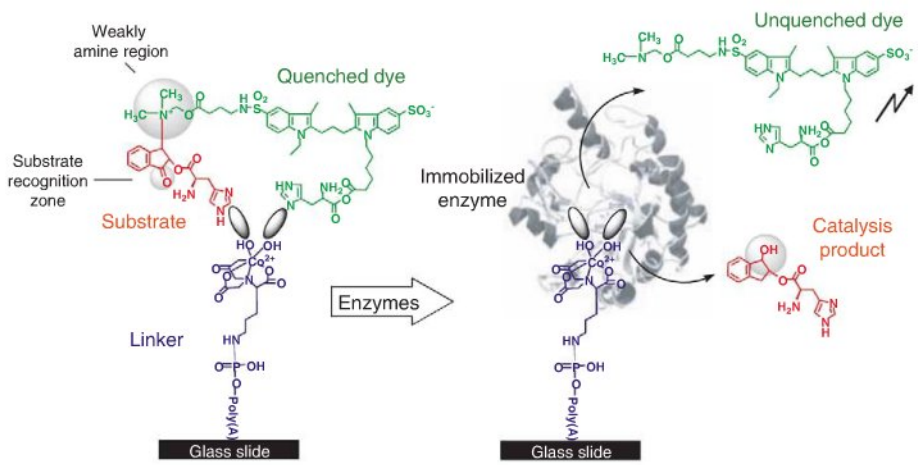

Fig. 1. The reactome strategy. The generic structure of reactome metabolites involves three linked components: the enzyme substrate-metabolite, the quenched dye, and the linker used to immobilize the complex on the array or on nanoparticles. The substrate-metabolite is linked to the quenched dye through a labile nitrogen bond, and both the dye and the substrate are anchored to the Co(II)-containing poly(A) linker by histidine "tags." Details of the synthetic strategy are provided in fig. S1. An enzyme-catalyzed chemical change in the substrate at a position adjacent to the weakly amine region causes rupture of the labile nitrogen:metabolite bond and release of the quenched Cy3 dye. This in turn provokes release of the reaction product and the histidine "tags" anchored to the Co(II), thereby exposing an active cobalt cation that ligates and immobilizes the enzyme on the array spot. The released dye is no longer quenched and gives a fluorescent signal. The nature of the reaction and the catalysis product is defined by the position to which the quenched dye and the substrate are linked (table S2).

[1]CSIC, Institute of Catalysis, 28049 Madrid, Spain. [2]CSIC, Centro Nacional de Biotecnología, 28049 Madrid, Spain. [3]HZI-Helmholtz Centre for Infection Research, 38124 Braunschweig, Germany. [4]Institute for Coastal Marine Environment, CNR, Messina 98122, Italy. [5]Universidad de Oviedo, 33006 Oviedo, Spain. [6]Institute of Microbiology, Carolo-Wilhelmina Technical University of Braunschweig, 38106 Braunschweig, Germany. [7]School of Biological Sciences, Bangor University, Gwynedd LL572 UW, UK. [8]Centre for Integrated Research in the Rural Environment, Aberystwyth University-Bangor University Partnership (CIRRE).

*These authors contributed equally to this work.
†These authors contributed equally to this work.
‡To whom correspondence should be addressed. E-mail: mferrer@icp.csic.es (M.F.); p.golyshin@bangor.ac.uk (P.N.G.)

outstrips our ability to analyze and usefully exploit this data (*16*). There is a lack of functional information about many open reading frames (ORFs) and an incorrect annotation of some others (*7*). To establish sequence:function relationships for proteins reacting with the array, we created a suite of 528 batches of gold nanoparticles, each batch covered with an individual metabolite found to be metabolized by the *P. putida* extract and collectively representing the entire Pp reactome. Each type of nanoparticle was separately reacted with the Pp cell lysate and recovered by centrifugation, and then the unbound enzyme was removed by washing with buffer. Captured enzyme(s) was released by imidazole and identified by trypsin digestion and mass spectrometry peptide sequencing (Fig. 2A). 549 proteins were captured by the nanoparticles, of which 191 enzymes acting on 158 of the 525 metabolites were unambiguously identified (table S4) and their functions assigned.

As shown in the left panel of Fig. 2B, overall the captured enzymes exhibited a noticeable bias toward functions relating to xenobiotic (33%) and amino acid metabolism (31%). New functional assignments and annotations were defined for 31 enzymes (16%) that had been previously predicted from genome sequence analysis but not characterized as proteins (Fig. 2B, middle panel). These include oxidoreductases, synthases, ligases, kinases, deacetylases, transferases, decarboxylases, nucleosidases, and DNA-metabolizing proteins and were assigned to pathways for xenobiotic (55%), amino acid (19%), carbohydrate (11%), and secondary metabolite (7%) metabolism. Biochemical characterization of 23 out of 31 hypothetical proteins identified by array mapping and further captured in essentially pure form confirmed their activities (Fig. 2C and fig. S6A). This analysis revealed enzymatic potential for *p*-cymene and 4-chlorobiphenyl metabolisms in *P. putida* that have not thus far been predicted by genome analysis of Pp (fig. S6B). The analysis of a further 25% resulted in improved annotations, and the activities of the remaining 59% of enzymes were consistent with current annotations in the databases (Fig. 2B, right panel). All together, these findings expand the extensive potential catabolic landscape of this bacterium (*17*) and will facilitate future genome annotations, because the majority of these genes are highly conserved in other organisms.

The reactomes of microbial communities of diverse habitats. The results obtained with model organisms for which genome sequences are available confirmed that the reactome array constitutes a means of obtaining a genome-wide overview of the metabolic status of a population of cells. Because all metabolic pathways documented in the main databases are represented by metabolites on the reactome array, and because a subset of these—the core metabolites—are characteristic of all life forms, it should enable such overviews to be obtained of the cells of essentially any organism, and even of communities of multiple species. In the latter case, the quality of the metabolic overview obtained will depend upon the complexity of the natural or experimental community, the sensitivity of the reactome array, and the possible inclusion on the array of additional metabolites specific to the habitat and metabolism of the habitat community members.

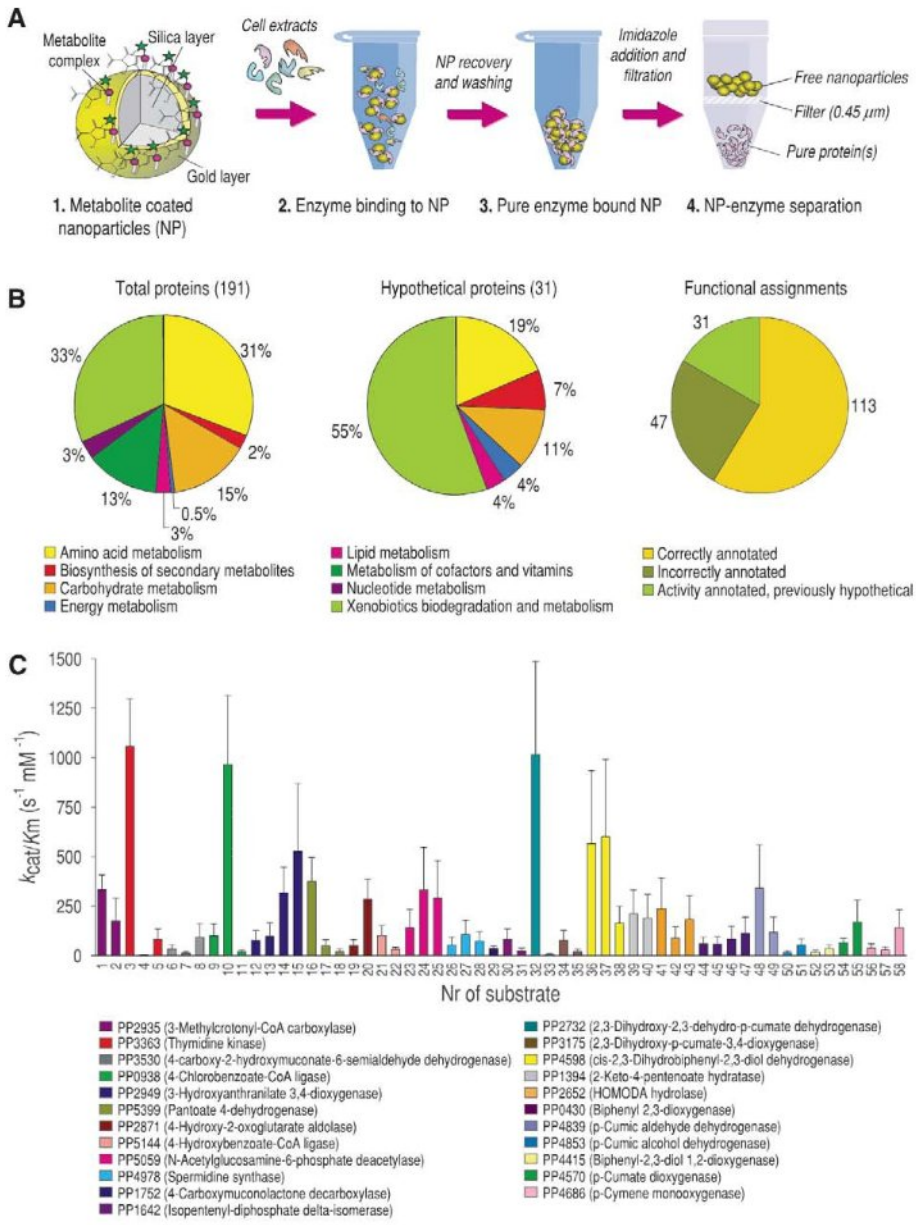

Fig. 2. Nanoparticle capture and functional characterization of hypothetical proteins of *P. putida*. (**A**) The nanoparticle (NP) strategy for protein capture and analysis is summarized in the scheme. NP coated with a single metabolite complex is allowed to react with the cell lysate. An enzyme able to transform the substrate becomes captured by the Co(II) cation of the linker and immobilized on the NP. After recovery of the NP by centrifugation, and washing to remove unbound enzymes, the specifically captured enzyme(s) is released by imidazole treatment of the NP, separated in pure form from the NP by filtration, sequenced, and functionally characterized. In the case where more than one enzyme binds to the substrate on the NP, a further separation will be necessary. (**B**) Functional assignments of *P. putida* proteins detected by the array. On the left is shown the distribution of functional classes of the 191 enzymes captured on NPs and further unambiguously identified and characterized. This provided a direct activity annotation and thereby allowed us to determine which previous genomic annotations were correct. The middle element shows the distribution of the functional classes of the 31 (previously) hypothetical proteins. On the right is shown the distribution of correctly and incorrectly genome-annotated enzymes and of new direct activity annotated proteins. (**C**) Substrate spectra and steady-state k_{cat}/K_m kinetic parameters of 23 previously hypothetical proteins that were NP-capture purified and that are color coded as indicated in the lower part of the figure. Substrate names (*14*) and K_m and k_{cat} values are shown in fig. S6. Other substrates tested but for which no activity was detected are shown in table S4C. Data represent the mean ± SEM of four independent measurements.

In some instances, environmental samples will not contain enough biomass for the array analysis, either because organism concentrations are very low or because only small samples can be acquired. In this case, the genetic information present in the samples can be harvested and archived in a laboratory host microbe, like *Escherichia coli* K-12, to create genomic libraries of multiple species, so-called "metagenomic libraries." We investigated whether useful information on the metabolic profiles of microbial communities can be obtained from such libraries, despite the differences in physiology and expression apparati of the donor organisms and those of *E. coli*, different habitat conditions, and so on. If so, this would allow functional exploration of communities characteristic of extreme and difficult-to-sample environments, such as hydrothermal vents, and of slow-growing communities in nutrient-poor habitats.

We obtained samples from three very distinct habitats: a low-nutrient, heavy metal–rich, acidic geothermal pool on Vulcano Island in the Tyrrhenian Sea (VUL); a nutrient-rich, organic pollutant–contaminated surface seawater near Kolguev Island in the Barents Sea (KOL); and the seawater-brine interface of the L'Atalante deep-sea hypersaline, anoxic lake (L'A) in the Eastern Mediterranean Sea. To obtain sufficient genomic DNA for library construction, we stimulated multiplication of the cells in the samples by adding growth substrates: Fe(II) to 100 mM plus yeast extract to 0.02% (VUL); crude oil to 0.2% (KOL); and D-glucose to 2 mM (L'A), and subsequently harvested the resulting microbial communities, extracted their total DNA, and established metagenome libraries in *E. coli*. To determine which species of microorganisms were present in each community, we used the DNA obtained from each sample as substrate for amplification of 16S rRNA genes by polymerase chain reaction (PCR). The amplicons thereby obtained were cloned to produce 16S rRNA gene libraries, and representative numbers of the clones were sequenced and taxonomically assigned through use of standard GenBank database homology search tools and phylogeny analysis packages (*14*). The compositions of the three communities are depicted in fig. S7. The VUL community was not very diverse and was dominated by acidophilic iron-oxidizing eubacterial species of *Acidithiobacillus* and acidophilic species of heterotrophic *Bacillus* and *Alicyclobacillus*. Species of the extremely acidophilic archaeon *Ferroplasma* were present in small amounts. In contrast, the KOL community was diverse and included various petroleum-degrading organisms belonging to the gamma- and epsilon-proteobacteria, such as species of *Pseudomonas*, the hydrocarbonoclastic bacterium *Thalassolituus*, and the denitrifying bacterium *Arcobacter*. The least diverse community was that of L'A, which consisted essentially of two strains distantly related to *Halanaerobium kushneri*.

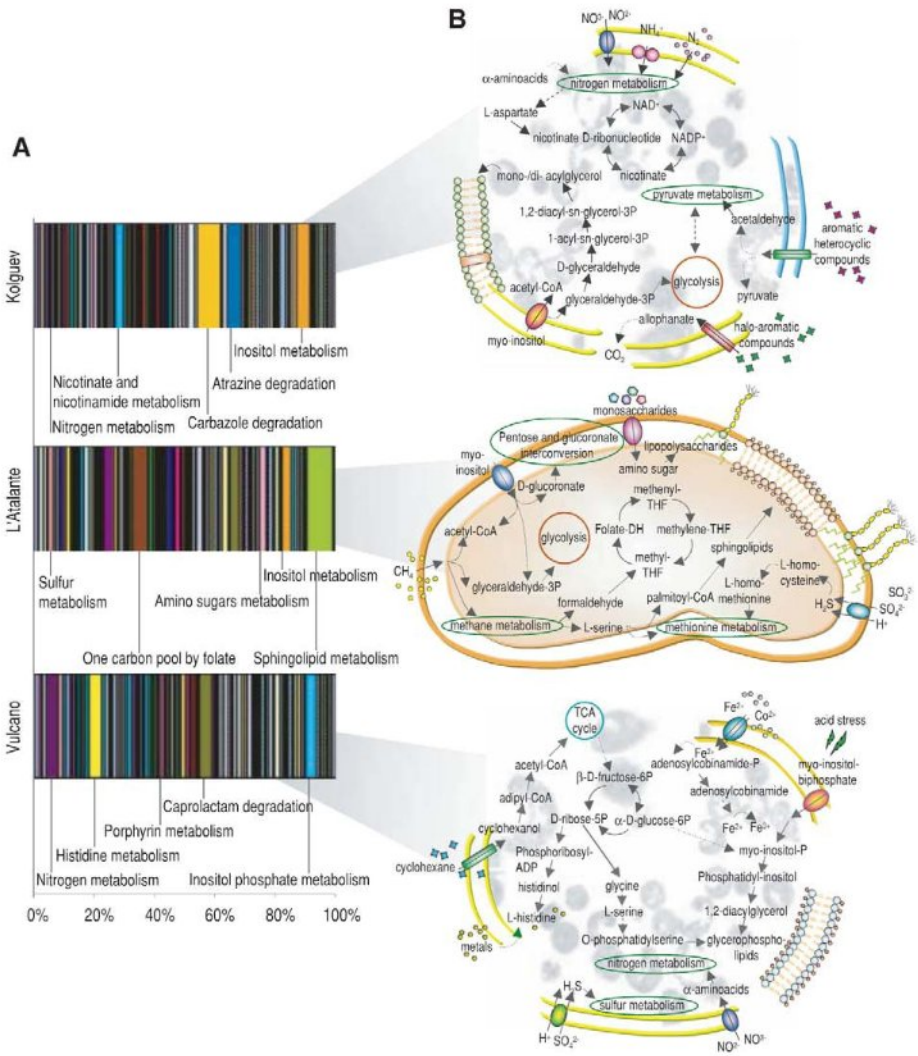

Fig. 3. Functional profiling and metabolic reconstruction of the metagenome library representations of the L'A, KOL, and VUL communities. (**A**) We used the relative proportion of *z* scores (log scale) provided in fig. S10 to rank KEGG functions in the three metagenome libraries. The detailed metabolic profiles (reactome "barcodes") are clearly distinct; the most distinctive metabolic characteristics are labeled. (**B**) Depiction of the distinguishing metabolic features of the communities in the context of their pan-metabolic networks. The L'A community consists essentially of two related species, so we have represented its metabolic network in the context of a single cell, whereas the other communities are diverse, with their pan-metabolic networks represented as a "meta cell," with fragmented membranes indicating facile exchange of metabolites between different community members of the "multicellular community organism." The metabolic networks depicted of the L'A, KOL, and VUL communities were constructed from the reactome array data from the 1676 metabolites that can be automatically found in KEGG. Tight coupling between major metabolic pathways is indicated.

The pan-reactomes of the three microbial communities were determined by application of cell lysates of pooled clones to the arrays (table S3; $P < 0.0381$, $N = 9$). Cell lysates of the parental, nonrecombinant *E. coli* strain used for library construction, and grown and treated under the same conditions, were used to produce a baseline pattern that was subtracted from those obtained with the library lysates to give the pan-reactome patterns (fig. S8). The VUL reactome consisted of enzymatic reactions involving 807 substrates, the KOL reactome involved 1493 compounds, and the L'A reactome included 2386 compounds (fig. S9). A total of 484 substrates were metabolized by extracts of all three communities, but the detailed metabolic profiles were clearly distinct (Fig. 3 and figs. S10 to S12), presumably reflecting niche-specific metabolic profiles expected of communities occupying distinct habitats.

The L'Atalante hypersaline lake has a high density, and its surface acts as a trap for organic detritus ("marine snow") and larger bioorganic material sedimenting through the water column (*18*). The major metabolic activities within the anoxic brine are sulfate reduction and methanogenesis (*16*). Metabolism in the brine-seawater interface is therefore expected to reflect (i) the slow input of diverse organic materials from above; (ii) the input of methane and sulfide from below, and other electron acceptors and donors and various metals, whose concentrations vary

steeply across the interface and which are cycled through various redox states and balances by the stratified microbial communities; and (iii) the steep gradients of salinity and redox potential.

Some of the features that distinguish the L'A reactome from those of VUL and KOL are high activity levels of sulfur, one-carbon pool-folate, amino-sugar and sphingolipid metabolisms, and low-nitrogen, porphyrin, nicotinate-nicotinamide and riboflavin metabolisms, pentose phosphate and glycolysis-gluconeogenesis pathway activity, and glycerol(phospho)lipid metabolism (Fig. 3 and fig. S12). The predominance of sulfur metabolism reflects the role of sulfide, produced by sulfate reduction in the underlying brine, as the primary source of energy in this system. The predominance of folate reactions (second highest Z_i value) (fig. S10) probably reflects a high proportion of one-carbon biochemistry (*19*). The predominance of inositol and amino-sugar pathways may reflect high-level production of osmoprotectants, as cellular adaptation to the prevailing high salt conditions and associated osmotic stress. Enzymes of sphingolipid metabolism represented almost 9% of the total reactome and 66% of all lipid biosynthetic pathways present on the array. Sphingolipids are thought to protect the cell surface against harmful environmental factors and can function as important signaling molecules involved in responses to a variety of stresses (*20*). Although the sample cultivations are expected to have resulted in population-level reductions of some microbial species present in the original source environment, sequence analysis of the 16S rRNA gene library created from the L'A sample (fig. S7) revealed that all of 96 clones analyzed belonged to a single group of halophilic anaerobes, the *Halanaerobium*-like organisms, that includes both fermenting and sulfur- and thiosulphate reducers (*H. congolensis*) (*21*). A pyrosequencing analysis of the L'A metagenome also indicated the presence of a methanogenic euryarchaeon related to *Methanosarcina* (*14*), which is consistent with methanogenic activity in the habitat. Thus, despite the biases inherent in both enrichment cultivations and metagenome libraries, there is reasonable consistency among habitat characteristics, the microbial community reactome, and the phylogeny and presumed physiology of the microbes present in the L'A sample.

KOL is a petroleum oil–enriched seawater sample from near the Port of Kolguev Island in the Barents Sea. Water in this area has a temperature of about 1°C in summer, when the sample was taken, and is chronically polluted from on-shore oil mining operations and shipping traffic. The main feature of the KOL metagenome reactome was a rich profile of hydrocarbon and organic utilization pathway activities, including those for the (halo)aromatics carbazole and atrazine (Fig. 3 and fig. S12). This is consistent both with the conditions prevailing in the source habitat and the sample enrichment culture derived from it and with the composition of the enrichment (determined by sequence analysis of a 16S rRNA gene library prepared from it), in which members of the genus *Thalassolituus*, hydrocarbonoclastic bacteria specialized in the degradation of aliphatic and aromatic fractions of crude oil (*22*), represent some 33% of the entire community (fig. S7). Other distinguishing features of the KOL reactome were a prevalence of carbon fixation and denitrification and nitrogen metabolism activities as energy-source mechanisms and weak signals for sulfur and methane metabolism. These are consistent with microbial photosynthetic, nitrogen fixation, and denitrification activities typically carried out in coastal surface waters and with the presence of *Roseobacter* sp. (4%), and *Arcobacter* (18%), *Pseudomonas* (40%) spp., and *Paracoccus denitrificans*, known specialists in phototrophic carbon fixation and nitrogen metabolism, respectively (table S5). Nicotinate and nicotinamide metabolism was also evident, which is consistent with a metabolism in which NAD-dependent enzymes, like dehydrogenases (*23*), play important roles.

The VUL sample represents an enrichment for ferrous iron- and sulfur-oxidizing microbes derived from the acidic sulfur- and iron-rich sediments of a hydrothermal (25 to 75°C) pool. The reactome of the metagenome library of VUL confirmed that nitrogen and sulfur pathways are major activities in this environment, consistent with two species, *Acidithiobacillus* and *Alicyclobacillus*, bacteria with iron- and sulfur-oxidizing activities and the ability to fix nitrogen (*24*), making up some 74% of the microbial community (fig. S7). One major feature of the reactome is the predominance of histidine pathway enzymes, which represent 24% of the entire amino acid metabolism activities and 4.3% of all metabolic activities measured by the array: This represents 4 to 5 times as many as that found with the other two communities (Fig. 3 and fig. S12). The hydrothermal pool contains iron-rich minerals, like jarosite [$KFe(III)_3(OH)_6(SO_4)_2$] and goethite [$FeO(OH)\cdot nH_2O$], at concentrations ranging from 3 to >500 mg per liter, and other heavy metals, which have maximum solubilities at low pH. Because intracellular histidine diminishes the pH-dependent toxicity of heavy metals, by sequestering them in the cytoplasm, the elevated histidine activity of the VUL sample might reflect adaptive responses to a selective pressure for histidine-mediated detoxification of heavy metals (*25*). The VUL community showed a high level of porphyrin metabolism, which represented about 20% of the entire cofactor and vitamin metabolism (up to 8 times as high as that in the other communities), and included cobalt-salvaging coenzyme B_{12} (cobalamin) precursor metabolism (fig. S13). It is possible that cobalt, an essential metal cofactor, is acquired and used more efficiently by the acidic community than the others (*26*, *27*). A feature of the VUL reactome not expected for the acidic hydrothermal pool was the high level of enzymatic activity with organic compounds like caprolactam, which suggests the presence of these or structurally related compounds in the source sediment, originating either from natural vent activity or anthropogenic pollution.

Applications of the reactome array. The reactome array reported here represents a tool to obtain a detailed and quantitative profile of the metabolic activity of a cell population or tissue, a cell consortium or organ, and an organism or consortium of organisms. It provides a "metabolic barcode" that can be compared with those of other samples. Because many of the metabolites on the array are connected in known pathway sequences, it is in principle possible to reconstruct much of the metabolic network operating in a cell or organism without any prior genomic information. Where genomic information is available, the array forges a link between metabolome and genome (fig. S3). The most detailed and cohesive metabolic network construction will be with a clonal population of cells, and the least cohesive with a diverse consortium of cell types, because of greater metabolic range and diversity, and cellular discontinuities in the global metabolism. Nevertheless, it is even possible to obtain useful information on the metabolic activity of microbial communities from environmental samples (fig. S14). This can lead to the discovery of unknown metabolic activities in organisms and communities (table S6), identification of metabolic components of niche specificity, and exposure of predominant microbial pathways shaping the characteristics of individual habitats.

The reactome array, and customized versions of it, may find applications in the large-scale metabolic characterization of cell lines, organisms, mutants, transgenes, and libraries thereof, or of mutant enzyme libraries, or in diagnostic tests. In evaluation of environmental pollution, the array would provide a measure of pollutant-metabolizing enzymes and thus a measure of the concentration of bioavailable pollutant. The rapidity of the reactome array and its format, which enables automation and high throughput, should facilitate its application in diagnostic procedures. The array may also contribute to enzyme discovery, because proteins can be identified and isolated directly from environmental samples or from source organisms, thereby circumventing expression cloning biases.

References and Notes

1. T. G. Whitham *et al.*, *Science* **320**, 492 (2008).
2. G. W. Tyson *et al.*, *Nature* **428**, 37 (2004).
3. M. T. P. Gilbert *et al.*, *Science* **317**, 1927 (2007).
4. J. F. Biddle *et al.*, *Proc. Natl. Acad. Sci. U.S.A.* **105**, 10583 (2008).
5. E. A. Dinsdale *et al.*, *Nature* **452**, 629 (2008).
6. M. G. Kalyuzhnaya *et al.*, *Nat. Biotechnol.* **26**, 1029 (2008).
7. T. Lombardot *et al.*, *Nucleic Acids Res.* **34**, D390 (2006).
8. J. Raes, P. Bork, *Nat. Rev. Microbiol.* **6**, 693 (2008).
9. T. A. Gianoulis *et al.*, *Proc. Natl. Acad. Sci. U.S.A.* **106**, 1374 (2009).
10. P. J. Turnbaugh, J. I. Gordon, *Cell* **134**, 708 (2008).
11. T. R. Northen *et al.*, *Proc. Natl. Acad. Sci. U.S.A.* **105**, 3678 (2008).
12. J. M. Vieites *et al.*, *FEMS Microbiol. Rev.* **33**, 236 (2009).
13. M. Kanehisa *et al.*, *Nucleic Acids Res.* **32**, D277 (2004).
14. Materials and methods are available as supporting material on *Science* online.
15. T. Fawcett, *Pattern Recognit. Lett.* **27**, 861 (2006).
16. R. F. Service, *Science* **311**, 1544 (2006).
17. J. I. Jimenez *et al.*, *Environ. Microbiol.* **4**, 824 (2002).
18. D. Daffonchio *et al.*, *Nature* **440**, 203 (2006).

19. E. Y. Huang *et al.*, *J. Bacteriol.* **179**, 5648 (1997).
20. Y. A. Hannun, C. Luberto, *Trends Cell Biol.* **10**, 73 (2000).
21. P. W. van der Wielen *et al.*, *Science* **307**, 121 (2005).
22. M. M. Yakimov *et al.*, *Curr. Opin. Biotechnol.* **18**, 257 (2007).
23. A. F. Pronk *et al.*, *J. Bacteriol.* **177**, 75 (1995).
24. O. V. Golyshina, K. N. Timmis, *Environ. Microbiol.* **7**, 1277 (2005).
25. D. A. Pearce, F. Sherman, *J. Bacteriol.* **181**, 4774 (1999).
26. J. D. Woodson *et al.*, *J. Bacteriol.* **185**, 7193 (2003).
27. Y. Jiao *et al.*, *Appl. Environ. Microbiol.* **71**, 4487 (2005).
28. This research was supported by the BIO2006-11738, CSD2007-00005, GEN2006-27750-C-4-E, BFU2008-04398-E/BMC, and KBBE-226977 projects. A.B and Y.A-R thank the Spanish MEC for the FPU and FPI fellowships. F.P. thanks the Spanish MEC for the BIO2006-15318 project. K.N.T, O.V.G., and P.N.G acknowledge the Federal Ministry for Science and Education (BMBF) for a grant in the framework of the BiotechGenoMik program, and K.N.T. thanks the Fonds der Chemischen Industrie for generous support. Authors are deeply indebted to A. Yanenko for sampling Kolguev Island coastal water and to the captain and crew of Research Vessel Urania for their assistance in deep-sea sampling in the Mediterranean Sea and to J. Manuel Franco for statistical analyses.

Supporting Online Material
www.sciencemag.org/cgi/content/full/326/5950/252/DC1
Materials and Methods
SOM Text
Figs. S1 to S14
Tables S1 to S6
References
Movie S1

26 March 2009; accepted 19 August 2009
10.1126/science.1174094

Unbiased Reconstruction of a Mammalian Transcriptional Network Mediating Pathogen Responses

Ido Amit,[1,2,3,4] Manuel Garber,[1]* Nicolas Chevrier,[2,3]* Ana Paula Leite,[1,5]* Yoni Donner,[1]* Thomas Eisenhaure,[2,3] Mitchell Guttman,[1,4] Jennifer K. Grenier,[1] Weibo Li,[2,3] Or Zuk,[1] Lisa A. Schubert,[6] Brian Birditt,[6] Tal Shay,[1] Alon Goren,[1,7] Xiaolan Zhang,[1] Zachary Smith,[1] Raquel Deering,[2,3] Rebecca C. McDonald,[2,3] Moran Cabili,[1] Bradley E. Bernstein,[1,3,7] John L. Rinn,[1] Alex Meissner,[1] David E. Root,[1] Nir Hacohen,[1,2,3]†‡ Aviv Regev[1,4,8]‡

Models of mammalian regulatory networks controlling gene expression have been inferred from genomic data but have largely not been validated. We present an unbiased strategy to systematically perturb candidate regulators and monitor cellular transcriptional responses. We applied this approach to derive regulatory networks that control the transcriptional response of mouse primary dendritic cells to pathogens. Our approach revealed the regulatory functions of 125 transcription factors, chromatin modifiers, and RNA binding proteins, which enabled the construction of a network model consisting of 24 core regulators and 76 fine-tuners that help to explain how pathogen-sensing pathways achieve specificity. This study establishes a broadly applicable, comprehensive, and unbiased approach to reveal the wiring and functions of a regulatory network controlling a major transcriptional response in primary mammalian cells.

Regulatory networks controlling gene expression serve as decision-making circuits within cells. For example, when immune dendritic cells (DCs) are exposed to viruses, bacteria, or fungi, they respond with transcriptional programs that are specific to each pathogen (*1*) and are essential for establishing appropriate immunological outcomes (*2*). These responses are initiated through specific receptors, such as Toll-like receptors (TLRs), that distinguish broad pathogen classes and are propagated through well-characterized signaling cascades (*2*). However, little is known about how the transcriptional network is wired to produce specific outputs.

Two major observational strategies have associated regulators with their putative targets on a genome scale (*3*): Cis-regulatory models rely on the presence of predicted transcription factor binding sites in the promoters of target genes (*3*–*5*), whereas trans-regulatory models are based on correlations between regulator and target expression (*3*–*6*). Because promoter binding sites and correlated expression are weak predictors of functional regulator-target linkages, such approaches are limited in their ability to produce reliable models of transcriptional networks (*3*). A complementary strategy is to systematically perturb every regulatory input and measure its effect on the expression of gene targets. This strategy has been successfully used in yeast (*7*–*9*) and sea urchin (*10*), but not in mammals.

A perturbation-based strategy for network reconstruction. We developed a perturbation strategy for reconstructing transcriptional networks in mammalian cells and used it to determine a network controlling the responses of DCs to pathogens (Fig. 1). First, we profiled gene expression at nine time points after stimulation with five pathogen-derived components and identified specific and shared genes that respond to each stimulus (fig. S1A). We used these profiles to identify 144 candidate regulators whose expression changed in response to at least one stimulus (*11*) (fig. S1B, top). We also identified a signature of 118 marker genes (fig. S1B, bottom) that captures the complexity of the response. We generated a validated lentiviral short hairpin RNA (shRNA) library for 125 of the 144 candidate regulators (fig. S1C, top), used it to systematically perturb each of the regulators in DCs, stimulated the cells with a pathogen component, and profiled the expression of the 118-gene signature (*12*) (fig. S1C, bottom). Finally, we used the measurements from the perturbed cells to derive a validated model of the regulatory network (fig. S1D).

Gene expression programs in response to TLR agonists. We measured genome-wide expression profiles in DCs exposed to PAM3CSK4 (PAM), a synthetic mimic of bacterial lipopeptides; polyinosine-polycytidylic acid [poly(I:C)], a viral-like double-stranded RNA; lipopolysaccharide (LPS), a purified component from Gram-negative *Escherichia coli*; gardiquimod, a small-molecule

[1]Broad Institute of MIT and Harvard, 7 Cambridge Center, Cambridge, MA 02142, USA. [2]Center for Immunology and Inflammatory Diseases, Massachusetts General Hospital, 149 13th Street, Charlestown, MA 02129, USA. [3]Harvard Medical School, Boston, MA 02115, USA. [4]Department of Biology, Massachusetts Institute of Technology, Cambridge, MA 02142, USA. [5]Computational and Systems Biology, Massachusetts Institute of Technology, Cambridge, MA 02139, USA. [6]NanoString Technologies, 530 Fairview Avenue N., Suite 2000, Seattle, WA 98109, USA. [7]Molecular Pathology Unit and Center for Cancer Research, Massachusetts General Hospital, Charlestown, MA 02129, USA. [8]Howard Hughes Medical Institute.
*These authors contributed equally to this work.
†To whom correspondence should be addressed. E-mail: nhacohen@partners.org
‡These authors contributed equally to this work.

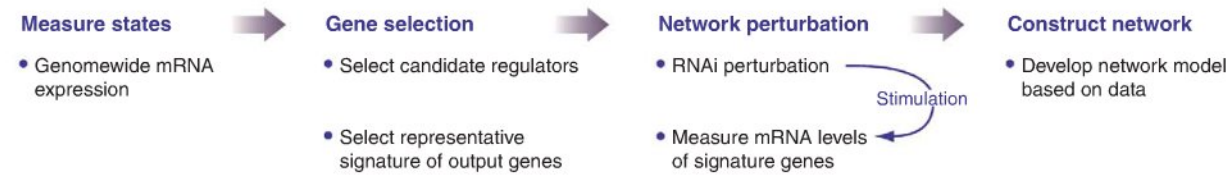

Fig. 1. A systematic strategy for network reconstruction. The strategy consists of four steps (left to right): state measurement using arrays; selection of regulators and response signatures; network perturbation with shRNAs against each regulator, followed by measurement of signature genes; and network reconstruction from the perturbational data.

agonist; and CpG, a synthetic single-stranded DNA. These compounds are known agonists of TLR2, TLR3, TLR4, TLR7, and TLR9, respectively. Poly(I:C) also activates the cytosolic viral RNA sensor MDA-5, and LPS can also act through co-receptors such as CD14; we therefore refer to the ligands rather than their receptors for clarity. On the basis of pilot experiments (fig. S2) (*11*), we measured mRNA expression at 0.5, 1, 2, 4, 6, 8, 12, 16, and 24 hours after stimulation with these pathogen components.

The observed transcriptional responses were classified into a "PAM-like" program and a "poly(I:C)-like" program, as well as a shared response [24.5% shared by PAM, poly(I:C), and LPS]. The LPS response (Fig. 2 and fig. S3) was largely the union of the "PAM-like" and "poly(I:C)-like" programs. This is partly explained by the known signaling pathways activated by these agonists. PAM binds TLR2 and signals through the MYD88 pathway; poly(I:C) binds TLR3 and MDA-5 and signals mostly through the TRIF and IPS-1 pathways, respectively; and LPS binds TLR4 and co-receptors and uses the MYD88 and TRIF pathways (*13*). It is also consistent with the known induction of an antiviral response by poly (I:C) and LPS (*14*). The "PAM-like" program is enriched for targets of the transcription factor NF-κB and for inflammatory responsive genes ($P < 6.1 \times 10^{-8}$), whereas the "poly(I:C)-like" program is enriched for interferon regulatory factors (IRFs) and for viral- and interferon-responsive genes (ISGs; $P < 8.3 \times 10^{-24}$). We thus term them the "inflammatory-like" and "antiviral-like" programs. A small number of genes are specific to a single stimulus. For example, ~250 genes are poly(I:C)-specific (1250 are shared with LPS), including several type I interferons (e.g., IFNA2, IFNA4; Fig. 2A). Surprisingly, 82% of the gardiquimod (TLR7) and CpG (TLR9) response was shared with the LPS response, but with a weaker antiviral component (fig. S4). This observation is unexpected given their different signaling mechanisms (*15*), but is highly reproducible and robust (fig. S4) (*11*).

Identification of candidate regulators and a response signature. To select potential regulators that mediate the observed transcriptional response, we focused on regulator genes whose expression changes during pathogen sensing [a reasonable assumption for many mammalian responses (*16*, *17*), including pathogen sensing (*1*, *4*)]. First, we reconstructed an observational trans-model of gene regulation (fig. S1B, top, and fig. S5A) (*11*) that associated 80 modules of co-regulated genes with 608 predictive regulators (fig. S5B) (*4*, *11*, *18*, *19*) automatically chosen out of a curated list of 3287 candidate regulators (*11*). Filtering identified 117 regulators above a minimal expression signal in at least one experiment (fig. S5B). These included known regulators from the NF-κB, STAT, and IRF families, as well as unexpected candidates such as the circadian regulator Timeless and the DNA methyltransferase Dnmt3a. Second, we added five constitutively expressed regulators whose cis-regulatory elements are enriched in the responsive genes (*11*). Third, to capture delayed responses or nonlinear relations, we incorporated 22 regulators whose expression changed by at least a factor of 2. This resulted in 144 candidate regulators, with a distribution of expression patterns similar to the general response (figs. S6 to S8 and table S1). The regulators' expression under LPS was conserved between DCs and functionally similar macrophages (Pearson correlation $r = \sim 0.9$ at 1 hour; fig. S9A) as well as between human macrophages and mouse DCs ($r = \sim 0.6$ at 2 hours; fig. S9B), supporting the functional relevance of the regulators' transcription.

To identify highly informative reporter genes for monitoring the effects of perturbing regulators, we devised GeneSelector (fig. S10A and table S2) (*11*). GeneSelector incrementally chooses genes (from our full expression data set) whose expression profile improves our discrimination of stimuli given the previously chosen genes. Using this approach, we identified the optimal time point (6 hours after activation; fig. S10B) and a set of 81 genes that distinguished the stimuli (*11*). We added 37 candidate regulators with

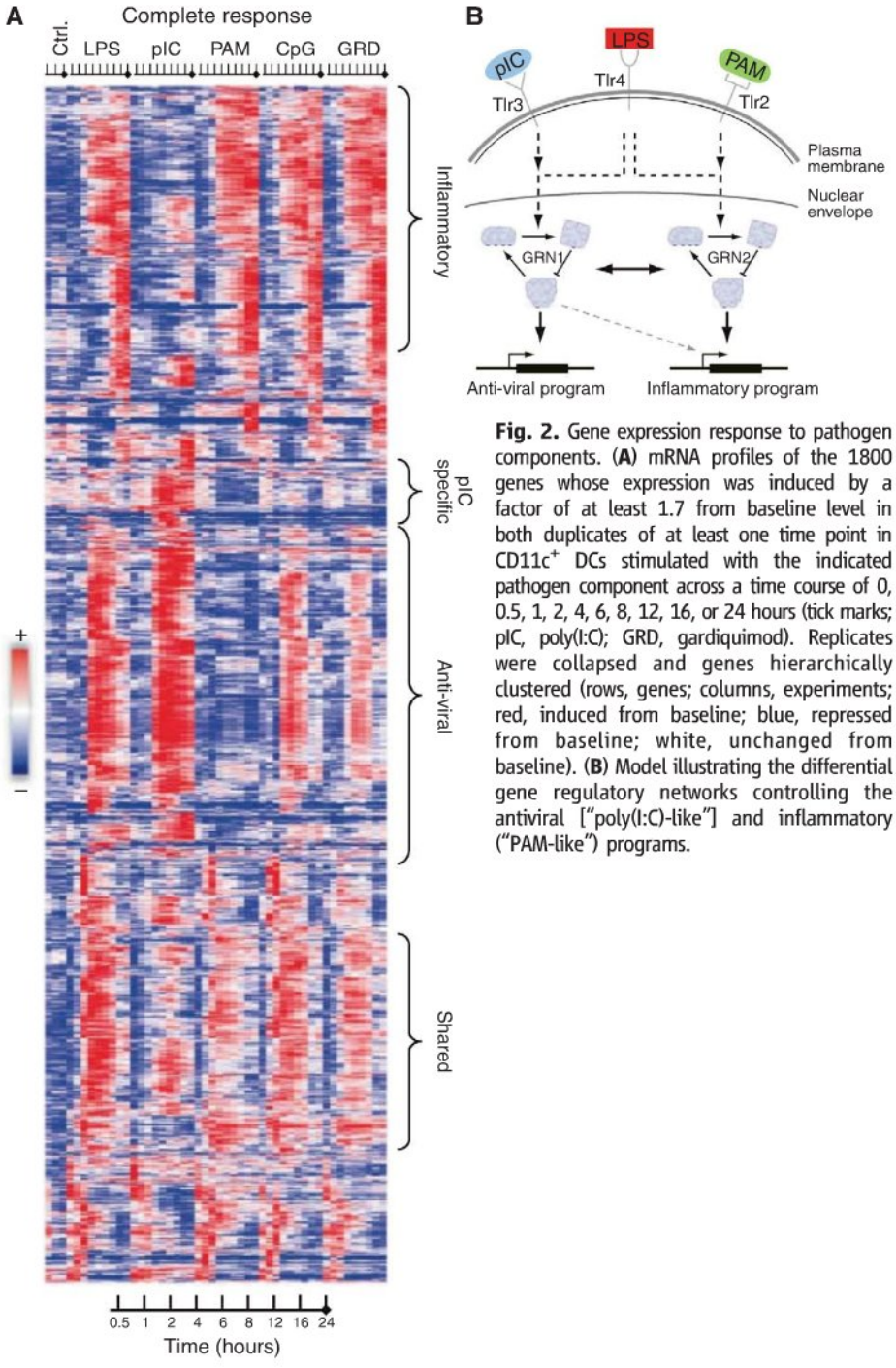

Fig. 2. Gene expression response to pathogen components. (**A**) mRNA profiles of the 1800 genes whose expression was induced by a factor of at least 1.7 from baseline level in both duplicates of at least one time point in $CD11c^+$ DCs stimulated with the indicated pathogen component across a time course of 0, 0.5, 1, 2, 4, 6, 8, 12, 16, or 24 hours (tick marks; pIC, poly(I:C); GRD, gardiquimod). Replicates were collapsed and genes hierarchically clustered (rows, genes; columns, experiments; red, induced from baseline; blue, repressed from baseline; white, unchanged from baseline). (**B**) Model illustrating the differential gene regulatory networks controlling the antiviral ["poly(I:C)-like"] and inflammatory ("PAM-like") programs.

detectable expression at the 6-hour time point, creating a signature of 118 genes. Finally, we added 10 control genes whose expression levels were unchanged under all stimuli, but whose (constant) basal levels varied from very low to high.

Perturbations, profiling, and modeling. We generated validated lentiviral shRNAs that knocked down the expression of 125 of our 144 candidate regulators in bone marrow DCs by at least 75% (fig. S11 and table S3) (*11*) and 32 shRNAs with no known gene targets as controls (figs. S12 and S13 and table S4) (*11*). To carry out our perturbational study, we selected a single treatment, LPS, that activates the majority of both the "inflammatory-like" and "antiviral-like" programs. After stimulation of shRNA-perturbed DCs with LPS for 6 hours, we used nCounter (*12*) to count transcripts of the 118 reporter and 10 control genes.

The changes in signature gene expression resulting from infection with each shRNA were used to construct a model that associated regulators to their targets. We expected increases in the transcript levels of reporter genes whose repressors are targeted by knockdown, and decreases in reporters whose activators are targeted. Our false discovery rate (FDR) model estimates the statistical significance of a change in transcripts in DCs infected with a given shRNA (*11*). We controlled for gene-specific noise by comparing to changes in the expression of each gene after perturbation with the control shRNAs (Fig. 3A), and for shRNA-specific noise by comparing to changes in the expression of the control genes after a given shRNA perturbation (Fig. 3B). We estimated the sensitivity of our calls from the 37 regulators, which are also included as target reporters (fig. S14) (*11*).

On the basis of these results, we identified a densely overlapping network with 2322 significant regulatory connections, including 1728 activations and 594 repressions (Fig. 3B, red and blue, respectively, at 95% confidence; tables S5 to S7). Of the 125 tested regulators, we confidently identified 100 with at least four targets. Among those were 24 hub regulators that were predicted to regulate more than 25% of the 118 genes measured, as well as 76 specific regulators each affecting the expression of 4 to 25 genes. On average, ~14 (±8; SD) regulators activated a target gene, and 5 (±5.8) regulators repressed it. Indirect effects may account for the large number of regulators we observed for each target.

Our perturbational model captured known regulatory features of the response, but also identified novel regulators. The reporter genes partitioned into two main clusters according to their response to perturbations (Fig. 3B and fig. S15A), consistent with the expression data: the "antiviral poly(I:C)–like" program reporters (e.g., Cxcl10, Isg15, and Ifit1) and the "inflammatory (PAM)–like" program reporters [e.g., IL1b, Cxcl2, IL6, and IL12b). We also found many known regulatory relations—for example, the NF-κB family of transcription factors (Rel, Rela, Relb, Nfkb1, Nfkb2, and Nfkbiz) regulating their known inflammatory gene targets. Our network provided evidence for the involvement of at least 68 additional regulators in the response to pathogens, of which 11 were hubs not previously associated with this system. Interestingly, 12 of the identified regulators (e.g., Hhex, Fus, Bat5, and Pa2g4) are in linkage disequilibrium with single-nucleotide polymorphisms (SNPs) associated with autoimmune and related diseases in genome-wide association studies (table S8).

The core inflammatory and antiviral programs. We next addressed how each regulator contributes to the generation of specific cell states. We first automatically defined the two major states induced by the five pathogen components with the use of non-negative matrix factorization (NMF) (*20*) and the original array data (*11*). This procedure identified two major expression components (termed "metagenes"): one predominantly determined by genes from the "inflammatory-like" program and the other by genes from the "antiviral-like" programs (Fig. 2A). Next, we quantified the effects of each regulator's knockdown on these two states (Fig. 3B, fig. S15A, and table S9) by classifying the nCounter expression measurements after a regulator's perturbation (*20*, *21*).

Finally, we used a regulator ranking score (*11*) to assign 33 (8 known) genes as regulators of the inflammatory state and 33 (15 known) genes as regulators of the antiviral state. This accurately classified the known activators of the inflammatory response (e.g., the NF-κB factors Rela, Nfkbiz, and Nfkb1; Fig. 3C, yellow in the inflammatory metagene) and of the antiviral response (e.g., Stat1, Stat2, Stat4, Irf8, and Irf9; Fig. 3C, yellow in the viral metagene). Although all perturbation experiments were conducted only under LPS stimulation (a bacterial component), we correctly classified factors known to mediate the response to other stimuli. Because 34 additional regulators were associated with both responses, it is possible that a single regulator can control genes in either state, depending on the differential timing of regulator activation, its level, or combinatorial regulation. Notably, for 12 of the transcription factors examined, we found an enriched cis-regulatory element in the appropriate metagene (*11*).

On the basis of the NMF scores (table S9), we identified an inflammatory subnetwork (fig. S15B), an antiviral subnetwork (Fig. 4A and fig. S15C), and several fine-tuning subnetworks that affect smaller numbers of genes from both responses (figs. S15D and S16) (*11*). The inflammatory subnetwork (fig. S15B) consisted of three regulatory modes: dominant activators (Cebpb, Bcl3, and Cited2) that induce more inflammatory targets than antiviral ones; cross-inhibitors (Nfkbiz, Nfkb1, Atf4, and Pnrc2) that induce inflammatory genes while repressing antiviral ones; and specific activators (Runx1 and Plagl2) that almost entirely target inflammatory genes. We observed that dominant activators mostly regulate effectors, whereas regulators are primarily controlled by cross-inhibitors.

Focusing on the network architecture, we found multiple feedforward circuits in this response, where an upstream regulator controls a target gene both directly and indirectly through a secondary regulator (*22*) (e.g., Fig. 4B and tables S10 and S11). The majority (76%, 4892 of 6444) of these feedforward circuits were found to be coherent (*22*), having the same direct and indirect effect on the regulated gene. The vast majority (80%) are type I loops (*23*) (Fig. 4B) with all-positive regulation (e.g., Nfkbiz activates E2f5 and both activate IL-6). Such feedforward circuits respond to persistent rather than transient stimulation, protecting the system from responding to spurious signals, as was shown for one circuit in LPS-stimulated macrophages (*24*). Our finding suggests that coherent feedforward loops, especially class I (*22*), are a general design principle in this system and may have a physiological impact on this response.

In the antiviral subnetwork, we identified a two-tiered regulatory circuit combining feedforward and feedback loops (Fig. 4A and table S11). This circuit has at the top the antiviral regulators Stat1 and Stat2, which regulate a full complement of antiviral reporters. The second-tier regulators Timeless, Rbl1, and Hhex are controlled by Stat1 and Stat2 and most likely form coherent feedforward loops that target specific subsets of genes. Timeless, Rbl1, and Hhex also feed back and promote the expression of the Stat regulators. This circuit is repressed through the cell cycle regulator and RNA binding protein Fus (*25*), acting as a single dominant inhibitor of 43 viral genes.

Finally, we derived a core network incorporating the regulators with the most substantial impact on each response, on the basis of the number, magnitude, and logic of targets that each regulator affects (*11*). The core network (Fig. 4C) has 24 regulators, 13 of which have previously been identified as key factors regulating the inflammatory or antiviral responses; the other 11 have not been previously implicated in either response. Of these 24 regulators, 19 are transcription factors, three are chromatin modifiers, and two are RNA binding proteins. The regulators apparently distinguish the two programs through cross-inhibition (Fig. 4C, gray lines) or dominant activation (Fig. 4C). The core network also explains how differential expression of secreted factors is specified, leading to the activation and migration of appropriate cell types for different pathogens (*11*, *26*) (fig. S17).

Embedded within the many known regulators of the antiviral response (Fig. 4C and fig. S15C), we found a large set of regulators not previously associated with this response. These included several known regulators of the cell cycle and the circadian rhythm, including Rbl1, Jun, Rb, E2f5, E2f8, Nmi, Fus, and Timeless, several of which were placed in our core network. This

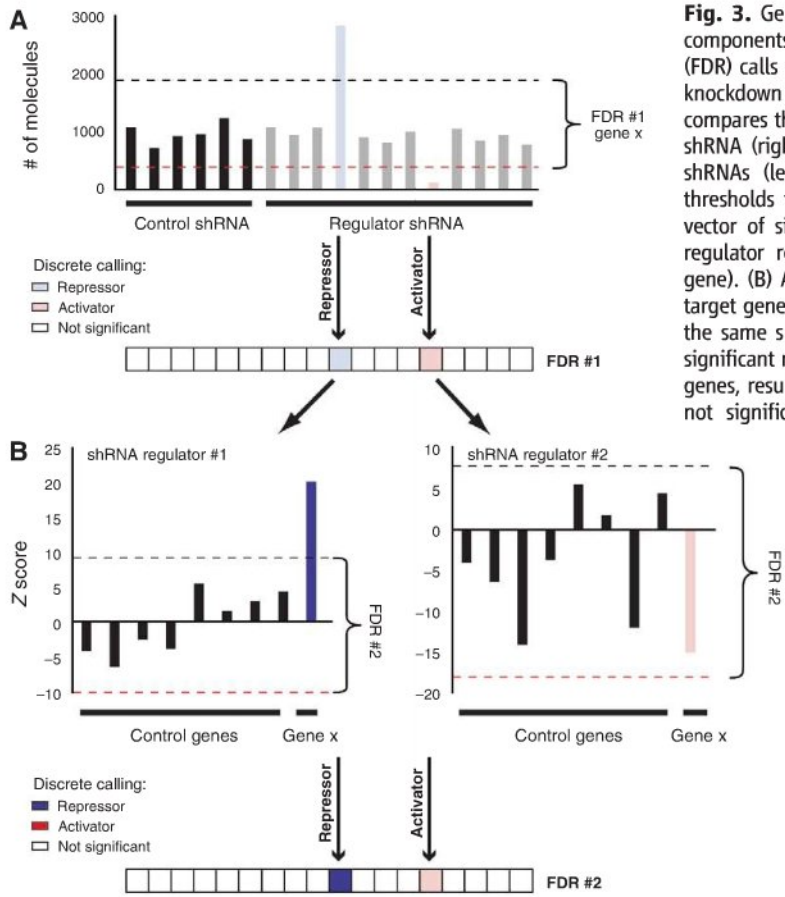

Fig. 3. Gene regulatory programs controlling the response to pathogen components. (**A** and **B**) A strategy to minimize the false discovery rate (FDR) calls of significant changes in an output target gene resulting from knockdown of a regulator gene. (A) The first FDR procedure (top) compares the expression of the gene after a perturbation with a regulator shRNA (right) to its expression upon perturbation with 32 nontargeting shRNAs (left). The dashed lines identify the gene-specific FDR-based thresholds for induction (blue line) and repression (red line). A discrete vector of significant calls (bottom) is derived from the raw data (blue, regulator represses the target gene; red, regulator induces the target gene). (B) A second FDR procedure (top) compares the expression of the target gene to that of eight control (target) genes upon perturbation with the same shRNA. In the example shown, the gene's induction (left) was significant relative to the variation in expression among the control target genes, resulting in a high score (bottom, dark blue), but its repression did not significantly differ from the controls, resulting in a lower score (bottom, weaker red). (**C**) All significant (95% confidence) relations between regulators (columns) and targets (rows), colored as in (B). The gray bar (right) represents the NMF-based calls for each target gene; black, antiviral program; dark gray, inflammatory program; light gray, control genes. The bottom bar shows the degree of effect by the regulator on each program as determined by the NMF projection of the regulator's perturbation profile (yellow, high; green, low).

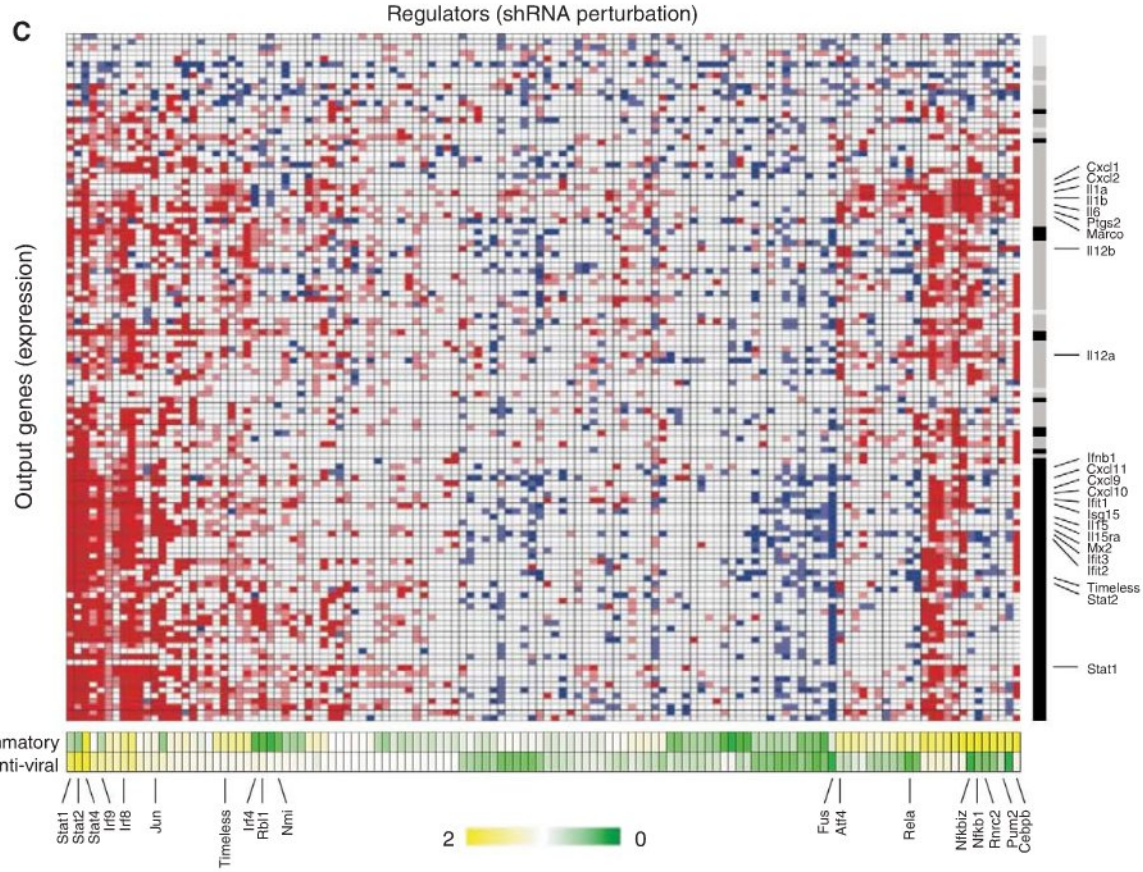

suggests that a cell cycle regulatory circuit was co-opted to function in the antiviral response in DCs (with no observable effect on cell cycle progression; fig. S18). Because we identified these antiviral regulatory relations in perturbation experiments using DCs stimulated with the bacterial component LPS, we silenced four regulators (Timeless, Rbl1, Jun, and Nmi) after exposure to the viral component poly(I:C). Each of the four regulators had a strong impact on the antiviral program, more than was observed under LPS stimulation (Fig. 4D), and on affected genes (e.g., type I IFNs) whose expression is poly(I:C)-specific. Nmi affected a smaller set of genes, consistent with the model's prediction. These results demonstrate our ability to correctly predict function in unobserved conditions.

Although most antiviral genes are induced after stimulation with the bacterial component LPS, a few critical ones are expressed specifically in poly(I:C) stimulation or follow distinct patterns in each stimulus. For example, in response to viral infection, cells induce the production of interferon β1 (Ifnb1), a crucial mediator of the antiviral response. Because high levels of Ifnb1 may be deleterious to the host if infected by specific bacteria (*27*), we predicted that specific mechanisms insulate Ifnb1's regulation from the response to LPS. Indeed, although Ifnb1 expression was induced in the first 2 hours of stimulation with LPS, this expression declined at subsequent time points, in contrast to its sustained induction after poly(I:C) treatment (Fig. 5A). Our model suggested that three regulators known to affect chromatin remodeling (*25*, *28*, *29*) are Ifnb1 repressors in LPS (Fig. 5B): the Polycomb complex subunit Cbx4 (*28*), Fus (*25*), and the DNA methyltransferase Dnmt3a (*29*). Cbx4 appeared to confer antiviral specificity to Ifnb1 induction because it was induced within the first 2 hours of PAM and LPS treatment but not by poly(I:C) (Fig. 5C), and Cbx4 knockdown caused induction of Ifnb1 mRNA and protein during LPS treatment (Fig. 5D and fig. S19A) but had no effect on the induction of the chemokine Cxcl10, a poly(I:C)- and LPS-induced gene (fig. S19B). Cbx4 knockdown did not affect Ifnb1 during PAM activation (Fig. 5E), when the antiviral response is not induced. Combined with evidence for chromatin changes around the Ifnb1 locus and its closest neighbor gene, Ptplad2 (fig. S20A), which has a similar dependence on Cbx4, these data are consistent with an effect by Cbx4 on local chromatin organization (fig. S20, B and C). Cbx4 knockdown affected few genes (~120 up-regulated and ~120 down-regulated genome-wide; table S12). Because most up-regulated

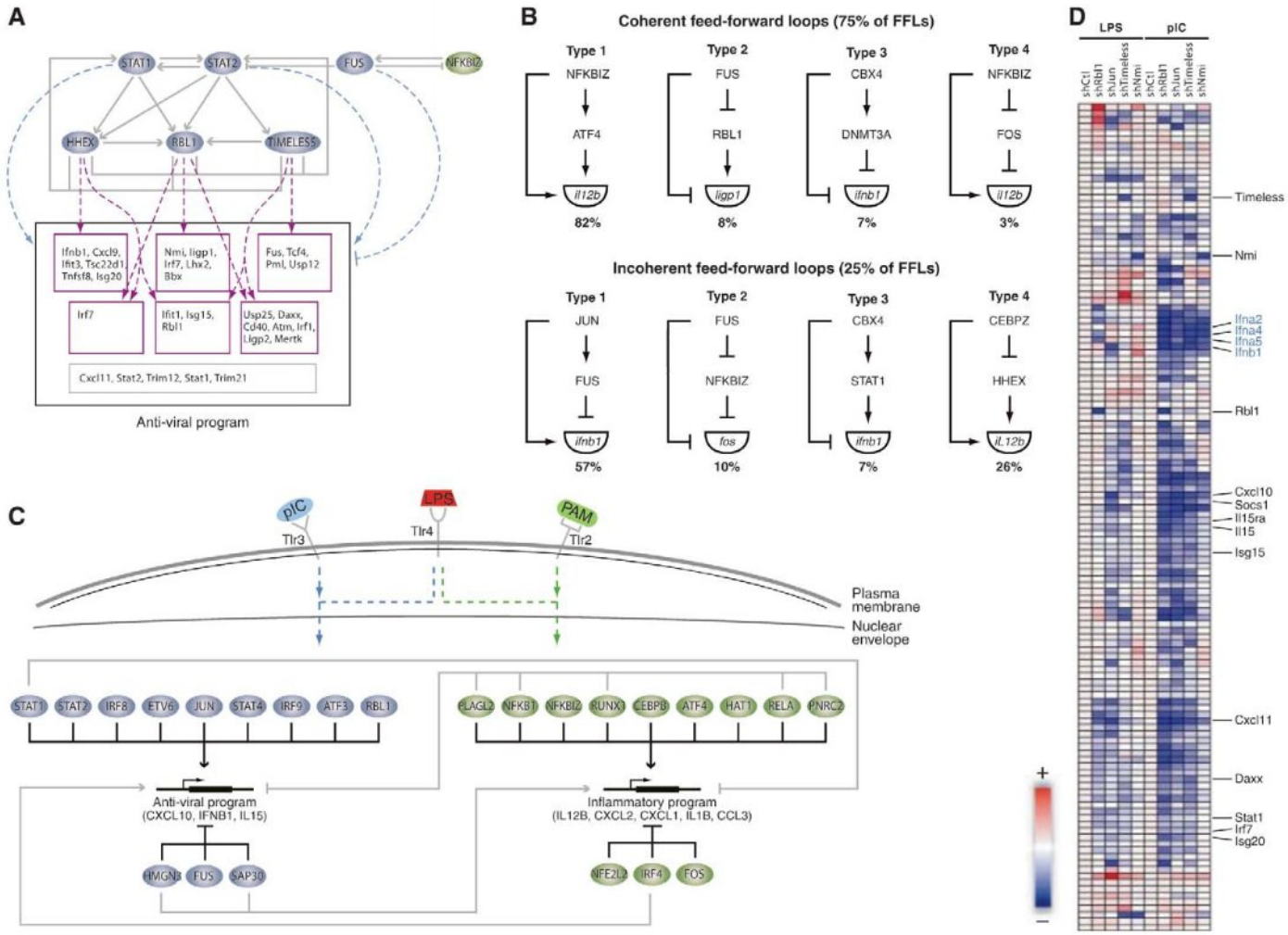

Fig. 4. The core regulatory circuits controlling the inflammatory and antiviral responses. (**A**) The antiviral subnetwork shows regulatory relations between the core antiviral regulators (blue nodes, top), their targets (boxes, bottom), each other, and inflammatory regulators (green node, top right). The two top regulators, Stat1 and Stat2, activate all antiviral targets (dashed blue arrows). The second-tier regulators activate subsets of targets (dashed purple arrows). (**B**) Examples of feedforward loop classes identified in the network, with fraction of each class. (**C**) A core regulatory network of the inflammatory and antiviral programs, consisting of the most distinct regulators, and their relation to ligands and receptors (top). Pointed arrows, induction; blunt arrows, repression; green ovals, inflammatory regulators; blue ovals, antiviral regulators. Example target genes are noted. (**D**) nCounter expression profiles for the target genes (rows) upon perturbation with shRNAs against a subset of viral regulators (columns) and followed by stimulation with LPS (left) or poly(I:C) (right). All values are normalized by expression in cells infected with a control shRNA and under the same stimulus (shCtl).

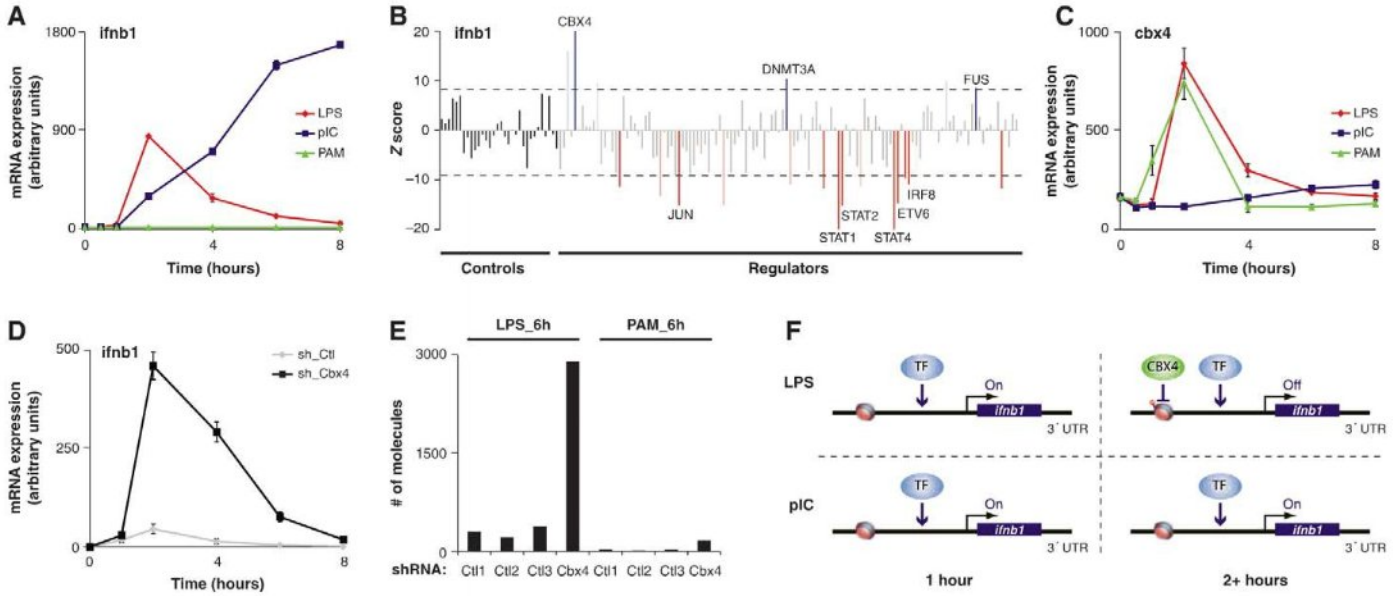

Fig. 5. The polycomb component Cbx4 selectively restricts Ifnb1 production under bacterial perturbations. (**A** and **C**) LPS (red), poly(I:C) (blue), and PAM (green)–induced expression of Ifnb1 (A) and Cbx4 (C) derived from data in Fig. 2A. (**B**) Ifnb1 expression (by nCounter) in response to LPS in DCs perturbed by control shRNAs or shRNAs targeting each of 125 regulators (format as in Fig. 3B). (**D**) Ifnb1 mRNA levels (by quantitative reverse transcription polymerase chain reaction) after LPS treatment in unsorted mouse bone marrow DCs perturbed with an shRNA against Cbx4 (black) or a control shRNA (gray); signals are relative to $t = 0$. (**E**) Ifnb1 mRNA levels (by nCounter) at 6 hours after exposure to LPS or PAM in bone marrow DCs perturbed with an shRNA against Cbx4 or one of three control shRNAs. (**F**) Model for bacterial-specific repression of Ifnb1 by Cbx4. Both poly(I:C) and LPS induce Ifnb1 expression early (left), but only LPS induces Cbx4, which then represses the *Ifnb1* locus at a later time (right, top).

genes show a precise temporal pattern in unperturbed cells akin to that of Cbx4—they are induced quickly and return to basal level by 2 to 4 hours (fig. S21, A to F)—we conclude that a chromatin modifier can act like a transcription factor controlling the precise expression of specific genes in the regulatory program.

Taken together, our results suggest a model of a transcriptional negative feedback loop, controlling Ifnb1 expression in LPS stimulation, wherein the induced proinflammatory regulator and chromatin modifier Cbx4 represses transcription by modifying the chromatin in the Ifnb1 locus, generating the specificity needed to drive the inflammatory versus the antiviral response (Fig. 5F). The type III coherent feedforward loop formed by Cbx4 and Dnmt3a (Fig. 4B) is consistent with a delayed repression of Ifnb1. Because neither regulator carries a sequence-specific DNA binding domain, the factors responsible for their guidance to the *Ifnb1* locus remain unknown.

Discussion. A central goal of our study was to address the mechanistic basis for pathogen-specific responses. Consistent with previous studies (*14*), we distinguished two key programs, a PAM (TLR2)–like inflammatory response and a poly(I:C) (TLR3/MDA-5)–like antiviral response, which are together induced by LPS, a Gram-negative bacterial component and a TLR4 ligand. These programs reflect both qualitative and quantitative differences between the required functional responses, and are consistent with the cross-protection between certain bacteria and virus infections (*14*). The broad effect of LPS allowed us to focus on a single stimulus and time point, but screens with other stimuli may identify additional unique regulators.

We found that these two responses are controlled by two corresponding regulatory arms, uncovering a mechanistic basis for the observed transcriptional responses. These two arms are integrated into a core network of 24 regulators that balance specific and shared responses through dominant activation and cross-inhibition. In the inflammatory response, we found several feed-forward loops, which may ensure response to only persistent and not sporadic signals. In the antiviral response, we discovered a two-tiered circuit involving feedback and feedforward loops, implicating a module of cell cycle regulators (Jun, Rbl1, Timeless, and Nmi), which we directly validated. More than 75 additional genes work to further fine-tune the regulation of gene targets. This perturbational model identifies many regulatory relations that would have been missed by nonsystematic approaches.

Our work establishes an unbiased, straightforward, and general framework for network reconstruction in mammalian cells (*11*), including several strategies to leverage shRNA for the study of gene regulation. This approach can be executed at substantial scale and reasonable cost, and is compatible with the challenge of deciphering the multiple regulatory systems that operate in mammals. It can be expanded to derive increasingly detailed models and to distinguish direct from indirect targets.

Our study will facilitate the development of new computational approaches to infer regulatory models. Although many computational approaches have attempted to derive observational models, their quality has been difficult to evaluate (*3*). The data generated here include expression profiles for training a model, as well as a perturbational unbiased screen for testing its quality (ftp://ftp.broadinstitute.org/pub/papers/dc_network). When we compared the perturbational model to our observational model, we found that many candidate regulators were correctly identified in both (figs. S5 and S22). However, there were also numerous false positive relations in the observational model, attributable to the fact that both the correct regulator and many others have indistinguishable expression (figs. S22 and S23).

The high-resolution map we constructed has important biomedical implications. By identifying regulators that mediate the differential control of specific gene pairs (e.g., IL-23 versus IL-12, fig. S17) and entire regulatory arms (e.g., viral versus inflammatory), it opens the way for therapeutic targeting of specific pathways to control disease or enhance vaccine efficacy. Furthermore, 12 of our regulators reside in genetic loci that were in linkage disequilibrium with SNPs associated with autoimmune and related diseases. The identified genes and their impact on DCs provide hypotheses to help explain how alleles of genes in a cascade may alter susceptibility to specific infections or immune disorders in humans.

References and Notes

1. Q. Huang *et al.*, *Science* **294**, 870 (2001).
2. T. Kawai, S. Akira, *Int. Immunol.* **21**, 317 (2009).

3. H. D. Kim, T. Shay, E. K. O'Shea, A. Regev, *Science* **325**, 429 (2009).
4. S. A. Ramsey *et al.*, *PLOS Comput. Biol.* **4**, e1000021 (2008).
5. H. Suzuki *et al.*, *Nat. Genet.* **41**, 553 (2009).
6. E. Segal *et al.*, *Nat. Genet.* **34**, 166 (2003).
7. A. P. Capaldi *et al.*, *Nat. Genet.* **40**, 1300 (2008).
8. Z. Hu, P. J. Killion, V. R. Iyer, *Nat. Genet.* **39**, 683 (2007).
9. C. T. Workman *et al.*, *Science* **312**, 1054 (2006).
10. D. H. Erwin, E. H. Davidson, *Nat. Rev. Genet.* **10**, 141 (2009).
11. See supporting material on *Science* Online.
12. G. K. Geiss *et al.*, *Nat. Biotechnol.* **26**, 317 (2008).
13. J. C. Kagan *et al.*, *Nat. Immunol.* **9**, 361 (2008).
14. S. Doyle *et al.*, *Immunity* **17**, 251 (2002).
15. T. Kawai *et al.*, *Nat. Immunol.* **5**, 1061 (2004).
16. I. Amit *et al.*, *Nat. Genet.* **39**, 503 (2007).
17. D. Pe'er, A. Regev, A. Tanay, *Bioinformatics* **18** (suppl. 1), S258 (2002).
18. S. I. Lee *et al.*, *PLoS Genet.* **5**, e1000358 (2009).
19. H. Zou, T. Hastie, *J. R. Stat. Soc. B* **67**, 301 (2005).
20. J. P. Brunet, P. Tamayo, T. R. Golub, J. P. Mesirov, *Proc. Natl. Acad. Sci. U.S.A.* **101**, 4164 (2004).
21. J. P. Daily *et al.*, *Nature* **450**, 1091 (2007).
22. S. Mangan, U. Alon, *Proc. Natl. Acad. Sci. U.S.A.* **100**, 11980 (2003).
23. U. Alon, *Nat. Rev. Genet.* **8**, 450 (2007).
24. V. Litvak *et al.*, *Nat. Immunol.* **10**, 437 (2009).
25. X. Wang *et al.*, *Nature* **454**, 126 (2008).
26. A. D. Luster, *Curr. Opin. Immunol.* **14**, 129 (2002).
27. T. Decker, M. Muller, S. Stockinger, *Nat. Rev. Immunol.* **5**, 675 (2005).
28. E. Bernstein *et al.*, *Mol. Cell. Biol.* **26**, 2560 (2006).
29. B. Li *et al.*, *Biochem. J.* **405**, 369 (2007).
30. We thank E. Lander, I. Wapinski, D. Pe'er, N. Friedman, J. Kagan, A. Luster, V. Kuchroo, and A. Citri for discussions and comments; L. Gaffney for assistance with artwork; S. Gupta and the Broad Genetic Analysis Platform for microarray processing; and T. Mikkelsen and the Broad Sequencing Platform for help with the ChIP-seq experiments. Supported by the Human Frontier Science Program Organization and a Claire and Emanuel G. Rosenblatt Award from the American Physicians Fellowship for Medicine in Israel (I.A.); NIH grant R21 AI71060 and the NIH New Innovator Award (N.H.); and a Career Award at the Scientific Interface from the Burroughs Wellcome Fund, an NIH Pioneer Award, and the Sloan Foundation (A.R.). A.R. is an Early Career Scientist of the Howard Hughes Medical Institute and an investigator of the Merkin Foundation for Stem Cell Research at the Broad Institute. Complete microarray data sets are available at the Gene Expression Omnibus (accession no. GSE17721).

Supporting Online Material

www.sciencemag.org/cgi/content/full/1179050/DC1
Materials and Methods
SOM Text
Figs. S1 to S23
Tables S1 to S16
References

14 July 2009; accepted 26 August 2009
Published online 3 September 2009;
10.1126/science.1179050
Include this information when citing this paper.

Mapping Excited-State Dynamics by Coherent Control of a Dendrimer's Photoemission Efficiency

Daniel G. Kuroda,[1]* C. P. Singh,[1]† Zhonghua Peng,[2] Valeria D. Kleiman[1]‡

Adaptive laser pulse shaping has enabled impressive control over photophysical processes in complex molecules. However, the optimal pulse shape that emerges rarely offers straightforward insight into the excited-state properties being manipulated. We have shown that the emission quantum yield of a donor-acceptor macromolecule (a phenylene ethynylene dendrimer tethered to perylene) can be enhanced by 15% through iterative phase modulation of the excitation pulse. Furthermore, by analyzing the pulse optimization process and optimal pulse features, we successfully isolated the dominant elements underlying the control mechanism. We demonstrated that a step function in the spectral phase directs the postexcitation dynamics of the donor moiety, thus characterizing the coherent nature of the donor excited state. An accompanying pump-probe experiment implicates a 2+1 photon control pathway, in which the optimal pulse promotes a delayed excitation to a second excited state through favorable quantum interference.

Since ancient times, humans have been trying to control the transformation of matter. For more than a century, absorption of light has been used to initiate photochemical reactions. It is only in the past 20 years, however, that researchers have devised techniques to steer the ensuing dynamics through modulation of the optical excitation field. Such quantum, or coherent, control schemes (*1*–*3*) use laser-derived electric fields to direct the motion of wave packets along excited-state potential energy surfaces (*4*–*6*). In principle, the phases and amplitudes in the applied field necessary to achieve a given outcome can be obtained from the field's coupling to the molecular Hamiltonian. In practice, rational design of the requisite pulse shapes remains an insurmountable problem for large molecules in condensed phase: The complete Hamiltonian is either unknown or too complex to be used in electric field calculations. Instead, researchers have relied on empirical methods whereby pulse shapes are determined through iterative optimization using the desired product (e.g., fluorescence quantum yield) as a feedback parameter (*7*). Thus, photoinduced processes can be actively manipulated without previous knowledge of the Hamiltonian and the light-matter couplings (*8*–*11*).

This closed-loop feedback technique has proven powerfully versatile. For example, modulation of isomerization yield in the natural photoreceptor bacteriorhodopsin (*11*), and control of quantum efficiency in both natural and artificial photosynthetic antennae by tuning spectral amplitude and phase in resonant linear excitation (*9*, *12*), were shown. Nonetheless, very few closed-loop experiments have yielded optimal pulse shapes that can be directly explained in terms of known molecular properties of the system under investigation (*9*, *11*, *13*–*15*). Major hindrances to attain such insight are the often intricate relationship between the variables to be optimized and the molecular response; the large number of parameters used for the generation of arbitrarily modulated pulses; and the often arbitrary, random pathways to optimization generated by the iteration algorithms. A major goal in the field is thus to develop a procedure for gleaning molecular insight from coherent control, especially in systems where the photophysical or photochemical pathways are presently unknown. For example, using optimal control, Branderhorst *et al.* (*15*) were able to identify wave packets with minimum position variance as candidates to minimize coupling to the bath and thus increase coherence robustness.

Our approach toward this end is to search for a confined set of parameters that directly govern the optimization. The idea is to express all the independent electric field parameters obtained from the collection of closed-loop optimization data as a combined set, filtering out those variables with redundant or negligible effects on the molecular response (*16*–*20*). Ideally, it ought to be more straightforward to associate these fewer parameters with a physical property.

We apply this approach to coherent control studies of the emissive properties of the phenylene ethynylene dendrimer $2G_2$-m-Per (Fig. 1) (*21*), designed to mimic natural light harvesting systems (*22*). Phenylene ethynylene dendrimers are rigid macromolecules with a high quantum yield for energy transfer from donor to ac-

[1]Department of Chemistry, Center for Chemical Physics, University of Florida, Gainesville, FL 32611–7200, USA. [2]Department of Chemistry, University of Missouri–Kansas City, Kansas City, MO 64110–2499, USA.

*Present address: Department of Chemistry, University of Pennsylvania, Philadelphia, PA 19104–6323, USA.
†On leave from Raja Ramanna. Centre for Advanced Technology, Indore, India.
‡To whom correspondence should be addressed. E-mail: kleiman@chem.ufl.edu

ceptor moieties (*22*–*24*). They present a folded geometry with the dendritic branches packed in a bouquet-like spatial arrangement (*23*). The donor consists of two indistinguishable monodendrons attached to a central phenyl ring at meta positions, disrupting the π conjugation between the two branches. In each monodendron, phenylene ethynylene units are connected in ortho and para substitution, creating extended π conjugated systems with broad absorption bands (*23*). Upon ultraviolet-visible absorption, the excitation is delocalized within each monodendron, from where energy can migrate to an acceptor—in this case, a perylene moiety mutually meta to both donors on the central phenyl ring (*23*). To better characterize the excited state dynamics, we also probed the acceptor-less system $2G_2$-m-OH and acceptor perylene separately.

Previous time-resolved spectroscopy showed that upon single-photon absorption, energy migrates toward the acceptor through two different pathways (*23*). One pathway (contributing to ~60% of the energy transfer yield) involves multistep exciton migration within the dendrimer backbone followed by transfer to the acceptor. This is an incoherent mechanism driven by an energy gradient. A parallel path (~40% contribution) appears to involve direct exciton migration from donor to acceptor (Fig. 1) (*23*). The possibility of coherence preservation in this latter process makes these macromolecules a compelling target for quantum control schemes.

Our experimental setup (fig. S1) comprises a femtosecond laser source, a pulse shaper to produce arbitrary phase and/or amplitude modulation, and a detection system to reveal the molecular response to excitation with tailored pulses (*25*). These molecules absorb linearly in the blue visible region only, lacking any one-photon absorption at $\lambda > 495$ nm. In the presence of an ~800-nm pulse, they are excited through two-photon absorption under the weak field limit (*25*). The samples consisted of dilute solutions of $2G_2$-m-Per (donor-acceptor) and $2G_2$-m-OH (donor) and perylene (acceptor) dissolved in dichloromethane (*26*).

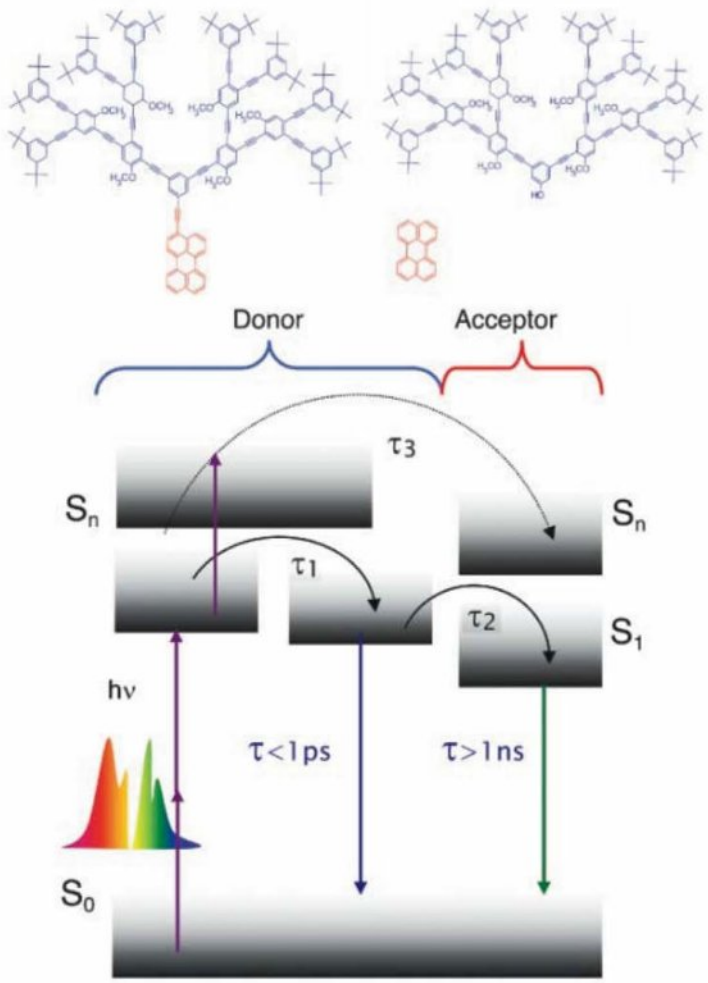

Fig. 1. Chemical structures (top from left to right) of donor-acceptor ($2G_2$-m-Per), acceptor (Per), and donor ($2G_2$-m-OH) molecules. The energy-level diagram for $2G_2$-m-Per shows two energy transfer pathways. Solid lines correspond to the cascade pathway (τ_1~500 fs, τ_2~750 fs), the dashed line to a not yet fully understood direct pathway (τ_3 ~ 400 fs) investigated in single-photon excitation experiments (*23*). Initial excitation energy is 3.14 eV (dendritic backbone), and detection is in the 2.6- to 2.1-eV range (perylene or backbone emission).

We began with a closed-loop optimization run directed toward maximizing two-photon absorption (TPA) by the $2G_2$-m-Per dendrimers. Specifically, we iteratively applied a set of phase-modulated pulses to the sample and then fed the results (in this case, overall emission intensity) into a customized genetic algorithm that in turn produced a new generation of pulses for further testing (*25*). We simultaneously measured two-photon induced current (TPIC) when the tailored pulses were focused onto a GaAsP photodiode. For a two-photon excitation process, the number of excited molecules should scale linearly with the TPIC. Thus, a relative quantum yield can be obtained by measuring or evaluating the ratio of fluorescence intensity to TPIC signal. When the objective was to increase emission intensity, this ratio reached its maximum value early on (less than ~20 generations) and then remained unchanged. Analysis of the optimization revealed that overall emission increased in parallel with TPIC [constant quantum yield (QY), Fig. 2A, green line] as pulse duration decreased. Hence, there was no coherent control over QY; shortening the pulses simply raised the two-photon absorption probability (*27*, *28*). The optimal pulse shape was the trivial transform limited (TL) case with full width at half maximum of 45 fs.

In contrast, when the QY was directly used as the feedback functional, the control process moved beyond modulation of the TPA (Fig. 2A, red line). Brixner *et al.* showed a similar response for the two-photon excitation of $[Ru(dpb)_3]^{2+}$ (*29*). For $2G_2$-m-Per, in the early generations the optimization pathway largely resembled that of the TPA-maximization experiment. The QY rose dramatically from a relative value of 0.6 (for the starting set of pulses with random phase) to a value of ~0.95 with a concomitant rise in the TPIC (indicative of increased absorption). Beyond that point, the results of each experiment differ, driven by distinct phase parametrizations leading to distinct optimal outcomes. In the QY-optimization case (Fig. 2A, red line), QY continued to grow with essentially no further accompanying increase in TPIC. Thus, the optimally shaped pulse raised the number of photons emitted without significantly changing the number of molecules excited. Specifically, the pulse induced 25% of the absorption observed with a TL pulse while improving the QY by 15% (reaching a maximum value of 1.13; dashed vertical line in Fig. 2A). The QY optimization yields an excitation pulse quite different from the TL pulse, as the optimal pulse includes information regarding the excited state and its dynamics after excitation (Fig. 2B).

To understand the changes occurring during the optimization process, we measured the second harmonic spectra and autocorrelations of

the best excitation pulses in each generation of the closed-loop experiment (Fig. 2C). The greatest changes occur during the first 20 generations, ultimately yielding a second-order spectrum resembling that of the TL pulse. In later generations, the spectrum remains centered at ~403 nm (indicating the absence of spectral selectivity during optimization) and shows only a slight flattening of its profile. Interestingly, this spectral broadening does not correlate with a decrease in pulse duration. Instead, the autocorrelation traces for the corresponding pulses show a narrow central peak with additional structure on its wings. These changes are consistent with the QY/TPIC correlation observed in Fig. 2A, where optimization of quantum yield proceeded first by uncovering the phase distribution necessary to maximize excitation and then subsequently by tuning the excited-state dynamics independent of the absorption probability.

As is often the case in closed-loop coherent control studies, the optimal pulse that emerged from our genetic algorithm exhibited a rather complex electric field (Fig. 2B, bottom panel) that offered limited direct insight into straightforward molecular properties. Our goal is to go beyond the optimization process and learn specific information about the molecular properties (*18*). We therefore sought to extract the essential parameters of the optimal pulse in the hope of attaining a simplified picture of the control process.

We applied partial least squares regression methods (*25*) to correlate spectral phase features with the improvement in quantum yield at each stage of the optimization. This statistical analysis uncovered two components crucial for reaching the final objective. One component accounts for the changes on pulse shape (G1 to G20 in Fig. 2C) improving two-photon absorption. It morphs the initial random phases into a flat spectral phase to create a short excitation pulse. The other component involves spectral steps; it has a significant contribution in explaining fitness evolution and accounts for the improvement on QY (*25*). Additionally, using the SHG-FROG (second-harmonic generation frequency resolved optical gating) technique, we retrieved the electric field for the experimental optimal pulse. It presents an asymmetric temporal profile with two distinguishable features: a ~50-fs spike followed by a ~1-ps-long tail (fig. S4B). The retrieved spectral phase function presents steps (fig. S4A) comparable to those associated with the second component identified in the statistical analysis (fig. S3).

Based on the foregoing analysis, we reduced the excitation pulse shape to its two most significant features: a short time component and a spectral phase with a steplike signature. Because we essentially understood the role of the short pulse component in optimizing excitation, we focused our attention on the meaning of the steplike signature observed in the spectral phase. We aimed to demonstrate that information extracted from the closed-loop experiment could be harnessed to control the excited-state dynamics without a priori knowledge of the molecular Hamiltonian, thereby offering insight into the control mechanism. To this end, we modulated the excitation pulses with a steplike phase function varied in sizes between 0 and 2π in steps of 0.1π. These (open-loop) experiments were performed without a feedback signal for optimization.

The two-photon induced absorption signal measured with the GaAsP photodiode (Fig. 3A, top panel) yielded a symmetric well and was modeled (solid line) considering two-photon absorption with phase-modulated pulses, assuming a step phase function and a small residual cubic phase (*30*). The measured QY from a solution containing only the acceptor molecule (perylene) showed a similarly symmetric phase dependence and did not improve relative to the response induced by a TL pulse (*25*). The response observed for the $2G_2$-m-OH (donor) and $2G_2$-m-Per (donor-acceptor) samples (Fig. 3A, middle panel) was strikingly different. Excitation with pulses modulated by a spectral phase step function with step sizes between 1.2π and 1.8π enhanced emission QY relative to the TL pulse (phase of 0 or 2π) response. The maximum ratio, at 1.4π for both samples, represents a 10% and 5% increase for $2G_2$-m-Per and $2G_2$-m-OH, respectively. The spectral step function recovers more than half of the QY improvement induced by the optimal pulse (QY for optimal pulse is 1.13 and for the 1.4π pulse is 1.09). The response from these macromolecules does not follow the model of two-photon absorption with phase-modulated pulses, implicating a mechanism in which the excited-state dynamics (as distinct from the excitation process) are purely controlled by phase.

We can further analyze the impact of the steplike spectral phase on energy transfer by comparing the results with the pure donor ($2G_2$-m-OH) to those with the donor-acceptor molecule ($2G_2$-m-Per). In $2G_2$-m-OH, the dendritic backbone acts as both absorber and emitter, whereas in $2G_2$-m-Per, the perylene trap emits after the energy transfer process (under steady-state conditions, less than 1% of the fluorescence arises from the donor when the perylene is present) (*23*). Variation of the $2G_2$-m-Per/$2G_2$-m-OH QY ratio with spectral phase step size shows that the energy transfer process itself is phase sensitive (Fig. 3A, bottom panel). For steps with phases between 0 and ~$\pi/2$, the relative QY remains unchanged, which implies that only the donor excited state is being controlled. For larger steps, the QY ratio becomes phase sensitive, peaking at a step size of π. At that point (π spectral phase step), the QY of $2G_2$-m-Per is 8% larger than

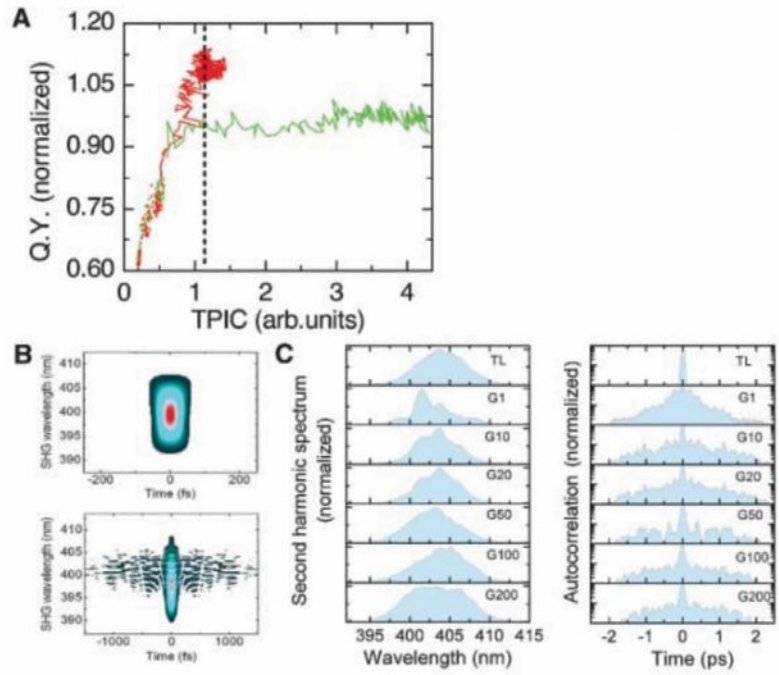

Fig. 2. Closed-loop experiments. (**A**) Green and red traces show optimization with the objective of maximizing overall emission or relative emission QY, respectively, in photoexcited $2G_2$-m-Per. The best individuals for each generation are plotted against a two-photon induced diode response (TPIC). Relative to a TPIC value of 1 for the optimal pulse, the first optimization yields a QY of 0.95, the second a QY of 1.13 for the same absorptivity (dashed line). (**B**) FROG image for a transform limited pulse (top) and the optimal pulse (bottom). Note the different time scales for the two pulses. (**C**) Second-order spectra (left) and the corresponding autocorrelations (right) of excitation pulses measured at different stages of the QY optimization procedure. From top to bottom: TL, generation 1 (random phase), 10, 20, 50, 100, and 200. The autocorrelations are plotted on a logarithmic scale to highlight the transformation of the long initial randomly phased pulse into the optimal pulse shape: a short spike with longer (1.5 ps) wings.

$2G_2$-m-OH; hence, the energy transfer yield was increased.

In the time domain, the impact of applying a step in the spectral phase function is to create a double pulse (fig. S6) with the relative timing and intensity of the subpulses dependent on the step size (*25*). Modulation with a 0.6π step pushes most of the intensity into the late component, whereas a 1.4π step creates the mirror image in time, with most of the intensity in the early component. The second-order spectra for both excitation pulses are identical (fig S6, second and third rows), but their induced emission quantum yields change from 0.73 to 1.09 (Fig. 3A at π ± 0.4π), a 35% difference. This observation rules out a substantial role of phase modulation in shifting the second-order spectrum to match the two-photon absorption and drive the QY enhancement (*25*).

It is important to emphasize that the results do not depend solely on the time delay between the excitation double pulses or on their relative intensities. Figure 3B shows the effect of varying the time delay between two equally intense pulses that have distinct relative phases. For the double pulses with zero relative spectral phase (green curve), the $2G_2$-m-Per QY increases above the value observed for a TL pulse, yielding the greatest enhancement for a delay of ~70 fs. This delay coincides with the delay calculated from the phase-stepped pulse that maximized QY (1.4π) (fig. S6). Experiments with $2G_2$-m-OH yielded a similar response. In contrast, when the relative phase of the subpulses was shifted to π (magenta), no enhancement relative to a TL pulse was observed, regardless of delay time. As expected for two-photon excitation, the QY signals decreased as the pair of pulses arrived at the sample with delays larger than their pulse width.

The sensitivity of emission yield to the relative phase between the two temporal components of the excitation pulse is a clear consequence of the quantum nature of the excited state formed. The optimum spectral phase evidently facilitates interference processes to modify the excited-state dynamics, which suppresses the coupling to undesired internal conversion pathways (*31*). One possible physical mechanism is that at ~70 fs, a new light-matter interaction occurs, moving the excited-state wave packet away from regions on the excited potential surface prone to nonradiative relaxation pathways. To explore this hypothesis, we performed a pump-probe experiment in which the sample was resonantly excited at ~400 nm (equivalent in frequency to the two-photon excitation at 800 nm) and probed at 800 nm. We sought with this experiment to uncover a second excited state that might further interact with the laser field after the initial excitation event. Indeed, Fig. 3C indicates that both the pure donor and donor-acceptor molecules have a strong photoinduced absorption around 800 nm, which grows within the instrument response time. A small decay was observed in $2G_2$-m-Per because of energy transfer to the acceptor.

Hence, there is an auxiliary excited state in the donor moiety that can be resonantly accessed by a briefly delayed 800-nm pulse in the quantum control experiment. For the right phase and temporal tuning, this process is enhanced, diminishing nonradiative decay and thus increasing overall QY. In the energy transfer process (*23*), only the direct pathway would be controllable by phase-modulated pulses; thus, the fraction of excited molecules that can undergo this 2+1 mechanism is limited and cannot be measured by a power dependence study.

This mechanism is bolstered by closed-loop experiments directed toward minimizing the emission quantum yield. The iteration cycle yielded only a smooth, long pulse, implying that absorption efficiency was reduced and thus that the excited state dynamics could not be actively manipulated (*25*).

Since the initial experiments on coherent control of light-matter interactions, several phase/amplitude sensitive mechanisms have been found to influence photoinduced processes (*32*–*34*). Here, we affirm that the control is exerted on the dynamics of the excited state. We therefore need to assess the possibility of contributions from intensity dependence of the two-photon absorption (Fig. 2) (*19*, *35*, *36*); spectral control; uniqueness of the phase function; direct excitation of the acceptor; and a mechanism of optimally "dumping" from the excited state, to the overall optimization. Evaluation of all these mechanisms are detailed in (*25*).

Through a succession of closed and open-loop optimization studies, we have discovered that a simple step function applied to the spectral phase of a photoexcitation pulse can enhance the emission quantum yield of a complex donor-acceptor molecule.

Closed-loop experiments taught us about an optimization based on different components: population transfer and excited-state dynamics control. We identified and manipulated previously unappreciated coherences in the donor-localized excited state of the molecule. Interferences on the excited state of the donor activate a delayed excitation, changing the overall coupling into nonradiative pathways. This mechanism affords a methodology to explore dynamical processes.

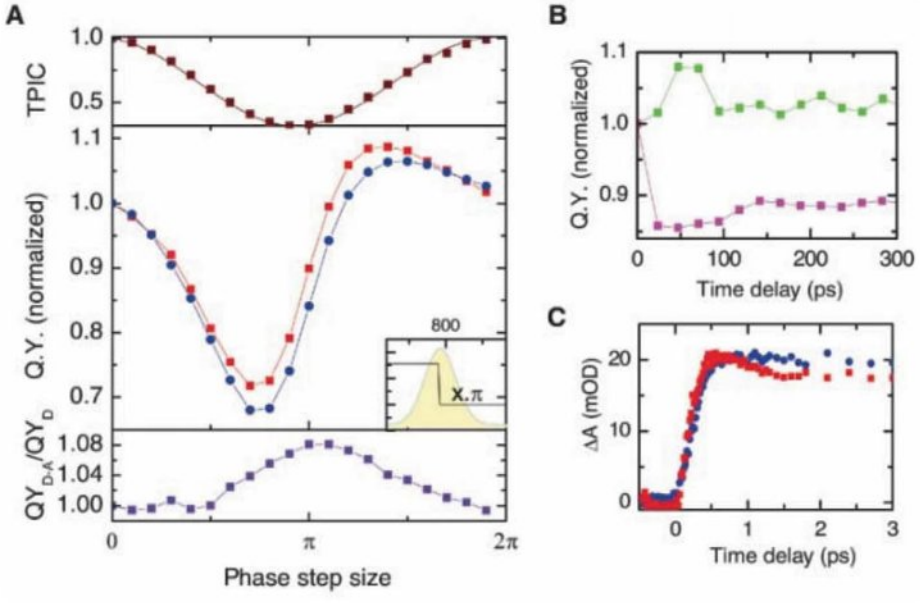

Fig. 3. Single-parameter experiments. Effect of varying the spectral phase step size applied to the excitation pulse (centered at ~800 nm) on [(**A**) top panel] two-photon induced diode response and [(A), middle panel)] emission QY measured for solutions of donor $2G_2$-m-OH (blue) and donor-acceptor $2G_2$-m-Per (red). The QY values show a maximum at 1.4π. [(A), bottom panel)] Ratio of red to blue curves. (**B**) QY of $2G_2$-m-Per after two-photon excitation with a pair of pulses (~800 nm). Each pair is modulated with 0 (green) and π (magenta) relative phase. The 70-fs delay (green curve maximum) corresponds well to the double-pulse separation in pulses shaped by a spectral phase step of 1.4π radians. (**C**) Transient absorption experiment performed on $2G_2$-m-OH (blue) and $2G_2$-m-Per (red) with 400-nm pump and 800-nm probe pulses. Photoinduced absorption in both molecules reveals a second excited state accessible by 800-nm absorption, confirming the possibility of a 2+1 mechanism for the coherent control.

References and Notes

1. S. A. Rice, *Science* **258**, 412 (1992).
2. W. S. Warren, H. Rabitz, M. Dahleh, *Science* **259**, 1581 (1993).
3. V. I. Prokhorenko, A. M. Nagy, R. J. D. Miller, *J. Chem. Phys.* **122**, 184502 (2005).
4. D. J. Tannor, S. A. Rice, *J. Chem. Phys.* **83**, 5013 (1985).
5. D. J. Tannor, S. A. Rice, *Adv. Chem. Phys.* **70**, 441 (1988).
6. K. Ohmori, *Annu. Rev. Phys. Chem.* **60**, 487 (2009).
7. R. S. Judson, H. Rabitz, *Phys. Rev. Lett.* **68**, 1500 (1992).
8. A. Assion *et al.*, *Science* **282**, 919 (1998).
9. J. L. Herek, W. Wohlleben, R. J. Cogdell, D. Zeidler, M. Motzkus, *Nature* **417**, 533 (2002).
10. R. J. Levis, G. M. Menkir, H. Rabitz, *Science* **292**, 709 (2001).

11. V. I. Prokhorenko *et al.*, *Science* **313**, 1257 (2006).
12. J. Savolainen *et al.*, *Proc. Natl. Acad. Sci. U.S.A.* **105**, 7641 (2008).
13. I. Otake, S. S. Kano, A. Wada, *J. Chem. Phys.* **124**, 014501 (2006).
14. C. Daniel *et al.*, *Science* **299**, 536 (2003).
15. M. P. A. Branderhorst *et al.*, *Science* **320**, 638 (2008).
16. R. A. Bartels, M. M. Murnane, H. C. Kapteyn, I. Christov, H. Rabitz, *Phys. Rev. A* **70**, 043404 (2004).
17. D. Cardoza, C. Trallero-Herrero, F. Langhojer, H. Rabitz, T. Weinacht, *J. Chem. Phys.* **122**, 124306 (2005).
18. M. A. Montgomery, R. R. Meglen, N. H. Damrauer, *J. Phys. Chem. A* **110**, 6391 (2006).
19. M. A. Montgomery, R. R. Meglen, N. H. Damrauer, *J. Phys. Chem. A* **111**, 5126 (2007).
20. J. L. White, B. J. Pearson, P. H. Bucksbaum, *J. Phys. At. Mol. Opt. Phys.* **37**, L399 (2004).
21. $2G_2$-m-Per is a second-generation dendrimer with two monodendrons on meta positions and an ethynylene perylene trap.
22. Z. H. Peng, J. S. Melinger, V. Kleiman, *Photosynth. Res.* **87**, 115 (2006).
23. E. Atas, Z. H. Peng, V. D. Kleiman, *J. Phys. Chem. B* **109**, 13553 (2005).
24. Z. H. Peng, Y. C. Pan, B. B. Xu, J. H. Zhang, *J. Am. Chem. Soc.* **122**, 6619 (2000).
25. Materials and methods are available as supporting material on *Science* Online.
26. S. F. Swallen, R. Kopelman, J. S. Moore, C. Devadoss, *J. Mol. Struct.* **486**, 585 (1999).
27. D. Meshulach, Y. Silberberg, *Nature* **396**, 239 (1998).
28. D. Meshulach, D. Yelin, Y. Silberberg, *Opt. Commun.* **138**, 345 (1997).
29. T. Brixner, N. H. Damrauer, B. Kiefer, G. Gerber, *J. Chem. Phys.* **118**, 3692 (2003).
30. M. H. B. Schmidt, G. Stobrawa, T. Feurer, LAB2-A virtual femtosecond laser lab, www.lab2.de.
31. L. G. C. Rego, L. F. Santos, V. S. Batista, *Annu. Rev. Phys. Chem.* **60**, 293 (2009).
32. D. Meshulach, Y. Silberberg, *Phys. Rev. A* **60**, 1287 (1999).
33. M. A. Montgomery, N. H. Damrauer, *J. Phys. Chem. A* **111**, 1426 (2007).
34. V. D. Kleiman, S. M. Arrivo, J. S. Melinger, E. J. Heilweil, *Chem. Phys.* **233**, 207 (1998).
35. T. Brixner, N. H. Damrauer, P. Niklaus, G. Gerber, *Nature* **414**, 57 (2001).
36. J. P. Ogilvie, K. J. Kubarych, A. Alexandrou, M. Joffre, *Opt. Lett.* **30**, 911 (2005).

37. This work was supported by the NSF, CHE-0239120.

Supporting Online Material

www.sciencemag.org/cgi/content/full/326/5950/263/DC1
Materials and Methods
SOM Text
Figs. S1 to S11
References

19 May 2009; accepted 31 August 2009
10.1126/science.1176524

Repetitive Readout of a Single Electronic Spin via Quantum Logic with Nuclear Spin Ancillae

L. Jiang,[1]*† J. S. Hodges,[1,2]* J. R. Maze,[1]* P. Maurer,[1] J. M. Taylor,[3]‡ D. G. Cory,[2] P. R. Hemmer,[4] R. L. Walsworth,[1,5] A. Yacoby,[1] A. S. Zibrov,[1] M. D. Lukin[1]§

Robust measurement of single quantum bits plays a key role in the realization of quantum computation and communication as well as in quantum metrology and sensing. We have implemented a method for the improved readout of single electronic spin qubits in solid-state systems. The method makes use of quantum logic operations on a system consisting of a single electronic spin and several proximal nuclear spin ancillae in order to repetitively readout the state of the electronic spin. Using coherent manipulation of a single nitrogen vacancy center in room-temperature diamond, full quantum control of an electronic-nuclear system consisting of up to three spins was achieved. We took advantage of a single nuclear-spin memory in order to obtain a 10-fold enhancement in the signal amplitude of the electronic spin readout. We also present a two-level, concatenated procedure to improve the readout by use of a pair of nuclear spin ancillae, an important step toward the realization of robust quantum information processors using electronic- and nuclear-spin qubits. Our technique can be used to improve the sensitivity and speed of spin-based nanoscale diamond magnetometers.

Efforts have recently been directed toward the manipulation of several qubits in quantum systems, ranging from isolated atoms and ions to solid-state quantum bits (*1*, *2*). These small-scale quantum systems have been successfully used for proof-of-concept demonstrations of simple quantum algorithms (*3*–*6*). In addition, they can be used for potentially important practical applications in areas such as quantum metrology (*1*). For example, techniques involving quantum logic operations on several trapped ions have been applied to develop an improved ion state readout scheme, resulting in a new class of atomic clocks (*7*, *8*). We developed a similar technique to enhance the readout of a single electronic spin in the solid state.

Our method makes use of quantum logic between a single electronic spin and nuclear spin qubits in its local environment for repetitive readout. Although such nuclear spins are generally the source of unwanted decoherence in the solid state, recent theoretical (*9*–*11*) and experimental (*12*–*18*) work has demonstrated that when properly controlled, the nuclear environment can become a very useful resource, in particular for long-term quantum memory.

Our experimental demonstration makes use of a single negatively charged nitrogen-vacancy (NV) center in diamond. The electronic ground state of this defect is an electronic spin triplet (with spin $S = 1$) and is a good candidate for a logic qubit on account of its remarkably long coherence times (*19*) and fast spin manipulation by use of microwave fields (*20*). Furthermore, the center can be optically spin-polarized and measured by combining confocal microscopy techniques with spin-selective rates of fluorescence (*12*). In practice, the NV spin readout under ambient room-temperature conditions is far from perfect. This is because laser radiation at 532 nm for readout repolarizes the electronic spin before a sufficient number of photons can be scattered for the state to be reliably determined.

Our approach is to correlate the electronic-spin logic qubit with nearby nuclear spins (*21*), which are relatively unperturbed by the optical readout, before the measurement process (*22*). Specifically, we used one or more ^{13}C nuclei (with nuclear spin $I = 1/2$) nuclear spins in the diamond lattice, coupled to the NV electronic spin via a hyperfine interaction, as memory ancillae qubits. For example, a single ^{13}C nuclear spin has eigenstates $|\uparrow\rangle_{n1}$ (aligned) or $|\downarrow\rangle_{n1}$ (anti-aligned) with the local magnetic field. The composite electronic-nuclear system was first prepared in a fiducial state, $|0\rangle_e\,|\downarrow\rangle_{n1}$, by using a sequence of optical, microwave, and radiofrequency (RF) pulses. Next, the electronic spin was prepared in an arbitrary state $|\Psi\rangle_e = \alpha|0\rangle_e + \beta|1\rangle_e$, where $|0,1\rangle_e$ denote electronic state with projected spin momentum m_S (m_S) = 0, 1. Before readout, we performed a sequence of gate operations resulting in the entangled electron-nuclear state $|\Psi\rangle_e\,|\downarrow\rangle_{n1} \rightarrow \alpha|0\rangle_e\,|\downarrow\rangle_{n1} + \beta|1\rangle_e\,|\uparrow\rangle_{n1}$. The optical measurement process projects this state into either $|0\rangle_e\,|\downarrow\rangle_{n1}$ or $|1\rangle_e\,|\uparrow\rangle_{n1}$. When optically excited, these two states fluoresce at different rates dependent on the value of m_S. Within a typical measurement period, less than one photon was counted before the electron spin was repolarized to $|0\rangle_e$, which indicates that the uncertainty of the electronic spin-state measurement is quite large.

The nuclear spin can thus reveal the former electronic state because of the correlations established before the electronic spin was reset. To achieve this repetitive readout, we performed a controlled-not operation, which mapped $|0\rangle_e\,|\downarrow\rangle_{n1} \rightarrow |0\rangle_e\,|\downarrow\rangle_{n1}$ and $|0\rangle_e\,|\uparrow\rangle_{n1} \rightarrow |1\rangle_e\,|\uparrow\rangle_{n1}$, and repeated the

[1]Department of Physics, Harvard University, Cambridge, MA 02138, USA. [2]Department of Nuclear Science and Engineering, Massachusetts Institute of Technology (MIT), Cambridge, MA 02139, USA. [3]Department of Physics, MIT, Cambridge, MA 02139, USA. [4]Department of Electrical and Computer Engineering, Texas A&M University, College Station, TX 77843, USA. [5]Harvard-Smithsonian Center for Astrophysics, Cambridge, MA 02138, USA.

*These authors contributed equally to this work.
†Present address: Institute for Quantum Information, California Institute of Technology, Pasadena, CA 91125, USA.
‡Present address: Joint Quantum Institute, University of Maryland, College Park, MD 20742, USA.
§To whom correspondence should be addressed. E-mail: lukin@fas.harvard.edu

optical measurement. Fluorescence counting of these two states can be added to prior measurements so as to decrease the uncertainty for electronic spin-state discrimination. If optical readout does not destroy the orientation of the nuclear spin, the uncertainty in the determination of the electronic spin can be reduced via repetitive measurements. In this way, the overall signal-to-noise of the measurement process of our logic qubit can be increased. After multiple readout cycles and many quantum logic operations, the nuclear spin orientation will finally be destroyed. However, it is possible to further improve the readout scheme by using a pair of ancillary nuclear spins and imprinting the electronic state into a Greenberger-Horne-Zeilinger (GHZ)–like state: $|\Psi\rangle_e\,|\downarrow\rangle_{n1}\,|\downarrow\rangle_{n2} \rightarrow \alpha|0\rangle_e\,|\downarrow\rangle_{n1}\,|\downarrow\rangle_{n2} + \beta|1\rangle_e\,|\uparrow\rangle_{n1}\,|\uparrow\rangle_{n2}$. In such a case, the state of the first nuclear spin after repetitive readout sequences can be periodically "refreshed" by using the information stored within the second nuclear spin. These schemes are closely related to a quantum nondemolition (QND) measurement (*23*, *24*) because the nuclear spin-population operators $\hat{I}_z^{n1,n2}$ do not evolve throughout the electronic-spin readout and constitute "good" QND observables. Although imperfect, optical NV electronic spin detection precludes an ideal QND measurement, our scheme nevertheless allows substantial improvement in the spin readout.

To implement the repetitive readout technique, we used a single NV center in diamond coupled to nearby ^{13}C nuclear spins. These nuclear spins can be polarized and fully controlled and provide a robust quantum memory, even in the presence of optical radiation necessary for electronic spin-state readout (*13*, *22*). This is achieved through a combination of optical, microwave, and RF fields (Fig. 1) and is discussed in (*25*).

To control a single nuclear spin, we chose a NV center with a well-resolved ^{13}C hyperfine coupling near 14 MHz. The degeneracy of the $|m_S = \pm 1\rangle_e$ spin states was lifted by applying a $B_0 = 30$ gauss magnetic field along the NV axis. Under these conditions, the transitions of the electronic spin (**e**) within the subspace of $\{|0\rangle_e, |1\rangle_e\}$ can be selectively addressed, conditioned on a certain nuclear state. The model Hamiltonian for this system (Fig. 1A) is

$$H = (\Delta + \gamma_e B_0)\hat{\mathcal{S}}_z + \gamma_C B_0 \hat{I}_z^{n1} + A\hat{\mathcal{S}}_z\hat{I}_z^{n1} \quad (1)$$

where $\Delta = 2\pi \times 2.87$ GHz is the zero field splitting, A is the hyperfine interaction, and γ_e and γ_C are the electronic- and nuclear-spin gyromagnetic ratios. $\hat{\mathcal{S}}_z = \frac{1}{2}\hat{\mathbf{1}} + \hat{S}_z$ is a pseudo-spin one-half operator for the electronic spin subspace, $\hat{\mathbf{1}}$ is the identity matrix, and $\hat{I}_z^{n1}$ and $\hat{S}_z$ are the spin-1/2 angular momentum operators. Coherent oscillations between the $|0\rangle_e$ and $|1\rangle_e$ states, conditioned on a single proximal nuclear spin ($\mathbf{n}_1$) in $|\downarrow\rangle_{n1}$ (or $|\uparrow\rangle_{n1}$), were selectively driven by the microwave field MW1 (or MW2). To control nuclear spin $\mathbf{n}_1$, a resonantly tuned RF field to address the levels $|1\rangle_e\,|\downarrow\rangle_{n1}$ and $|1\rangle_e\,|\uparrow\rangle_{n1}$, which are energetically separated because of the hyperfine interaction (Fig. 1A), was used. After the initialization of spin **e**, spin $\mathbf{n}_1$ was polarized by applying MW1 and RF π pulses, which transfers the polarization from spin **e** to spin $\mathbf{n}_1$. Rabi oscillations of spin $\mathbf{n}_1$ were demonstrated (Fig. 1E) by preparing spin **e** in the $|1\rangle_e$ state irrespective of the state of spin $\mathbf{n}_1$ (by using MW1 and MW2 π-pulses) and increasing the RF pulse length. These data indicate that we can achieve spin $\mathbf{n}_1$ preparation (polarization) and readout with combined fidelity $F \equiv \langle\downarrow|\,\rho'\,|\downarrow\rangle \geq 75\%$, where ρ' is the reduced density operator for spin $\mathbf{n}_1$.

We now describe the repetitive readout technique. As illustrated in Fig. 1D, the direct readout of electronic spin is imperfect. We define n^0 and n^1 as the total number of photons detected for the $|0\rangle_e$ and $|1\rangle_e$ states, respectively, during a single measurement interval. The signal is defined as the difference in average counts between the two spin states: $A_0 = n^0 - n^1 \approx 0.005$ (Fig. 1D). Experimentally, photon shot-noise dominated the fluctuations in the counts. Because of this shot

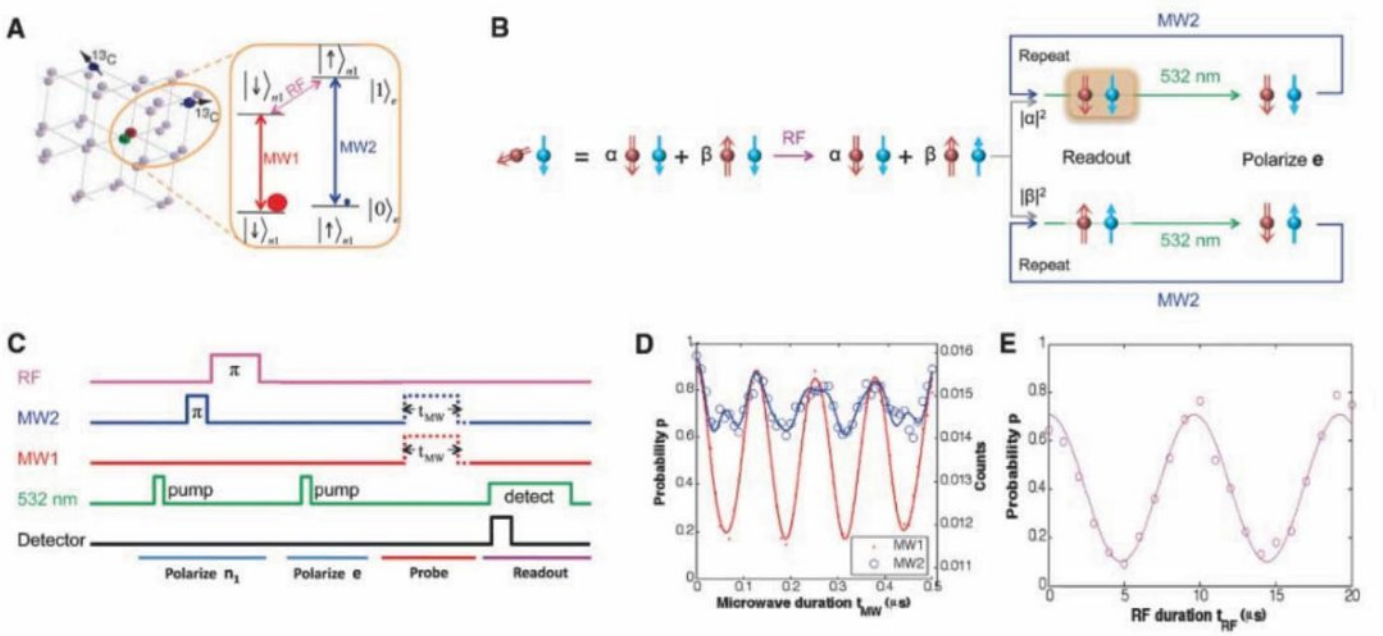

Fig. 1. Repetitive readout of an electronic spin. (**A**) Illustration of the NV center and its proximal ^{13}C nuclear spins. (Inset) Energy levels of the coupled spin system formed by the NV electronic spin (**e**) and the first proximal ^{13}C nuclear spin ($\mathbf{n}_1$). With a static magnetic field applied along the NV axis, spin $\mathbf{n}_1$ keeps the same quantization axis when spin **e** is $|0\rangle_e$ or $|1\rangle_e$ (*25*). When spin $\mathbf{n}_1$ is $|\downarrow\rangle_{n1}$ (or $|\uparrow\rangle_{n1}$), the microwave field MW1 (or MW2) resonantly drives spin **e** between $|0\rangle_e$ and $|1\rangle_e$, which can implement the $C_{n1}NOT_e$ gate. When spin **e** is $|1\rangle_e$, the RF field resonantly drives spin $\mathbf{n}_1$ between $|\downarrow\rangle_{n1}$ and $|\uparrow\rangle_{n1}$, which can implement the C_eNOT_{n1} gate. (**B**) Illustration of repetitive readout. The red down arrow represents the electronic spin state $|0\rangle_e$, the red up arrow represents the electronic spin state $|1\rangle_e$, the blue down arrow represents the nuclear spin state $|\downarrow\rangle_{n1}$, and the blue up arrow represents the nuclear spin state $|\uparrow\rangle_{n1}$. (**C**) Experimental pulse sequences that polarize spin $\mathbf{n}_1$ to $|\downarrow\rangle_{n1}$ and spin **e** to $|0\rangle_e$, followed by various probe operations, before fluorescence readout of spin **e**. (**D**) Measured electronic spin Rabi oscillations driven by MW1 and MW2 fields for polarized spin $\mathbf{n}_1$. The small wiggles for MW2 are due to off-resonant driving of the majority population in the $|\downarrow\rangle_{n1}$ state. The data are in agreement for finite detunings and microwave power (solid curves). The right vertical axis shows the average counts for a single readout. The left vertical axis shows the probability in the $|0\rangle_e$ state, obtained from the average counts (*25*). (**E**) Measured nuclear spin Rabi oscillation driven by the RF field.

noise and the low average count ($n^0 \approx 0.016$), we needed to average over $N \sim 10^5$ experimental runs in order to obtain the data in Fig. 1D.

To improve the signal, we used two spins: **e** and $\mathbf{n}_1$. Both spins were first polarized to the initial state $|0\rangle_e\,|\downarrow\rangle_{n1}$. Next, we performed a unitary operation $U(t)$, which prepares the superposition state $|\Psi_1\rangle = (\alpha|0\rangle_e + \beta|1\rangle_e)\,|\downarrow\rangle_{n1}$ that we wanted to measure. Instead of immediately reading out the electronic spin, we use a controlled-not gate (C_eNOT_{n1}, achieved with an RF π pulse) to correlate spin **e** with spin $\mathbf{n}_1$ (Fig. 2A). We then optically readout/pumped spin **e**, leaving the spin system in the post-readout state: $\rho_{post} = |0\rangle\langle 0|_e \otimes (|\alpha|^2\,|\downarrow\rangle\langle\downarrow| + |\beta|^2\,|\uparrow\rangle\langle\uparrow|)_{n1}$. The state of spin $\mathbf{n}_1$ via the electronic spin **e** by performing a controlled-not operation ($C_{n1}NOT_e$, achieved with an MW1 or MW2 π pulse) was then readout. This completes a one-step readout of spin $\mathbf{n}_1$, which can be repeated.

As a direct illustration of the enhanced readout technique, Fig. 2C shows the accumulated signal for Rabi oscillations of the electronic spin obtained by adding M subsequent repetitive readouts for each experimental run. This procedure results in a 10-fold enhancement of spin signal amplitude.

In order to further quantify the performance of this technique, the noise added with each additional repetitive readout must be considered. The repetitive readout spin signal is defined as a weighted sum of difference counts A_m associated with mth readout: $S_w(M) = \sum_{m=1}^{M} w_m A_m$. The average values of A_m were determined experimentally by measuring the difference in average counts associated with Rabi oscillations for each mth repeated readout. The w_m allowed us to weight the contribution of each repetitive readout to the overall signal. The noise corresponding to the repetitive readout signal is $\Delta S_w(M) = \sqrt{\sum_{m=1}^{M} w_m^2 \sigma_m^2}$. Here, σ_m is the uncertainty of the measurement of A_m. Experimentally, this uncertainty was found to be independent of m.

The signal-to-noise figure of merit is defined as $SNR\ (M) = S_w(M)/\Delta S_w(M)$. The w_m weights were chosen by noting that the larger values of A_m allow us to extract more information given the fixed uncertainty of each measurement, and we should emphasize these readouts more. As proven in (*25*), the optimal choice of weights corresponds to $w_m = |A_m|/\sigma_m^2$, and the optimized SNR is given by

$$\mathrm{SNR}_{opt}(M) = \sqrt{\sum_{m=1}^{M} \left|\frac{A_m}{\sigma_m}\right|^2} \qquad (2)$$

In the ideal QND case, each repetitive readout would yield the same $|A_m|$, and the SNR would scale with $\sqrt{M}$. For our experiment, the SNR saturates (Fig. 2E) because of the decay of the normalized amplitudes (Fig. 3D). Nevertheless, the experimental data shown in Fig. 2E indicate the enhancement of SNR by more than 220%.

In assessing this result, it is noted that various imperfections can affect the repetitive readout, which leads to the imperfect first readout $|A_1|/|A_0| < 1$, the sharp decrease in $|A_2|$, and the subsequent exponential reduction $|A_m| = |A_2|\eta^{(m-2)}$, with $\eta \approx 0.95$. These behaviors can be attributed to three major imperfections (*25*): (i) errors from microwave pulses (about 7% error probability for each π pulse), (ii) imperfect optical pumping of the electronic spin after each readout; and most substantially (iii) the depolarization of the nuclear-spin memory under optical illumination.

To quantify the latter process, we studied the decay times for ^{13}C nuclear spins in the presence of optical illumination. For an illumination time t_L longer than 1 μs, the nuclear spin polarization decays exponentially, with a characteristic time of $\tau_{n1} = 13\ (1)$ μs (Fig. 3B). Because τ_{n1} is much longer than the time for optical readout and optical spin polarization of the NV electronic spin (350 ns), repetitive readout of **e** is possible. [In the absence of optical illumination, the ^{13}C nuclear spin decay times are >>1 ms (*12*, *13*).] Despite the relatively long τ_{n1}, after many cycles the nuclear spin depolarizes. This degrades the repetitive optical readout for larger m, yielding the overall exponential decay in the amplitude $|A_m|$ with increasing m (*25*).

As an indication of how this limit can be circumvented, the use of two ancillary nuclear spins

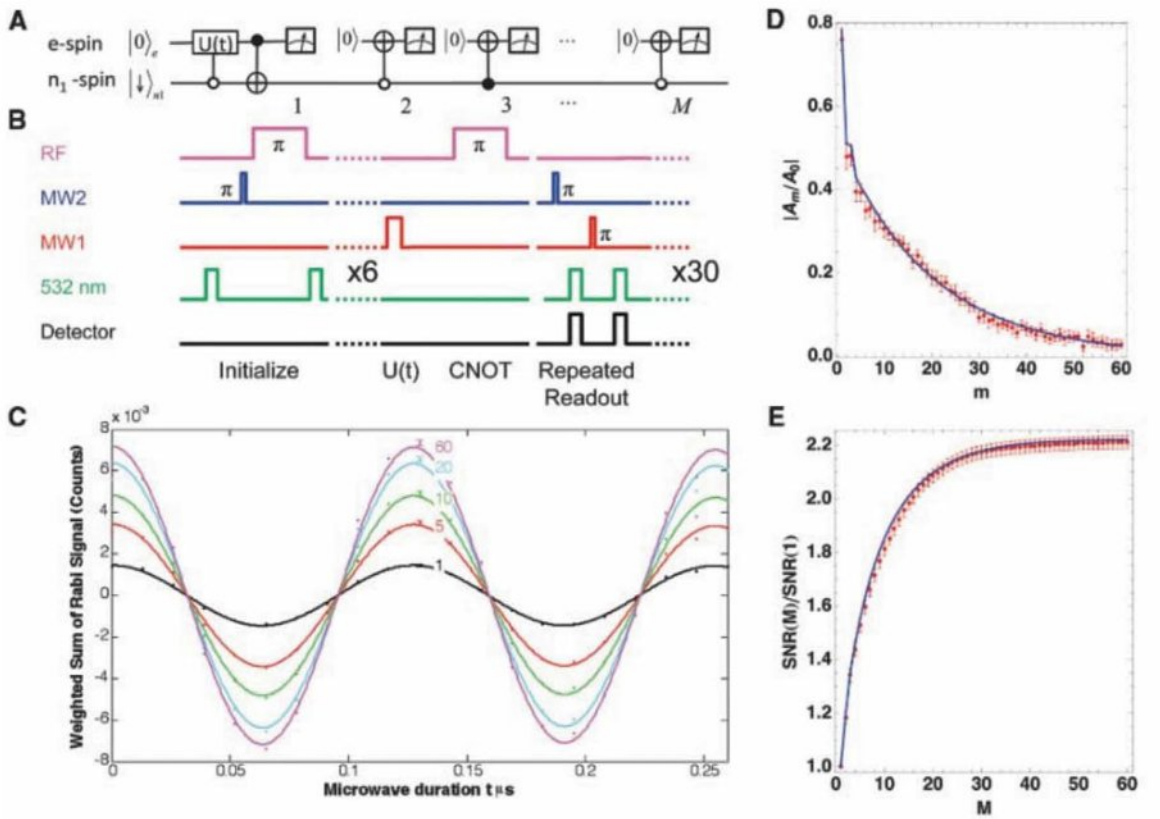

Fig. 2. Realization of repetitive readout. (**A**) Quantum circuit for M-step repetitive readout scheme assisted by spin $\mathbf{n}_1$. (**B**) Operations and pulse sequences for $M = 60$. The initial state $|0\rangle_e\,|\downarrow\rangle_{n1}$ is prepared with a six-step pumping of spins **e** and $\mathbf{n}_1$. The MW1 pulse of duration t induces the Rabi rotation $U(t)$ of spin **e**, whose parity information is imprinted to spin $\mathbf{n}_1$ with an RF π pulse (the C_eNOT_{n1} gate). After fluorescence readout of spin **e**, $(M - 1)$–repetitive readouts of spin $\mathbf{n}_1$ are performed by means of MW1 or MW2 π pulses ($C_{n1}NOT_e$ gates) followed by fluorescence readout. The $m = 1$ readout is not preceded by a MW1 pulse. (**C**) Cumulative signal obtained from repetitive readout measurements, summed from $m = 1$ to M, for $M = 1$, 5, 10, 20, and 60 repetitions. Constant background counts are subtracted. (**D**) Amplitudes $|A_m|$ for Rabi oscillation measurements obtained from the mth readout normalized to the signal amplitude without repetitive readout (A_0). (**E**) Improvement in SNR using the repetitive readout scheme. Blue curves in (D) and (E) are simulations with imperfection parameters estimated from independent experiments (*25*).

was considered. The state of spin **e** may be correlated with a more distant spin $\mathbf{n}_2$ in addition to proximal spin $\mathbf{n}_1$. As the decay time of spin $\mathbf{n}_2$ is longer than that of spin $\mathbf{n}_1$ because of a weaker interaction with spin **e**, the information stored in spin $\mathbf{n}_2$ persists after spin $\mathbf{n}_1$ has been depolarized under optical illumination. This remaining $\mathbf{n}_2$ polarization can then be transferred to spin $\mathbf{n}_1$ and repetitively readout again.

Control of two nuclear spins is achieved by using the strongly coupled nuclear spin $\mathbf{n}_1$ as a probe for the second nearby ^{13}C nuclear spin $\mathbf{n}_2$, which cannot be directly observed via the NV center. By placing the NV electronic spin in $|0\rangle_e$ state, the hyperfine coupling is removed. This enables proximal ^{13}C nuclear spins with similar Zeeman energy to flip-flop and exchange spin population. Figure 3D shows that the nuclear population, $p_{n1,\uparrow}(\tau)$, oscillates between $p_{n1,\uparrow}(0) \approx 0.2$ and $p_{n1,\uparrow}(T/2) \approx 0.5$ with a period of $T = 117$ (1) μs (Fig. 3, A and C). The relatively high contrast of these oscillations suggests an interaction with a second nuclear spin ($\mathbf{n}_2$) as the two nuclei flip-flop between the states $|\uparrow\rangle_{n1}|\downarrow\rangle_{n2}$ and $|\downarrow\rangle_{n1}|\uparrow\rangle_{n2}$. Such an excitation exchange requires a similar Zeeman splitting for the two spins, indicating that the second nucleus is also a ^{13}C. The nuclear spin-spin interaction strength determined by our measurements, $b = \pi/T = 4.27$ (3) kHz, is several times that of a bare dipolar coupling (2 kHz for two ^{13}C nuclei separated by the nearest neighbor distance, 1.54 Å), signifying that their interaction is mediated by the NV electronic spin (Fig. 3A, inset) (*25*), which is described by the interaction hamiltonian $H_{\text{int}} = b(I_{1+}I_{2-} + I_{1-}I_{2+})$. This interaction can be used to effectively control the state of the second nucleus and of the entire three-spin system. Specifically, a half period of nuclear spin oscillation, $T/2$, constitutes a SWAP (*1*) operation between the two nuclear spins. This operation can be used, for example, to polarize the second nuclear spin (Fig. 3, C and D). In addition, by modifying the initial state of spin $\mathbf{n}_1$, we can prepare the initial state of the two nuclei in any of the four possible configurations: ↑↑, ↑↓, ↓↑, or ↓↓ (*25*). Further control is provided by putting the electronic spin into the $|1\rangle_e$ state, in which case the flip-flop dynamics between spins $\mathbf{n}_1$ and $\mathbf{n}_2$ disappears (fig. S1). This is because spins $\mathbf{n}_1$ and $\mathbf{n}_2$ typically have very distinct hyperfine splittings that introduce a large energy difference ($\Delta E >> b$) between $|\uparrow\rangle_{n1}|\downarrow\rangle_{n2}$ and $|\downarrow\rangle_{n1}|\uparrow\rangle_{n2}$ and quench the interaction. Therefore, we can implement a controlled-SWAP operation between spins $\mathbf{n}_1$ and $\mathbf{n}_2$, enabling full control over spin $\mathbf{n}_2$. We further observed that spin $\mathbf{n}_2$ has a decay time of $\tau_{n2} = 53$ (1) μs (Fig. 3B, inset) under

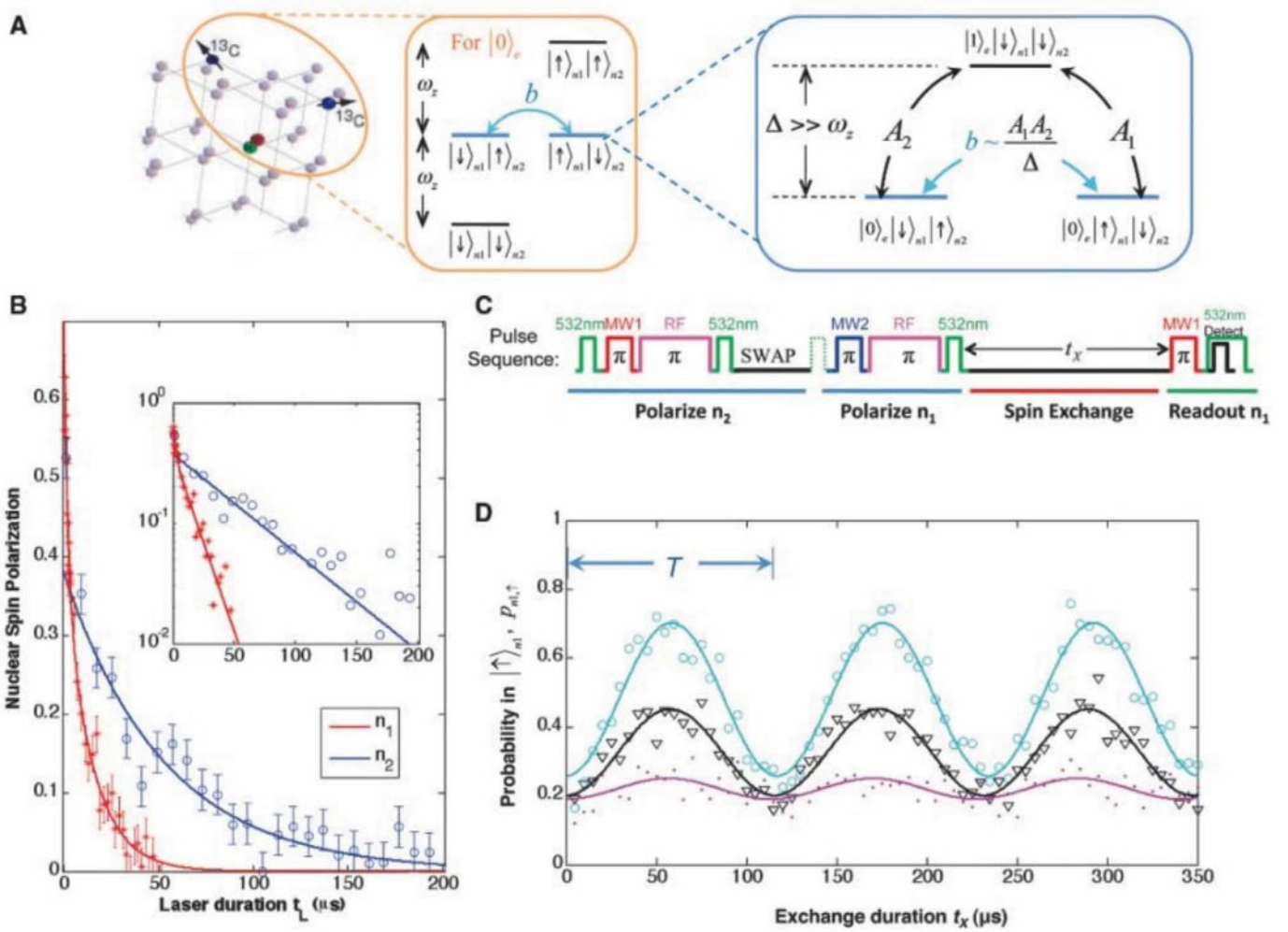

Fig. 3. Coherence and control of two nuclear spins. (**A**) The coupled spin system formed by the NV electronic spin (**e**) and two proximal ^{13}C nuclear spins ($\mathbf{n}_1$ and $\mathbf{n}_2$). (Middle) Energy levels for spins $\mathbf{n}_1$ and $\mathbf{n}_2$ when spin **e** is in the $|0\rangle_e$ state. (Right) Schematic of flip-flop between spins $\mathbf{n}_1$ and $\mathbf{n}_2$, which is electron-mediated by the second-order hopping via $|1\rangle_e|\downarrow\rangle_{n1}|\downarrow\rangle_{n2}$. (**B**) Measured depolarization of spins $\mathbf{n}_1$ and $\mathbf{n}_2$ under optical illumination. For the duration of optical illumination t_L longer than 1 μs, the polarizations for spins $\mathbf{n}_1$ and $\mathbf{n}_2$ decay exponentially with characteristic times $\tau_{n1} = 13$ (1) μs and $\tau_{n2} = 53$ (5) μs, respectively. For t_L less than 1 μs, the decay is slightly faster, which is probably associated with dynamics of the spin-fluctuator model that describe optically induced depolarization of single nuclei (*22*, *25*). These decay times are much longer than the optical readout/pump time of the electronic spin (about 350 ns). (Inset) Log-linear plot. (**C**) Operations and pulse sequence to probe dynamics between spins $\mathbf{n}_1$ and $\mathbf{n}_2$. (**D**) Measured spin flip-flop dynamics between spins $\mathbf{n}_1$ and $\mathbf{n}_2$. For three different preparations of the initial state [$|\downarrow\rangle_{n1}|\uparrow\rangle_{n2}$ (blue), $|\downarrow\rangle_{n1}$ and n_2 in thermal state (black), and $|\downarrow\rangle_{n1}|\downarrow\rangle_{n2}$ (purple)], the observed population, $p_{n1,\uparrow}(t)$, oscillates with the same period $T = 117$ (1) μs. These observations verify the theoretical prediction, with flip-flop coupling strength $b = 4.27$ (3) kHz.

optical illumination. Compared with spin $\mathbf{n}_1$, spin $\mathbf{n}_2$ is less perturbed by the optical transitions between different electronic states because it has a weaker hyperfine coupling to the electron (*22*).

To demonstrate concatenated readout experimentally, both nuclear spins were initialized in the state $|\downarrow\rangle_{n1}\,|\downarrow\rangle_{n2}$, and a single NV electronic spin that we would like to detect was prepared in a superposition state $(\alpha|0\rangle + \beta|1\rangle)_e$. First, the operation ($C_eNOT_{n1}$-SWAP-$C_eNOT_{n1}$) was used to prepare the GHZ-type state $|\Psi\rangle = \alpha|0\rangle_e\,|\downarrow\rangle_{n1}\,|\downarrow\rangle_{n2} + \beta|1\rangle_e\,|\uparrow\rangle_{n1}\,|\uparrow\rangle_{n2}$. Next, we optically readout/pumped spin **e**, leaving the system in state $\rho'_{post} = |\alpha|^2\,|0\downarrow\downarrow\rangle\langle 0\downarrow\downarrow| + |\beta|^2\,|0\uparrow\uparrow\rangle\langle 0\uparrow\uparrow|$. $M-1$ repetitive readouts of spin $\mathbf{n}_1$ were then performed in the manner described above until spin $\mathbf{n}_1$ was depolarized. At that point, spin $\mathbf{n}_2$ was still directly correlated with the first measurement of the **e** spin. This information can be transferred to spin $\mathbf{n}_1$ by means of a nuclear SWAP gate. Thus, the parity information can be measured again by performing a second round of M-step repetitive readout. These operations are summarized in the quantum circuit (Fig. 4A) and pulse sequences (Fig. 4B).

Experimentally, the "revival" in the signal amplitude $|A_m|$ after the SWAP was demonstrated (Fig. 4C), which led to an associated jump in the SNR curve (Fig. 4D) for $M' = 61$. This shows that the second nuclear spin can be used to further enhance the readout efficiency. Although ideally the repetitive readout scheme assisted by two nuclear spins should improve the absolute SNR more than a single nuclear spin, in the present experimental realization this is not yet so because more errors are accumulated for the two-nuclear-spin scheme because of initialization and pulse imperfections. These errors reduce the optical signal amplitudes for the readout assisted by two nuclear spins, compromising the overall SNR improvement. Nevertheless, the experiments clearly demonstrate that it is in principle possible to further boost the relative SNR by using additional nuclear spins.

Although we have demonstrated an enhancement for coherent Rabi oscillations, any set of pulses acting on the electronic spin (such as a spin echo sequence) can be implemented. This should have immediate applications to NV-based nanomagnetometry (*26*, *27*). Because the duration of the entire repetitive readout sequence (~150 μs in Fig. 2B) is shorter than the typical echo duration in pure diamond, SNR improvements directly translate into enhanced sensitivity and increased speed of nanoscale diamond magnetometer (*28*). This may have important applications in probing time-varying processes in biophysical systems. The repetitive readout can also be used to achieve single-shot readout of NV centers. At room temperature, with optimized collection efficiency, an improvement in spin signal on the order of a few hundred is needed to achieve single-shot readout. Potentially, this improvement can be obtained by using nuclei more robust to optical depolarization, such as the nitrogen nuclear spin of the NV center in isotopically pure ^{12}C diamond (*19*) and by using advanced control techniques (*29*, *30*) to suppress the imperfections from microwave pulses. Furthermore, resonant optical excitations [wavelength $\lambda \approx 637$ nm] can be used for NV centers at cryogenic temperatures. Here, the resolved spin structure of optical excited states (*20*, *31*, *32*) can be exploited to readout the electronic spin much more efficiently with reduced perturbation to the nuclear spin (*22*). Under these conditions, a 10-fold spin signal improvement may be sufficient to enable single-shot readout of the NV electronic spin. In turn, this can be used to perform robust, adaptive QND measurements of nuclear-spin qubits, which will be of direct use for distributed quantum networks (*13*, *21*). Our experiments demonstrate that manipulation of several nuclear-spin ancillae surrounding a central electronic spin can be used to implement useful quantum algorithms in solid-state systems.

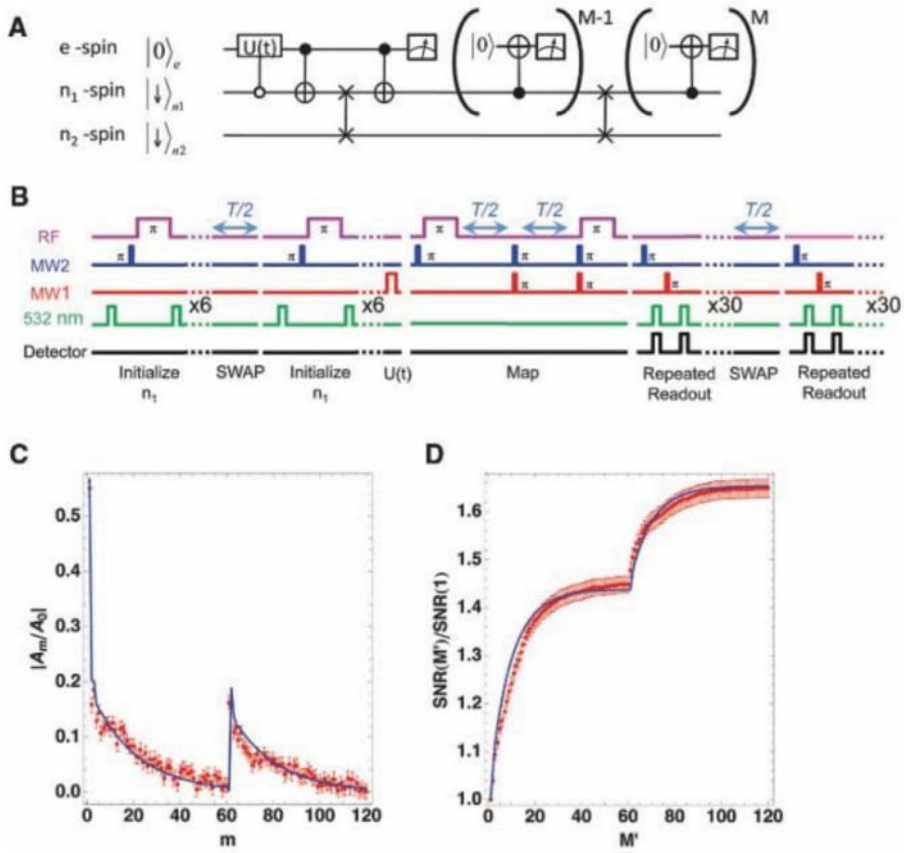

Fig. 4. Demonstration of the two-level concatenated readout procedure. (**A**) Quantum circuit for concatenated M-step repetitive readout scheme assisted by both spins $\mathbf{n}_1$ and $\mathbf{n}_2$. (**B**) Operations and pulse sequences for $M = 60$. Ideally, the GHZ-like state $\alpha|0\rangle_e\,|\downarrow\rangle_{n1}\,|\downarrow\rangle_{n2} + \beta|1\rangle_e\,|\uparrow\rangle_{n1}\,|\uparrow\rangle_{n2}$ with the parity information of spin **e** imprinted on both spins $\mathbf{n}_1$ and $\mathbf{n}_2$ is created before the first readout. After the first round of M-step repetitive readout, spin $\mathbf{n}_1$ is depolarized, but spin $\mathbf{n}_2$ maintains its polarization. The spin state of spin $\mathbf{n}_2$ is swapped to spin $\mathbf{n}_1$, which is then detected during the second round of M-step repetitive readouts. (**C**) Normalized amplitude $|A_m|/|A_0|$ obtained from the mth readout. (**D**) Measured improvement in the SNR by use of the double repetitive readout scheme. The blue curves in (C) and (D) are simulations with imperfection parameters estimated from independent experiments (*25*).

References and Notes

1. R. Blatt, D. Wineland, *Nature* **453**, 1008 (2008).
2. R. Hanson, D. D. Awschalom, *Nature* **453**, 1043 (2008).
3. M. Riebe *et al.*, *Nature* **429**, 734 (2004).
4. R. Reichle *et al.*, *Nature* **443**, 838 (2006).
5. L. DiCarlo *et al.*, *Nature* **460**, 240 (2009).
6. C. A. Ryan, C. Negrevergne, M. Laforest, E. Knill, R. Laflamme, *Phys. Rev. A* **78**, 012328 (2008).
7. T. Rosenband *et al.*, *Science* **319**, 1808 (2008).
8. D. B. Hume, T. Rosenband, D. J. Wineland, *Phys. Rev. Lett.* **99**, 120502 (2007).
9. W. M. Witzel, S. Das Sarma, *Phys. Rev. B* **77**, 165319 (2008).
10. J. Maze, J. M. Taylor, M. D. Lukin, *Phys. Rev. B* **78**, 094303 (2008).
11. W. A. Coish, J. Fischer, D. Loss, *Phys. Rev. B* **77**, 125329 (2008).
12. F. Jelezko *et al.*, *Phys. Rev. Lett.* **93**, 130501 (2004).
13. M. V. G. Dutt *et al.*, *Science* **316**, 1312 (2007).
14. P. Neumann *et al.*, *Science* **320**, 1326 (2008).
15. R. Hanson, V. V. Dobrovitski, A. E. Feiguin, O. Gywat, D. D. Awschalom, *Science* **320**, 352 (2008).
16. J. J. L. Morton *et al.*, *Nat. Phys.* **2**, 40 (2006).
17. J. S. Hodges, J. C. Yang, C. Ramanathan, D. G. Cory, *Phys. Rev. A* **78**, 010303 (2008).
18. J. J. L. Morton *et al.*, *Nature* **455**, 1085 (2008).
19. G. Balasubramanian *et al.*, *Nat. Mater.* **8**, 383 (2009).
20. G. D. Fuchs *et al.*, *Phys. Rev. Lett.* **101**, 117601 (2008).
21. L. Jiang, J. M. Taylor, A. S. Sorensen, M. D. Lukin, *Phys. Rev. A* **76**, 062323 (2007).
22. L. Jiang *et al.*, *Phys. Rev. Lett.* **100**, 073001 (2008).
23. S. Haroche, J. M. Raimond, *Exploring the Quantum: Atoms, Cavities, and Photons* (Oxford Univ. Press, New York, 2006).
24. M. Sarovar, K. C. Young, T. Schenkel, K. B. Whaley, *Phys. Rev. B* **78**, 245302 (2008).
25. Materials and methods are available as supporting material on *Science* Online.

26. J. R. Maze *et al.*, *Nature* **455**, 644 (2008).
27. G. Balasubramanian *et al.*, *Nature* **455**, 648 (2008).
28. J. M. Taylor *et al.*, *Nat. Phys.* **4**, 810 (2008).
29. N. Khaneja, T. Reiss, C. Kehlet, T. Schulte-Herbruggen, S. J. Glaser, *J. Magn. Reson.* **172**, 296 (2005).
30. P. Cappellaro, L. Jiang, J. S. Hodges, M. D. Lukin, *Phys. Rev. Lett.* **102**, 210502 (2009).
31. N. B. Manson, J. P. Harrison, M. J. Sellars, *Phys. Rev. B* **74**, 104303 (2006).
32. A. Batalov *et al.*, *Phys. Rev. Lett.* **102**, 195506 (2009).

33. We thank P. Cappellaro, L. Childress, J. Doyle, M. V. G. Dutt, J. MacArthur, A. Sorenson, P. Stanwix, E. Togan, and A. Trifonov for many stimulating discussions and experimental help. This work was supported by the Defense Advanced Research Projects Agency, NSF, the Packard Foundation, and the Pappalardo Fellowship. The content of the information does not necessarily reflect the position or the policy of the U.S. Government, and no official endorsement should be inferred.

Supporting Online Material
www.sciencemag.org/cgi/content/full/1176496/DC1
Materials and Methods
Figs. S1 to S4
References

19 May 2009; accepted 29 July 2009
Published online 10 September 2009;
10.1126/science.1176496
Include this information when citing this paper.

Persistent Currents in Normal Metal Rings

A. C. Bleszynski-Jayich,[1] W. E. Shanks,[1] B. Peaudecerf,[1] E. Ginossar,[1] F. von Oppen,[2] L. Glazman,[1,3] J. G. E. Harris[1,3]

Quantum mechanics predicts that the equilibrium state of a resistive metal ring will contain a dissipationless current. This persistent current has been the focus of considerable theoretical and experimental work, but its basic properties remain a topic of controversy. The main experimental challenges in studying persistent currents have been the small signals they produce and their exceptional sensitivity to their environment. We have developed a technique for detecting persistent currents that allows us to measure the persistent current in metal rings over a wide range of temperatures, ring sizes, and magnetic fields. Measurements of both a single ring and arrays of rings agree well with calculations based on a model of non-interacting electrons.

An electrical current induced in a resistive circuit will rapidly decay in the absence of an applied voltage. This decay reflects the tendency of the circuit's electrons to dissipate energy and relax to their ground state. However, quantum mechanics predicts that the electrons' many-body ground state (and, at finite temperature, their thermal equilibrium state) may contain a persistent current (PC), which flows through the resistive circuit without dissipating energy or decaying. A dissipationless equilibrium current flowing through a resistive circuit is counterintuitive, but it has a familiar analog in atomic physics: Some atomic species' electronic ground states possess nonzero orbital angular momentum, which is equivalent to a current circulating around the atom.

One of the major insights of mesoscopic condensed-matter physics is that this analogy remains valid even when the electrons experience a static disorder potential, as in a resistive metal (*1*). Theoretical treatments of PCs in resistive metal rings have been developed over a number of decades [see (*1*, *2*) and references therein]. Calculations that take into account the electrons' inevitable coupling to the static disorder potential and a fluctuating thermal bath predict several general features. A micrometer-diameter ring will support a PC of $I \sim 1$ nA at temperatures $T \lesssim 1$ K. A magnetic flux Φ threading the ring will break time-reversal symmetry, allowing the PC to flow in a particular direction around the ring. Furthermore, the Aharonov-Bohm effect will require I to be periodic in Φ with period $\Phi_0 = h/e$, thereby providing a clear-cut experimental signature of the PC.

These predictions have attracted considerable interest, but measuring the PC is challenging for a number of reasons. For example, the PC flows only within the ring and so cannot be measured with a conventional ammeter. Experiments to date (*2*, *3*) have mostly used superconducting quantum interference devices (SQUIDs) to infer the PC from the magnetic field it produces. Interpretation of these measurements has been complicated by the SQUID's low signal-to-noise ratio (SNR) and the uncontrolled back action of the SQUID's ac Josephson oscillations, which may drive nonequilibrium currents in the rings. In addition, SQUIDs perform optimally in low magnetic fields; this limits the maximum Φ that can be applied to the rings, allowing observation of only a few oscillations of $I(\Phi)$ and complicating the subtraction of background signals unrelated to the PC.

Experiments to date have produced a number of confusing results in apparent contradiction with theory and even among the experiments themselves (*2*, *3*). These conflicts have remained without a clear resolution for nearly 20 years, suggesting that our understanding of how to measure and/or calculate the ground-state properties of as simple a system as an isolated metal ring may be incomplete.

More recent theoretical work has predicted that the PC is highly sensitive to a variety of subtle effects, including electron-electron interactions (*4*–*7*), the ring's coupling to its electromagnetic environment (*8*), and trace magnetic impurities within the ring (*9*). These theories have not explained all of the experimental results to date, but they do indicate that accurate measurements of the PC would be able to address a number of interesting questions in many-body condensed-matter physics (in addition to resolving the long-standing controversy described above).

We measured the PC in resistive metal rings using a micromechanical detector with orders of magnitude greater sensitivity and lower back-action than SQUID-based detectors. Our approach allows us to measure the PC in a single ring and arrays of rings as a function of ring size, temperature, and the magnitude and orientation of the magnetic field over a much broader range than has been possible previously. Quantitative agreement is found between these measurements and calculations based on a model of diffusive, non-interacting electrons. This agreement is supported by independent measurements of the rings' electrical properties.

Figure 1, A to C, shows single-crystal Si cantilevers with integrated Al rings [their fabrication is described elsewhere (*10*)]. All the PC measurements were made in magnetic fields well above the critical field of Al, ensuring that the rings were in their normal (rather than superconducting) state. The parameters of the four ring samples measured are given in Table 1.

In the presence of a magnetic field $\vec{B}$, each ring's current I produces a torque on the cantilever $\vec{\tau} = \vec{\mu} \times \vec{B}$ as well as a shift $\delta\nu$ in the cantilever's resonant frequency ν. Here $\vec{\mu} = \pi r^2 I \hat{n}$ is the magnetic moment of the PC, r is the ring radius, and $\hat{n}$ is the unit vector normal to the ring. We infer $I(B)$ from measurements of $\delta\nu(B)$; the conversion between $\delta\nu(B)$ and $I(B)$ is described in the supporting online material (SOM) text.

To monitor ν, we drive the cantilever in a phase-locked loop. The cantilever is driven via a piezoelectric element, and the cantilever's displacement is monitored by a fiber-optic interferometer (*11*). The cantilever's thermally limited force sensitivity is ~2.9 aN/Hz$^{1/2}$ at $T = 300$ mK, corresponding to a magnetic moment sensitivity of ~11 μ_B/Hz$^{1/2}$ and a current sensitivity of ~20 pA/Hz$^{1/2}$ for a ring with $r = 400$ nm at $B = 8$ T. By comparison, SQUID magnetometers achieve a current sensitivity $\gtrsim$5 nA/Hz$^{1/2}$ for a similar ring (*12*–*14*). The noise temperature of the cantilever and the electron temperature of a metal sample at the end of a cantilever both equilibrate with the fridge temperature for the conditions we used (*11*).

The frequency shift of a cantilever containing an array of $N = 1680$ lithographically identical rings with $r = 308$ nm at $T = 323$ mK is shown (Fig. 1D) as a function of B. Oscillations with a period $\approx$20 mT, corresponding to a flux h/e through each ring, are visible in the raw data. Depending on r and θ (the angle between $\vec{B}$ and the plane of

[1]Department of Physics, Yale University, New Haven, CT 06520, USA. [2]Institut für Theoretische Physik, Freie Universität Berlin, Fachbereich Physik, 14195 Berlin, Germany. [3]Department of Applied Physics, Yale University, New Haven, CT 06520, USA.

the ring), we observe as many as 450 oscillations over a 5.5-T range of B (figs. S12 to S17).

Figure 1E shows the data from Fig. 1D after subtracting the smooth background and converting the data from $\delta\nu(B)$ to $I(B)$ using the expressions in the SOM text. The lefthand axis in Fig. 1E shows I_Σ, the total PC inferred from the measurement, which is the sum of the PC from each ring in the array. The righthand axis shows the estimated typical single-ring PC: $I_{typ} = I_\Sigma/\sqrt{N}$. This relationship between I_{typ} and I_Σ arises because the PC in each ring is predicted to oscillate as a function of B with a phase that depends on the ring's microscopic disorder, and thus is assumed to be random from ring to ring. This assumption is verified below.

To establish that $\delta\nu$ provides a reliable measure of the PC, $I_{typ}(B)$ was measured as a function of several experimental conditions: the laser power incident on the cantilever, the amplitude and frequency of the cantilever's motion, the polarity and orientation of the magnetic field, and the presence or absence of room-temperature electronics connected to the cryostat. These data are shown in the SOM text and indicate that the measurements of $I_{typ}(B)$ are independent of these parameters (for the conditions of our experiment) and reflect the equilibrium PC in the rings.

Figure 2, A to C, shows $I_{typ}(B)$ for arrays of rings with three different radii: $r = 308$, 418, and 793 nm. We have also measured a single ring with $r = 418$ nm (Fig. 2D). Figure 2, E to H, shows $|\tilde{I}_{typ}(f_\Phi)|$, the absolute value of the Fourier transform of the data in Fig. 2, A to D [f_Φ is the flux frequency in units of $(h/e)^{-1}$]. Figure 2, I to L, shows $G_{typ}(\delta B)$, the autocorrelation of $I_{typ}(B)$ for each of these samples. $G_{typ}(\delta B)$ is calculated from measurements of $I_{typ}(B)$ taken over a much broader range of B than is shown in Fig. 2, A to D; the complete data are shown in the SOM text.

A number of conclusions can be drawn from a qualitative examination of these data. First, $I_{typ}(B)$ oscillates with a period $\approx h/e$ but also contains an aperiodic modulation that broadens the peaks in $\tilde{I}_{typ}(f_\Phi)$ and causes $G_{typ}(\delta B)$ to decay at large δB. This modulation is due to the fact that we apply a uniform B to the sample, leading to magnetic flux inside the metal of each ring given by $\Phi_M = BA_M$ where A_M is the area of the metal projected along $\vec{B}$. This leads to a new effective disorder potential [and hence a randomization of the phase of the $I(B)$ oscillations] each time Φ_M changes by $\sim\Phi_0$ (*15*). As a result, the peaks in $\tilde{I}_{typ}(f_\Phi)$ span a band of f_Φ roughly bounded by the rings' inner and outer radii (the blue bars in Fig. 2, E to H), and the decay of $G_{typ}(\delta B)$ is found to occur on a field scale [defined as the half width at half maximum of $G_{typ}(\delta B)$(*15*)] $B_c = \kappa\Phi_0/A_M$. Here κ is a constant that is predicted (*16*) to be ≈ 1; we find $1 < \kappa < 3$ in these samples. For the array samples, ring-to-ring variations in r (estimated to be ~1%) should contribute negligibly to B_c and the peak widths in $\tilde{I}_{typ}(f_\Phi)$. The fact that the $r = 418$ nm array and the $r = 418$ nm single ring show similar peak width and B_c indicates that ring-to-ring variations in r do not affect the signal appreciably.

It is clear from Fig. 2 that the PC is smaller in larger rings. This is consistent with the prediction (*17*) that the typical amplitude $I_{h/e}(T = 0)$ of the h/e-periodic Fourier component of $I(\Phi)$ at $T = 0$ corresponds roughly to the current produced by a single electron diffusing around the ring at the Fermi energy, and hence should scale as $1/r^2$. In addition, $I_{h/e}(T)$ is predicted (*17*) to decrease on a temperature scale (known as the Thouless temperature) $T_T \propto 1/r^2$, corresponding to the scale of disorder-induced correlations in the ring's spectrum of single-electron states.

In Fig. 2E, a small peak at $f_\Phi = 2$ can be seen, corresponding to the second harmonic of $I(\Phi)$. This harmonic has attracted particular attention because under some conditions, it has a component that is not random from ring to ring (*4*, *12*, *18*, *19*). The signal from such a nonrandom "average" current would scale as $I_\Sigma^{(avg)} \propto N$ rather than $\sqrt{N}$. Furthermore, the amplitude of $I_\Sigma^{(avg)}$ can be strongly enhanced by electron-electron interactions (*4*–*6*) and other effects (*8*, *9*). However, $I_\Sigma^{(avg)}$ arises because of time-reversal symmetry within the metal, which in our experiments is broken by Φ_M. We calculate that Φ_M suppresses $I_\Sigma^{(avg)}$ by a factor $\sim e^{-2\pi r/1.3\ell_B}$ (where the magnetic

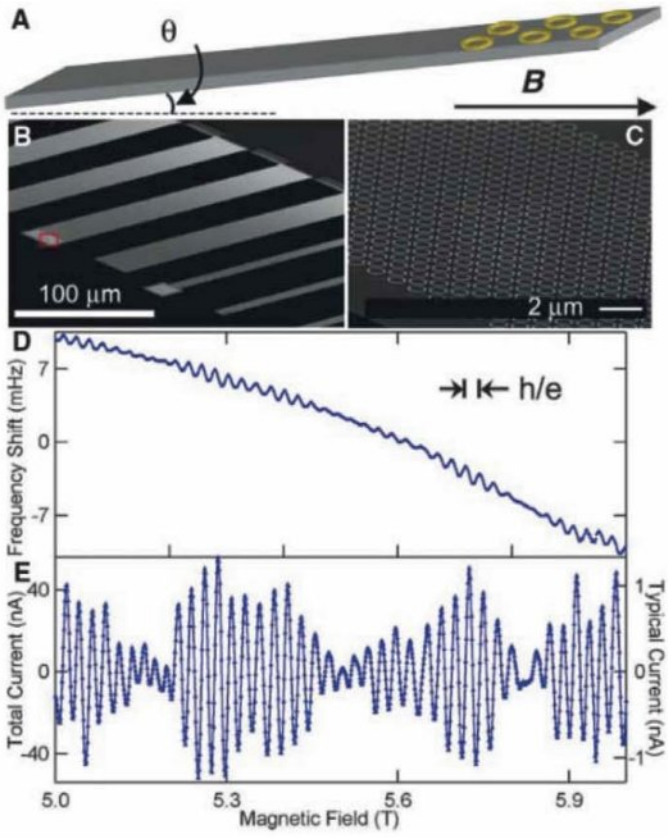

Fig. 1. (**A**) Cantilever torque magnetometry schematic. An array of metal rings is integrated onto the end of a cantilever. The cantilever is mounted in a ^{3}He refrigerator. A magnetic field B is applied at an angle θ from the plane of the rings. The out-of-plane component of B provides magnetic flux Φ through the ring. The in-plane component of B exerts a torque on the rings' magnetic moment and causes a shift in the cantilever's resonant frequency $\delta\nu$. Laser interferometry is used to monitor the cantilever's motion and to determine $\delta\nu$. (**B**) A scanning electron micrograph of several Si cantilevers similar to those used in the experiment. The light regions at the end of some of the cantilevers are arrays of Al rings. The individual rings are visible in (**C**), which shows a magnified view of the region in (**B**) outlined in red. (**D**) Raw data showing $\delta\nu$ as a function of B for an array of $N = 1680$ rings with $r = 308$ nm at $T = 365$ mK and $\theta = 45°$. (**E**) PC inferred from the frequency shift data in (D) after subtracting a smooth background from the raw data. The lefthand axis shows the total current I_Σ in the array, and the righthand axis shows the estimated typical per-ring current $I_{typ} = I_\Sigma/\sqrt{N}$. Oscillations with a characteristic period of ~20 mT (corresponding to $\Phi = h/e$) are visible in (D) and (E).

Table 1. Sample parameters. For each of the four ring samples, the rings' mean radius r, linewidth w, and thickness d are listed, along with the number N of rings in the sample. The electrons' diffusion constant D, extracted from the fits in Fig. 3, is given. The stated errors are statistical errors in the fits. An additional 6% error in D is estimated for uncertainties in the overall calibration, as discussed in the SOM text. The fifth sample is the codeposited wire used in the transport measurements described in the SOM text. For this sample, D was determined from the wire's resistivity.

Sample	r (nm)	w (nm)	d (nm)	N	D (cm^2/s)
308-nm array	308	115	90	1680	271 ± 2.6
418-nm array	418	85	90	990	214 ± 3.3
793-nm array	793	85	90	242	205 ± 6.5
418-nm ring	418	85	90	1	215 ± 4.6
Wire (see SOM text)	289,000 (length)	115	90	1	260 ± 12

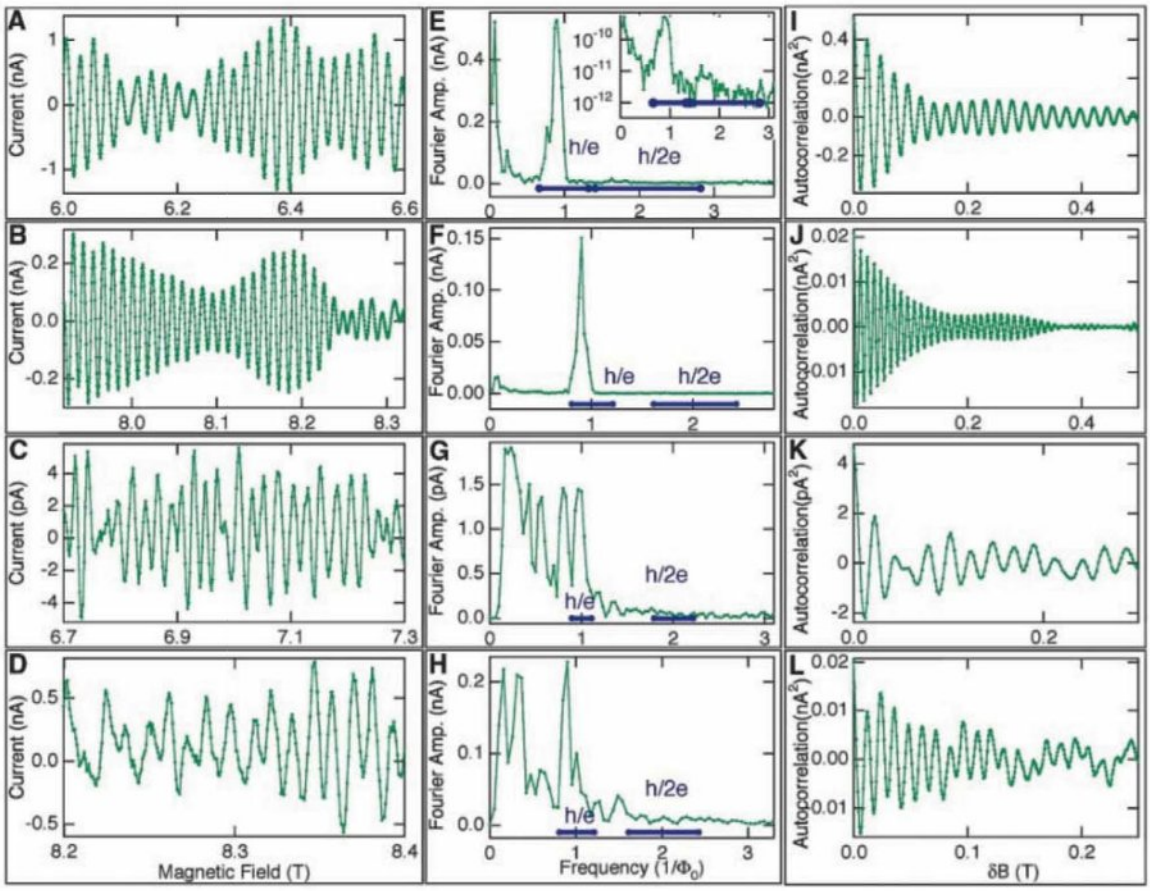

Fig. 2. PC versus magnetic field in (**A**) the 308-nm array for T = 365 mK, $\theta = 45°$; (**B**) the 418-nm array for T = 365 mK, $\theta = 45°$; (**C**) the 793-nm array for T = 323 mK, $\theta = 6°$; and (**D**) the 418-nm ring for 365 mK, $\theta = 45°$. In each case, a smooth background has been removed. (**E** to **H**) Fourier transforms of the data in (A) to (D). The expected *h/e* and *h/2e* periodicities are indicated by the horizontal blue bars. The bars' widths reflect the rings' linewidth w. A small *h/2e* peak is present in (E) (visible in the log-scale graph, inset). (**I** to **L**) The autocorrelation functions of the data shown in (A) to (D), but computed over a field range ΔB larger than shown in (A) to (D): ΔB = (I) 5.4 T, (J) 5.3 T, (K) 0.6 T, and (L) 1.1 T (full data are shown in the SOM text).

length $\ell_B = \sqrt{h/eB}$), which for this experiment should render $I_\Sigma^{(\mathrm{avg})}$ unobservably small. As a result, the peak in Fig. 2E at $f_\Phi = 2$ presumably reflects the random component of the second harmonic of $I(\Phi)$, which is predicted (*17*) to have a zero-temperature amplitude $I_{h/2e}(0) = I_{h/e}(0)/2^{3/2}$, to be suppressed on a temperature scale $= T_T/4$, and to produce a signal with the same $\sqrt{N}$ scaling as $I_{h/e}$.

We now turn to a more quantitative analysis of the data. Theory predicts (*17*) that, for each independent realization of the disorder potential, $I_{h/pe}$ [the p^{th} harmonic of $I(\Phi)$] is drawn randomly from a distribution with a mean $\langle I_{h/pe}\rangle = 0$ and a root mean square (rms) value $\langle I_{h/pe}^2\rangle^{1/2}$, which in general is nonzero. Here $\langle\cdots\rangle$ represents an average over disorder potentials. The quantity $\langle I_{h/pe}^2\rangle^{1/2}$ can be calculated explicitly as a function of r, T, p, and the electrons' diffusion constant D for a variety of models.

To compare our data against these calculations, we make use of the fact that $\langle I_{h/pe}^2\rangle^{1/2}$ can be extracted from a measurement of $I_\Sigma(B)$ when the measurement record spans many B_c. When this condition is satisfied, averages performed with respect to B are equivalent to averages performed with respect to disorder realizations, and it is straightforward to show that the area under a peak in $|\tilde{I}_{\mathrm{typ}}(f_\Phi)|^2$ (Fig. 2, E to H) at $f_\Phi = p$ is simply related to $\langle I_{h/pe}^2\rangle^{1/2}$

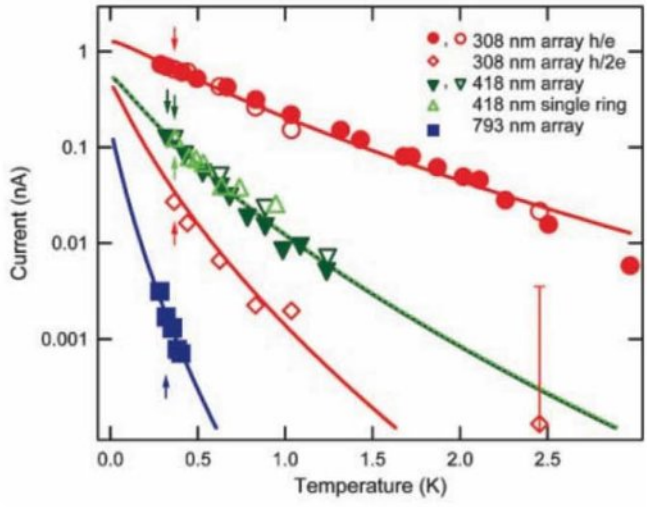

Fig. 3. Temperature dependence of the *h/e* and *h/2e* Fourier components of the current per ring. The vertical axis indicates $\langle I_{h/e}^2\rangle^{1/2}$ and $\langle I_{h/2e}^2\rangle^{1/2}$, the rms values of the Fourier amplitudes of the persistent current. In each data set, the open points were taken with $\theta = 45°$, whereas for the solid points, $\theta = 6°$. The arrows indicate the data points derived from $I(B)$ measurements taken over a magnetic field range much greater than B_c; other data points are derived from the scaling of $I(B)$ measured over a smaller range of B, as described in the SOM text. The lines (solid for array samples, dotted for the single ring) are fits to the prediction for non-interacting diffusive electrons. The electron diffusion constant D is the only fitting parameter and is listed in Table 1.

$$\left[(f_\Phi^+ - f_\Phi^-)^{-1}\int_{f_\Phi^-}^{f_\Phi^+}\left(|\tilde{I}_{\mathrm{typ}}(f_\Phi)|^2 - b(f_\Phi)\right)df_\Phi\right]^{1/2} = \left\langle I_{h/pe}^2\right\rangle^{1/2} \quad (1)$$

Here b is the noise floor in $|\tilde{I}_{\mathrm{typ}}(f_\Phi)|^2$ and is estimated from the portions of the data away from the peaks. We take the limits of integration f_Φ^+ and f_Φ^- to be roughly the values of f_Φ corresponding to *h/pe* flux periodicity through the outer and inner radii of the ring, respectively. In previous experiments, $\langle I_{h/pe}^2\rangle$ could only be determined by measuring several rings, one ring at a time (*3*, *20*). This approach was limited by the low SNR achieved in single-ring measurements and practical limits on the number of nominally identical rings (≈15) that could be measured.

Measurements of $\langle I^2_{h/e}\rangle^{1/2}$ for each sample and $\langle I^2_{h/2e}\rangle^{1/2}$ for the smallest rings are shown as a function of T for $\theta = 45°$ (open symbols) and $\theta = 6°$ (solid symbols) (Fig. 3). It can be seen that the PC in larger rings decays more quickly with T than in smaller rings, and that $\langle I^2_{h/2e}\rangle^{1/2}$ decays more quickly than $\langle I^2_{h/e}\rangle^{1/2}$, which is consistent with the discussion above. In addition, the agreement between the data for the $r =$ 418 nm array and the $r = 418$ nm single ring indicates that the PC signal scales as $\sqrt{N}$ and hence that the PC is random from ring to ring.

The solid lines are fits to theoretical predictions in which $\langle I^2_{h/pe}\rangle^{1/2}$ is calculated for diffusive non-interacting electrons. This calculation closely follows that of (*17*) but takes into account the presence of the large magnetic field B inside the metal (which lifts the spin degeneracy and breaks time-reversal symmetry) as well as spin-orbit scattering (the rings' circumference exceeds the spin-orbit scattering length, as discussed in the SOM text). We find

$$\left\langle I^2_{h/pe}(T)\right\rangle = g\left(p^2\frac{T}{T_T}\right)\left\langle I^2_{h/pe}(0)\right\rangle \qquad (2)$$

where $g(x) = \frac{\pi^6}{3}x^2\sum_{n=1}^{\infty} n\,\exp[-(2\pi^3 nx)^{1/2}]$, $\langle I^2_{h/pe}(0)\rangle^{1/2} = 0.37p^{-3/2}\frac{3eD}{(2\pi r)^2}$, and $T_T = \frac{h\pi^2 D}{k_B(2\pi r)^2}$.

The data from each sample were fit separately, in each case using D as the only fitting parameter. The best-fit values of D are listed in Table 1. These values are typical for high-purity evaporated Al wires of the dimensions used here (*21*, *22*); however, to further constrain the comparison between our data and theory, we also independently determined D from the resistivity of a co-deposited wire (the wire's properties are listed in Table 1). This measurement is described in detail in the SOM text and provides a value of D in good agreement with the values extracted from the PC measurements. The values of D in Table 1 show a correlation with the samples' linewidths, which may reflect the increased contribution of surface scattering in the narrower samples.

The calculation leading to Eq. 2 assumes the phase-coherent motion of free electrons around the ring. Measurements of the phase coherence length $L_\Phi(T)$ in the co-deposited wire are described in the SOM text and show that $L_\Phi \gg 2\pi r$ for nearly all the temperatures at which the PC is observable. The closest approach between L_Φ and $2\pi r$ at a temperature where the PC can still be observed occurs in the 308-nm array at $T = 3$ K, where we find $L_\Phi(3\text{ K}) = 1.86 \times (2\pi r)$. It is conceivable that the more rapid decrease in $\langle I^2_{h/e}\rangle^{1/2}$ observed in this sample above $T = 2$ K (Fig. 3) is due to dephasing; however, it is not possible to test this hypothesis in the other samples, because the larger rings' PC is well below the noise floor when $L_\Phi(T) = 1.86 \times (2\pi r)$. To the best of our knowledge the effect of dephasing on the PC has not been calculated.

Our measurement of the PC in normal metal rings over a wide range of temperatures, ring sizes, array sizes, magnetic field magnitudes, and magnetic field orientations with high SNR, excellent background rejection, and low measurement back-action indicates that the rings' equilibrium state is well described by the diffusive non-interacting electron model. In addition to providing a clear experimental picture of PCs in simple metallic rings, these results open the possibility of using measurements of the PC to search for ultra–low temperature phase transitions (*6*) or to study a variety of many-body and environmental effects relevant to quantum phase transitions and quantum coherence in solid-state qubits (*23*, *24*). Furthermore, the micromechanical detectors used here are well suited to studying the PC in circuits driven out of equilibrium (for example, by the controlled introduction of microwave radiation) (*8*). The properties of PCs in these regimes have received relatively little attention to date but could offer new insights into the behavior of isolated nanoelectronic systems.

References and Notes

1. M. Buttiker, I. Imry, R. Landauer, *Phys. Lett.* **96A**, 365 (1983).
2. L. Saminadayar, C. Bäuerle, D. Mailly, *Encycl. Nanosci. Nanotech* **3**, 267 (2004).
3. H. Bluhm, N. C. Koschnick, J. A. Bert, M. E. Huber, K. A. Moler, *Phys. Rev. Lett.* **102**, 136802 (2009).
4. V. Ambegaokar, U. Eckern, *Phys. Rev. Lett.* **65**, 381 (1990).
5. V. Ambegaokar, U. Eckern, *Europhys. Lett.* **13**, 733 (1990).
6. H. Bary-Soroker, O. Entin-Wohlman, Y. Imry, *Phys. Rev. Lett.* **101**, 057001 (2008).
7. U. Eckern, P. Schwab, *Adv. Phys.* **44**, 387 (1995).
8. V. E. Kravtsov, V. I. Yudson, *Phys. Rev. Lett.* **70**, 210 (1993).
9. P. Schwab, U. Eckern, *Z. Phys. B* **103**, 97 (1997).
10. A. C. Bleszynski-Jayich, W. E. Shanks, R. Ilic, J. G. E. Harris, *J. Vac. Sci. Technol. B* **26**, 1412 (2008).
11. A. C. Bleszynski-Jayich, W. E. Shanks, J. G. E. Harris, *Appl. Phys. Lett.* **92**, 013123 (2008).
12. E. M. Q. Jariwala, P. Mohanty, M. B. Ketchen, R. A. Webb, *Phys. Rev. Lett.* **86**, 1594 (2001).
13. M. E. Huber *et al.*, *Rev. Sci. Instrum.* **79**, 053704 (2008).
14. D. Mailly, C. Chapelier, A. Benoit, *Phys. Rev. Lett.* **70**, 2020 (1993).
15. W. J. Skocpol *et al.*, *Phys. Rev. Lett.* **56**, 2865 (1986).
16. P. A. Lee, A. D. Stone, H. Fukuyama, *Phys. Rev. B* **35**, 1039 (1987).
17. E. K. Riedel, F. von Oppen, *Phys. Rev. B* **47**, 15449 (1993).
18. L. P. Levy, G. Dolan, J. Dunsmuir, H. Bouchiat, *Phys. Rev. Lett.* **64**, 2074 (1990).
19. B. L. Altshuler, Y. Gefen, Y. Imry, *Phys. Rev. Lett.* **66**, 88 (1991).
20. V. Chandrasekhar *et al.*, *Phys. Rev. Lett.* **67**, 3578 (1991).
21. P. LaFarge, P. Joyez, D. Esteve, C. Urbina, M. H. Devoret, *Nature* **365**, 422 (1993).
22. C. Song *et al.*, *Phys. Rev. B* **79**, 174512 (2009).
23. P. Cedraschi, V. V. Ponomarenko, M. Büttiker, *Phys. Rev. Lett.* **84**, 346 (2000).
24. A. Kopp, K. Le Hur, *Phys. Rev. Lett.* **98**, 220401 (2007).

25. We thank M. Devoret, R. Ilic, T. Ojanen, and J. C. Sankey for their assistance. A.C.B.-J., W.E.S., and J.G.E.H. are supported by NSF grants 0706380 and 0653377. F.v.O. is supported in part by the Deutsche-Israelische Projektkooperation. J.G.E.H. acknowledges support from the Sloan Foundation. A.C.B.-J. acknowledges support from UNESCO-L'Oreal. L.G. is supported in part by U. S. Department of Energy grant DE-FG02-08ER46482. F.v.O and L.G. acknowledge the hospitality of the Kavli Institute for Theoretical Physics in the final stages of this work.

Supporting Online Material

www.sciencemag.org/cgi/content/full/326/5950/272/DC1
SOM Text
Figs. S1 to S18
References and Notes

23 June 2009; accepted 8 September 2009
10.1126/science.1178139

The Shape and Surface Variation of 2 Pallas from the Hubble Space Telescope

B. E. Schmidt,[1]* P. C. Thomas,[2] J. M. Bauer,[3] J.-Y. Li,[4] L. A. McFadden,[4] M. J. Mutchler,[5] S. C. Radcliffe,[6] A. S. Rivkin,[7] C. T. Russell,[1] J. Wm. Parker,[8] S. A. Stern[8]

We obtained Hubble Space Telescope images of 2 Pallas in September 2007 that reveal distinct color and albedo variations across the surface of this large asteroid. Pallas's shape is an ellipsoid with radii of 291 (±9), 278 (±9), and 250 (±9) kilometers, implying a density of 2400 (±250) kilograms per cubic meter—a value consistent with a body that formed from water-rich material. Our observations are consistent with the presence of an impact feature, 240 (±25) kilometers in diameter, within Pallas's ultraviolet-dark terrain. Our observations imply that Pallas is an intact protoplanet that has undergone impact excavation and probable internal alteration.

In the current paradigm, the largest asteroids were among the first solar system bodies to form and were the building blocks of planets [e.g., (*1*) and references therein]. Pallas is the second largest and third most massive asteroid, with a mean radius of 272 km; 1 Ceres is 475 km (*2*) and 4 Vesta is 265 km (*3*). These three bodies are the archetypes of their spectral classes: Ceres is the largest of the rare G-types, Vesta is the likely parent body of the Vestoid V-type asteroids and the associated howardite, eucrite, and diogenite (HED) meteorites [e.g., (*1*)], and Pallas is the largest of the B-types. Like Vesta, Pallas is linked to an orbital family sharing its orbital and spectral parameters. The largest of these is 5222 Ioffe, with a diameter of 22 km (*4*). It is assumed that

[1]Institute of Geophysics and Planetary Physics, University of California, Los Angeles, CA 90095, USA. [2]Department of Astronomy, Cornell University, Ithaca, NY 14853, USA. [3]Jet Propulsion Laboratory, Pasadena, CA 91109, USA. [4]Department of Astronomy, University of Maryland, College Park, MD 20742, USA. [5]Space Telescope Science Institute (STScI), Baltimore, MD 80302, USA. [6]Hydraulx, Santa Monica, CA 90401, USA. [7]Applied Physics Laboratory, Laurel, MD 20723, USA. [8]Southwest Research Institute, Boulder, CO 80302, USA.

*To whom correspondence should be addressed. E-mail: britneys@ucla.edu

the family formed when one or more large impacts on Pallas ejected pieces of the asteroid into space, but no craters or satellites of Pallas have been reliably detected. Like Ceres, Pallas has a surface covered with hydrated minerals and a semimajor axis near 2.7 AU, consistent with the bodies forming from a common reservoir of water-rich material (*5*, *6*). Pallas differs from Ceres in that it does not appear to have a hydrostatically relaxed shape, yet it is far from irregularly shaped. Ceres and Vesta are best regarded as intact, differentiated "protoplanets," minor bodies whose properties are closer to those of planets than to those of small asteroids [e.g., (*7*)]. Pallas has been less well characterized because until recently no spatially resolved observations existed. In 2007 we observed Pallas near its opposition in five filters with the Wide Field and Planetary Camera 2 (WFPC2) onboard the Hubble Space Telescope (HST), resolving its shape and surface.

We used calibrated WFPC2 images (*8*) to generate a first-order triaxial model for Pallas's shape and size, following a method similar to that of (*9*). The model is based on fits to Pallas's limb with interactive modification to match the nonellipsoidal shape (*8*). Our best fits yielded semiaxes of 291 (±9) km, 278 (±9) km, and 250 (±9) km. We found a rotational pole of RA 42° (±10°), Dec −12° (±10°), within uncertainties of recent measurements (*10*, *11*). We observed Pallas with sub-Earth latitude near 30°S so that the visible surface extended from 60°N through the south pole. The HST solution has a mean radius within 6 km of an occultation-derived shape of 287 (±10) km by 263 (±10) km by 250 (±10) km (*12*), which provides the best check of absolute scale but is up to 19 km larger than other estimates (*8*, *10*, *11*, *13*) (table S1). Our shape and the best estimate of Pallas's mass [see (*8*) for discussion], 1.026 (±0.028) × 10^{-10} solar masses (2.04 × 10^{20} kg) (*14*), imply a density of 2400 (±250) kg/m^3. Agreement with occultation data (*12*) indicates that Pallas has a density intermediate between Ceres at 2077 kg/m^3 (*2*) and Vesta at 3480 kg/m^3 (*3*, *14*).

After measuring Pallas's size, we deconvolved the images to enhance the sharpness of the limb and surface features (*8*). To first order, Pallas's shape is a triaxial ellipsoid, but closer examination of the deconvolved images reveals departures from a regular shape (Fig. 1). Because the observations were made at low phase, the shape of the asteroid's limb results from topography. We observed more than 80% of a full rotation with small coverage gaps, during which Pallas's apparent shape varied from oblate to an irregular spheroid to "egg-shaped." Along the southeastern limb of the image at 348°E (Fig. 1) is a large depression that cuts into the body and could have been caused by impact. This feature is face-on in three subsequent images (central longitudes 62°, 74°, and 75°E), corresponding to Pallas's darkest terrain, and is the largest topographic feature we detected. Similarly shaped smaller features are seen on the limbs of the images at 0°E and 62°E.

To visualize the asteroid's shape, we modeled Pallas by fitting a three-dimensional triaxial ellipsoid to individual WFPC2 images with the modeling program Maya (Fig. 2) (*15*). A digital model with Pallas's dimensions and pole was generated, placed over each image, and fit by hand to the limb's shape. The model was then rotated to the next sub-Earth longitude, mimicking Pallas's rotation between the HST exposures, and shaped again. These steps were repeated for each image until a fully three-dimensional, rotating model of Pallas was complete. The result is a model that matches the images and, by interpolating a smooth body between the available data, allows surface topography to be viewed. Combined interpretation of images and the model shows that Pallas is irregular on scales of ~100 km with several depressions at varying sizes. The largest of these features is centered near 30°S, 75°E and measures about 240 ± 25 km in diameter, visible at several geometries (Fig. 3). Pallas's surface gravity is near 0.18 m/s, close to that of Vesta (*3*). Vesta's large south polar crater has a diameter of 460 km with a prominent central peak (*3*). Following the same gravity scaling laws as for Vesta and the Moon (*3*, *16*, *17*), a 240-km crater on Pallas lies near the transition between simple and complex craters. Vesta's large crater has an estimated depth of 13 km, but a crater's depth is dependent on its type. A bowl-shaped simple crater of ~15 km depth and 240 km diameter would eject a volume of ~3.5 × 10^5 km^3, exceeding the ~5575 km^3 maximum volume of Ioffe, the orbital family's largest member other than Pallas. Therefore, a single impact of this size may be sufficient to have created the Pallas family.

Previous studies of Pallas limited its surface albedo variation to 2% (*18*); however, albedo markings are clearly visible in the deconvolved images (Fig. 1). Pallas's average reflectance properties were obtained from photometry before deconvolution by integrating over the entire visible surface (*8*). The shape of a light curve is related to the size of the body by the relationship

$$\log(b/a) \leq \Delta M(-0.4) \quad (1)$$

(*19*), where a and b are the long and intermediate axes, and ΔM is light-curve amplitude. The max-

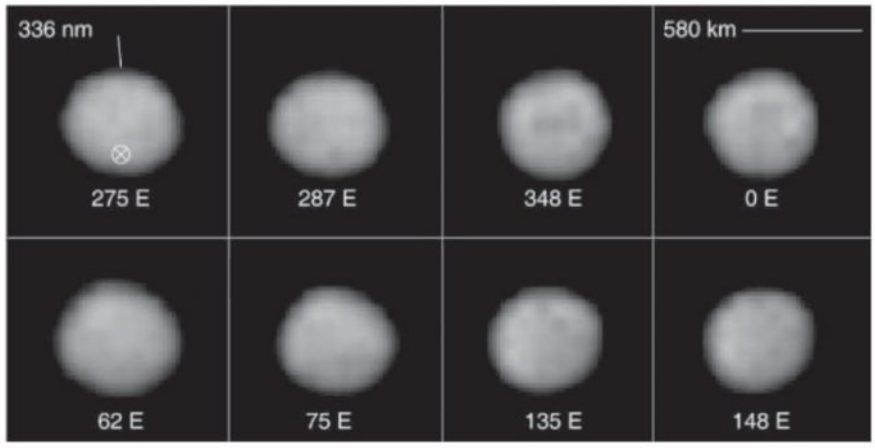

Fig. 1. Deconvolved 336-nm WFPC2 images of Pallas from 8 September 2007. We observed Pallas at an angular size of 0.326 arc sec and a phase of 4.2°, resulting in a scale of ~75 km/pixel. Pallas' spin pole (pointing upward) and south pole (⊗) are marked, and the corresponding sub-Earth longitude is labeled; north is up and east is right in this panel.

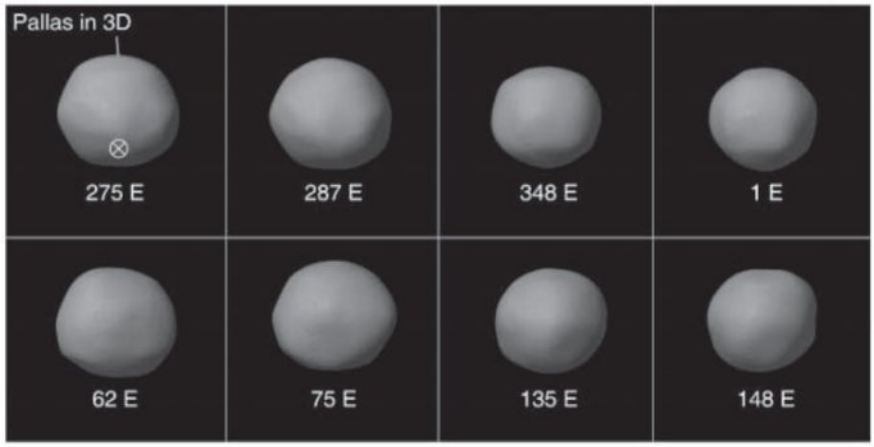

Fig. 2. Three-dimensional topography model of Pallas based on images. The aspects are identical to those in Fig. 1. The approximate orientation of the spin axis and location of the south pole are shown. The texture of the surface is for presentation only.

imum light-curve amplitude in U (*9*) is 0.113 (±0.002) magnitudes, whereas it is 0.091, 0.090, 0.081, and 0.088 (±0.002) magnitudes in the B, V, R, and I filters, respectively (fig. S1). With its *b*/*a* axis ratio of 0.96, this is roughly consistent with the amplitude of the B, V, R, and I light curves deriving from Pallas's shape with a small enhancement due to spatial variation. However, the amplitude in U [near-ultraviolet (UV)] is more than twice that expected from Pallas's shape, suggesting a bright region near 270°E and a dark spot at 70°E. The near-UV wavelength map of Pallas confirms the existence of albedo features, and the locations of the dark and bright terrain agree with those predicted by the light curves (Fig. 4). These terrains correspond to the maxima and minima of the color plot (Fig. 4), confirming that these regions have different colors from each other and from the rest of Pallas's surface. The actual brightness variations across the surface are ~10% above and below the mean. There are also both gradual trends from bright to dark and distinct albedo regions: bright areas near 15°S, 170°E and 45°S, 290°E, and dark regions at 30°S, 0°E and 0°S, 95°E.

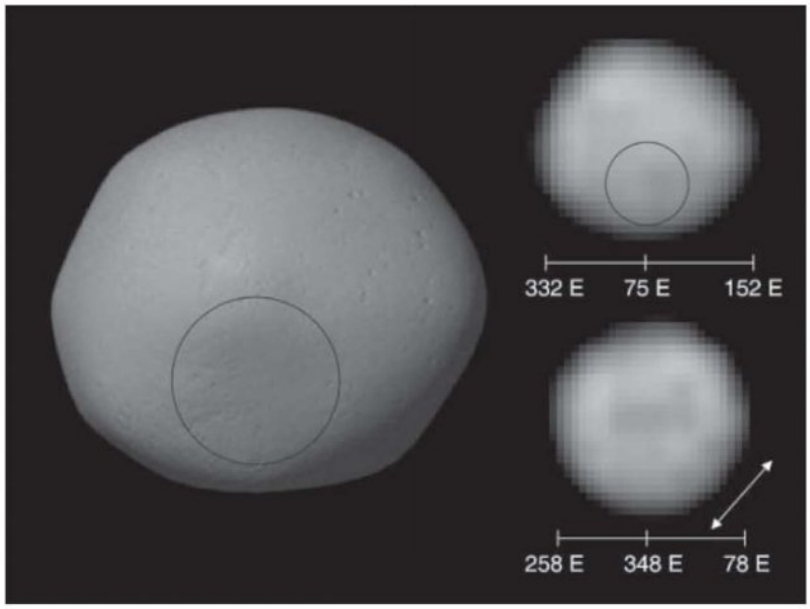

Fig. 3. Pallas's largest crater-like feature seen in the digital model (left) and from two perspectives: appearing face-on (upper right) and edge-on along the limb (lower right). The flat region indicated by the arrow rotates through multiple projections, manifests as the depression in the center of the model, and has a diameter of 240 ± 25 km.

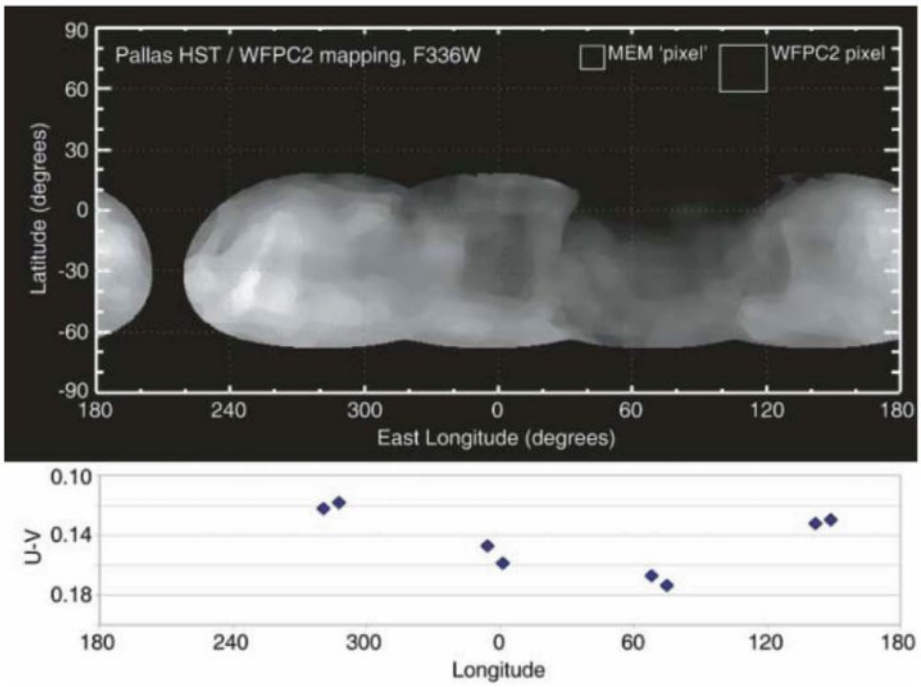

Fig. 4. Map of Pallas in the UV along with its U-V colors constructed from the deconvolved images. The map has been stretched to ± 20% contrast to show variations more clearly. The color plot compares the disk-averaged brightness of the surface in two wavelengths, minimizing shape effects. We show the relative pixel scales of the raw and deconvolved images in the upper right. Any feature smaller than a WFPC2 pixel is beyond our resolution.

Within observational limitations, small, undifferentiated asteroids usually have compositionally homogeneous surfaces, with variations in albedo dominated by regolith effects (*20*, *21*). By contrast, Ceres and Vesta, which are thermally altered bodies, have been shown to possess surface color variation caused by regional differences in processing or composition (*22*, *23*). Both Pallas and Ceres show surface variation that is most pronounced in the near-UV (*22*), and on Ceres, large circular albedo features have been interpreted as craters (*22*, *24*). On Pallas, local topography is on a scale similar to that of albedo features, and the largest potential crater is centered near the UV-dark terrain. Because the albedo trends on Pallas are regionally distinct and wavelength-dependent, the variation is most likely due to a difference in composition or in processing, and not to shadows or regolith effects. Two hypotheses have been presented for altering the UV color of C-type asteroids: space weathering [e.g., (*25*)] and heating (*26*). International Ultraviolet Explorer (IUE) data show that space weathering may brighten the surface in the UV, increasing its spectral slope (*25*), meaning that young surfaces will appear darkest. Additionally, laboratory heating of chondritic material has been shown to increase the material's UV absorption, effectively darkening the material (*26*). The production of darker material could be due to either impact heating or exposure of deeper, more internally heated layers. In either case, impacts are expected to produce UV-dark material, consistent with the interpretation that the UV-dark surfaces on Pallas have undergone impact excavation.

Our measurement of Pallas's shape and surface properties is consistent with a body that has undergone alteration. Because Pallas is too large for significant porosity (*27*), its density implies that Pallas probably formed from a mix of ice, rock, and hydrated silicate. The largest uncertainty in Pallas's interior state arises from uncertainties in its mass (*8*), but its surface materials provide further clues. The hydrated material that covers Pallas has reflective properties similar to those of chondritic material (*28*), and chondrites heated in the lab to temperatures above 400°C have similar UV properties (*26*). If Pallas's surface material is derived from the asteroid and not from meteoritic infall, this suggests that Pallas's surface and interior were thermally altered by impact or internal heat while the body contained a large amount of water. By analogy to evolution scenarios suggested for Ceres (*29*), Pallas contained enough rocky material to undergo

significant internal heating and could differentiate if it formed before the decay of ^{26}Al. Indeed, if Pallas and Ceres did form contemporaneously with similar initial composition, Pallas could retain less heat and water because of its smaller size. Our fit shape is close to that of a hydrostatically relaxed spheroid, which for a mean density of 2400 kg/m^3 would have a and c axes of 283.4 and 251.6 km, respectively, at Pallas's current spin period. These dimensions correspond to the undifferentiated case; our uncertainties would not allow any discrimination of the few-kilometer difference reasonable differentiated models would make. In either case, Pallas's density and spectral properties are suggestive of a body in which water has played a key role. These new measurements of Pallas's size, shape, and reflectance build the case that it joins Ceres and Vesta as the third intact protoplanet: an evolved body with planet-like properties.

References and Notes

1. C. T. Russell *et al.*, *Earth Moon Planets* **101**, 65 (2007).
2. P. C. Thomas *et al.*, *Nature* **437**, 224 (2005).
3. P. C. Thomas *et al.*, *Science* **277**, 1492 (1997).
4. S. Foglia, G. Masi, *Minor Planet Bull.* **31**, 100 (2004).
5. M. A. Feierberg, L. A. Lebofsky, H. P. Larson, *Geochim. Cosmochim. Acta* **14**, 719 (1981).
6. A. S. Rivkin, E. S. Howell, F. Vilas, L. A. Lebofsky, in *Asteroids III*, W. F. Bottke Jr., A. Cellino, P. Paolicchi, R. P. Binzel, Eds. (Univ. of Arizona Press, Tucson, AZ, 2002), pp. 235–253.
7. T. B. McCord, L. A. McFadden, C. T. Russell, C. Sotin, P. C. Thomas, *Eos* **87**, 105 (2006).
8. See supporting material on *Science* Online.
9. P. C. Thomas *et al.*, *Icarus* **135**, 175 (1998).
10. J. D. Drummond, J. Christou, *Icarus* **197**, 480 (2008).
11. B. Carry *et al.*, *Lunar Planet. Inst. Contrib.* **1805**, 8303 (2008).
12. D. W. Dunham *et al.*, *Astron. J.* **99**, 1636 (1990).
13. J. D. Drummond, W. J. Cocke, *Icarus* **78**, 323 (1989).
14. A. S. Konopliv, C. F. Yoder, E. M. Standish, D. N. Yuan, W. L. Sjogren, *Icarus* **182**, 23 (2006).
15. Maya is distributed through the Autodesk EULA agreement.
16. W. Hale, R. A. Grieve, *J. Geophys. Res.* **87**, A65 (1982).
17. H. J. Melosh, *Impact Craters: A Geologic Process* (Oxford Univ. Press, New York, 1989).
18. O. Saint Pe, M. Combes, F. Rigaut, *Icarus* **105**, 263 (1993).
19. K. Meech, J. M. Bauer, O. R. Hainaut, *Astron. Astrophys.* **326**, 1268 (1997).
20. D. B. J. Bussey *et al.*, *Icarus* **155**, 38 (2002).
21. A. Fujiwara *et al.*, *Science* **312**, 1330 (2006).
22. J.-Y. Li *et al.*, *Icarus* **182**, 143 (2006).
23. R. P. Binzel *et al.*, *Icarus* **128**, 95 (1997).
24. B. Carry *et al.*, *Astron. Astrophys.* **478**, 235 (2008).
25. A. R. Hendrix, F. Vilas, *LPI Contrib.* **1805**, 8361 (2008).
26. T. Hiroi, M. E. Zolensky, C. M. Pieters, M. E. Lipschutz, *Meteoritics* **31**, 321 (1996).
27. D. Britt, D. Yeomans, K. Housen, G. Consolmagno, in *Asteroids III*, W. F. Bottke Jr., A. Cellino, P. Paolicchi, R. P. Binzel, Eds. (Univ. of Arizona Press, Tucson, AZ, 2002), pp. 485–500.
28. H. P. Larson, M. A. Feierberg, L. A. Lebofsky, *Icarus* **56**, 398 (1983).
29. T. B. McCord, C. Sotin, *J. Geophys. Res.* **110**, E05009 (2005).

30. Based on observations made with the NASA/ESA Hubble Space Telescope, obtained at the Space Telescope Science Institute, which is operated by the Association of Universities for Research in Astronomy Inc. under NASA contract NAS 5-26555. The observations are associated with program 11115. Supported by STScI grant HST-GO-11115.01 (C.T.R.).

Supporting Online Material

www.sciencemag.org/cgi/content/full/326/5950/275/DC1
Materials and Methods
Tables S1 and S2
Fig. S1
References

15 June 2009; accepted 21 August 2009
10.1126/science.1177734

Evolutionary Development of the Middle Ear in Mesozoic Therian Mammals

Qiang Ji,[1] Zhe-Xi Luo,[2]* Xingliao Zhang,[3] Chong-Xi Yuan,[1] Li Xu[3]

The definitive mammalian middle ear (DMME) is defined by the loss of embryonic Meckel's cartilage and disconnection of the middle ear from the mandible in adults. It is a major feature distinguishing living mammals from nonmammalian vertebrates. We report a Cretaceous trechnotherian mammal with an ossified Meckel's cartilage in the adult, showing that homoplastic evolution of the DMME occurred in derived therian mammals, besides the known cases of eutriconodonts. The mandible with ossified Meckel's cartilage appears to be paedomorphic. Reabsorption of embryonic Meckel's cartilage to disconnect the ear ossicles from the mandible is patterned by a network of genes and signaling pathways. This fossil suggests that developmental heterochrony and gene patterning are major mechanisms in homplastic evolution of the DMME.

Stem therian mammals of the Mesozoic are relatives to modern marsupials and placentals that make up 99% of living mammals today. The marsupial-placental clade, also known as living Theria, is successively nested within the boreosphenidan mammals, the pretribosphenic mammals, and trechnotherians (*1*–*6*). The trechnotherian clade of living therians and spalacotheroids is one of 20 or so Mesozoic mammaliaform clades (*1*, *5*).

Spalacotheroids are a basal group of the trechnotherian clade (*6*–*10*), characterized by the acute triangulation of the molar cusp pattern, a precursor condition to the tribosphenic molars of the common ancestor to marsupials and placentals (*1*–*10*). Spalacotheroids have ancestral skeletal features of living therians (*9*, *10*). Here, we describe an Early Cretaceous spalacotheroid (Figs. 1 and 2) that sheds light on the evolution of the definitive mammalian middle ear (DMME) (*11*). Whether this key mammalian feature had a singular origin or had evolved multiple times is still being debated (*11*–*16*).

Maotherium asiaticus sp. nov. (*17*) shows a diagnostic pattern of main molar cusps arranged in an almost symmetric triangle, thus also known as symmetrodont molars. The postcanines show an increasingly acute (smaller) angle between cusps B′-A-C from the premolar toward the more posterior molars, a gradient in all symmetrodont mammals but most prominently developed in spalacotheroids (*6*–*10*). The upper cusps B′ and C are slightly conical, more closely resembling those of zhangheotheriids than those of other spalacotheroids. A wear facet is developed along the preparacrista (prevallum) between cusp A (paracone) and cusp B′ on M1 and M2, which erupted first in the molar series. However, the facet is not yet developed on the more posterior molars that would erupt later (*6*, *7*, *9*). Thus, the match of upper and lower wear facets occurred after eruption and after substantial occlusal contact of the upper-lower molars. The triangulated shearing surfaces on the molars suggest that *M. asiaticus* was an insectivorous mammal.

M. asiaticus was a generalized terrestrial mammal. It represented a common ecomorphotype and lifestyle among a wide range of ecomorphotypes of Mesozoic mammals (*18*–*21*). *M. asiaticus* is estimated to have a total body length from 150 mm to 155 mm and to weigh between 72 (scaling from its 28.5-mm mandibular length) and 83 g (scaling from skull length of 36.5 mm) [details in (*22*)]. In the hind-foot digit ray III of *M. asiaticus* and *M. sinensis*, the intermediate phalanx is short relative to the proximal phalanx; the proximal and intermediate phalanges are short relative to the metatarsal. Both suggest a terrestrial habit for *Maotherium*. That *M. sinensis* is a terrestrial mammal is also shown by its manual terminal phalanx shape and by phalangeal ratio that can be correlated with the terrestrial ecomorphotypes of extant mammals (*23*). *Zhangheotherium* and *Maotherium* are basal among spalacotheroids, and both had terrestrial habits (*9*, *10*), suggesting that spalacotheroids ancestrally were terrestrial with generalized locomotory function (*9*, *10*, *24*).

M. asiaticus has an ossified Meckel's cartilage. The cartilage has a compressed and tapering anterior limb that is solidly lodged in the

[1]Institute of Geology, Chinese Academy of Geological Sciences, Beijing 100037, China. [2]Carnegie Museum of Natural History, Pittsburgh, PA 15213, USA. [3]Henan Geological Museum, Zhengzhou 450003, China.

*To whom correspondence should be addressed. E-mail: LuoZ@CarnegieMNH.Org

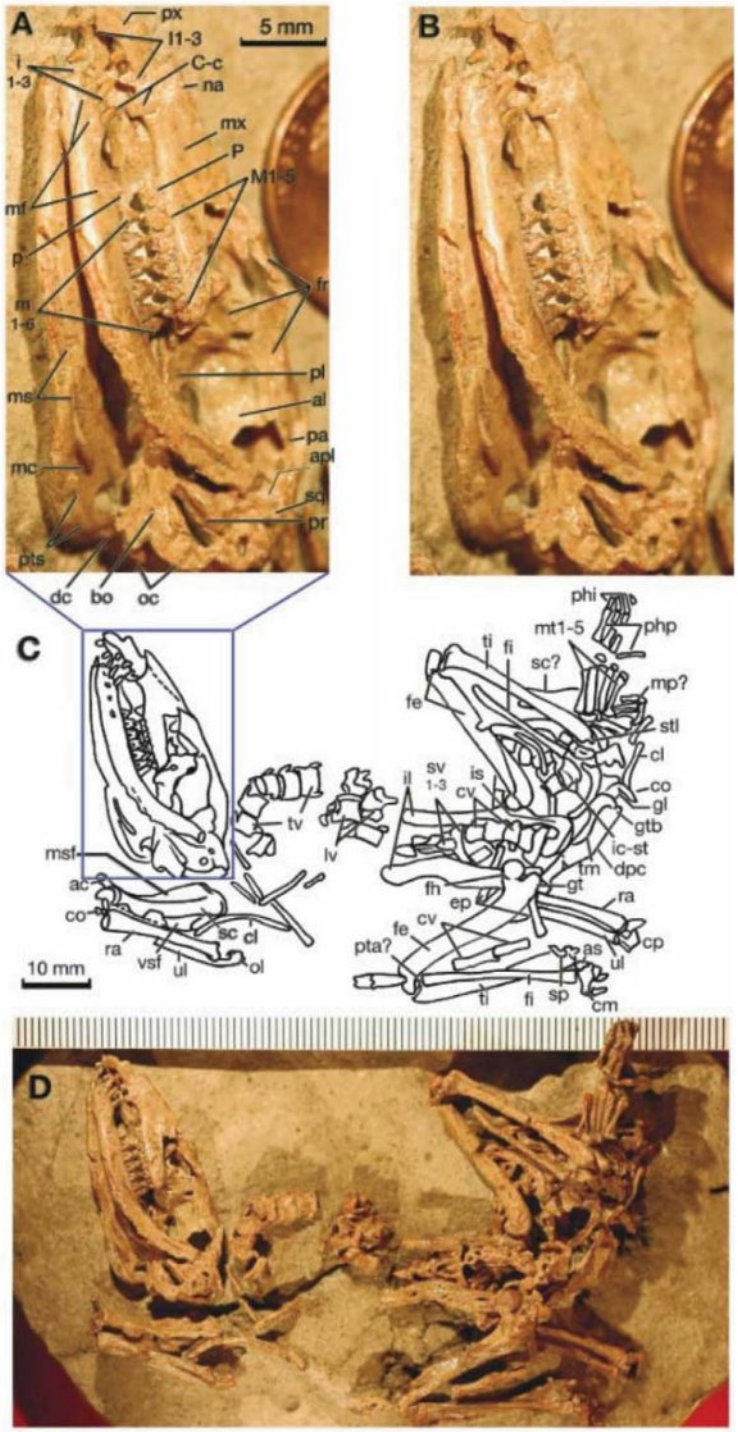

Fig. 1. Skeleton and skull of the Cretaceous spalacotheroid therian mammal *Maotherium asiaticus* [Henan Geological Museum (HGM) 41H-III-0321; holotype]. (**A** and **B**) Stereophotos of the skull with the ossified and in situ Meckel's cartilage connected to the mandible. (**C** and **D**) Skeletal feature identification and specimen photo. Abbreviations are as follows: ac, acromion; al, alisphenoid; apl, anterior lamina of petrosal; as, astragalus; bo, basioccipital; C and c, upper and lower canines; cl, clavicle; cm, calcaneum; co, coracoid process (scapula); cp, carpals; cv, caudal vertebrae; dc, dentary condyle; dpc, deltopectoral crest; ep, epipubis; fe, femur; fh, femoral head; fi, fibula; fr, frontal; gl, glenoid of scapula; gt, greater trochanter of femur; gtb, greater tubercle of humerus; I and i, incisors; ic, interclavicle; il, ilium; is, ischium; lv, lumbar vertebrae; M and m, upper and lower molars; mc, Meckel's cartilage; mf, mental foramina; msf, medial scapular facet; mp?, metacarpals?; mt, metatarsal; mx, maxillary; na, nasal; oc, occipital condyle; ol, olecranon process (ulna); P and p, upper and lower premolars; pa, parietal; phi, intermediate phalanges; php, proximal phalanges; pl, palatine; pr, petrosal promontorium; pta?, patella?; pts, pterygoid shelf; px, premaxillary; ra, radius; sc, scapula; sp, extratarsal spur; sq, squamosal; st, sternal manubrium?; stl, distal styloid of tibia; sv, sacral vertebrae; tm, teres major process; tv, thoracic vertebrae; ul, ulna; and vsf, ventral scapular facet.

Meckelian groove of the mandible (Fig. 2, A and C). The cartilage is curved at mid-length, and its posterior limb is twisted relative to the anterior limb so the posterior end diverges away from the mandible (Fig. 2A, red and blue arrows). Its preserved part in *Maotherium* is more gracile than the Meckel's cartilage in situ with connection to the mandible in *Repenomamus* (*12*). It is identical to the Meckel's cartilage preserved in *Gobiconodon* (*13*) and the ossified Meckel's cartilage in *Yanoconodon*, which is connected to the ectotympanic and malleus (*15*). Thus, we infer that *Maotherium* has a similar, ossified connection between the mandible and the middle ear (Fig. 3C) as in eutriconodonts.

Basal mammaliaforms have both a postdentary trough and a Meckelian groove. The middle ear and its associated postdentary rod (partly homologous to the ossified Meckel's cartilage) are lodged in the postdentary trough. A classic problem of Mesozoic mammals is whether the absence of the postdentary trough would mean the loss of the connection between the middle ear and the mandible (*14*, *16*). In *Maotherium*, the middle ear is connected by Meckel's cartilage to the mandible without a postdentary trough. Thus, the absence of a postdentary trough cannot exclude the possibility that the middle ear was still attached to the mandible. It adds to the evidence that Meckel's cartilage is evolutionarily labile within the spalacotheroid clade. Because the Meckelian groove is present in the Early Cretaceous spalacotheroids *Maotherium* and *Zhangheotherium* but absent in the derived spalacotheroids of the Late Cretaceous (*6*), the adult retention of Meckel's cartilage occurred only in Early Cretaceous taxa of this clade and was likely lost in its Late Cretaceous members that show no trace of Meckel's groove (*6*).

Maotherium corroborates an earlier observation that its related genus *Zhangheotherium* has a disarticulated Meckel's cartilage (*12*), but the new fossil of *Maotherium* (HGM 41H-III-0321) shows that the Meckel's cartilage is connected to the mandible in spalacotheroids and adds new anatomical information. Compared with *Yanoconodon*, the Meckel's cartilage in *M. asiaticus* indicates that the middle ear is oriented at an angle to the mandible (Figs. 2C and 3). The mid-length curvature of Meckel's cartilage made it feasible for its anterior limb to be nestled in the Meckel's groove on the mandible, whereas its posterior limb was separated mediolaterally from the mandible (Fig. 2, A and C). From the curvature of Meckel's cartilage, it can be inferred that the ectotympanic ring and the malleus manubrium should be oriented obliquely to the vertical coronoid-angular part of the mandible (Fig. 2) (*15*). Observation of *Maotherium* and *Yanoconodon* suggests that, before its disconnection from the mandible, the ancestral middle ear was already mediolaterally separated from the mandible (*12*, *15*, *25*).

DMME in extant mammals is accomplished by two ontogenetic steps (*25*–*27*): first, a mediolateral separation of the middle ear anlagen from

the mandible in embryonic stages (seen in extant monotremes and placentals); second, a loss of connection to the mandible by reabsorption of Meckel's cartilage in fetal stages. In *Maotherium* and eutriconodonts, the mediolateral separation of the middle ear from the mandible had already occurred. However, Meckel's cartilage is ossified, and its reabsorption never happened, resulting in retention of a middle ear connection to the mandible otherwise seen only in the embryonic or fetal stage of extant mammals.

The middle ear of *Maotherium* and eutriconodonts shows a paedomorphic resemblance to the embryonic pattern of modern monotremes and placentals in which the middle ear is mediolaterally separated from the mandible but still connected via Meckel's cartilage to the mandible (*25*–*27*). All that is necessary for adult eutriconodonts and spalacotheroids to retain this paedomorphic mandibular ear connection is a relatively earlier timing in ossification of the Meckel's cartilage. The homoplastic separation of the middle ear from the mandible in Mesozoic mammals is correlated with ontogenetic heterochrony.

By parsimony of all characters (*1*–*6*, *15*), *Maotherium* and its spalacotheroid clade are more closely related to living therians than to multituberculates and eutriconodonts, all within Mammalia (Fig. 3) (*22*). *Maotherium* is similar to eutriconodonts in having the middle ear connected to the mandible in adults (Fig. 3 right side, DMME absent) but conspicuously different from living therians, multituberculates (*22*, *28*), and modern monotremes (and possibly *Hadrocodium*), in which the middle ear is separated from the mandible in adults (Fig. 3 left side, DMME present). The separation of the middle ear in mammalian phylogeny may have occurred by two alternative evolutionary scenarios: (i) DMME was present in the common ancestor of Mammalia (Fig. 3, node 3), but eutriconodonts and spalacotheroids reevolved the middle ear attachment to the mandible; or (ii) DMME was absent in the common ancestor of mono-

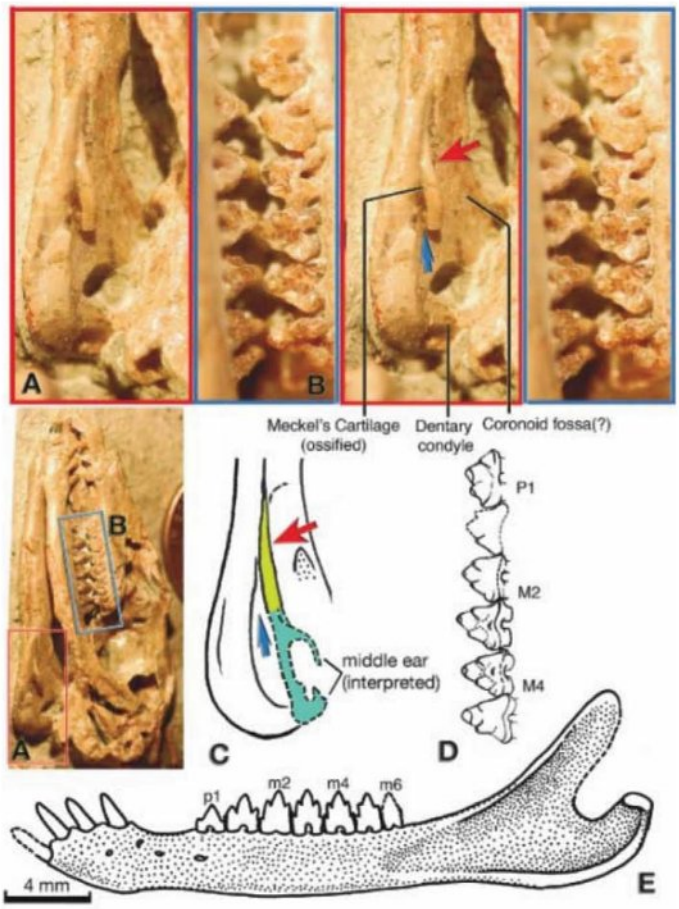

Fig. 2. Dentition and mandible of *Maotherium asiaticus* (HGM 41H-III-0321; holotype) and interpretation of its middle ear. (**A**) The preserved Meckel's cartilage (ossified) and its attachment to the mandible (stereophotos). (**B**) Upper postcanines (P1 to M5) (stereophotos). (**C**) Interpretive restoration of the middle ear (dashed line) and its attachment to the mandible [as in (A)]. Red arrow, mid-length curvature of Meckel's cartilage (identical to eutriconodonts); blue arrow, mediolateral separation; the ectotympanic and malleus are conjectural, based on the middle ears of multituberculates and *Yanoconodon*. (**D**) Upper premolar and molars [oblique view, as in (B)]. (**E**) Mandible (reconstruction, lateral view).

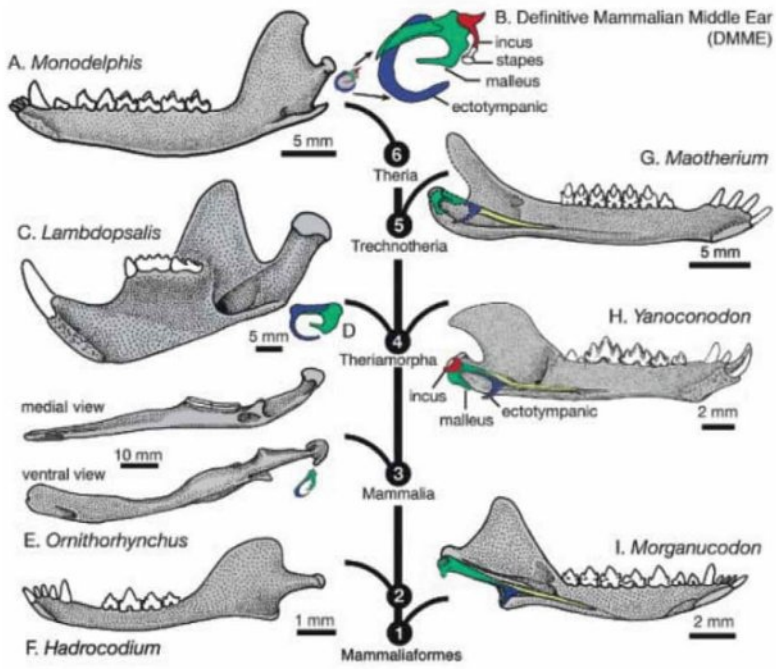

Fig. 3. Homoplastic evolution of the mammalian middle ear by paedomorphic retention of ossified Meckel's cartilage among extinct clades of mammaliaforms. Right, ancestral conditions of ossified Meckel's element in premammalian mammaliaforms, and in paedomorphic retention of ossified Meckel's cartilage in extinct clades of Mammalia. Left, living mammal and mammaliaform clades achieved the reabsorption of embryonic Meckel's cartilage and the DMME. (**A** and **B**) Extant therian *Monodelphis*: mandible [(A), medial view] and middle ear [(B) medial view]. (**C** and **D**) Extinct multituberculate mammal *Lambdopsalis*: absence of Meckel's cartilage on the mandible [(C) medial view] and separated middle ear ossicles [(D) ventral view] in adult [modified from (*28*)]. (**E**) Extant monotreme *Ornithorhynchus*: reabsorption of embryonic Meckel's cartilage and separation of middle ear from the mandible (top, medial view; bottom, ventral view) in adult. (**F**) Mammaliaform *Hadrocodium*: mandible (medial view) without Meckel's groove for middle ear attachment. (**G**) Partial restoration of the spalacotheroid *Maotherium asiaticus*: ossified Meckel's cartilage connecting the middle ear to mandible (medial view); hypothetical restoration of ear ossicle based on other Mesozoic mammals. (**H**) The eutriconodont *Yanoconodon* (and gobiconodontids): ossified Meckel's cartilage connecting middle ear to the mandible but ossicles partially (mediolaterally) separated from the mandible. (**I**) Mammaliaform *Morganucodon*: ossified Meckel's elements and the middle ear in the postdentary trough and Meckel's groove of the mandible. [Tree simplified from the phylogeny in (*22*)]; phylogenetic tree nodes 1 and 3 to 6 as labeled; node 2 (*Hadrocodium*) represents an unnamed mammaliaform clade.

tremes, eutriconodonts, and the living therians, and this ancestral feature is retained in eutriconodonts and spalacotheroids; but DMME evolved in extant monotremes (*14*) and in multituberculates for a second time, and then again for a third time in marsupials and placentals.

Paedomorphosis, or retention of fetal or juvenile characteristics of ancestors and/or relatives through developmental heterochrony, is a common phenomenon in vertebrate evolution. Scenario i gains support from the paedomorphic similarity of the ossified Meckel's cartilage in eutriconodonts and spalacotheroids to that of extant mammalian embryos (*15*). The premature ossification of Meckel's cartilage represents a simple developmental change in timing (heterochrony), for which a genetic mechanism has been established (*29*, *30*).

A mutant genetic and signaling network that can result in a premature ossification of Meckel's cartilage in mammalian embryogenesis has been characterized by recent genetic studies. Meckel's cartilage derives from cranial neural crest cells; it serves as scaffolding for development of mandibular and middle ear elements. Normal development of the Meckel's cartilage and its derivatives in vertebrates requires a wide range of structural and homeobox genes, such as *Bapx1*, *Gsc*, *Emx2*, *Sox9*, and *Type II Col.*, which are expressed in the mammalian middle ear structure [reviewed by (*30*)]. Morphogenesis of Meckel's cartilage also requires a variety of growth factors, some of which are ubiquitous in mammalian development. This complex signaling network for Meckel's normal development includes transforming growth factors–β (*Tgf*-β) (*29*), connective tissue growth factors (*Ctgf*) (*29*), fibroblast growth factor (*Fgf*) (*30*), epidermal growth factor (*Egf*) (*31*), and bone morphogenetic proteins (*Bmp*), among others.

In normal chondrogenesis of Meckel's cartilage of *Mus* (wild type), the signaling pathway from *Tgf*-β (upstream) to *Ctgf* (downstream) stimulates the proliferation, and inhibits the terminal differentiation, of chondrocytes (*29*). Mutant *Tgfbr2*$^{fl/fl}$*;Wnt1-Cre* genes (a mutant of *Tgf*-β) accelerate chondrocyte proliferation and cause ossification of Meckel's cartilage in mutant *Mus* (*29*). The phenotype of ossified Meckel's cartilage in *Tgfbr2*$^{fl/fl}$*;Wnt1-Cre* mutant mice is similar to the fossilized and (prematurely) ossified Meckel's cartilage in the spalacotheroids (Fig. 2) and eutriconodonts (Fig. 3). This suggests that some similar developmental pathway had underlined the ossification of Meckel's cartilage in extinct Mesozoic mammals.

Among living mammals, an ossified Meckel's cartilage occurs only in certain mutant mice; the cartilage is retained only in pathological cases among humans. However, ossified Meckel's cartilage evolved at least twice in Mesozoic spalacotheroids and eutriconodonts. The absence of ossified Meckel's cartilage in the adult in extant monotremes, marsupials, and placentals represents a more-canalized development of the middle ear for these living lineages, in contrast to a much more labile evolutionary development of middle ear features, made possible by a greater diversity of about 20 Mesozoic mammaliaform clades (*1*, *5*).

References and Notes

1. Z. Kielan-Jaworowska, R. L. Cifelli, Z.-X. Luo, *Mammals from the Age of Dinosaurs—Origins, Evolution, and Structure* (Columbia Univ. Press, New York, 2004).
2. Z.-X. Luo *et al.*, *Acta Palaeontol. Pol.* **47**, 1 (2002).
3. T. Martin, O. W. M. Rauhut, *J. Vertebr. Paleontol.* **25**, 414 (2005).
4. G. W. Rougier *et al.*, *American Mus. Nov.* **3566**, 1 (2007).
5. Z.-X. Luo, *Nature* **450**, 1011 (2007).
6. C. L. Cifelli, S. K. Madsen, *Geodiversitas* **21**, 167 (1999).
7. T. Tsubamoto *et al.*, *Acta Palaeontol. Pol.* **49**, 329 (2004).
8. S. C. Sweetman, *Palaeontology* **51**, 1367 (2008).
9. G. W. Rougier *et al.*, *Acta Geol. Sin.* **77**, 7 (2003).
10. G. Li, Z.-X. Luo, *Nature* **439**, 195 (2006).
11. E. F. Allin, J. A. Hopson, "The auditory apparatus of advanced mammal-like reptiles and early mammals," in *The Evolutionary Biology of Hearing*, D. B. Webster, *et al.*, Eds. (Springer-Verlag, New York, 1992), pp. 587–614.
12. J. Meng *et al.*, *Zool. J. Linn. Soc.* **138**, 431 (2003).
13. C.-K. Li *et al.*, *Chinese Sci. Bull. (English Ed.)* **48**, 1129 (2003).
14. T. H. Rich, J. A. Hopson, A. M. Musser, T. F. Flannery, P. Vickers-Rich, *Science* **307**, 910 (2005).
15. Z.-X. Luo *et al.*, *Nature* **446**, 288 (2007).
16. T. Rowe *et al.*, *Proc. Natl. Acad. Sci. U.S.A.* **105**, 1238 (2008).
17. Systematics: Class Mammalia; Clade Trechnotheria (*1*); Superfamily Spalacotheroidea (*9*, *10*); Family *Zhangheotheriidae*; Genus *Maotherium* (*10*); sp. nov. *Maotherium asiaticus*. Holotype: Henan Geological Museum, Zhengzhou, China (HGM 41H-III-0321; Figs. 1 and 2), an almost complete skull, and most of the postcranial skeleton. Etymology: *asiaticus*, Latin for the Asiatic provenance of zhangheotheriids. Locality and Age: Lujiatun Locality (120°54′41″E, 41°36′26″N), Beipiao, Liaoning Province, China; the Yixian Formation. The site dated to be 123.2 ± 1.0 million years old (*22*). Diagnosis: I3, C1, P1, M5; i3, c1, p1, m6. *M. asiaticus* is referred to *Maotherium* by apomorphies shared by *Maotherium sinensis* (type species): deep precondylar notch of mandible, a deep ectoflexus on upper molars with cusp B′, a gradient in increasingly acute angle in triangulation of molar cusps toward the posterior molar, sigmoidal shape of the posterior ventral border of mandible. Differs from *M. sinensis* in having apomorphies of low central cusp between B′ and C; *M. asiaticus* has the tibial distal styloid process and the proximolateral process of the metatarsal 5 (all three features absent in *M. sinensis*). Full diagnosis in (*22*).
18. Z.-X. Luo, A. W. Crompton, A.-L. Sun, *Science* **292**, 1535 (2001).
19. Z.-X. Luo, J. R. Wible, *Science* **308**, 103 (2005).
20. Q. Ji, Z.-X. Luo, C.-X. Yuan, A. R. Tabrum, *Science* **311**, 1123 (2006).
21. J. Meng *et al.*, *Nature* **444**, 889 (2006).
22. Materials and methods are available as supporting material on *Science* Online.
23. E. C. Kirk *et al.*, *J. Hum. Evol.* **55**, 278 (2008).
24. Z.-X. Luo, Q. Ji, J. R. Wible, C.-X. Yuan, *Science* **302**, 1934 (2003).
25. W. Maier, in *Mammal Phylogeny*, F. S. Szalay *et al.*, Eds. (Springer-Verlag, New York, 1993), vol. 1, pp. 165–181.
26. M. R. Sánchez-Villagra *et al.*, *J. Morphol.* **251**, 219 (2002).
27. T. Rowe, *Science* **273**, 651 (1996).
28. J. Meng, A. R. Wyss, *Nature* **377**, 141 (1995).
29. K. Oka *et al.*, *Dev. Biol.* **303**, 391 (2007).
30. A. S. Tucker *et al.*, *Development* **131**, 1235 (2004).
31. L. Shum *et al.*, *Development* **118**, 903 (1999).

32. We thank G. Cui for fossil preparation; M. R. Dawson for improving the manuscript; and R. Asher, Y. Chai, and A. Tucker for discussion. Support from the 973 Project of Ministry of Science and Technology of China (Q.J.); from Institute of Geology of Chinese Academy of Geological Sciences (Beijing) (C.-X.Y.), from NSF (USA), National Natural Science Foundation (China), and National Geographic Society (Z.-X.L.); and from Henan Provincial Government (to Z.-L.Z. and L.X.).

Supporting Online Material

www.sciencemag.org/cgi/content/full/326/5950/278/DC1
Materials and Methods
SOM Text
References

1 July 2009; accepted 17 August 2009
10.1126/science.1178501

Daily Electrical Silencing in the Mammalian Circadian Clock

Mino D. C. Belle,[1] Casey O. Diekman,[2,4] Daniel B. Forger,[3,4] Hugh D. Piggins[1]*

Neurons in the brain's suprachiasmatic nuclei (SCNs), which control the timing of daily rhythms, are thought to encode time of day by changing their firing frequency, with high rates during the day and lower rates at night. Some SCN neurons express a key clock gene, *period 1* (*per1*). We found that during the day, neurons containing *per1* sustain an electrically excited state and do not fire, whereas non-*per1* neurons show the previously reported daily variation in firing activity. Using a combined experimental and theoretical approach, we explain how ionic currents lead to the unusual electrophysiological behaviors of *per1* cells, which unlike other mammalian brain cells can survive and function at depolarized states.

In mammals, behavior and physiology are regulated on a daily basis by the brain's master circadian (~24-hour) clock in the suprachiasmatic nuclei (SCNs). The *period 1* (*per1*) gene is a key component of the molecular mechanism of this clock (*1*); its expression in the SCN peaks during the day and is low at night, and can be used as a marker of clock-containing SCN neurons and their circadian phase (*2*, *3*). SCN neurons are also thought to express time of day by changing their firing frequency, with high rates during the day and lower rates at night (*4*–*6*). A fundamental question in circadian biology is how the intracellular molecular circadian clock regulates the electrophysiology of SCN neurons. A Hodgkin-Huxley–type model of SCN neurons shows that circadian changes in ionic conductances can account for the circadian variation

in firing rate (*7*). This model also predicts that the molecular clock can drive SCN neurons to exhibit an unusual depolarized rest state not previously reported experimentally. Because not all SCN neurons appear to contain the molecular clock machinery (*8*), a further prediction of this model is that SCN neurons that express the key clock genes (such as *per1*) will have different electrical properties than those that do not express these genes.

To measure time-dependent changes in the membrane properties and excitability of SCN neurons in vitro, and to investigate potential differences among these neurons, we made targeted whole-cell recordings from SCN of mice expressing an enhanced green fluorescent protein (EGFP) reporter of *per1*. We sampled from 309 "*per1*" neurons showing detectable EGFP and 109 neurons in which EGFP could not be detected ("non-*per1*"). We found a marked difference in the electrophysiological behavior during the day of these two populations.

Sampling from *per1* and non-*per1* neurons throughout the SCN across the projected day-night cycle revealed large circadian variation in resting membrane potential (RMP), membrane input resistance (R_{input}), and overall electrophysiological behaviors (Figs. 1 and 2). In the morning [Zeitgeber Time (ZT) 2 to 4.25, where ZT0 represents lights-on and ZT12 represents lights-off], *per1* neurons were at moderate RMP (V_m = –44 ± 0.6 mV; n = 47 neurons) and generated action potentials (APs) (4.3 ± 0.1 Hz) (Figs. 1 and 2). In the afternoon (ZT5.25 to 10.75), *per1* neurons were spontaneously depolarized and either showed low-amplitude 2- to 7-Hz oscillations in membrane potential (MP) (mean V_m = –35 ± 0.7 mV; n = 50 neurons) or were completely silent (V_m = –27 ± 0.4 mV; n = 50 neurons) (Figs. 1 and 2). Around dusk (ZT10.75 to 12.75), these cells were again at moderate RMP (–46 ± 1 mV; n = 45 neurons) and generated APs, but at lower frequency than in the morning (1 ± 0.1 Hz) (Figs. 1 and 2). This progression from moderate RMP in the morning to depolarized states (–25 to –34 mV) in the afternoon and back to moderate RMP at dusk was specific to *per1* neurons; non-*per1* cells remained at moderate RMP (V_m = –46 ± 0.9 mV; n = 48 neurons) and continued to generate APs until dusk (Figs. 1 and 2). In contrast, during the early night (ZT13 to 15.25) both *per1* and non-*per1* neurons became robustly hyperpolarized and showed no APs (*per1*, –68 ± 0.5 mV; n = 40 neurons; non-*per1*, –66 ± 1.1 mV; n = 24 neurons), but later in the night (ZT16.75 to 23) both *per1* and non-*per1* neurons were at or close to moderate RMP and generated APs (Figs. 1 and 2).

In many studies, unusually depolarized neurons are considered unhealthy, so we were careful to establish that such *per1* neurons were physiologically sound. Indeed, depolarized states were only observed in cells recorded during the afternoon and never in cells tested in morning, dusk, or night. Further, silent *per1* cells characteristic of the state attained in the afternoon had extremely high R_{input} and, by application of steady-state hyperpolarizing currents, could be induced to fire regular APs like those of cells measured in the morning (R_{input} at –25 mV = 2.9 ± 0.1 gigohm, n = 38 neurons) (fig. S1). Alternatively, steady-state depolarizing currents reversibly silenced regular AP-firing *per1* cells in the morning, rendering them indistinguishable from neurons measured in the afternoon portion of the light cycle (n = 26 neurons) (fig. S1). Depolarization of non-*per1* neurons in a similar manner compromises their electrophysiological properties. Thus, *per1* neurons appear to be healthy and functioning within normal whole-cell electrophysiological parameters.

We used mathematical modeling to determine whether these observed electrical behaviors could be explained by existing data on the ionic currents measured within SCN neurons. To simulate *per1* neurons at various circadian phases, we first adapted a model of unidentified SCN neurons (*7*) to account for the enhanced electrical excitability of *per1* neurons (fig. S2). We then incorporated into the model circadian variations in K^+ and Ca^{2+} conductances (fig. S3), and intracellular Ca^{2+} concentration (fig. S4), from published experimental observations (*9*–*11*). Although a circadian variation in only one ionic current could cause transitions from a hyperpolarized

[1]Faculty of Life Sciences, A. V. Hill Building, University of Manchester, Manchester M13 9PT, UK. [2]Department of Industrial and Operations Engineering, University of Michigan, Ann Arbor, MI 48109, USA. [3]Department of Mathematics, University of Michigan, Ann Arbor, MI 48109, USA. [4]Center for Computational Medicine and Bioinformatics, University of Michigan, Ann Arbor, MI 48109, USA.

*To whom correspondence should be addressed. E-mail: hugh.d.piggins@manchester.ac.uk

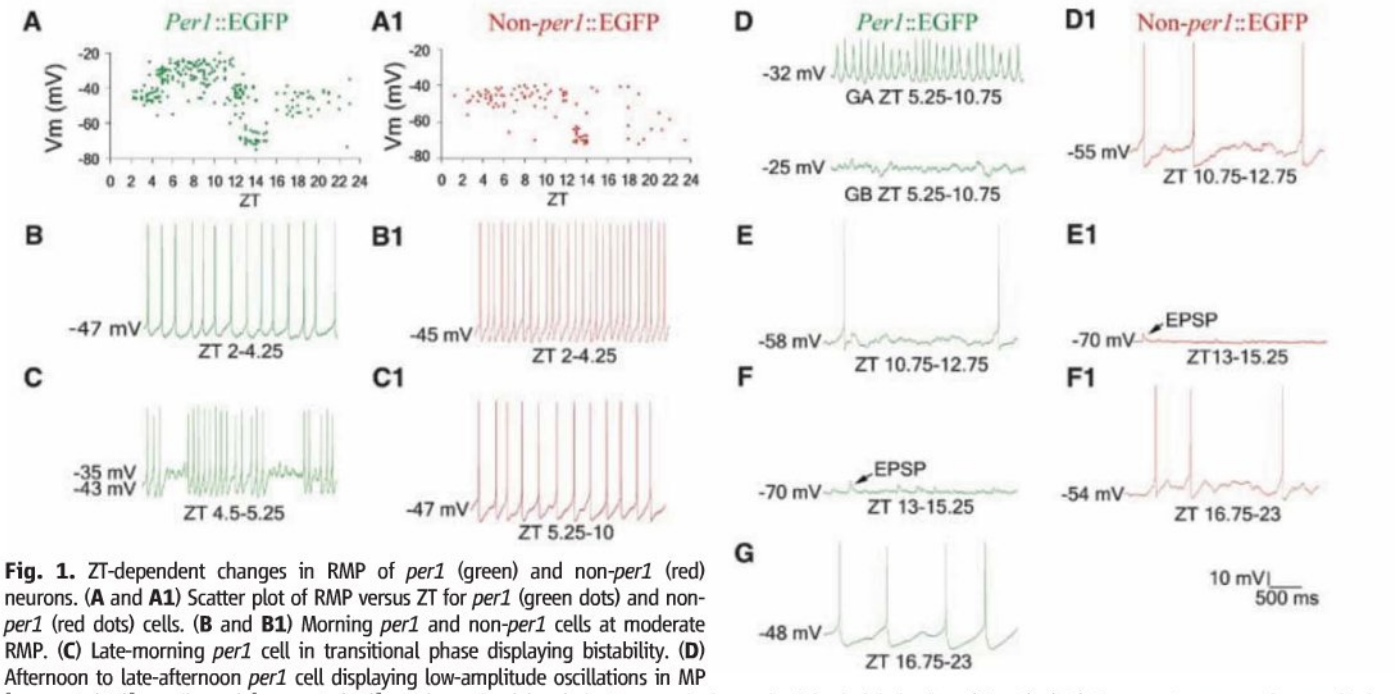

Fig. 1. ZT-dependent changes in RMP of *per1* (green) and non-*per1* (red) neurons. (**A** and **A1**) Scatter plot of RMP versus ZT for *per1* (green dots) and non-*per1* (red dots) cells. (**B** and **B1**) Morning *per1* and non-*per1* cells at moderate RMP. (**C**) Late-morning *per1* cell in transitional phase displaying bistability. (**D**) Afternoon to late-afternoon *per1* cell displaying low-amplitude oscillations in MP [group A (GA)] or silenced [group B (GB)] as determined by their R_{input} and electrophysiological behaviors (Fig. 2). (**C1**) Non-*per1* neurons do not display bistability or depolarized RMP, but remained at moderate RMP, generating APs. (**E** and **D1**) Dusk *per1* and non-*per1* cells at moderate RMP around the time of lights-off. (**F** and **E1**) Early night *per1* and non-*per1* cells hyperpolarized and silenced, receiving excitatory postsynaptic potentials (EPSPs). (**G** and **F1**) Late-night *per1* and non-*per1* neurons at moderate RMP.

steady state to repetitive firing, and also from repetitive firing to a depolarized steady state (figs. S5 and S6), circadian rhythms in both K^+ and Ca^{2+} currents were required to faithfully reproduce the fine details of these transitions (Fig. 1, B to G, and Fig. 3).

Mathematical analysis revealed that as the day progresses, transitions in the behavior of *per1* neurons occur when a quiescent state gains or loses stability through Hopf bifurcations (fig. S3). This common mathematical structure has been found in many other neural systems and corresponds to Type II excitability (spiking emerging with nonzero frequency) in Hodgkin's original classification system (*12*). The changes in stability of the hyperpolarized rest state we observed at night in *per1* neurons are similar in character to those seen in other neurons (*13*). However, *per1* neurons are different in that a second Hopf bifurcation occurs during the day, when an unusually depolarized rest state becomes stable or unstable. The physiological importance of these bifurcations is that minor, molecular clock–driven changes in certain ionic conductances can have a major effect on the bioelectrical output of the neuron. Near bifurcation points, neurons can exhibit the types of behaviors seen in *per1* neurons, such as low-amplitude oscillations in MP or noise-induced transitions between oscillatory and quiescent states (*12*, *14*). These behaviors do not appear to depend on the initial state of the neuron (fig. S3) and can be achieved with a variety of parameter choices (figs. S4, S5, S6, and S7).

In both *per1* and non-*per1* cells, the cyclical changes in RMP were closely associated and in phase with alterations in R_{input} (Fig. 2). For *per1* cells, the amplitude of the circadian variation in RMP and R_{input} were 42 mV [day, –27 ± 0.4 mV; night, –68 ± 0.5 mV; $P < 1 \times 10^{-5}$; all P values were determined by means of analysis of variance (ANOVA) and post-hoc Bonferroni test unless otherwise stated] and 2.1 gigohm (day, 2.9 ± 0.1 gigohm; night, 0.8 ± 0.03 gigohm; $P < 1 \times 10^{-5}$), respectively. The measured membrane time constant was also significantly larger during the day than at night (afternoon, 48.3 ms; early night, 23.3 ms; $P < 0.001$; $n = 20$ neurons). These differences between day and night *per1* cells were not associated with any change in cell capacitance (day, 9.4 ± 0.04 pF; night, 9.3 ± 0.05 pF; $n = 10$ neurons), and thus are not a result of changes in cell size. In non-*per1* cells, the differences in RMP and R_{input} between the day and night were 20 mV (day, –46 ± 0.9 mV; night, –66 ± 1.1 mV; $P < 0.001$) and 0.9 gigohm (day, 1.6 ± 0.1 gigohm; night, 0.7 ± 0.1 gigohm; $P < 0.001$), respectively.

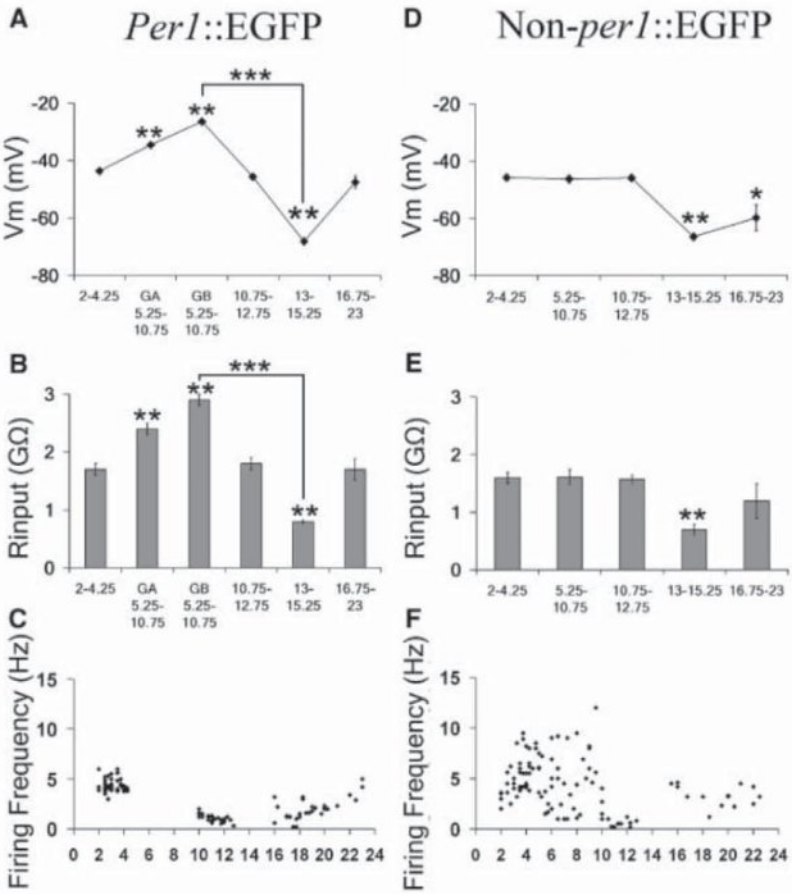

Fig. 2. Changes in RMP and associated changes in R_{input} and firing frequency of *per1* and non-*per1* cells across a day-night cycle. *Per1* cells in GA and GB at ZT5.25 to 10.75 were determined by their electrophysiological behaviors (Fig. 1) and R_{input} ($P < 0.01$) (Fig. 2B). GA cells displayed low-amplitude 2- to 7-Hz oscillations in MP, whereas GB cells were silent. (**A**) Changes in RMP of *per1* cells and (**B**) associated changes in their R_{input}. (**C**) Scatter plot of firing frequency versus ZT for *per1* cells, showing *per1* cells generating APs in the morning, at dusk, and during late night; however, *per1* cells were completely silent during the afternoon and early night. (**D**) Changes in RMP of non-*per1* cells, and (**E**) associated changes in their R_{input}. (**F**) Scatter plots of firing frequency versus ZT for non-*per1* cells, showing the previously reported daily variation in firing frequency of these cells. *$P < 0.05$; **$P < 0.001$; ***$P < 1 \times 10^{-5}$. Numerical data represent ±SEM

Our measurements and modeling indicate that a clock-controlled reduction in K^+ channel conductance causes depolarization in *per1* cells in the afternoon, and an increase in K^+ channel conductance at night causes the hyperpolarization. We also reasoned that L-type Ca^{2+} channels may contribute to determining the RMP of these cells (*9*, *15*, *16*). We therefore bath-applied tetraethylammonium (TEA; a broad spectrum K^+ channel blocker) or nimodipine (an L-type Ca^{2+} channel blocker) during the night or the morning.

TEA (30 mM) caused a significant depolarization in *per1* cells recorded in the morning (from –43 ± 1.2 mV to –28 ± 0.9 mV; $P < 0.001$, $n = 8$ neurons, ANOVA and post hoc test), and significantly increased their R_{input} (1.5 ± 0.03 to 2.9 ± 0.2; $P < 0.001$, ANOVA and post hoc test) (fig. S8). Nimodipine (2 μM) depolarized *per1* cells recorded in the morning so that their cellular behaviors and RMP were similar to those *per1* cells tested in the afternoon (fig. S8). Nimodipine also caused cells whose RMP was near –33 mV to depolarize to –25 mV (fig. S8). Antagonizing L-type Ca^{2+} channels in SCN neurons inhibits Ca^{2+}-dependent K^+ channels (K_{ca}) (*15*), and in many neuronal systems inhibition of K_{ca} channels causes depolarization (*17*). So, we tested whether the large- (BK_{Ca}) and/or the small-conductance (SK_{Ca}) K_{ca} are involved in setting the RMP of *per1* neurons. Iberiotoxin (IbTX; BK_{Ca}-selective receptor antagonist) (100 nM) causes small depolarization (2 to 3 mV) in early- and late-morning *per1* cells. However, concomitant application of IbTX and apamin (SK_{Ca} selective receptor antagonist) (100 to 200 nM) during early and late morning caused significant and irreversible depolarization (13 to 15 mV) in *per1* cells, and significantly increased their R_{input} (1.6 ± 0.03 to 3 ± 0.2; $P < 0.001$) to values that were indistinguishable from those of *per1* cells measured in the afternoon (Figs. 2 and 4). During the apamin- and IbTX-induced depolarization, morning *per1* cells displayed behaviors and membrane properties that were typical of afternoon *per1* cells (figs. S9 and S10). Thus, spontaneous depolarization and associated change in R_{input} observed in *per1* neurons between dawn and dusk result from a clock-controlled reduction in BK_{Ca} and SK_{Ca} conductances. IbTX and apamin had little effect on the RMP of non-*per1* cells

during the day (fig. S11). Although TEA ($n = 6$ neurons) dose-dependently depolarized cells in the early-night state and increased their R_{input} to values similar to those of cells measured in the morning (Fig. 2 and figs. S8 and S12), these night effects were not seen with nimodipine, IbTX, or apamin ($n = 7$ neurons) (fig. S12). This suggests that BK_{Ca}, SK_{Ca}, and L-type Ca^{2+} channels minimally influence the RMP of *per1* neurons during the night.

Blocking of AP-dependent presynaptic potentials with TTX (200 nM to 1 μM; $n = 8$ neurons) or inhibition of postsynaptic receptors for glutamate and γ-aminobutyric acid, alone or in combination, had no effect on the RMP of *per1* cells at any time (fig. S13). This suggests that the observed changes in RMP of *per1* cells were cell autonomous and do not rely on the network properties of the SCN (*18*).

Both our experimental and modeling results establish that like invertebrate circadian clock neurons (*19*–*21*), *per1*-containing SCN cells exhibit clock-controlled, high-amplitude circadian oscillations in key electrophysiological properties. A loss of BK_{Ca} and SK_{Ca} channel conductances underpin the depolarization of RMP seen in *per1* neurons during the afternoon, whereas multiple K^+ channels contribute to hyperpolarization of these cells during the night. In contrast, SCN neurons lacking detectable EGFP expression showed much smaller day-night differences in electrophysiological parameters but do exhibit the characteristic circadian differences in AP frequency (*4*–*6*). The level of *per1*-driven EGFP peaks about two hours before the day-night transition (*4*), with its morning and dusk phases showing strong association with AP generation. However, in the middle of the afternoon, neurons containing *per1* are in an excited state but do not fire APs. This temporal dissociation between clock gene expression and AP generation, at this time of day, demonstrates that the relationships between *per1* expression and neuronal membrane properties are much more complex than first supposed (*22*–*24*). Our study also indicates that the neurophysiology of *per1* neurons may not obey conventional electrophysiological principles.

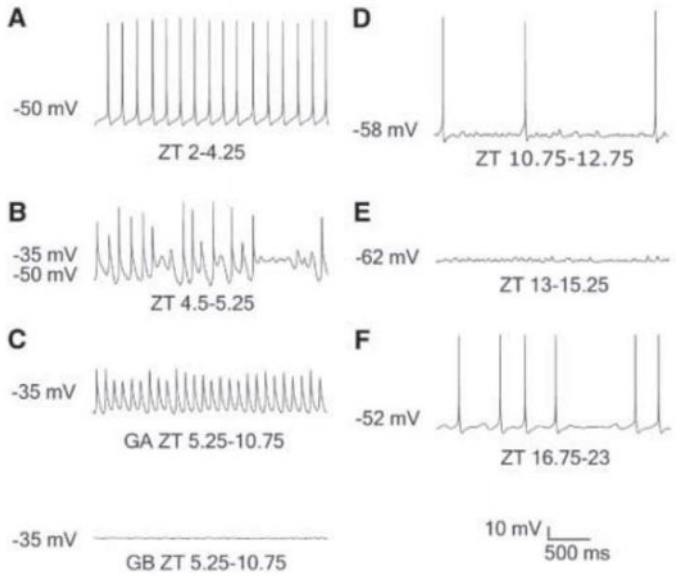

Fig. 3. Mathematical simulations predict the electrophysiological behavior of SCN clock neurons observed throughout a day-night cycle. These simulations use a revised version of the Sim-Forger model (*7*) specific for *per1* neurons and incorporate randomly generated postsynaptic potentials (fig. S2). (**A** to **F**) Panels are similar to experimental data in Fig. 1, B to G, and show that known rhythms in ionic currents (fig. S3) can explain the experimentally observed behaviors.

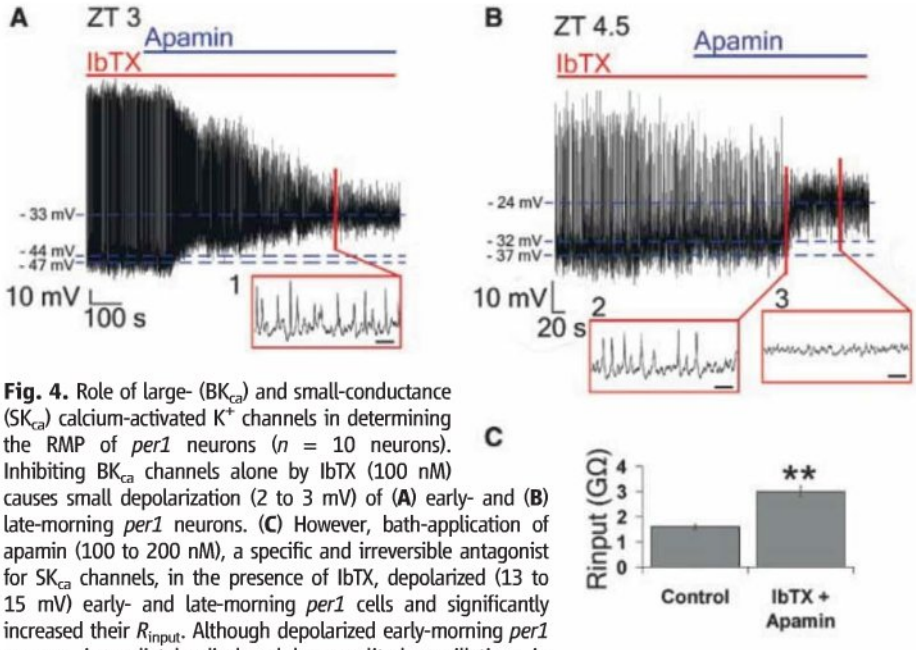

Fig. 4. Role of large- (BK_{ca}) and small-conductance (SK_{ca}) calcium-activated K^+ channels in determining the RMP of *per1* neurons ($n = 10$ neurons). Inhibiting BK_{ca} channels alone by IbTX (100 nM) causes small depolarization (2 to 3 mV) of (**A**) early- and (**B**) late-morning *per1* neurons. (**C**) However, bath-application of apamin (100 to 200 nM), a specific and irreversible antagonist for SK_{ca} channels, in the presence of IbTX, depolarized (13 to 15 mV) early- and late-morning *per1* cells and significantly increased their R_{input}. Although depolarized early-morning *per1* neurons immediately displayed low-amplitude oscillations in MP [(A), inset 1], late morning *per1* cells first show low-amplitude oscillations in MP during depolarization [(B), inset 2] and then became silent [(B), inset 3]. These behaviors were typical of afternoon *per1* cells (Fig. 1 and figs. S1 and S8). $^{**}P < 0.001$. Numerical data represent ±SEM.

References and Notes

1. C. H. Ko, J. S. Takahashi, *Hum. Mol. Genet.* **15**, R271 (2006).
2. H. Tei *et al.*, *Nature* **389**, 512 (1997).
3. A. T. L. Hughes *et al.*, *J. Neurochem.* **106**, 1646 (2008).
4. M. U. Gillette *et al.*, *Ciba Found. Symp.* **183**, 134 (1995).
5. M. Mrugala, P. Zlomanczuk, A. Jagota, W. J. Schwartz, *Am. J. Physiol. Regul. Integr. Comp. Physiol.* **278**, R987 (2000).
6. D. J. Cutler *et al.*, *Eur. J. Neurosci.* **17**, 197 (2003).
7. C. K. Sim, D. B. Forger, *J. Biol. Rhythms* **22**, 445 (2007).
8. S. Yamaguchi *et al.*, *Science* **302**, 1408 (2003).
9. C. M. Pennartz, M. T. de Jeu, N. P. Bos, J. Schaap, A. M. Geurtsen, *Nature* **416**, 286 (2002).
10. G. R. Pitts, H. Ohta, D. G. McMahon, *Brain Res.* **1071**, 54 (2006).
11. M. Ikeda *et al.*, *Neuron* **38**, 253 (2003).
12. J. Rinzel, G. B. Ermentrout, in *Methods in Neuronal Modeling*, C. Koch, I. Segev, Eds. (MIT Press, Cambridge, MA, ed. 2, 1998), pp. 251–292.
13. D. Paydarfar, D. B. Forger, J. R. Clay, *J. Neurophysiol.* **96**, 3338 (2006).
14. E. M. Izhikevich, *Dynamical Systems in Neuroscience* (MIT Press, Cambridge, MA, 2007).
15. A. C. Jackson, G. L. Yao, B. P. Bean, *J. Neurosci.* **24**, 7985 (2004).
16. R. P. Irwin, C. N. Allen, *J. Neurosci.* **27**, 11748 (2007).
17. X. Liu, A. E. Herbison, *Endocrinology* **149**, 3598 (2008).
18. T. M. Brown, H. D. Piggins, *Prog. Neurobiol.* **82**, 229 (2007).
19. G. Cao, M. N. Nitabach, *J. Neurosci.* **28**, 6493 (2008).
20. V. Sheeba, H. Gu, V. K. Sharma, D. K. O'Dowd, T. C. Holmes, *J. Neurophysiol.* **99**, 976 (2008).
21. S. Michel, M. E. Geusz, J. J. Zaritsky, G. D. Block, *Science* **259**, 239 (1993).
22. S. J. Kuhlman, R. Silver, S. J. Le, A. Bult-Ito, D. G. McMahon, *J. Neurosci.* **23**, 1441 (2003).
23. M. J. Vansteensel *et al.*, *Curr. Biol.* **13**, 1538 (2003).
24. M. H. Hastings, E. D. Herzog, *J. Biol. Rhythms* **19**, 400 (2004).

25. We thank D. McMahon, Vanderbilt University, for providing us with the *per1*::2dGFP mice and R. Lucas and R. Baines, University of Manchester, C. Diniz Behn, University of Michigan, and D. Paydarfar, University of Massachusetts Medical School, for their critical reading of the manuscript. This work was funded by a project grant from the Biotechnology and Biological Sciences Research Council awarded to H.D.P. (BB/E00511X). M.D.C.B. is a Research Associate. C.O.D. is a NSF Graduate Research Fellow. D.B.F. is an Air Force Office of Scientific Research Young Investigator (FA 9550-08-01-0076).

Supporting Online Material

www.sciencemag.org/cgi/content/full/326/5950/281/DC1
Materials and Methods
Figs. S1 to S18
References

11 December 2008; accepted 24 August 2009
10.1126/science.1169657

Broad and Potent Neutralizing Antibodies from an African Donor Reveal a New HIV-1 Vaccine Target

Laura M. Walker,[1]* Sanjay K. Phogat,[2]*‡ Po-Ying Chan-Hui,[3] Denise Wagner,[2] Pham Phung,[4] Julie L. Goss,[4] Terri Wrin,[4] Melissa D. Simek,[5] Steven Fling,[1] Jennifer L. Mitcham,[3] Jennifer K. Lehrman,[5] Frances H. Priddy,[5] Ole A. Olsen,[3] Steven M. Frey,[3] Phillip W. Hammond,[3] Protocol G Principal Investigators,† Stephen Kaminsky,[2] Timothy Zamb,[2] Matthew Moyle,[3] Wayne C. Koff,[5] Pascal Poignard,[1] Dennis R. Burton[1,6]‡

Broadly neutralizing antibodies (bNAbs), which develop over time in some HIV-1–infected individuals, define critical epitopes for HIV vaccine design. Using a systematic approach, we have examined neutralization breadth in the sera of about 1800 HIV-1–infected individuals, primarily infected with non–clade B viruses, and have selected donors for monoclonal antibody (mAb) generation. We then used a high-throughput neutralization screen of antibody-containing culture supernatants from about 30,000 activated memory B cells from a clade A–infected African donor to isolate two potent mAbs that target a broadly neutralizing epitope. This epitope is preferentially expressed on trimeric Envelope protein and spans conserved regions of variable loops of the gp120 subunit. The results provide a framework for the design of new vaccine candidates for the elicitation of bNAb responses.

Despite more than two decades of research, a protective vaccine against HIV-1 remains elusive. It is widely accepted that such a vaccine will require the elicitation of both T cell–mediated immunity and a broadly neutralizing antibody (bNAb) response (*1*–*3*). All of the known bNAbs provide protection in the best available primate models (*4*–*9*) and, therefore, are considered to be the types of antibodies that should be elicited by a vaccine. Unfortunately, these antibodies tend to display limited breadth and potency against non–clade B viruses, which make up the majority of infections outside North America and Europe, and they recognize epitopes on the virus that so far have failed to elicit bNAb responses when incorporated into a diverse range of immunogens (*10*–*12*). Therefore, in order to develop a successful vaccine, it is of high priority to identify new bNAbs that bind to epitopes that may be more amenable to immunogen design.

We have screened serum from ~1800 HIV-1–infected donors from Thailand, Australia, the United Kingdom, the United States, and several sub-Saharan African countries for neutralization activity and have identified donors who exhibit broad and potent neutralizing serum activity (*13*, *14*). Monoclonal antibodies (mAbs) are currently being generated from these donors by different approaches. In this study, we used a high-throughput strategy to screen immunoglobulin G (IgG)–containing culture supernatants from ~30,000 activated memory B cells from a clade A–infected donor for binding to monomeric recombinant envelope glycoproteins gp120 (HIV-1 primary isolate JR-CSF) and gp41 (HIV-1 strain HxB2) (trimeric gp120 and gp41 complexes, referred to as Env, mediate viral entry) and neutralization activity against HIV-1 primary isolates JR-CSF and SF162 (table S1) (*15*). The memory B cells were cultured at near clonal density, which enabled us to reconstitute the authentic antibody heavy and light chain pair from each culture well.

[1]Department of Immunology and Microbial Science, and IAVI Neutralizing Antibody Center, The Scripps Research Institute, La Jolla, CA 92037, USA. [2]AIDS Vaccine Design and Development Laboratory, International AIDS Vaccine Initiative, New York, NY 11220, USA. [3]Theraclone Sciences, Seattle, WA 98104, USA. [4]Monogram Biosciences, Inc., South San Francisco, CA 94080, USA. [5]International AIDS Vaccine Initiative, New York, NY 10038, USA. [6]Ragon Institute of Massachusetts General Hospital, Massachusetts Institute of Technology, and Harvard, Boston, MA 02114, USA.

*These authors contributed equally to this work.
†Protocol G Principal Investigators are listed at the end of the manuscript.
‡To whom correspondence should be addressed. E-mail: burton@scripps.edu (D.R.B.); SPhogat@iavi.org (S.K.P.)

A

Clade	No. of viruses	Median IC_{50} (μg/ml) against viruses neutralized with an IC_{50} <50 μg/ml						
		b12	2G12	2F5	4E10	PG9	PG16	PGC14
A	27	6.98	17.10	5.70	6.20	0.16	0.11	41.59
B	31	0.80	0.82	2.41	5.22	0.43	0.70	21.88
C	27	6.46	2.93	31.51	2.97	0.22	0.25	11.97
D	25	1.47	7.71	3.17	4.60	0.10	0.02	38.57
CRF01_AE	10	21.53	>50	0.26	0.51	0.08	0.03	>50
CRF_AG	10	10.40	0.95	0.64	1.42	0.80	0.03	45.10
G	15	3.07	31.03	1.24	1.44	0.29	1.21	>50
F	15	>50	9.23	1.78	2.30	0.09	0.08	25.71
Total	162	2.82	2.43	2.30	3.24	0.22	0.15	25.99

B

Clade	No. of viruses	Percent viruses neutralized						
		b12	2G12	2F5	4E10	PG9	PG16	PGC14
		With an IC_{50} <50 μg/ml						
A	27	30	37	74	96	85	85	11
B	31	58	71	68	97	74	74	29
C	27	33	11	7	96	78	78	19
D	25	48	24	56	96	76	60	8
CRF01_AE	10	30	0	89	100	100	100	0
CRF_AG	10	30	50	80	100	80	60	10
G	15	13	20	80	100	87	73	7
F	15	0	21	87	100	67	64	13
Total	162	35	32	60	98	79	73	15
		With an IC_{50} <1.0 μg/ml						
A	27	0	4	4	0	70	63	0
B	31	32	39	23	0	45	42	3
C	27	7	0	0	11	56	48	0
D	25	12	8	12	8	48	44	0
CRF01_AE	10	11	0	88	80	70	70	0
CRF_AG	10	10	30	60	30	40	50	0
G	15	0	0	27	0	60	33	0
F	15	0	14	13	28	80	79	0
Total	162	11	12	19	12	57	51	1

Table 1. Neutralization activity of mAbs. (**A**) Neutralization potency. Boxes are color-coded as follows: white, median potency >50 μg/ml; green, median potency between 20 and 50 μg/ml; yellow, median potency between 2 and 20 μg/ml; orange, median potency between 0.2 and 2 μg/ml; red, median potency <0.2 μg/ml. CRF_07BC and CRF_08BC viruses are not included in the clade analysis, but are counted toward the total number of neutralized viruses, because there was only one virus tested from each of these clades. (**B**) Neutralization breadth. Boxes are color-coded as follows: white, no viruses neutralized; green, 1 to 30% of viruses neutralized; yellow, 31 to 60% of viruses neutralized; orange, 61 to 90% of viruses neutralized; red, 91 to 100% of viruses neutralized. CRF_07BC and CRF_08BC viruses are not included in the clade analysis, but are counted toward the total number of neutralized viruses, because there was only one virus tested from each of these clades.

Unexpectedly, 97.7% of B cell culture supernatants that neutralized HIV-$1_{JR\text{-}CSF}$ and 46.5% that neutralized HIV-$1_{SF\text{-}162}$ did not bind to monomeric $gp120_{JR\text{-}CSF}$ or $gp41_{HxB2}$, and only 2% of cultures with neutralization activity could neutralize both viruses (fig. S1). Antibody genes were obtained from five B cell cultures that exhibited differing functional profiles; one bound to gp120 and only neutralized HIV-1_{SF162} (PGC14); two bound to gp120 and weakly neutralized both viruses (PGG14 and PG20); and two potently neutralized HIV-$1_{JR\text{-}CSF}$, failed to neutralize HIV-1_{SF162}, and did not bind to gp120 or gp41 in an enzyme-linked immunosorbent assay (ELISA) (PG9 and PG16) (*15*). Analysis of the antibody variable genes revealed two pairs of somatic variants, one of which contained long, heavy-chain complementarity-determining region 3 (CDRH3) loops (PG9 and PG16) (table S2). Long CDRH3 loops have been previously associated with polyreactivity (the ability to bind to a variety of structurally dissimilar antigens with moderate affinity) (*16*); thus, we tested PG9 and PG16 for reactivity against a panel of antigens and confirmed that the antibodies were not polyreactive (fig. S2) (*15*).

All five antibodies were first tested for neutralization activity against a multiclade 16-pseudovirus panel (table S3) (*15*). Two of the antibodies that bound to gp120 in the initial screen (PGG14 and PG20) did not show substantial neutralization breadth or potency against any of the viruses tested, and the third antibody that bound to gp120 (PGC14) neutralized 4 out of 16 viruses with varying degrees of potency. In contrast, the two antibodies that failed to bind recombinant gp120 or gp41 and did not neutralize HIV-1_{SF162} in the initial screen (PG9 and PG16) neutralized a large proportion of the viruses at concentrations less than 1 μg/ml. The observation that 93.3% of B cell cultures that neutralized HIV-$1_{JR\text{-}CSF}$ did not bind to gp120 or gp41 or neutralize HIV-1_{SF162} suggests that this donor's NAb response against HIV-$1_{JR\text{-}CSF}$ might be mediated by antibodies of the PG9 and PG16 type. We next evaluated PG9, PG16, and PGC14 on a large multiclade pseudovirus panel

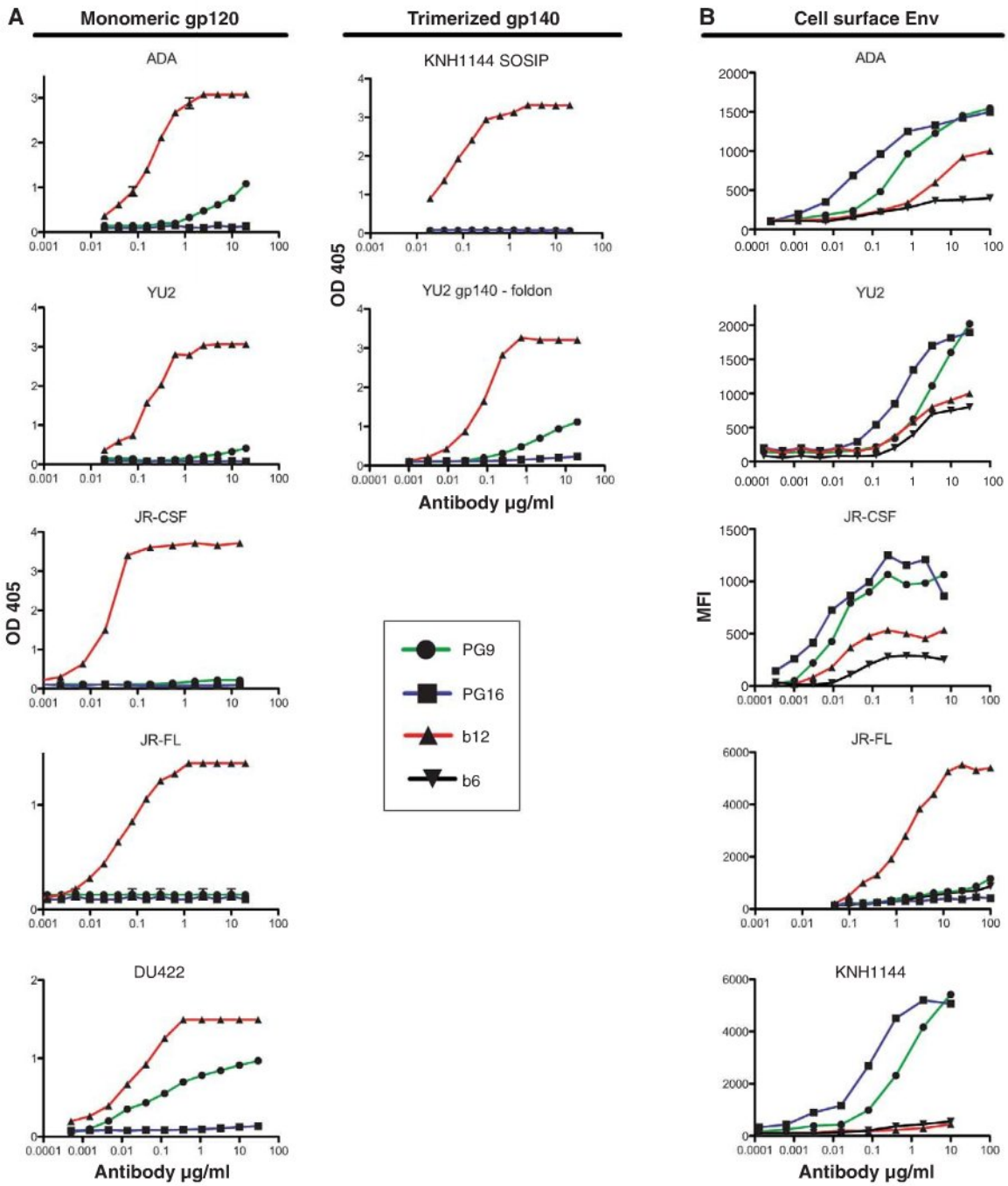

Fig. 1. Antigen-binding properties of PG9 and PG16. (**A**) Binding of PG9 and PG16 to monomeric gp120 and artificially trimerized gp140 constructs as determined by ELISA. Antigens were coated directly onto ELISA wells in the experiments shown, but similar results were also obtained when antigens were captured onto wells with antibodies against noncompetitive epitopes. OD, optical density (absorbance at 450 nm). (**B**) Binding of PG9 and PG16 to Env expressed on the surface of 293T cells as determined by flow cytometry. The bNAb b12 was used as a control for ELISA assays; b12, which binds with similar affinity to both cleaved and uncleaved forms of Env, and the nonneutralizing antibody b6, which only binds to uncleaved Env, are included in the cell surface–binding assays to show the expected percentages of cleaved and uncleaved Env expressed on the cell surface (*19*). Experiments were performed in duplicate, and data are representative of at least three independent experiments. MFI, mean fluorescence intensity.

consisting of 162 viruses, to further assess the neutralization breadth and potency of these three antibodies (Table 1, and tables S4 and S5). The bNAbs b12, 2G12, 2F5, and 4E10, and the donor's serum, were also included in the panel for comparison. Overall, PG9 and PG16 demonstrated a remarkable combination of neutralization breadth and potency. PG9 neutralized 127 out of 162 and PG16 119 out of 162 viruses with a potency that frequently considerably exceeded that noted for the four control bNAbs. The antibody concentration required to inhibit HIV activity by 50% or 90%, respectively (IC_{50} and IC_{90} values), for neutralized viruses across all clades were an order of magnitude lower for PG9 and PG16 than for any of the four existing bNAbs (Table 1A, and tables S4 and S5), and both mAbs showed an overall greater breadth of neutralization than b12, 2G12, and 2F5 (Table 1B, and tables S4 and S5). At low antibody concentrations, PG9 and PG16 also demonstrated greater neutralization breadth than 4E10 (Table 1B). Furthermore, both mAbs potently neutralized one virus (IAVI-C18) that exhibits resistance to all four existing bNAbs (table S4). Inspection of the mAb neutralization curves revealed that, whereas the PG9 neutralization curves usually exhibited sharp slopes, the neutralization curves for PG16 sometimes exhibited gradual slopes or plateaued at less than 100% neutralization (fig. S3 and table S3). Although neutralization curves with similar profiles have been reported previously (*17*, *18*), the mechanism for this is not well understood. Comparison of the neutralization profile of the serum with the neutralization profile of PG9, PG16, and PGC14 revealed that these three antibodies could recapitulate the breadth of the serum neutralization in most cases (table S4). For example, almost all of the viruses that were neutralized by the serum with an IC_{50} > 1:500 were neutralized by PG9 and/or PG16 at <0.05 μg/ml. The one case where this did not occur was against HIV-1_{SF162}, but this virus was potently neutralized by PGC14. Although PG9 and PG16 are somatic variants, they exhibited different degrees of potency against a number of the viruses tested. For instance, PG9 neutralized HIV-$1_{6535.30}$ ~185 times as potently as PG16, and PG16 neutralized HIV-$1_{MGRM\text{-}AG\text{-}001}$ ~440 times as potently as PG9. In some cases, the two antibodies also differed in neutralization breadth; PG9 neutralized nine viruses that were not sensitive to PG16, and PG16 neutralized two viruses that were not sensitive to PG9. On the basis of these results, it appears that this donor's broad serum neutralization might be mediated by somatic antibody variants that recognize slightly different epitopes and display varying degrees of neutralization breadth and

Table 2. Alanine mutations that decrease PG9 or PG16 neutralization activity. Amino acid numbering is based on the sequence of HIV-1_{HxB2}. Boxes are color coded as follows: white, the amino acid is identical among 0 to 49% of all HIV-1 isolates; light blue, the amino acid is identical among 50 to 90% of isolates; dark blue, the amino acid is identical among 90 to 100% of isolates. Amino acid identity was determined based on a sequence alignment of HIV-1 isolates listed in the HIV sequence database at http://hiv-web.lanl.gov/content/hiv-db/mainpage.html. In descriptions of the gp120 domains, C refers to constant domains and V refers to variable loops. Neutralization activity is reported as fold increase in IC_{50} value relative to WT JR-CSF and was calculated using the equation [(IC_{50} mutant)/(IC_{50} WT)]. Boxes are color coded as follows: green, substitutions that had a negligible effect on neutralization activity; yellow, 4- to 9-fold IC_{50} increase; orange, 10- to 100-fold IC_{50} increase; red, >100-fold IC_{50} increase. Experiments were performed in triplicate, and values represent an average of at least three independent experiments.

Mutation	Gp120 domain	Fold IC_{50} increase relative to wild-type	
		PG9	PG16
V127A	C1 (V1/V2 stem)	30	57
N134A	V1	5	23
N156A	C1 (V1/V2 stem)	280	1500
S158A	C1 (V1/V2 stem)	>2000	>2000
F159A	C1 (V1/V2 stem)	>2000	>2500
N160K	V2	>2000	>2500
T162A	V2	>2000	>2500
D167A	V2	5	30
Y173A	V2	1400	1000
F176A	V2	>5000	>7000
V181A	V2	200	250
P299A	V3 (base)	200	1400
K305A	V3 (stem)	50	2800
I307A	V3 (tip)	10	3000
I309A	V3 (tip)	9	150
F317A	V3 (tip)	3	1400
Y318A	V3 (tip)	2	1000
N392A	V4	7	23
I420A	C4	9	11
I423A	C4	40	14
I424A	C4	10	9

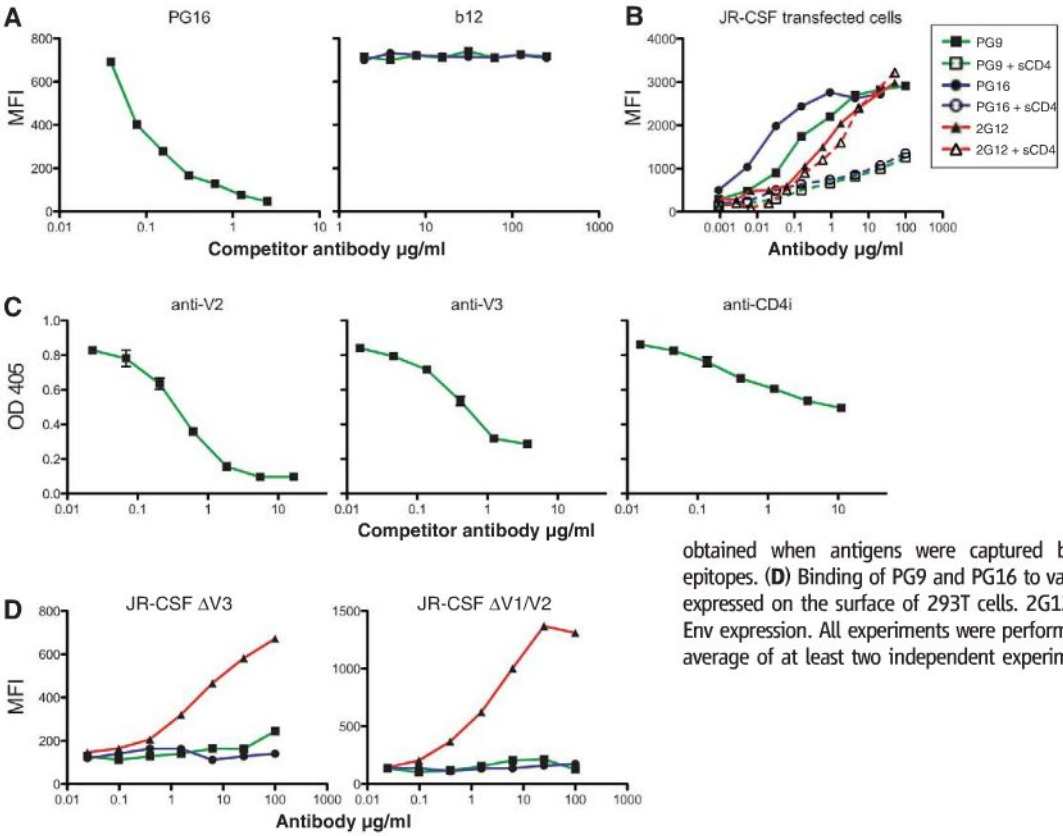

Fig. 2. Mapping the PG9 and PG16 epitopes. (**A**) Competition of PG9 and PG16 with each other and with the CD4–binding site (CD4bs) antibody b12 for cell surface Env binding. The competitor antibody is indicated at the top of each graph. MFI, mean fluorescence intensity. (**B**) Effect of soluble CD4 (sCD4) on the binding of PG9 and PG16 to cell surface Env. 2G12 is included to control for CD4-induced shedding of gp120. (**C**) Competition of PG9 with antibodies against the V2 loop (10/76b), V3 loop (F425/b4e8), and the CD4i site (X5) for gp120 binding. Antigens were coated directly onto ELISA wells in the experiments shown, but similar results were also obtained when antigens were captured by antibodies against noncompetitive epitopes. (**D**) Binding of PG9 and PG16 to variable loop–deleted HIV-$1_{JR\text{-}CSF}$ variants expressed on the surface of 293T cells. 2G12 is included to control for cell surface Env expression. All experiments were performed in duplicate, and data represent an average of at least two independent experiments.

potency against any given virus. Selection for these types of antibodies may reflect the immune system's response to an ever-evolving viral envelope target.

The inability of PG9 and PG16 to bind monomeric $gp120_{JR\text{-}CSF}$ or $gp41_{HxB2}$ in the initial screen while potently neutralizing HIV-$1_{JR\text{-}CSF}$ suggested that the epitope targeted by these antibodies might be preferentially expressed on trimeric HIV Env. This possibility was investigated by comparing the ability of PG9 and PG16 to bind monomeric gp120 from several different strains, artificially trimerized gp140 constructs, and trimeric Env expressed on the surface of transfected cells (*15*). Although both antibodies bound with high affinity to cell surface Env, PG16 did not bind to any of the soluble gp120 or gp140 constructs, and PG9 bound only weakly to monomeric gp120 and trimerized gp140 from certain strains (Fig. 1). We hypothesized that PG9 and PG16 do not exhibit exclusive specificity for cleaved HIV-1 trimers because it has been previously shown that a substantial fraction of cell surface Env is composed of uncleaved gp160 molecules (*19*). Indeed, this was confirmed by the fact that both antibodies bound with high affinity to cleavage-defective HIV-1_{YU2} trimers expressed on the surface of transfected cells (fig. S4) (*15*). These results suggest that there are significant structural differences between soluble, recombinant gp140 and uncleaved gp160 expressed on the surface of transfected cells.

We next sought to define the PG9 and PG16 epitopes. We suspected that they would recognize the same or overlapping epitopes because the two antibodies are somatic variants. Indeed, both antibodies competed for binding to HIV-$1_{JR\text{-}CSF}$–transfected cells (Fig. 2A) (*15*). Soluble CD4, a soluble version of the receptor for Env, diminished binding of both PG9 and PG16 to cell surface Env, although neither antibody competed with the CD4–binding site antibody b12 for trimer binding (Fig. 2, A and B). This result suggests that conformational changes induced by CD4 binding cause a loss of the epitope targeted by the antibodies. Competition ELISAs revealed that PG9 competed for gp120 binding with antibodies against the V2 and V3 variable loops of gp120, and to a lesser extent, with CD4-induced (CD4i) antibodies (which recognize an epitope on gp120 dependent on CD4 binding) (Fig. 2C and fig. S5) (*15*). Neither PG9 nor PG16 bound to HIV-$1_{JR\text{-}CSF}$ variants with deleted V1 and V2, or V3, variable loops expressed on the surface of transfected cells, which further suggested that the variable loops are critical components of the epitopes (Fig. 2D). To dissect the fine specificity of PG9 and PG16, we performed alanine scanning using a large panel of HIV-$1_{JR\text{-}CSF}$ Env alanine mutants that have been described previously (*20*–*23*), as well as several new alanine mutants. We generated pseudoviruses incorporating single Env alanine mutations, and PG9 and PG16 were tested for neutralization activity against each mutant pseudovirus (*15*). Mutations that resulted in viral escape from PG9 and PG16 neutralization were considered important for formation of the PG9 and PG16 epitopes (Table 2 and table S6). On the basis of these data, and consistent with the competition experiments, residues that form the epitopes recognized by PG9 and PG16 are primarily located in conserved regions of the V2 and V3 loops of gp120 (Table 2 and fig. S6). Certain co-receptor binding site mutations also had an effect on PG9 and PG16 neutralization, albeit to a lesser extent (table S6). PG9 and PG16 were largely dependent on the same residues, although PG16 was more sensitive to V3 loop substitutions than PG9. Although neither antibody bound to wild-type HIV-$1_{JR\text{-}FL}$–transfected cells, a glutamic acid to lysine (E to K) mutation at position 168 in the V2 loop of HIV-$1_{JR\text{-}FL}$ generated high-affinity PG9 and PG16 recognition (fig. S7). Asparagines N156 and N160, sites of V2 N-glycosylation, were critical in forming the PG9 and PG16 epitopes because substitutions at these positions resulted in escape from antibody neutralization (Table 2 and fig. S8). HIV-1_{SF162} contains a rare N to K polymorphism at position 160 (which is nonpermissive for N-glycosylation), and mutation of this residue to an N renders this isolate sensitive to PG9 and PG16 (fig. S9). Deglycosylation of monomeric gp120 abolished binding of PG9 (fig. S8), which confirmed that glycans are important, directly or indirectly, in forming the epitope (*15*).

The preferential binding of PG9 and PG16 to native trimers could either be because their epitopes span more than one gp120 subunit or because the antibodies recognize a single subunit in a conformation that is stabilized on the trimer. To address this question, we studied the binding profiles of PG9 and PG16 to mixed HIV-1_{YU2} trimers, in which two gp120 subunits contained point mutations to abolish binding of the two antibodies (*15*). A third substitution that abrogates binding of 2G12, which binds with high affinity to both monomeric gp120 and trimeric Env, was also introduced into the same construct as an internal control. Cell surface–binding analysis revealed that all three antibodies bound to the mixed trimers with similar apparent affinity compared with wild-type trimers, and all binding was saturated at a similar lower level (fig. S10). This result suggests that the preference of PG9 and PG16 for trimeric Env is due to gp120 subunit presentation in the context of the trimeric spike rather than gp120 cross-linking.

Others have shown that NAbs that bind to epitopes encompassing parts of the V2 or both the V2 and V3 domains can exhibit potency comparable to that of PG9 and PG16, although these antibodies have thus far displayed strong strain-specificity (*17*, *24*). The epitopes recognized by these antibodies have been shown to differ from that of the clade B consensus sequence only by single–amino acid substitutions, which suggested the existence of a relatively conserved structure within the V2 domain (*17*, *18*). Here, we have confirmed that this region serves as a potent neutralization target and demonstrated that antibodies that recognize conserved parts of V2 and V3 can have broad reactivity.

Given that this is the first attempt at direct functional screening of such a large number of antibodies, it seems likely that the approach will generate further bNAbs, in particular those that bind poorly to recombinant forms of Env. The neutralization breadth exhibited by PG9 and PG16, particularly against non–clade B isolates, suggests that vaccine-induced antibodies of similar specificity might provide protection against a diverse range of the most prevalent HIV-1 isolates circulating worldwide. Furthermore, the exceptional neutralization potency exhibited by these antibodies in vitro suggests that antibodies of this specificity might provide protection at relatively modest serum concentrations achievable by vaccination. Immunogens designed to focus the immune response on conserved regions of variable loops in the context of the trimeric spike will determine whether these types of antibodies can be readily elicited by a vaccine.

References and Notes

1. M. I. Johnston, A. S. Fauci, *N. Engl. J. Med.* **356**, 2073 (2007).
2. D. H. Barouch, *Nature* **455**, 613 (2008).
3. B. D. Walker, D. R. Burton, *Science* **320**, 760 (2008).
4. R. S. Veazey *et al.*, *Nat. Med.* **9**, 343 (2003).
5. A. J. Hessell *et al.*, *PLoS Pathog.* **5**, e1000433 (2009).
6. P. W. Parren *et al.*, *J. Virol.* **75**, 8340 (2001).
7. J. R. Mascola, *Vaccine* **20**, 1922 (2002).
8. J. R. Mascola *et al.*, *Nat. Med.* **6**, 207 (2000).
9. J. R. Mascola *et al.*, *J. Virol.* **73**, 4009 (1999).
10. S. Phogat, R. Wyatt, *Curr. Pharm. Des.* **13**, 213 (2007).
11. M. Montero, N. E. van Houten, X. Wang, J. K. Scott, *Microbiol. Mol. Biol. Rev.* **72**, 54 (2008).
12. C. N. Scanlan, J. Offer, N. Zitzmann, R. A. Dwek, *Nature* **446**, 1038 (2007).
13. M. D. Simek *et al.*, *J. Virol.* **83**, 7337 (2009).
14. L. Stamatatos, L. Morris, D. R. Burton, J. R. Mascola, *Nat. Med.* **15**, 866 (2009).
15. Materials and methods are available as supporting material on *Science* Online.
16. Y. Ichiyoshi, P. Casali, *J. Exp. Med.* **180**, 885 (1994).
17. W. J. Honnen *et al.*, *J. Virol.* **81**, 1424 (2007).
18. A. Pinter *et al.*, *J. Virol.* **79**, 6909 (2005).
19. M. Pancera, R. Wyatt, *Virology* **332**, 145 (2005).
20. R. Pantophlet *et al.*, *J. Virol.* **77**, 642 (2003).
21. R. Pantophlet, M. Wang, R. O. Aguilar-Sino, D. R. Burton, *J. Virol.* **83**, 1649 (2009).
22. R. Darbha *et al.*, *Biochemistry* **43**, 1410 (2004).
23. C. N. Scanlan *et al.*, *J. Virol.* **76**, 7306 (2002).
24. M. K. Gorny *et al.*, *J. Virol.* **79**, 5232 (2005).

25. We thank R. Aguilar-Sino for technical assistance at The Scripps Research Institute; C. Ward, W. Cieplak, and M. Branum for technical assistance at Theraclone Sciences; R. Pejchal for assistance in structural modeling; S. M. Eagol and C. Williams for assistance with figures; E. Anton from Monogram R&D and the Monogram Clinical Reference Laboratory staff; all the study participants and research staff at each of the Protocol G clinical centers; and Protocol G project team members for all of the support that they have provided for this study (individuals and affiliations are listed in the supporting online material text as notes). We also thank A. Pinter for supplying the antibodies 10/76b and c108 g, W. Olson and J. Moore for providing the KNH1144 SOSIP trimer, and R. Wyatt for providing the $YU2_{gp140}$-foldon trimer. This work was supported by the International AIDS Vaccine Initiative (IAVI) through the contributions of a number of government and private donors who are listed on the Web site www.iavi.org, as well as IAVI's Innovation Fund (which is cofunded by the

Bill & Melinda Gates Foundation); the U.S. Agency for International Development (USAID); and the National Institute of Allergy and Infectious Diseases, NIH, AI33292 (D.R.B.). The contents are the responsibility of the authors and do not necessarily reflect the views of USAID or the U.S. government. The authors declare competing financial interests. Protocol G Principal Investigators: G. Miiro, J. Serwanga, A. Pozniak, D. McPhee, O. Manigart, L. Mwananyanda, E. Karita, A. Inwoley, W. Jaoko, J. DeHovitz, L. G. Bekker, P. Pitisuttithum, R. Paris, and S. Allen.

Supporting Online Material

www.sciencemag.org/cgi/content/full/1178746/DC1
Materials and Methods
SOM Text
Figs. S1 to S10
Tables S1 to S6
References

7 July 2009; accepted 26 August 2009
Published online 3 September 2009;
10.1126/science.1178746
Include this information when citing this paper.

Comprehensive Mapping of Long-Range Interactions Reveals Folding Principles of the Human Genome

Erez Lieberman-Aiden,[1,2,3,4]* Nynke L. van Berkum,[5]* Louise Williams,[1] Maxim Imakaev,[2] Tobias Ragoczy,[6,7] Agnes Telling,[6,7] Ido Amit,[1] Bryan R. Lajoie,[5] Peter J. Sabo,[8] Michael O. Dorschner,[8] Richard Sandstrom,[8] Bradley Bernstein,[1,9] M. A. Bender,[10] Mark Groudine,[6,7] Andreas Gnirke,[1] John Stamatoyannopoulos,[8] Leonid A. Mirny,[2,11] Eric S. Lander,[1,12,13]† Job Dekker[5]†

We describe Hi-C, a method that probes the three-dimensional architecture of whole genomes by coupling proximity-based ligation with massively parallel sequencing. We constructed spatial proximity maps of the human genome with Hi-C at a resolution of 1 megabase. These maps confirm the presence of chromosome territories and the spatial proximity of small, gene-rich chromosomes. We identified an additional level of genome organization that is characterized by the spatial segregation of open and closed chromatin to form two genome-wide compartments. At the megabase scale, the chromatin conformation is consistent with a fractal globule, a knot-free, polymer conformation that enables maximally dense packing while preserving the ability to easily fold and unfold any genomic locus. The fractal globule is distinct from the more commonly used globular equilibrium model. Our results demonstrate the power of Hi-C to map the dynamic conformations of whole genomes.

The three-dimensional (3D) conformation of chromosomes is involved in compartmentalizing the nucleus and bringing widely separated functional elements into close spatial proximity (*1*–*5*). Understanding how chromosomes fold can provide insight into the complex relationships between chromatin structure, gene activity, and the functional state of the cell. Yet beyond the scale of nucleosomes, little is known about chromatin organization.

[1]Broad Institute of Harvard and Massachusetts Institute of Technology (MIT), MA 02139, USA. [2]Division of Health Sciences and Technology, MIT, Cambridge, MA 02139, USA. [3]Program for Evolutionary Dynamics, Department of Organismic and Evolutionary Biology, Department of Mathematics, Harvard University, Cambridge, MA 02138, USA. [4]Department of Applied Mathematics, Harvard University, Cambridge, MA 02138, USA. [5]Program in Gene Function and Expression and Department of Biochemistry and Molecular Pharmacology, University of Massachusetts Medical School, Worcester, MA 01605, USA. [6]Fred Hutchinson Cancer Research Center, Seattle, WA 98109, USA. [7]Department of Radiation Oncology, University of Washington School of Medicine, Seattle, WA 98195, USA. [8]Department of Genome Sciences, University of Washington, Seattle, WA 98195, USA. [9]Department of Pathology, Harvard Medical School, Boston, MA 02115, USA. [10]Department of Pediatrics, University of Washington, Seattle, WA 98195, USA. [11]Department of Physics, MIT, Cambridge, MA 02139, USA. [12]Department of Biology, MIT, Cambridge, MA 02139, USA. [13]Department of Systems Biology, Harvard Medical School, Boston, MA 02115, USA.

*These authors contributed equally to this work.
†To whom correspondence should be addressed. E-mail: lander@broadinstitute.org (E.S.L.); job.dekker@umassmed.edu (J.D.)

Long-range interactions between specific pairs of loci can be evaluated with chromosome conformation capture (3C), using spatially constrained ligation followed by locus-specific polymerase chain reaction (PCR) (*6*). Adaptations of 3C have extended the process with the use of inverse PCR (4C) (*7*, *8*) or multiplexed ligation-mediated amplification (5C) (*9*). Still, these techniques require choosing a set of target loci and do not allow unbiased genomewide analysis.

Here, we report a method called Hi-C that adapts the above approach to enable purification of ligation products followed by massively parallel sequencing. Hi-C allows unbiased identification of chromatin interactions across an entire genome.We briefly summarize the process: cells are crosslinked with formaldehyde; DNA is digested with a restriction enzyme that leaves a 5′ overhang; the 5′ overhang is filled, including a biotinylated residue; and the resulting blunt-end fragments are ligated under dilute conditions that favor ligation events between the cross-linked DNA fragments. The resulting DNA sample contains ligation products consisting of fragments that were originally in close spatial proximity in the nucleus, marked with biotin at the junction. A Hi-C library is created by shearing the DNA and selecting the biotin-containing fragments with streptavidin beads. The library is then analyzed by using massively parallel DNA sequencing, producing a catalog of interacting fragments (Fig. 1A) (*10*).

We created a Hi-C library from a karyotypically normal human lymphoblastoid cell line (GM06990) and sequenced it on two lanes of an Illumina Genome Analyzer (Illumina, San Diego, CA), generating 8.4 million read pairs that could be uniquely aligned to the human genome reference sequence; of these, 6.7 million corresponded to long-range contacts between segments >20 kb apart.

We constructed a genome-wide contact matrix M by dividing the genome into 1-Mb regions ("loci") and defining the matrix entry m_{ij} to be the number of ligation products between locus i and locus j (*10*). This matrix reflects an ensemble average of the interactions present in the original sample of cells; it can be visually represented as a heatmap, with intensity indicating contact frequency (Fig. 1B).

We tested whether Hi-C results were reproducible by repeating the experiment with the same restriction enzyme (HindIII) and with a different one (NcoI). We observed that contact matrices for these new libraries (Fig. 1, C and D) were extremely similar to the original contact matrix [Pearson's $r = 0.990$ (HindIII) and $r = 0.814$ (NcoI); P was negligible ($<10^{-300}$) in both cases]. We therefore combined the three data sets in subsequent analyses.

We first tested whether our data are consistent with known features of genome organization (*1*): specifically, chromosome territories (the tendency of distant loci on the same chromosome to be near one another in space) and patterns in subnuclear positioning (the tendency of certain chromosome pairs to be near one another).

We calculated the average intrachromosomal contact probability, $I_n(s)$, for pairs of loci separated by a genomic distance s (distance in base pairs along the nucleotide sequence) on chromosome n. $I_n(s)$ decreases monotonically on every chromosome, suggesting polymer-like behavior in which the 3D distance between loci increases with increasing genomic distance; these findings are in agreement with 3C and fluorescence in situ hybridization (FISH) (*6*, *11*). Even at distances greater than 200 Mb, $I_n(s)$ is always much greater than the average contact probability between different chromosomes (Fig. 2A). This implies the existence of chromosome territories.

Interchromosomal contact probabilities between pairs of chromosomes (Fig. 2B) show that small, gene-rich chromosomes (chromosomes 16, 17, 19, 20, 21, and 22) preferentially interact with each other. This is consistent with FISH studies showing that these chromosomes frequently colocalize in the center of the nucleus

(*12*, *13*). Interestingly, chromosome 18, which is small but gene-poor, does not interact frequently with the other small chromosomes; this agrees with FISH studies showing that chromosome 18 tends to be located near the nuclear periphery (*14*).

We then zoomed in on individual chromosomes to explore whether there are chromosomal regions that preferentially associate with each other. Because sequence proximity strongly influences contact probability, we defined a normalized contact matrix M^* by dividing each entry in the contact matrix by the genome-wide average contact probability for loci at that genomic distance (*10*). The normalized matrix shows many large blocks of enriched and depleted interactions, generating a plaid pattern (Fig. 3B). If two loci (here 1-Mb regions) are nearby in space, we reasoned that they will share neighbors and have correlated interaction profiles. We therefore defined a correlation matrix C in which c_{ij} is the Pearson correlation between the ith row and jth column of M^*. This process dramatically sharpened the plaid pattern (Fig. 3C); 71% of the resulting matrix entries represent statistically significant correlations ($P \leq 0.05$).

The plaid pattern suggests that each chromosome can be decomposed into two sets of loci (arbitrarily labeled A and B) such that contacts within each set are enriched and contacts between sets are depleted. We partitioned each chromosome

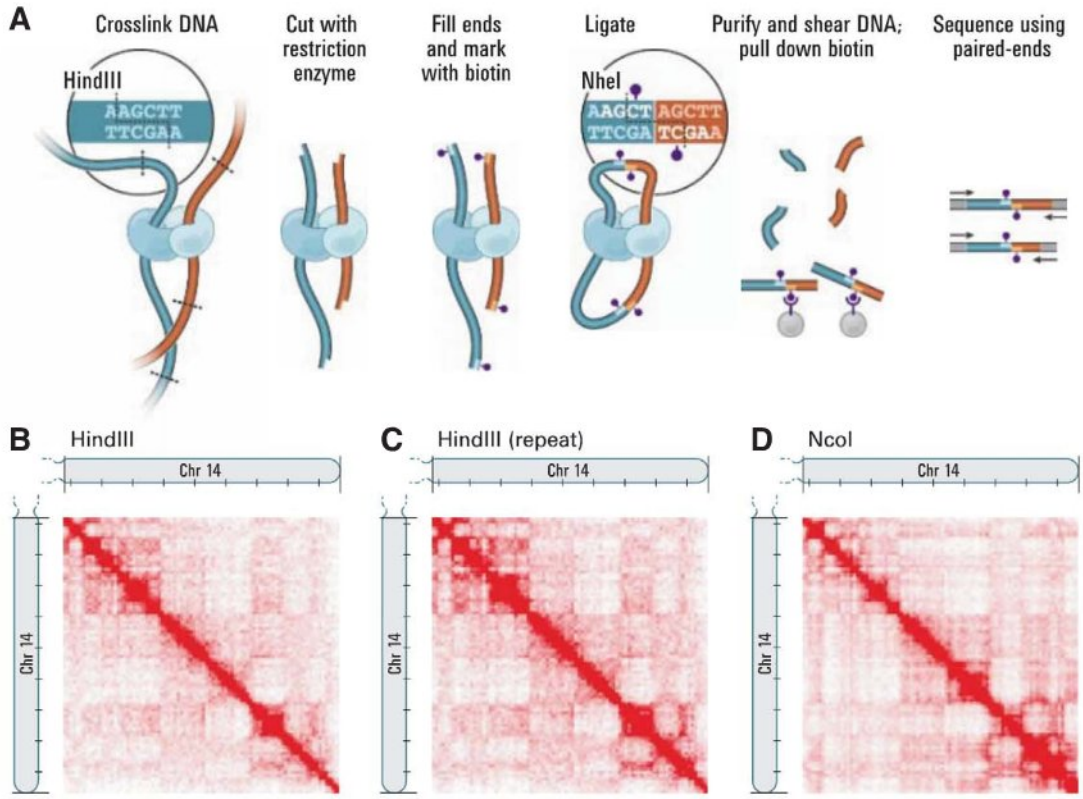

Fig. 1. Overview of Hi-C. (**A**) Cells are cross-linked with formaldehyde, resulting in covalent links between spatially adjacent chromatin segments (DNA fragments shown in dark blue, red; proteins, which can mediate such interactions, are shown in light blue and cyan). Chromatin is digested with a restriction enzyme (here, HindIII; restriction site marked by dashed line; see inset), and the resulting sticky ends are filled in with nucleotides, one of which is biotinylated (purple dot). Ligation is performed under extremely dilute conditions to create chimeric molecules; the HindIII site is lost and an NheI site is created (inset). DNA is purified and sheared. Biotinylated junctions are isolated with streptavidin beads and identified by paired-end sequencing. (**B**) Hi-C produces a genome-wide contact matrix. The submatrix shown here corresponds to intrachromosomal interactions on chromosome 14. (Chromosome 14 is acrocentric; the short arm is not shown.) Each pixel represents all interactions between a 1-Mb locus and another 1-Mb locus; intensity corresponds to the total number of reads (0 to 50). Tick marks appear every 10 Mb. (**C** and **D**) We compared the original experiment with results from a biological repeat using the same restriction enzyme [(C), range from 0 to 50 reads] and with results using a different restriction enzyme [(D), NcoI, range from 0 to 100 reads].

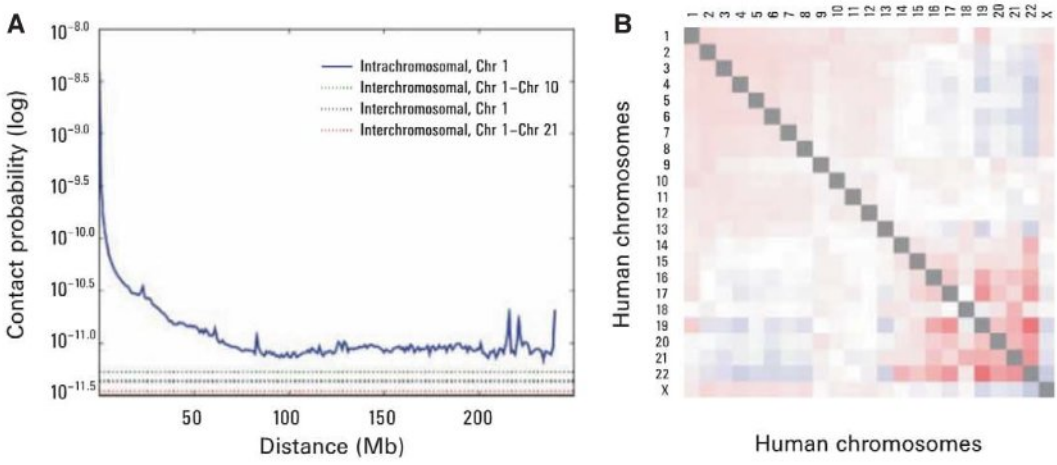

Fig. 2. The presence and organization of chromosome territories. (**A**) Probability of contact decreases as a function of genomic distance on chromosome 1, eventually reaching a plateau at ~90 Mb (blue). The level of interchromosomal contact (black dashes) differs for different pairs of chromosomes; loci on chromosome 1 are most likely to interact with loci on chromosome 10 (green dashes) and least likely to interact with loci on chromosome 21 (red dashes). Interchromosomal interactions are depleted relative to intrachromosomal interactions. (**B**) Observed/expected number of interchromosomal contacts between all pairs of chromosomes. Red indicates enrichment, and blue indicates depletion (range from 0.5 to 2). Small, gene-rich chromosomes tend to interact more with one another, suggesting that they cluster together in the nucleus.

in this way by using principal component analysis. For all but two chromosomes, the first principal component (PC) clearly corresponded to the plaid pattern (positive values defining one set, negative values the other) (fig. S1). For chromosomes 4 and 5, the first PC corresponded to the two chromosome arms, but the second PC corresponded to the plaid pattern. The entries of the PC vector reflected the sharp transitions from compartment to compartment observed within the plaid heatmaps. Moreover, the plaid patterns within each chromosome were consistent across chromosomes: the labels (A and B) could be assigned on each chromosome so that sets on different chromosomes carrying the same label had correlated contact profiles, and those carrying different labels had anticorrelated contact profiles (Fig. 3D). These results imply that the entire genome can be partitioned into two spatial compartments such that greater interaction occurs within each compartment rather than across compartments.

The Hi-C data imply that regions tend be closer in space if they belong to the same compartment (A versus B) than if they do not. We tested this by using 3D-FISH to probe four loci (L1, L2, L3, and L4) on chromosome 14 that alternate between the two compartments (L1 and L3 in compartment A; L2 and L4 in compartment B) (Fig. 3, E and F). 3D-FISH showed that L3 tends to be closer to L1 than to L2, despite the fact that L2 lies between L1 and L3 in the linear genome sequence (Fig. 3E). Similarly, we found that L2 is closer to L4 than to L3 (Fig. 3F). Comparable results were obtained for four consecutive loci on chromosome 22 (fig. S2, A and B). Taken together, these observations confirm the spatial compartmentalization

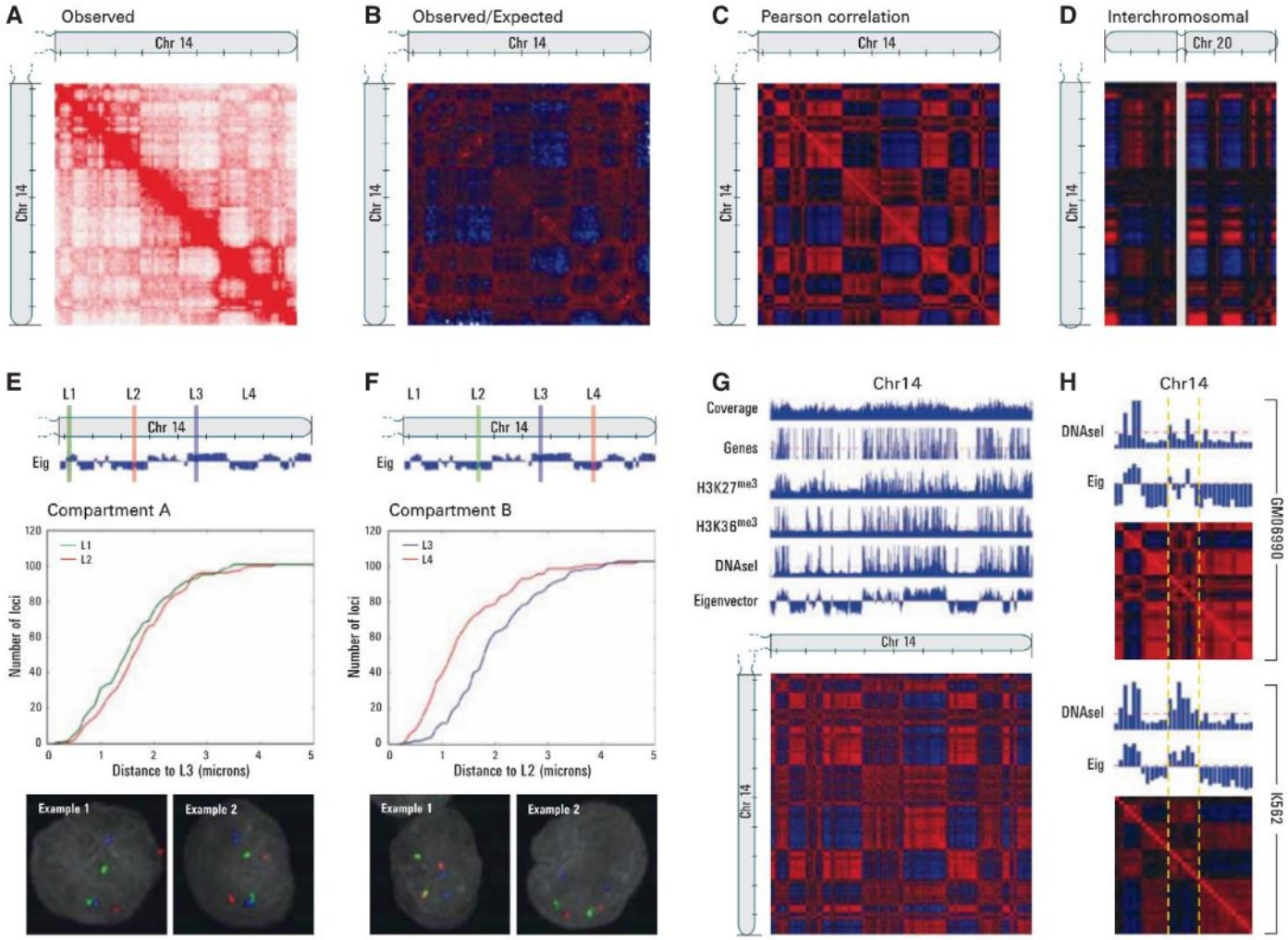

Fig. 3. The nucleus is segregated into two compartments corresponding to open and closed chromatin. (**A**) Map of chromosome 14 at a resolution of 1 Mb exhibits substructure in the form of an intense diagonal and a constellation of large blocks (three experiments combined; range from 0 to 200 reads). Tick marks appear every 10 Mb. (**B**) The observed/expected matrix shows loci with either more (red) or less (blue) interactions than would be expected, given their genomic distance (range from 0.2 to 5). (**C**) Correlation matrix illustrates the correlation [range from – (blue) to +1 (red)] between the intrachromosomal interaction profiles of every pair of 1-Mb loci along chromosome 14. The plaid pattern indicates the presence of two compartments within the chromosome. (**D**) Interchromosomal correlation map for chromosome 14 and chromosome 20 [range from –0.25 (blue) to 0.25 (red)]. The unalignable region around the centromere of chromosome 20 is indicated in gray. Each compartment on chromosome 14 has a counterpart on chromosome 20 with a very similar genome-wide interaction pattern. (**E** and **F**) We designed probes for four loci (L1, L2, L3, and L4) that lie consecutively along chromosome 14 but alternate between the two compartments [L1 and L3 in (compartment A); L2 and L4 in (compartment B)]. (E) L3 (blue) was consistently closer to L1 (green) than to L2 (red), despite the fact that L2 lies between L1 and L3 in the primary sequence of the genome. This was confirmed visually and by plotting the cumulative distribution. (F) L2 (green) was consistently closer to L4 (red) than to L3 (blue). (**G**) Correlation map of chromosome 14 at a resolution of 100 kb. The PC (eigenvector) correlates with the distribution of genes and with features of open chromatin. (**H**) A 31-Mb window from chromosome 14 is shown; the indicated region (yellow dashes) alternates between the open and the closed compartments in GM06990 (top, eigenvector and heatmap) but is predominantly open in K562 (bottom, eigenvector and heatmap). The change in compartmentalization corresponds to a shift in chromatin state (DNaseI).

of the genome inferred from Hi-C. More generally, a strong correlation was observed between the number of Hi-C reads m_{ij} and the 3D distance between locus i and locus j as measured by FISH [Spearman's $\rho = -0.916$, $P = 0.00003$ (fig. S3)], suggesting that Hi-C read count may serve as a proxy for distance.

Upon close examination of the Hi-C data, we noted that pairs of loci in compartment B showed a consistently higher interaction frequency at a given genomic distance than pairs of loci in compartment A (fig. S4). This suggests that compartment B is more densely packed (*15*). The FISH data are consistent with this observation; loci in compartment B exhibited a stronger tendency for close spatial localization.

To explore whether the two spatial compartments correspond to known features of the genome, we compared the compartments identified in our 1-Mb correlation maps with known genetic and epigenetic features. Compartment A correlates strongly with the presence of genes (Spearman's $\rho = 0.431$, $P < 10^{-137}$), higher expression [via genome-wide mRNA expression, Spearman's $\rho = 0.476$, $P < 10^{-145}$ (fig. S5)], and accessible chromatin [as measured by deoxyribonuclease I (DNAseI) sensitivity, Spearman's $\rho = 0.651$, P negligible] (*16*, *17*). Compartment A also shows enrichment for both activating (H3K36 trimethylation, Spearman's $\rho = 0.601$, $P < 10^{-296}$) and repressive (H3K27 trimethylation, Spearman's $\rho = 0.282$, $P < 10^{-56}$) chromatin marks (*18*). We repeated the above analysis at a resolution of 100 kb (Fig. 3G) and saw that, although the correlation of compartment A with all other genomic and epigenetic features remained strong (Spearman's $\rho > 0.4$, P negligible), the correlation with the sole repressive mark, H3K27 trimethylation, was dramatically attenuated (Spearman's $\rho = 0.046$, $P < 10^{-15}$). On the basis of these results we concluded that compartment A is more closely associated with open, accessible, actively transcribed chromatin.

We repeated our experiment with K562 cells, an erythroleukemia cell line with an aberrant karyotype (*19*). We again observed two compartments; these were similar in composition to those observed in GM06990 cells [Pearson's $r = 0.732$,

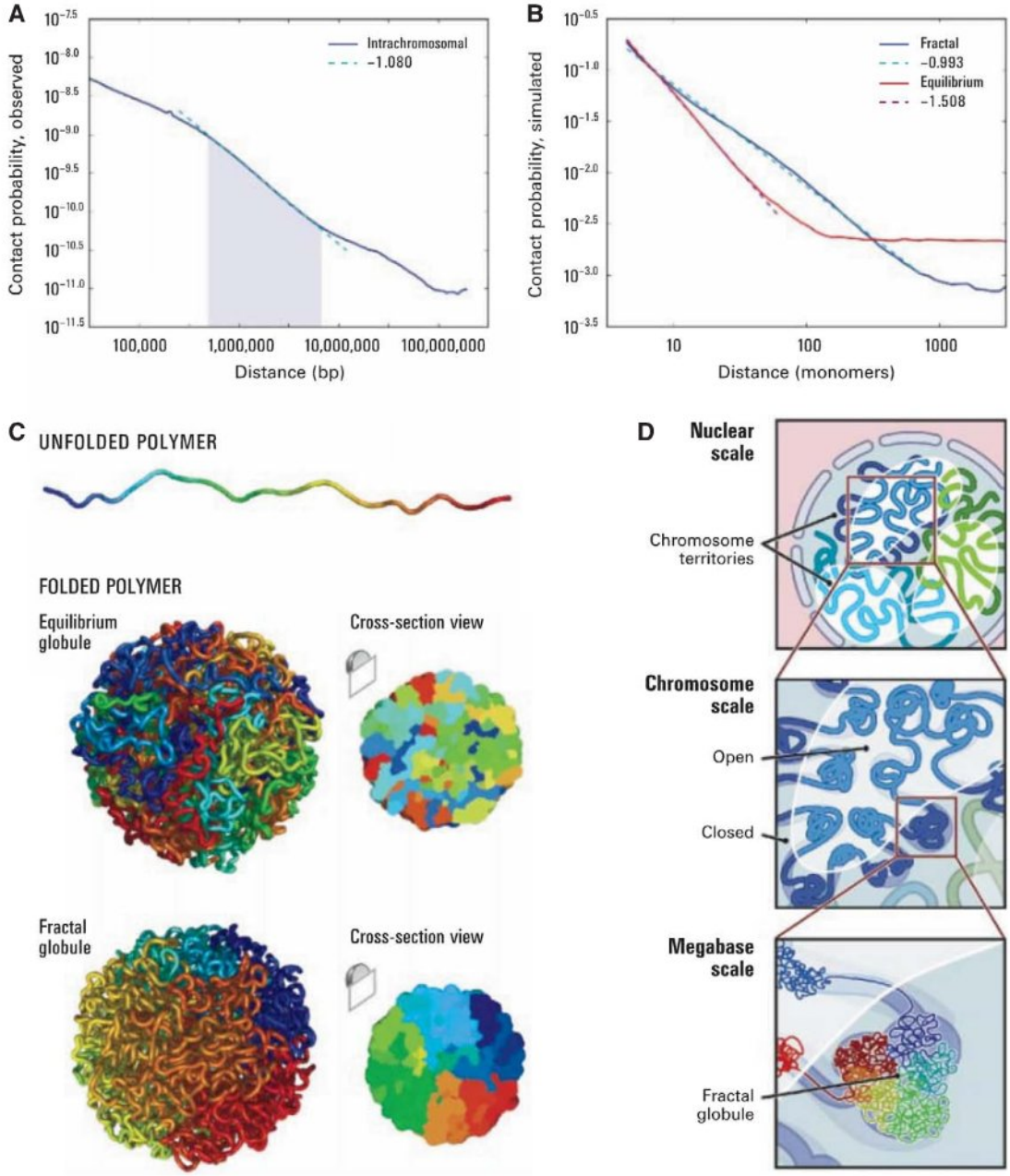

Fig. 4. The local packing of chromatin is consistent with the behavior of a fractal globule. (**A**) Contact probability as a function of genomic distance averaged across the genome (blue) shows a power law scaling between 500 kb and 7 Mb (shaded region) with a slope of −1.08 (fit shown in cyan). (**B**) Simulation results for contact probability as a function of distance (1 monomer ~ 6 nucleosomes ~ 1200 base pairs) (*10*) for equilibrium (red) and fractal (blue) globules. The slope for a fractal globule is very nearly −1 (cyan), confirming our prediction (*10*). The slope for an equilibrium globule is −3/2, matching prior theoretical expectations. The slope for the fractal globule closely resembles the slope we observed in the genome. (**C**) (Top) An unfolded polymer chain, 4000 monomers (4.8 Mb) long. Coloration corresponds to distance from one endpoint, ranging from blue to cyan, green, yellow, orange, and red. (Middle) An equilibrium globule. The structure is highly entangled; loci that are nearby along the contour (similar color) need not be nearby in 3D. (Bottom) A fractal globule. Nearby loci along the contour tend to be nearby in 3D, leading to monochromatic blocks both on the surface and in cross section. The structure lacks knots. (**D**) Genome architecture at three scales. (Top) Two compartments, corresponding to open and closed chromatin, spatially partition the genome. Chromosomes (blue, cyan, green) occupy distinct territories. (Middle) Individual chromosomes weave back and forth between the open and closed chromatin compartments. (Bottom) At the scale of single megabases, the chromosome consists of a series of fractal globules.

P negligible (fig. S6)] and showed strong correlation with open and closed chromatin states as indicated by DNaseI sensitivity (Spearman's $\rho = 0.455$, $P < 10^{-154}$).

The compartment patterns in K562 and GM06990 are similar, but there are many loci in the open compartment in one cell type and the closed compartment in the other (Fig. 3H). Examining these discordant loci on karyotypically normal chromosomes in K562 (*19*), we observed a strong correlation between the compartment pattern in a cell type and chromatin accessibility in that same cell type (GM06990, Spearman's $\rho = 0.384$, $P = 0.012$; K562, Spearman's $\rho = 0.366$, $P = 0.017$). Thus, even in a highly rearranged genome, spatial compartmentalization correlates strongly with chromatin state.

Our results demonstrate that open and closed chromatin domains throughout the genome occupy different spatial compartments in the nucleus. These findings expand on studies of individual loci that have observed particular instances of such interactions, both between distantly located active genes and between distantly located inactive genes (*8*, *20*–*24*).

Lastly, we sought to explore chromatin structure within compartments. We closely examined the average behavior of intrachromosomal contact probability as a function of genomic distance, calculating the genome-wide distribution $I(s)$. When plotted on log-log axes, $I(s)$ exhibits a prominent power law scaling between ~500 kb and ~7 Mb, where contact probability scales as s^{-1} (Fig. 4A). This range corresponds to the known size of open and closed chromatin domains.

Power-law dependencies can arise from polymer-like behavior (*25*). Various authors have proposed that chromosomal regions can be modeled as an "equilibrium globule": a compact, densely knotted configuration originally used to describe a polymer in a poor solvent at equilibrium (*26*, *27*). [Historically, this specific model has often been referred to simply as a "globule"; some authors have used the term "equilibrium globule" to distinguish it from other globular states (see below).] Grosberg *et al.* proposed an alternative model, theorizing that polymers, including interphase DNA, can self-organize into a long-lived, non-equilibrium conformation that they described as a "fractal globule" (*28*, *29*). This highly compact state is formed by an unentangled polymer when it crumples into a series of small globules in a "beads-on-a-string" configuration. These beads serve as monomers in subsequent rounds of spontaneous crumpling until only a single globule-of-globules-of-globules remains. The resulting structure resembles a Peano curve, a continuous fractal trajectory that densely fills 3D space without crossing itself (*30*). Fractal globules are an attractive structure for chromatin segments because they lack knots (*31*) and would facilitate unfolding and refolding, for example, during gene activation, gene repression, or the cell cycle. In a fractal globule, contiguous regions of the genome tend to form spatial sectors whose size corresponds to the length of the original region (Fig. 4C). In contrast, an equilibrium globule is highly knotted and lacks such sectors; instead, linear and spatial positions are largely decorrelated after, at most, a few megabases (Fig. 4C). The fractal globule has not previously been observed (*29*, *31*).

The equilibrium globule and fractal globule models make very different predictions concerning the scaling of contact probability with genomic distance s. The equilibrium globule model predicts that contact probability will scale as $s^{-3/2}$, which we do not observe in our data. We analytically derived the contact probability for a fractal globule and found that it decays as s^{-1} (*10*); this corresponds closely with the prominent scaling we observed ($s^{-1.08}$).

The equilibrium and fractal globule models also make differing predictions about the 3D distance between pairs of loci ($s^{1/2}$ for an equilibrium globule, $s^{1/3}$ for a fractal globule). Although 3D distance is not directly measured by Hi-C, we note that a recent paper using 3D-FISH reported an $s^{1/3}$ scaling for genomic distances between 500 kb and 2 Mb (*27*).

We used Monte Carlo simulations to construct ensembles of fractal globules and equilibrium globules (500 each). The properties of the ensembles matched the theoretically derived scalings for contact probability (for fractal globules, s^{-1}, and for equilibrium globules, $s^{-3/2}$) and 3D distance (for fractal globules $s^{1/3}$, for equilibrium globules $s^{1/2}$). These simulations also illustrated the lack of entanglements [measured by using the knot-theoretic Alexander polynomial (*10*, *32*)] and the formation of spatial sectors within a fractal globule (Fig. 4B).

We conclude that, at the scale of several megabases, the data are consistent with a fractal globule model for chromatin organization. Of course, we cannot rule out the possibility that other forms of regular organization might lead to similar findings.

We focused here on interactions at relatively large scales. Hi-C can also be used to construct comprehensive, genome-wide interaction maps at finer scales by increasing the number of reads. This should enable the mapping of specific long-range interactions between enhancers, silencers, and insulators (*33*–*35*). To increase the resolution by a factor of n, one must increase the number of reads by a factor of n^2. As the cost of sequencing falls, detecting finer interactions should become increasingly feasible. In addition, one can focus on subsets of the genome by using chromatin immunoprecipitation or hybrid capture (*36*, *37*).

References and Notes

1. T. Cremer, C. Cremer, *Nat. Rev. Genet.* **2**, 292 (2001).
2. T. Sexton, H. Schober, P. Fraser, S. M. Gasser, *Nat. Struct. Mol. Biol.* **14**, 1049 (2007).
3. J. Dekker, *Science* **319**, 1793 (2008).
4. T. Misteli, *Cell* **128**, 787 (2007).
5. S. T. Kosak, M. Groudine, *Genes Dev.* **18**, 1371 (2004).
6. J. Dekker, K. Rippe, M. Dekker, N. Kleckner, *Science* **295**, 1306 (2002).
7. Z. Zhao *et al.*, *Nat. Genet.* **38**, 1341 (2006).
8. M. Simonis *et al.*, *Nat. Genet.* **38**, 1348 (2006).
9. J. Dostie *et al.*, *Genome Res.* **16**, 1299 (2006).
10. Materials and methods are available as supporting material on *Science* Online.
11. H. Yokota, G. van den Engh, J. E. Hearst, R. K. Sachs, B. J. Trask, *J. Cell Biol.* **130**, 1239 (1995).
12. S. Boyle *et al.*, *Hum. Mol. Genet.* **10**, 211 (2001).
13. H. Tanabe, F. A. Habermann, I. Solovei, M. Cremer, T. Cremer, *Mutat. Res.* **504**, 37 (2002).
14. J. A. Croft *et al.*, *J. Cell Biol.* **145**, 1119 (1999).
15. J. Dekker, *J. Biol. Chem.* **283**, 34532 (2008).
16. P. J. Sabo *et al.*, *Nat. Methods* **3**, 511 (2006).
17. J. R. Hesselberth *et al.*, *Nat. Methods* **6**, 283 (2009).
18. T. S. Mikkelsen *et al.*, *Nature* **448**, 553 (2007).
19. S. Naumann, D. Reutzel, M. Speicher, H. J. Decker, *Leuk. Res.* **25**, 313 (2001).
20. C. S. Osborne *et al.*, *Nat. Genet.* **36**, 1065 (2004).
21. J. M. Brown *et al.*, *J. Cell Biol.* **182**, 1083 (2008).
22. A. F. Dernburg *et al.*, *Cell* **85**, 745 (1996).
23. L. S. Shopland *et al.*, *J. Cell Biol.* **174**, 27 (2006).
24. P. Fraser, W. Bickmore, *Nature* **447**, 413 (2007).
25. P. G. d. Gennes, *Scaling Concepts in Polymer Physics* (Cornell Univ. Press, Ithaca, NY, 1979).
26. C. Munkel, J. Langowski, *Phys. Rev. E* **57**, 5888 (1998).
27. J. Mateos-Langerak *et al.*, *Proc. Natl. Acad. Sci. U.S.A.* **106**, 3812 (2009).
28. A. Y. Grosberg, S. K. Nechaev, E. I. Shakhnovich, *J. Phys. France* **49**, 2095 (1988).
29. A. Grosberg, Y. Rabin, S. Havlin, A. Neer, *Europhys. Lett.* **23**, 373 (1993).
30. B. B. Mandelbrot, *The Fractal Geometry of Nature* (Freeman, New York, ed. 2, 1983).
31. O. A. Vasilyev, S. K. Nechaev, *Theor. Math. Phys.* **134**, 142 (2003).
32. G. Kolesov, P. Virnau, M. Kardar, L. A. Mirny, *Nucleic Acids Res.* **35**, W425 (2007).
33. E. M. Blackwood, J. T. Kadonaga, *Science* **281**, 60 (1998).
34. A. C. Bell, A. G. West, G. Felsenfeld, *Science* **291**, 447 (2001).
35. J. E. Phillips, V. G. Corces, *Cell* **137**, 1194 (2009).
36. M. H. Kuo, C. D. Allis, *Methods* **19**, 425 (1999).
37. A. Gnirke *et al.*, *Nat. Biotechnol.* **27**, 182 (2009).

38. Supported by a Fannie and John Hertz Foundation graduate fellowship, a National Defense Science and Engineering graduate fellowship, an NSF graduate fellowship, the National Space Biomedical Research Institute, and grant no. T32 HG002295 from the National Human Genome Research Institute (NHGRI) (E.L.); a fellowship from the American Society of Hematology (T.R.); award no. R01HL06544 from the National Heart, Lung, and Blood Institute and R37DK44746 from the National Institute of Diabetes and Digestive and Kidney Diseases (M.G.); NIH grant U54HG004592 (J.S.); i2b2 (Informatics for Integrating Biology and the Bedside), the NIH-supported Center for Biomedical Computing at Brigham and Women's Hospital (L.A.M.), grant no. HG003143 from the NHGRI, and a Keck Foundation distinguished young scholar award (J.D.). We thank J. Goldy, K. Lee, S. Vong, and M. Weaver for assistance with DNaseI experiments; A. Kosmrlj for discussions and code; A. P. Aiden, X. R. Bao, M. Brenner, D. Galas, W. Gosper, A. Jaffer, A. Melnikov, A. Miele, G. Giannoukos, C. Nusbaum, A. J. M. Walhout, L. Wood, and K. Zeldovich for discussions; and L. Gaffney and B. Wong for help with visualization. We also acknowledge the ENCODE chromatin group at Broad Institute and Massachusetts General Hospital. Hi-C sequence data has been deposited at the GEO database (www.ncbi.nlm.nih.gov/geo/), accession no. GSE18199. Expression data are also available at GEO, accession no. GSE18350. Chromatin immunoprecipitation sequence (ChIP-Seq) data and DNaseI sensitivity data are available at the University of California Santa Cruz (UCSC) browser (http://genome.ucsc.edu/). Additional visualizations are available at http://hic.umassmed.edu. A provisional patent on the Hi-C method (no. 61/100,151) is under review.

Supporting Online Material

www.sciencemag.org/cgi/content/full/326/5950/289/DC1
Materials and Methods
Figs. S1 to S32

1 September 2009; accepted 18 September 2009
10.1126/science.1181369

Arterial-Venous Segregation by Selective Cell Sprouting: An Alternative Mode of Blood Vessel Formation

Shane P. Herbert,[1,2] Jan Huisken,[1] Tyson N. Kim,[3] Morri E. Feldman,[4] Benjamin T. Houseman,[5] Rong A. Wang,[3] Kevan M. Shokat,[5] Didier Y. R. Stainier[1]*

Blood vessels form de novo (vasculogenesis) or upon sprouting of capillaries from preexisting vessels (angiogenesis). With high-resolution imaging of zebrafish vascular development, we uncovered a third mode of blood vessel formation whereby the first embryonic artery and vein, two unconnected blood vessels, arise from a common precursor vessel. The first embryonic vein formed by selective sprouting of progenitor cells from the precursor vessel, followed by vessel segregation. These processes were regulated by the ligand EphrinB2 and its receptor EphB4, which are expressed in arterial-fated and venous-fated progenitors, respectively, and interact to orient the direction of progenitor migration. Thus, directional control of progenitor migration drives arterial-venous segregation and generation of separate parallel vessels from a single precursor vessel, a process essential for vascular development.

During early stages of vertebrate embryogenesis, coordinated sorting and segregation of arterial- and venous-fated angioblasts into distinct networks of arteries and veins is essential to establish a functional vasculature. Recent studies in mouse and zebrafish have elucidated key roles for a number of signaling pathways and transcriptional regulators in arterial-venous specification (*1*, *2*). However, we still lack a basic mechanistic understanding of how mixed populations of specified arterial-venous cells coordinate their behavior to segregate and form distinct vessels.

During zebrafish vascular development, angioblasts migrate from the lateral plate mesoderm to the midline (*3*, *4*) and eventually give rise to the first embryonic artery (dorsal aorta, DA) and vein (caudal vein, CV). Notochord-derived Sonic hedgehog, which induces the ex-

[1]Department of Biochemistry and Biophysics, Programs in Developmental Biology, Genetics and Human Genetics, Cardiovascular Research Institute, University of California, San Francisco, CA 94158, USA. [2]Multidisciplinary Cardiovascular Research Centre and Institute of Molecular and Cellular Biology, Faculty of Biological Sciences, University of Leeds, Leeds LS2 9JT, UK. [3]Laboratory for Accelerated Vascular Research, Division of Vascular Surgery, Department of Surgery, University of California, San Francisco, CA 94143, USA. [4]Graduate Group in Biophysics, University of California, San Francisco, CA 94158, USA. [5]Howard Hughes Medical Institute and Department of Cellular and Molecular Pharmacology, University of California, San Francisco, CA 94158, USA.

*To whom correspondence should be addressed. E-mail: Didier.Stainier@ucsf.edu

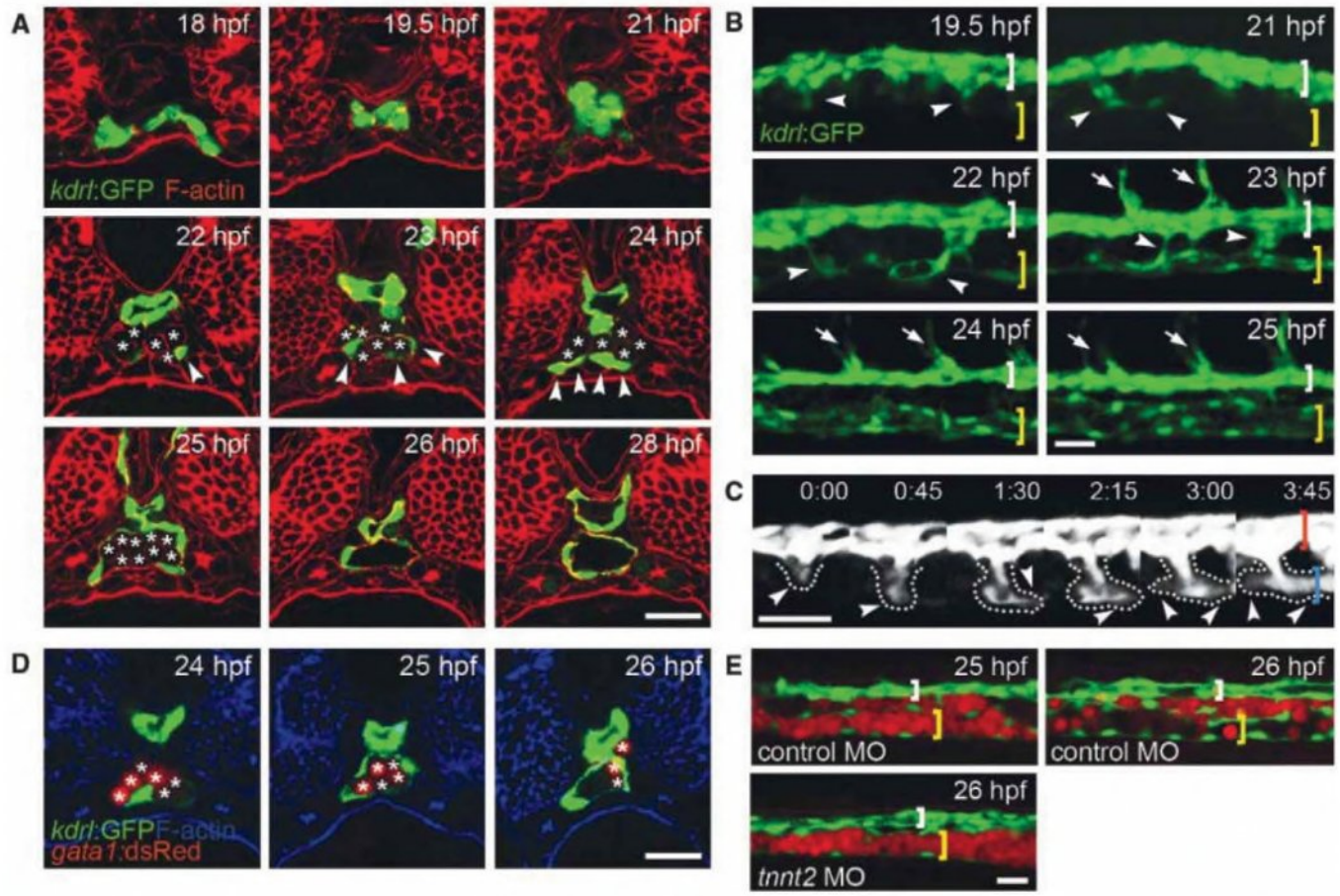

Fig. 1. The CV forms by selective angioblast sprouting. (**A** to **E**) Mid-trunk transverse sections [(A) and (D)], lateral views [(B) and (E)], or lateral time-lapse [(C) and movie S1] of *Tg(kdrl:GFP)*^{s843} [(A) to (C)] or *Tg(kdrl:GFP)*^{s843}; *Tg(gata1:dsRed)*^{sd2} [(D) and (E)] embryos. Angioblasts coalesce and remodel to form the DA by 22 hpf [white and red brackets; (A) to (C)]. Between 21 and 24 hpf, venous angioblasts sprout ventrally from the DA [arrowheads and dotted lines, (A) to (C)] and contribute to the CV primordium [yellow and blue brackets, (A) to (C)]. ISVs sprout dorsally from 23 hpf [arrows, (B)]. By 25 hpf, venous angioblasts surround *Tg(gata1:*dsRed*)* ^{sd2}-positive erythrocytes [asterisks, (A) and (D); red cells, (D) and (E)]. Erythrocyte displacement typically clears the CV lumen by 26 hpf [(A), (D), and (E)] but not in *tnnt2* MO–injected embryos (E). Scale bars indicate 35 μm.

pression of vascular endothelial growth factor a (Vegfa) in the ventral somites, is essential for angioblast differentiation (*5*). Vegfa-induced activation of Notch signaling (*5*, *6*), as well as other factors (*2*, *7*–*9*), subsequently promotes arterial specification in a subset of angioblasts (*4*), before arterial-venous segregation. To investigate mechanisms of arterial-venous angioblast sorting and segregation, we analyzed vascular development with high temporal resolution in *Tg(kdrl:GFP)*^{s843} (*4*) embryos (*10*). These transgenic embryos express green fluorescent protein (GFP) in the endothelial lineage, enabling the tracking of angioblasts during early stages of vascular development. GFP-positive angioblasts coalesced at the midline to form a single vascular cord by the 21-somite stage (19.5 hours postfertilization; hpf; Fig. 1, A and B, and fig. S1). Subsequent cord remodeling led to the formation of a lumenized DA primordium by 22 hpf. From 21 to 23 hpf, a subpopulation of angioblasts sprouted ventrally from the DA primordium and connected (anastomosed) with adjacent cells to form the CV primordium by 24 hpf (Fig. 1, A to C; figs. S1, S2, and S4; and movies S1 and S2). Hence, the first artery and vein share a common vessel primordium. Dorsal intersegmental vessel (ISV) sprouting occurred at regular intervals along the DA and was initiated later than ventral sprouting (23 hpf; Fig. 1B), suggesting that distinct mechanisms govern dorsal versus ventral sprouting behaviors. Thus, the DA forms by classical vasculogenesis, whereas formation of the CV involves an alternative mechanism whereby selective sprouting of venous-fated angioblasts, subsequent sprout termination, and cell-cell segregation allow distinct arterial and venous vessels to form. Hence, unlike angiogenesis in which new capillaries form a continuous network with the original vessel, two unconnected blood vessels can derive from a common group of cells.

Differences between DA and CV tube formation were further highlighted by contrasting modes of lumen formation. DA lumen formation involved hollowing of the vascular cord (*11*), whereas a functional CV lumen was generated differently (Fig. 1, A, D, and E; figs. S1, S2, S5, and S6; and movies S3 and S4). By using *Tg(gata1:dsRed)*^{sd2} embryos that express the fluorescent protein dsRed in erythrocytes (*12*) and selective plane illumination microscopy (*13*), we found that initial hollowing of the CV primordium was followed by rapid luminal expansion upon the invasion of erythrocytes positioned ventral to the DA (fig. S6 and movies S3 and S4). Shortly thereafter, the CV lumen was cleared upon the flow-dependent displacement of erythrocytes, a process that failed to occur in *cardiac troponin t2* (*tnnt2*) morpholino oligonucleotide (MO)–injected embryos, which lack circulation (*14*) (Fig. 1E).

We hypothesized that arterial-venous segregation and generation of two separate vessels might be achieved by selective incorporation of venous-fated angioblasts into ventral sprouts while limiting the ventral migratory behavior of arterial-fated angioblasts. Vegfa was recently shown to differentially regulate angioblast sprouting behavior by promoting the expression of the Notch ligand *delta-like 4* (*dll4*) (*15*–*17*). Expression of Dll4 in ISV tip cells activates Notch signaling in adjacent cells, thereby limiting their dorsal sprouting behavior. Injection of embryos with *vegfa* MO revealed that Vegfa signaling also limits the ventral migratory behavior of angioblasts (Fig. 2, table S1, fig. S7, and movies S5 and S6). In *vegfa* MO–injected embryos, angioblasts initially coalesced to form a vascular cord but then migrated ventrally excessively, failed to segregate, and ultimately generated a single vascular tube encircling *Tg(gata1:*dsRed*)*^{sd2}-positive erythrocytes. Hence, Vegfa-mediated arterial specification is required for the control and termination of angioblast ventral migration and maintenance of an intact DA. A similar phenotype was observed on injection of MO to *plcγ1*, which encodes a key downstream component of Vegfa signaling (*6*), and on inhibition of Vegfa receptor activation using SU5416 (Fig. 2, table S1, fig. S7, and movies S5 and S7). ISV sprouting was also disrupted in Vegfa-deficient embryos,

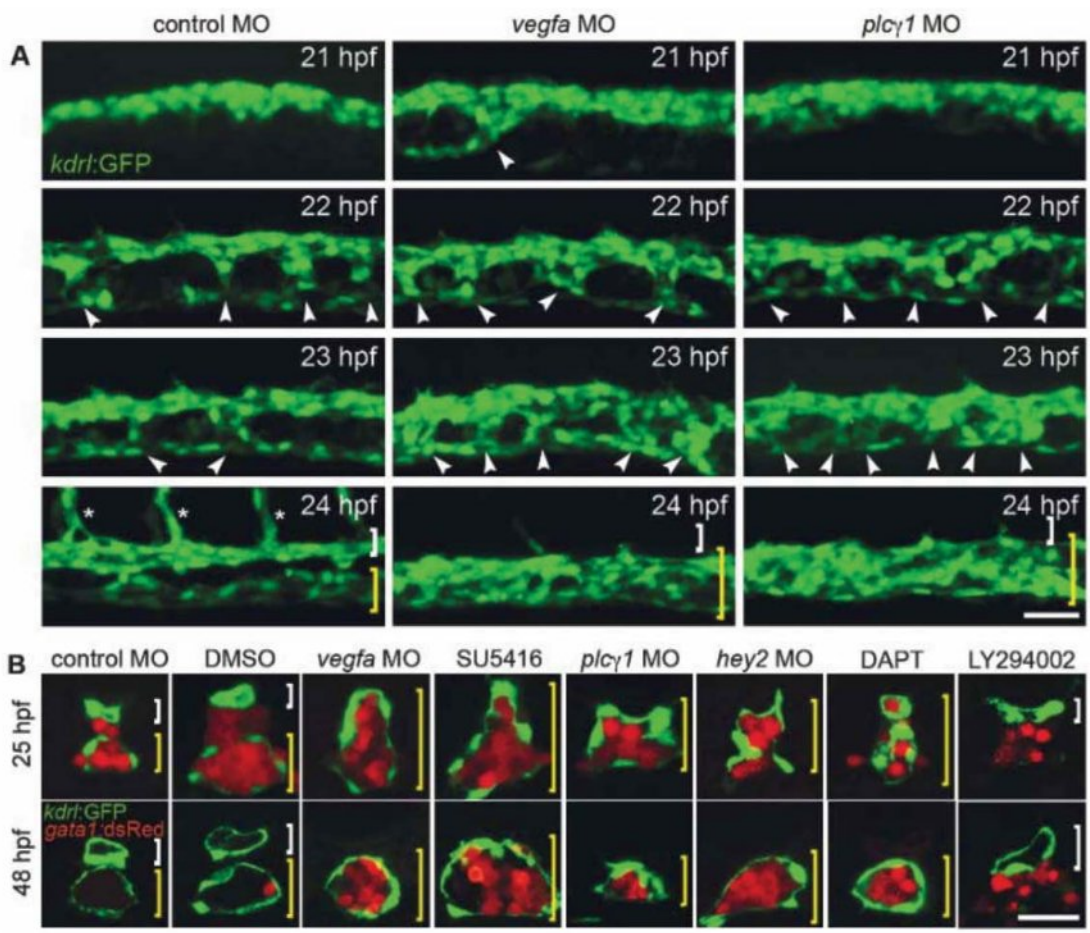

Fig. 2. Vegf signaling limits ventral sprouting. (**A** and **B**) Lateral views of *Tg(kdrl:GFP)*^{s843} embryos (A) or transverse sections of *Tg(kdrl:GFP)*^{s843};*Tg(gata1:dsRed)*^{sd2} embryos (B) injected with control, *vegfa*, *plcγ1* or *hey2* MO, or exposed to dimethyl sulfoxide (DMSO), SU5416, DAPT, or LY294002. *vegfa* or *plcγ1* MO–injection blocks ISV sprouting (asterisks), promotes excessive ventral sprouting (arrowheads), leads to loss of the DA (white bracket) and generates a single venous tube (yellow bracket). SU5416, DAPT, or *hey2* MO–injection also promote loss of the DA, whereas LY294002 blocks CV morphogenesis. Scale bars, 35 μm.

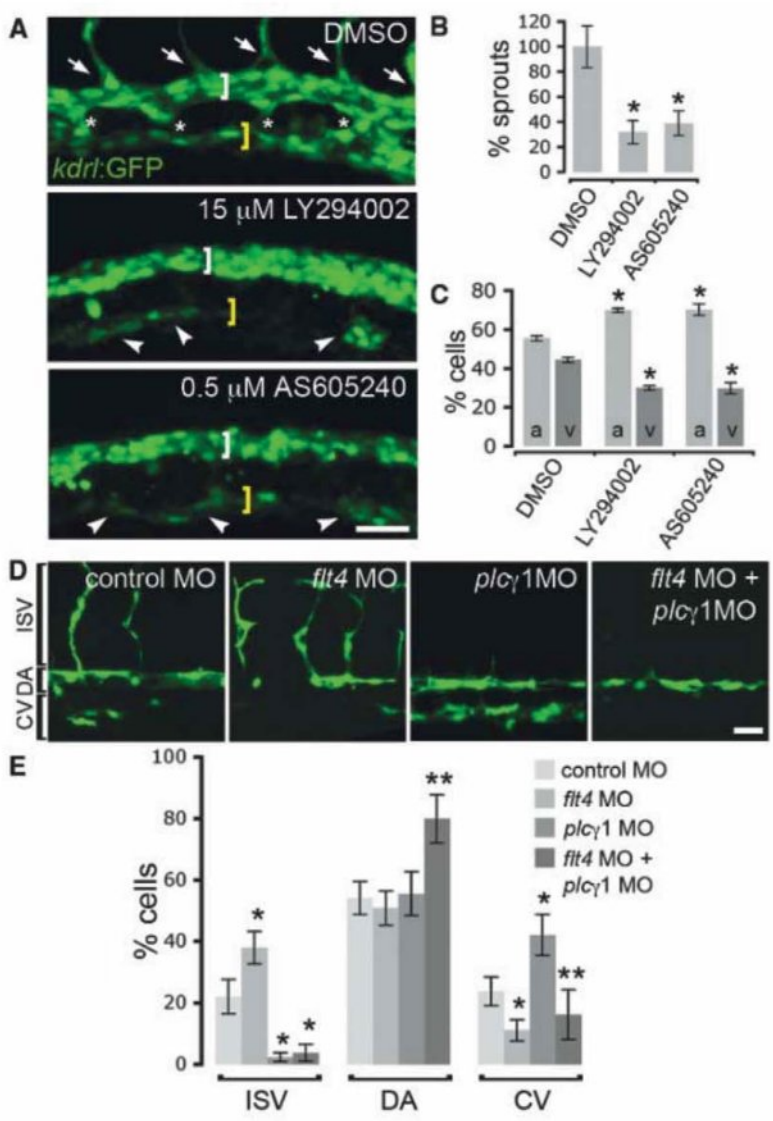

Fig. 3. Flt4/PI3K signaling mediates venous angioblast migration. (**A** to **C**) *Tg(kdrl:GFP)*^{s843} embryos were exposed to DMSO, LY294002, or AS605240, processed for microscopy [23 hpf, (A)], and then scored for (B) the number of ventral sprouts (as a percentage of DMSO-treated embryos) or (C) the percentage of cells in the DA (white bracket, a in graph) or CV (yellow bracket, v in graph). PI3K inhibition blocks ISV sprouting (arrows), venous sprouting (asterisks), and angioblast ventral migration (arrowheads). Lateral images (**D**) and quantification (**E**) of donor-derived *Tg(kdrl:GFP)*^{s843} cells in wild-type hosts at 48 hpf. Fewer cells from *flt4* MO–injected donors contribute to the CV versus controls. Excessive ventral migration of angioblasts from *plcγ1* MO–injected donors is reduced on coinjection with *flt4* MO. Scale bars, 35 μm. Error bars represent mean ± SEM. *$P < 0.05$ versus control, **$P < 0.05$ versus *plcγ1* MO, Student's *t* test.

consistent with opposing roles for Vegfa signaling in the induction of dorsal sprouting (*6*) and restraint of ventral sprouting. Vegfa influences dorsal sprouting behavior by indirectly activating Notch signaling (*15*–*17*). Accordingly, N-[N-(3,5-difluorophenacetyl)-1-alanyl]-S-phenylglycine t-butyl ester (DAPT)–mediated inhibition of Notch signaling promoted excessive ventral sprouting (Fig. 2B). Moreover, excessive ventral migration was also observed on injection of MO to *gridlock/hey2*, which encodes a key transcriptional effector of notch signaling (*7*). Thus, termination of ventral sprouting is regulated by genes downstream of Vegfa and Notch signaling.

In contrast, vein morphogenesis was strikingly disrupted by the broad range phosphoinositide 3-kinase (PI3K) inhibitor LY294002 (Fig. 2B). Although LY294002 treatment did not affect total angioblast numbers, suggesting no proliferation defects (table S2), ventral sprouting was disrupted, and significantly more cells were retained in the DA (Fig. 3, A to C), consistent with a role for PI3K in angioblast ventral sprouting [supporting online material (SOM) text S1]. Cell migration during angiogenic sprouting selectively requires signaling via the p110α isoform of PI3K downstream of Vegf receptor activation (*18*). Consequently, we tested the hypothesis that a similar p110α-dependent mechanism may control ventral sprouting and CV formation. We interrogated the group I PI3K family (p110α, p110β, p110δ, and p110γ) with isoform-selective inhibitors (*19*, *20*) (table S3) to avoid the early developmental defects and compensatory interactions associated with genetically silencing individual isoforms (*19*, *21*, *22*). Consistent with a role for p110α, exposure of embryos to inhibitors at concentrations that inhibit p110α blocked vein morphogenesis (fig. S12 and SOM text S2). Application of LY294002 or the isoform selective inhibitor, AS605240, at concentrations that blocked ventral sprouting also disrupted dorsal sprouting (Fig. 3, A to C), indicating a general requirement for PI3K in arterial-venous sprouting.

A common role for p110α in dorsal and ventral angioblast sprouting indicated that similar signaling pathways regulate these processes. Vegfa promotes dorsal ISV sprouting on activation of its receptor, Flk1, and downstream p110α-mediated signaling (*18*). Restricted venous expression of the related Vegfc receptor gene *flt4* (fig. S8) suggested a role for p110α in vein morphogenesis downstream of Flt4-mediated signaling. Although angioblast ventral sprouting and migration was significantly delayed in *vegfc* or *flt4* MO–injected embryos (fig. S13 and table S4), possible functional redundancy with other Vegf signaling components or compensation by alternate mechanisms enabled vein formation at later time points. However, a role for Flt4 signaling in angioblast ventral sprouting was confirmed on transplantation of cells from *Tg(kdrl:GFP)*^{s843} donors into nontransgenic wild-type hosts. Significantly fewer *flt4* MO–injected than control MO-injected, donor-derived cells contributed to the CV (Fig. 3, D and E, and table S5). Furthermore, the excessive contribution of *plcγ1* MO–injected, donor-derived cells to the CV was blocked on *flt4* MO–co-injection. Hence,

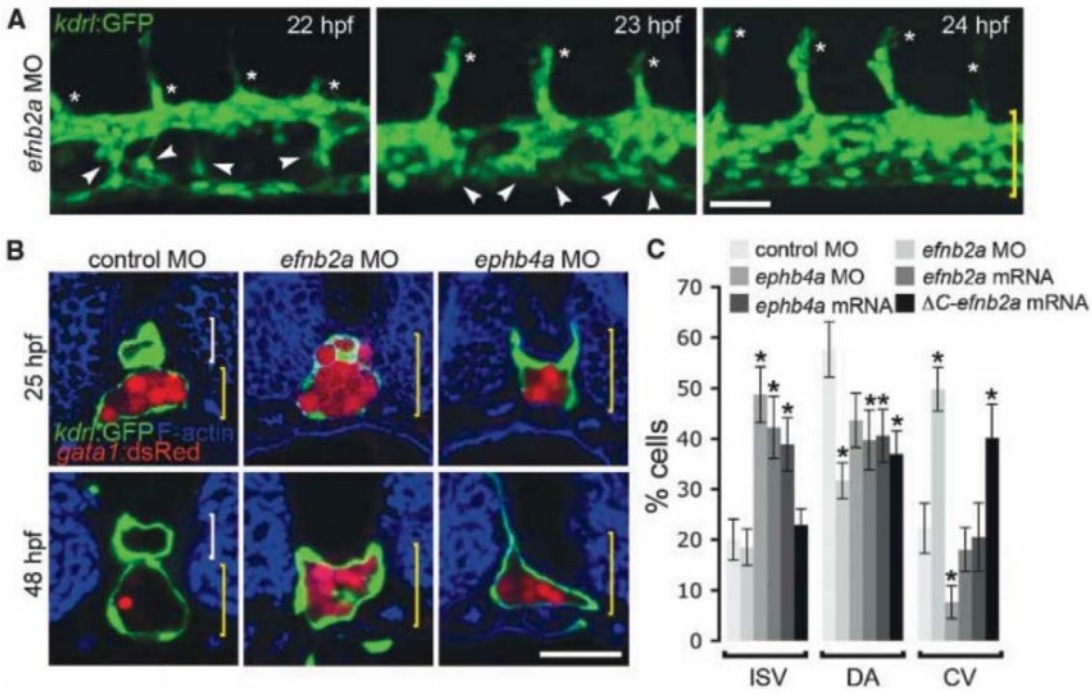

Fig. 4. Ephb4a-Efnb2a signaling determines the direction of angioblast migration. (**A** and **B**) Lateral projections of *Tg(kdrl:GFP)*^{s843} embryos (A) or transverse sections of *Tg(kdrl:GFP)*^{s843}; *Tg(gata1:dsRed)*^{sd2} embryos (B) injected with control, *efnb2a*, or *ephb4a* MO. Reduced Efnb2a expression promotes excessive ventral sprouting [(A), arrowheads], loss of the DA [(B), white bracket], and formation of a single vessel [(A) and (B), yellow bracket] without affecting initiation of ISV sprouting [(A), asterisks]. Similarly, posterior arterial-venous segregation is disrupted in *ephb4a* MO–injected embryos. (**C**) Quantification of donor-derived *Tg(kdrl:GFP)*^{s843} cells in wild-type hosts at 30 hpf. More cells from *efnb2a* MO–injected or Δ*C-efnb2a*-overexpressing donors contribute to the CV versus controls, whereas fewer cells from *ephb4a* MO–injected donors contribute to the CV. Overexpression of *efnb2a* or *ephb4a* enhances the number of donor cells contributing to ISVs. Scale bars, 35 μm. Error bars represent mean ± SEM (*$P < 0.05$, Student's *t* test).

Vegfa/Flk1 and Vegfc/Flt4 signaling regulate multidirectional arterial-venous sprouting. However, *vegfc* is not expressed ventral to the DA but in the DA itself (fig. S14), indicating that other mechanisms must orient the direction of venous angioblast migration ventrally.

The EphB4 receptor tyrosine kinase and its plasma-membrane-spanning ligand, EphrinB2 (EfnB2), demarcate venous and arterial domains, respectively (*23*). Studies of EphB4- and EfnB2-null mice have revealed roles for forward and reverse EphB4-EfnB2 signaling in vascular morphogenesis (*23*–*25*); however, the exact function and mode of action of bidirectional EphB4-EfnB2 signaling remain unknown (*1*). Observations that zebrafish Efnb2a expression is restricted to the dorsal-most cells of the vascular cord (*4*) (fig. S15) and is tightly regulated by Vegfa (figs. S11 and S16) as well as Notch signaling (*5*–*7*) led us to hypothesize a role for Ephb4a-Efnb2a in the directional control of angioblast migration. Consistent with this hypothesis, the generation of distinct arterial and venous vessels was disrupted, and the PI3K-dependent ventral migration of angioblasts deregulated, in *efnb2a* or *ephb4a* MO–injected embryos (Fig. 4, A and B, fig. S17, and table S6). In contrast to *vegfa* MO–injected embryos, *efnb2a* and *ephb4a* MO–injected embryos still formed ISVs (Figs. 2A and 4, A and B), indicating that angioblasts migrate both dorsally and ventrally but fail to segregate. To elucidate the distinct functions of Efnb2a and Ephb4a in arterial-venous segregation, we transplanted cells from *Tg(kdrl:GFP)*^{s843} donors into nontransgenic wild-type hosts. *efnb2a* MO–injected donor-derived cells contributed to the CV at over twice the frequency of control cells (Fig. 4C, table S6, and figs. S18 and S19). In contrast, significantly fewer *ephb4a* MO–injected, donor-derived cells contributed to the CV compared to controls. Thus, Efnb2a limits the ventral migration of arterial angioblasts, whereas Ephb4a promotes the ventral migration of venous angioblasts, suggesting a role for bidirectional Ephb4a-Efnb2a–mediated repulsion between arterial and venous cells in the directional control of angioblast sprouting (fig. S19). Furthermore, donor cells overexpressing *efnb2a* or *ephb4a* preferentially contributed to ISVs, consistent with increased repulsion of arterial angioblasts away from *ephb4a*-expressing venous cells in response to elevated Efnb2a or a potential forced Ephb4a-Efnb2a cis-interaction in response to elevated Ephb4a (Fig. 4C, table S6, and figs. S18 and S19). Donor cells overexpressing reverse signaling–deficient Efnb2a (*26*) (ΔC-Efnb2a) were not retained in the DA (Fig. 4C, table S6, and figs. S18 and S19), confirming a role for reverse Ephb4a-Efnb2a signaling in the regulation of arterial-venous segregation. Hence, Vegfa-induced *efnb2a* expression and bidirectional Ephb4a-Efnb2a signaling selectively exclude arterial angioblasts from venous sprouts while promoting the ventral migration of venous angioblasts. These data support the concept that Notch, EfnB2, and EphB4 can regulate the size of developing arteries and veins and that endothelial cells from the DA may contribute to the formation of the CV in mouse (*27*). Thus, repulsive Ephb4a-Efnb2a signaling regulates the directional control of angioblast sprouting behavior.

Previous work focused on identifying signals that modulate specification of arterial-venous angioblasts, but how these signals ultimately affect cell behavior to sort and segregate angioblasts into distinct vessels was unknown. Our data provide a cellular framework for arterial-venous tube morphogenesis whereby coordinated regulation of dorsal and ventral angioblast sprouting behaviors by Vegf, Notch, and Ephb4a-Efnb2a signaling efficiently fashions the embryonic vasculature (fig. S20 and SOM text S3) and shed light on how multidirectional arterial and venous sprouting can be achieved while maintaining the integrity of a precursor vessel. Most importantly, we have uncovered an alternative mode of vascular development that allows the segregation of cells into discrete arterial and venous vessels from one common precursor vessel.

References and Notes

1. R. H. Adams, K. Alitalo, *Nat. Rev. Mol. Cell Biol.* **8**, 464 (2007).
2. F. J. Lin, M. J. Tsai, S. Y. Tsai, *EMBO Rep.* **8**, 920 (2007).
3. M. Gering, R. Patient, *Dev. Cell* **8**, 389 (2005).
4. S. W. Jin, D. Beis, T. Mitchell, J. N. Chen, D. Y. Stainier, *Development* **132**, 5199 (2005).
5. N. D. Lawson, A. M. Vogel, B. M. Weinstein, *Dev. Cell* **3**, 127 (2002).
6. N. D. Lawson, J. W. Mugford, B. A. Diamond, B. M. Weinstein, *Genes Dev.* **17**, 1346 (2003).
7. T. P. Zhong, S. Childs, J. P. Leu, M. C. Fishman, *Nature* **414**, 216 (2001).
8. S. Cermenati *et al.*, *Blood* **111**, 2657 (2008).
9. H. Pendeville *et al.*, *Dev. Biol.* **317**, 405 (2008).
10. Materials and methods are available as supporting material on *Science* Online.
11. L. H. Parker *et al.*, *Nature* **428**, 754 (2004).
12. D. Traver *et al.*, *Nat. Immunol.* **4**, 1238 (2003).

13. J. Huisken, J. Swoger, F. Del Bene, J. Wittbrodt, E. H. Stelzer, *Science* **305**, 1007 (2004).
14. A. J. Sehnert *et al.*, *Nat. Genet.* **31**, 106 (2002).
15. M. Hellstrom *et al.*, *Nature* **445**, 776 (2007).
16. A. F. Siekmann, N. D. Lawson, *Nature* **445**, 781 (2007).
17. J. D. Leslie *et al.*, *Development* **134**, 839 (2007).
18. M. Graupera *et al.*, *Nature* **453**, 662 (2008).
19. Z. A. Knight *et al.*, *Cell* **125**, 733 (2006).
20. L. M. Sly *et al.*, *Blood* **113**, 2945 (2009).
21. L. Bi, I. Okabe, D. J. Bernard, A. Wynshaw-Boris, R. L. Nussbaum, *J. Biol. Chem.* **274**, 10963 (1999).
22. K. Ueki *et al.*, *Proc. Natl. Acad. Sci. U.S.A.* **99**, 419 (2002).
23. R. H. Adams *et al.*, *Genes Dev.* **13**, 295 (1999).
24. R. H. Adams *et al.*, *Cell* **104**, 57 (2001).
25. S. S. Foo *et al.*, *Cell* **124**, 161 (2006).
26. T. Sato, T. Hamaoka, H. Aizawa, T. Hosoya, H. Okamoto, *J. Neurosci.* **27**, 5271 (2007).
27. Y. H. Kim *et al.*, *Development* **135**, 3755 (2008).
28. We thank J. E. Cooke, S. Schulte-Merker, and H. Okamoto for reagents and D. Shin, P. Gut, and S. Woo for critical reading of the manuscript. S.P.H. is a Wellcome Trust Sir Henry Wellcome postdoctoral fellow. J.H. was supported by the Human Frontier Science Program Organization and is supported by a Cardiovascular Research Institute fellowship. This study was supported in part by grants from the NIH (HL54737) and Packard Foundation to D.Y.R.S.

Supporting Online Material
www.sciencemag.org/cgi/content/full/326/5950/294/DC1
Materials and Methods
SOM Text
Figs. S1 to S20
Tables S1 to S6
Movies S1 to S7

2 July 2009; accepted 19 August 2009
10.1126/science.1178577

KLF Family Members Regulate Intrinsic Axon Regeneration Ability

Darcie L. Moore,[1,2]* Murray G. Blackmore,[3]* Ying Hu,[1] Klaus H. Kaestner,[4] John L. Bixby,[2,3] Vance P. Lemmon,[2,3] Jeffrey L. Goldberg[1,2]†

Neurons in the central nervous system (CNS) lose their ability to regenerate early in development, but the underlying mechanisms are unknown. By screening genes developmentally regulated in retinal ganglion cells (RGCs), we identified Krüppel-like factor–4 (KLF4) as a transcriptional repressor of axon growth in RGCs and other CNS neurons. RGCs lacking KLF4 showed increased axon growth both in vitro and after optic nerve injury in vivo. Related KLF family members suppressed or enhanced axon growth to differing extents, and several growth-suppressive KLFs were up-regulated postnatally, whereas growth-enhancing KLFs were down-regulated. Thus, coordinated activities of different KLFs regulate the regenerative capacity of CNS neurons.

Adult mammalian central nervous system (CNS) axons are unable to regenerate after injury, but immature CNS neurons regenerate axons robustly (*1*–*3*). In addition to the development of an inhibitory CNS environment (*4*, *5*), a developmental loss in neurons' intrinsic capacity for axon growth is thought to contribute to regeneration failure. For example, after birth, axonal outgrowth from rat retinal ganglion cells (RGCs, a type of CNS neuron) slows substantially (*6*). Similar developmental declines in axon growth ability have been observed in mammalian tissue explants of brainstem (*7*), cerebellum (*8*, *9*), entorhinal cortex (*10*), and retina (*2*). Various cell-autonomous factors such as cAMP (cyclic adenosine 3′,5′-monophosphate) and CREB (cAMP response element–binding protein) (*11*, *12*), Bcl-2 (B cell lymphoma/leukemia 2) (*13*, *14*), Rho/ROCK (Rho-associated kinase) (*15*), Cdh1-APC (anaphase-promoting complex) (*16*, *17*), and PTEN (phosphatase and tensin homolog) (*18*) have been suggested to play roles in this process. However, manipulating these regulators of axon growth, even when simultaneously overcoming environmental inhibition, only partially restores regeneration, suggesting that additional intrinsic axon growth regulators remain to be identified.

To investigate the molecular basis for the developmental loss of axon growth ability in RGCs, we took advantage of the fact that coculture with amacrine cell membranes is sufficient to signal embryonic RGCs to decrease their rapid axon growth (*6*). Addition of the transcriptional inhibitor actinomycin D blocked this effect of amacrine membranes, and embryonic RGCs retained their capacity for axon growth (Fig. 1A). These data suggest that gene transcription is required for the developmental loss of intrinsic axon growth ability in RGCs.

To identify candidate genes, we profiled gene expression from embryonic day 17 (E17) through postnatal day 21 (P21) RGCs (*19*), spanning the period when axon growth ability declines in vivo (*6*, *13*). We screened 111 candidates whose expression changed more than threefold by overexpression in embryonic hippocampal neurons, and used automated image acquisition and neurite tracing (KSR instrument, Cellomics) for rapid, unbiased quantification of neurite length (*20*); the investigator (D.L.M.) was blinded to gene identity until the screen was complete. The zinc-finger transcription factor, Krüppel-like factor–4 (KLF4), was the most effective suppressor of neurite outgrowth, decreasing average length by 50% (Fig. 1B). In a separate, blinded screen examining growth cone morphologies, KLF4 again emerged as the most interesting candidate gene as growth cones in KLF4-overexpressing hippocampal neurons were consistently enlarged (e.g., Fig. 1C).

Although KLF4 regulates cell survival in other systems (*21*–*23*), we detected no differences in

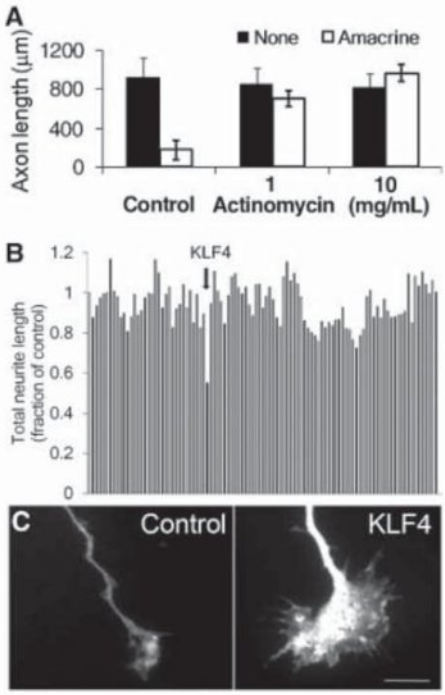

Fig. 1. A screen of developmentally regulated genes identifies KLF4 as an inhibitor of neurite growth. (**A**) Purified embryonic RGCs were cultured in the presence (white bars) or absence (black bars) of amacrine cell membranes for 3 days, and replated away from amacrine cell membranes, after which RGC axon growth was measured. Actinomycin D blocked RGCs' decrease in axon growth caused by amacrine cell membranes (mean ± SEM). (**B** and **C**) E18 hippocampal neurons were cotransfected with 111 candidate genes and enhanced green fluorescent protein (EGFP), cultured for 3 days on laminin, and immunostained for Tau to visualize neurites. (B) Neurite length of cotransfected (EGFP+) neurons. Bars represent average neurite length normalized to EGFP control (far left). KLF4 (arrow) decreased neurite growth by 50%. (C) EGFP+ growth cones of EGFP+/KLF4-transfected neurons (right) were enlarged compared to control-transfected neurons (left). Scale bar, 10 μm.

[1]Bascom Palmer Eye Institute, University of Miami Miller School of Medicine, Miami, FL 33136, USA. [2]Neuroscience Program, University of Miami Miller School of Medicine, Miami, FL 33136, USA. [3]Miami Project to Cure Paralysis, University of Miami Miller School of Medicine, Miami, FL 33136, USA. [4]Department of Genetics, University of Pennsylvania, Philadelphia, PA 19104, USA.

*These authors contributed equally to this work.
†To whom correspondence should be addressed. E-mail: jgoldberg@med.miami.edu

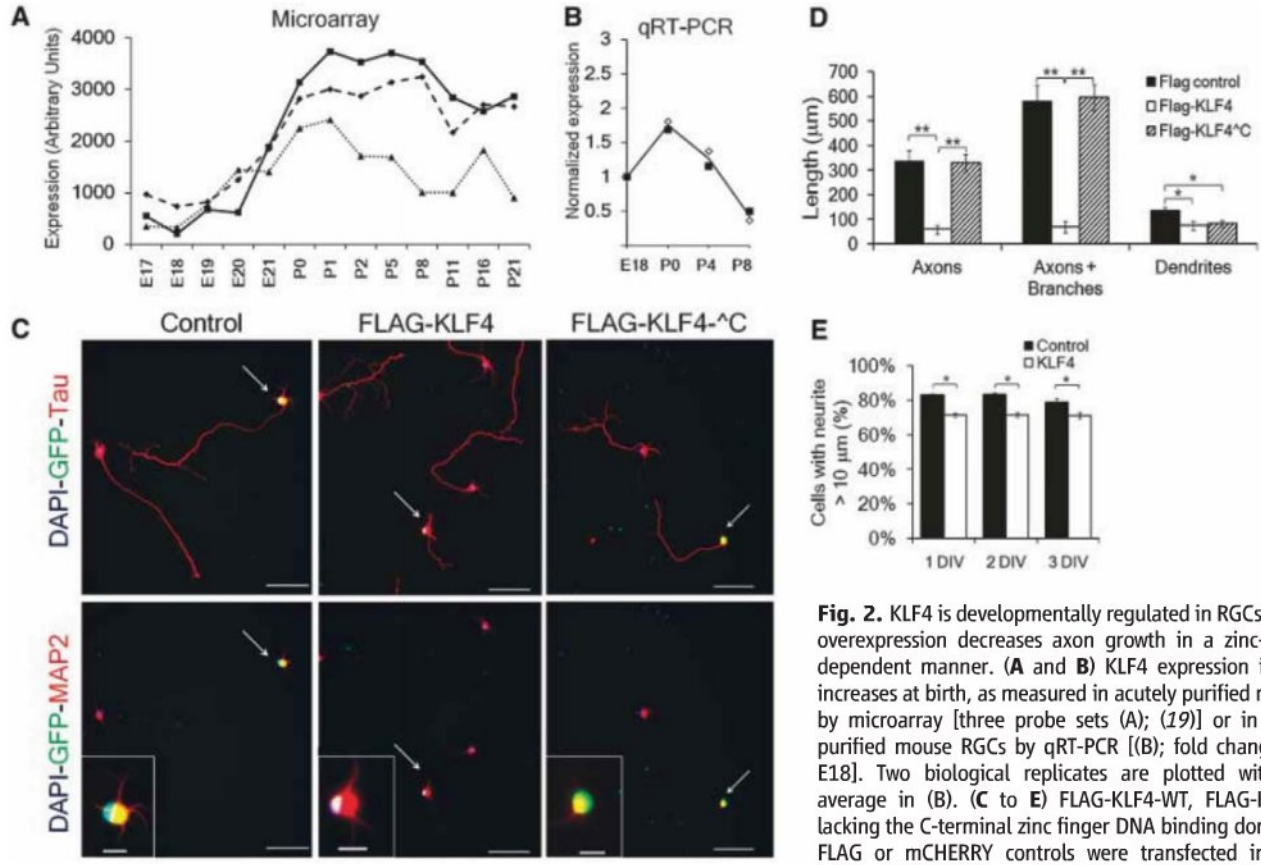

Fig. 2. KLF4 is developmentally regulated in RGCs, and its overexpression decreases axon growth in a zinc-finger–dependent manner. (**A** and **B**) KLF4 expression in RGCs increases at birth, as measured in acutely purified rat RGCs by microarray [three probe sets (A); (*19*)] or in acutely purified mouse RGCs by qRT-PCR [(B); fold change from E18]. Two biological replicates are plotted with their average in (B). (**C** to **E**) FLAG-KLF4-WT, FLAG-KLF4-^C lacking the C-terminal zinc finger DNA binding domain, or FLAG or mCHERRY controls were transfected into E20 RGCs. (C) After 2 days, RGCs were immunostained for FLAG or GFP (green, transfected cells), and Tau or MAP2 (red) as marked [nuclear DAPI (4′,6-diamidino-2-phenylindole) is blue]. Scale bar, 50 μm (main panels), 10 μm (inset). (D) Hand-tracing revealed that FLAG-KLF4-WT overexpression decreased axon growth; overexpression of FLAG-KLF4-^C was similar to that of controls (**$P < 0.001$, *$P < 0.02$, unpaired t test, post-Bonferroni correction; mean ± SEM). (E) E20 RGCs were transfected with either mCherry-pIRES2-eGFP (control) or KLF4-pIRES2-EGFP and plated for 1, 2 or 3 days in vitro (DIV). At 1 to 3 DIV, more control-transfected RGCs extended at least one neurite >10 μm than KLF4-transfected RGCs (*$P < 0.001$, paired t test; mean ± SEM).

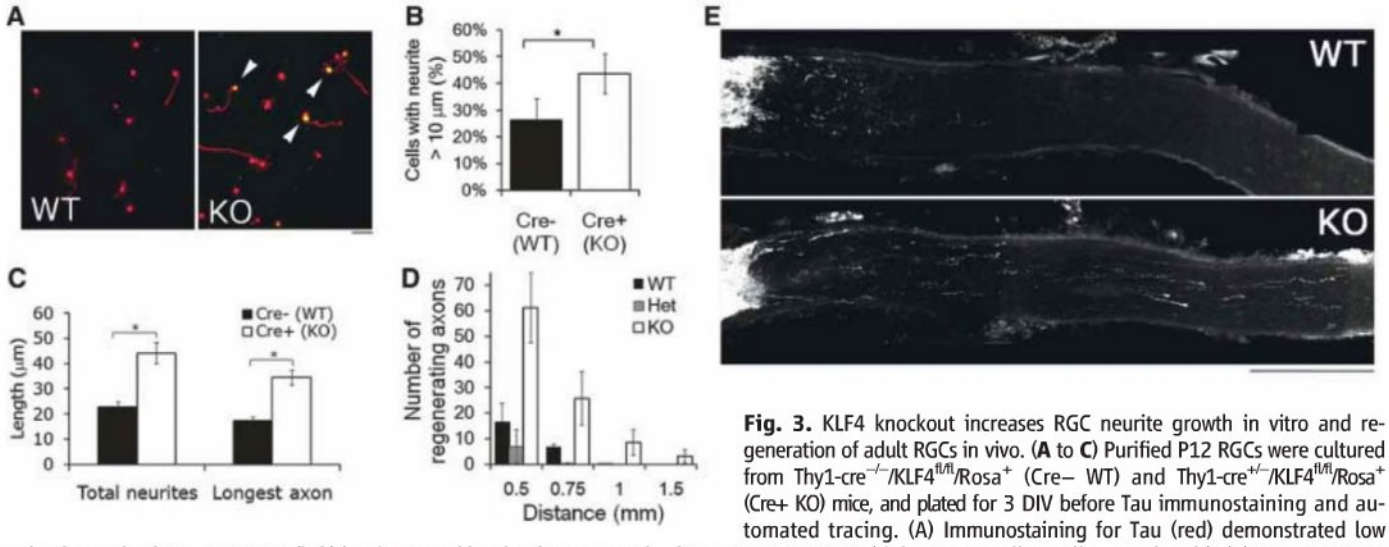

Fig. 3. KLF4 knockout increases RGC neurite growth in vitro and regeneration of adult RGCs in vivo. (**A** to **C**) Purified P12 RGCs were cultured from Thy1-cre$^{-/-}$/KLF4$^{fl/fl}$/Rosa^{+} (Cre– WT) and Thy1-cre$^{+/-}$/KLF4$^{fl/fl}$/Rosa^{+} (Cre+ KO) mice, and plated for 3 DIV before Tau immunostaining and automated tracing. (A) Immunostaining for Tau (red) demonstrated low levels of growth of Cre– WT RGCs (left) but increased levels of axon growth of Cre+ KLF4-KO RGCs (right; Rosa+ yellow cells, arrowheads). (B) KLF4-KO RGCs have a higher percentage of cells with neurites, compared to controls ($N = 3$; *$P < 0.02$, t test; mean ± SEM). (C) When all YFP+ RGCs were measured, KLF4 KO RGCs extended longer neurites than WT RGCs (representative experiment shown; *$P < 0.001$; mean ± SEM). (**D** and **E**) Two weeks after optic nerve crush of Thy1-cre^{+}/KLF4$^{+/+}$ (WT), Thy1-cre^{+}/KLF4$^{fl/+}$ (Het), and Thy1-cre^{+}/KLF4$^{fl/fl}$ (KO) mice, regenerating fibers were anterogradely labeled by intravitreal injection of Alexa 594–labeled cholera toxin B. Regenerating fibers were counted at specified distances from the lesion site. (D) More fibers regenerate in KO mice compared to WT or Het ($n = 10$ WT, 4 Het, and 7 KO mice; $P < 0.001$ for KO versus WT or Het; no difference between WT and Het by mixed-model analysis of covariance; mean ± SEM). (E) Partial projections of sectioned optic nerve from WT and KO mice show regenerating axons more than 1 mm distal to the lesion site in KO nerve. Scale bar, 200 μm.

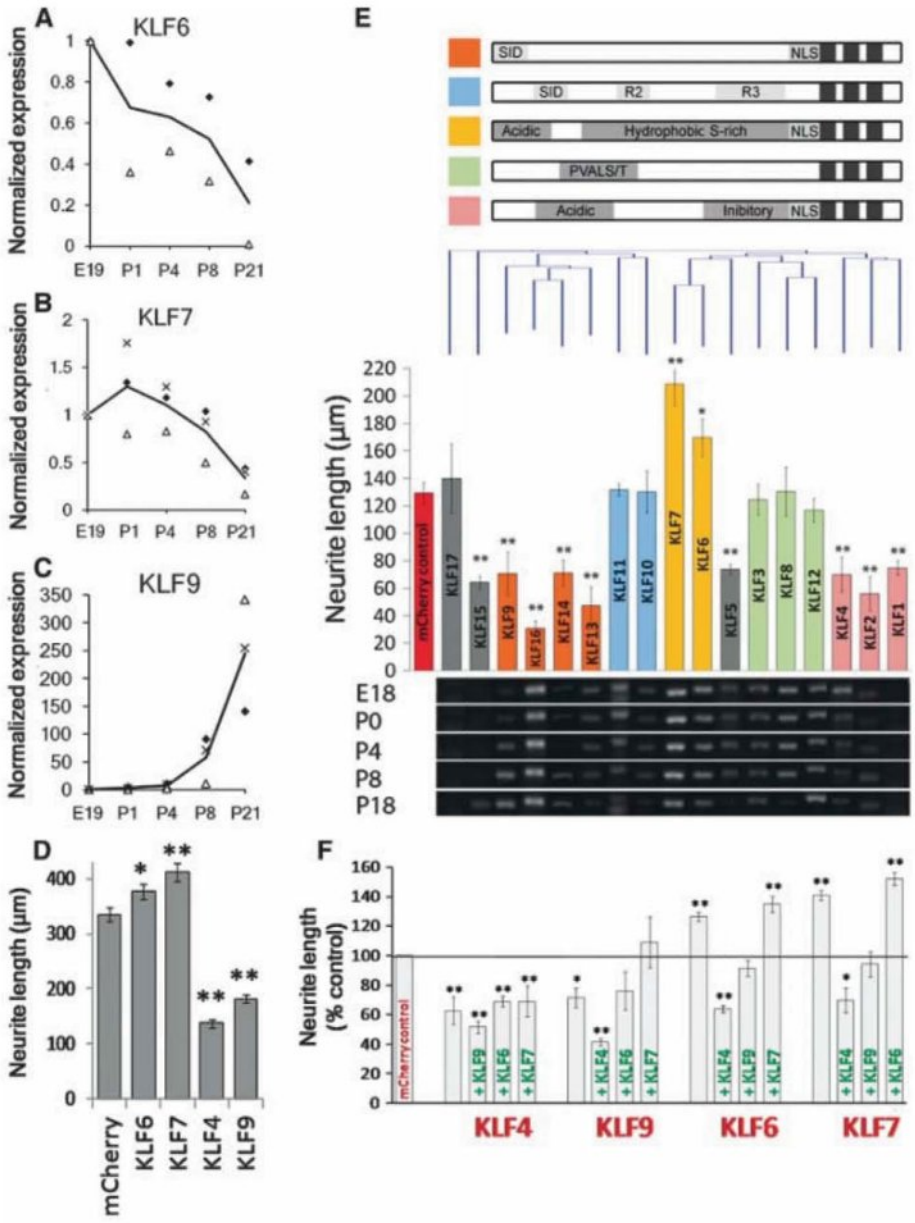

Fig. 4. Multiple KLF family members are developmentally regulated in RGCs and differentially affect CNS neurite growth. (**A** to **C**) RGCs from multiple ages were purified by immunopanning and analyzed by qRT-PCR. Transcript abundance is normalized to E19. KLF6 (A) and KLF7 (B) decrease more than 5-fold postnatally, whereas KLF9 (C) increases 250-fold. Each marker type is a separate experiment, and the line shown is the average; $N = 2$ to 3. (**D**) P4 RGCs were cotransfected with KLFs and EGFP and plated for 2 days on laminin. Bars represent average total neurite length of transfected (EGFP+) neurons [$n > 700$; $^*P < 0.05$, $^{**}P < 0.01$; analysis of variance (ANOVA) with post hoc Dunnett's test; mean ± SEM; pooled data from two replicate experiments]. (**E**) P5 cortical neurons were cotransfected with individual KLFs and mCherry, plated for 3 days on laminin, and immunostained for β-III tubulin. (Top) KLF family members are grouped according to defined structural domains (*27*) and clustered by amino acid similarity (Clustal analysis, Vector NTI). (Middle) Bars represent average total neurite length of transfected (mCherry+) neurons and are colored by the presence of known motifs (above). Nine KLFs significantly decreased neurite length, and two increased neurite length ($N > 3$, $n > 100$; $^*P < 0.05$, $^{**}P < 0.01$, ANOVA with post hoc Dunnett's test; mean ± SEM). (Bottom) Purified RGCs from different ages were analyzed by RT-PCR with KLF-specific primers, ordered according to the overlying bar graph. Transcripts for all KLFs except KLF1 and -17 were detected in developing RGCs. (**F**) P5 cortical neurons were cotransfected with combinations of KLFs with IRES-mCherry (red) or IRES-EGFP (green) reporters and cultured as above (DNA loading controls, fig. S13). Bars represent average neurite length of dually transfected neurons (mCherry+, EGFP+). Coexpression of KLF4 or -9 blocked the growth-promoting effects of KLF6 or -7 ($N = 3$, $n > 25$; $^*P < 0.05$, $^{**}P < 0.01$, ANOVA with post hoc Dunnett's test; mean ± SEM).

survival between KLF4- and control-transfected hippocampal neurons (fig. S1A). To determine if the growth-suppressive effect was specific either to axons or dendrites, we manually traced Tau+ and MAP2+ neurites (fig. S1B). Overexpression of KLF4 in embryonic hippocampal neurons significantly decreased the lengths of both axons (Tau+/MAP2–) and dendrites (Tau+/MAP2+) (figs. S1 and S2). We also observed a reduction in branching (fig. S3) and in the percentage of neurons that extended neurites (fig. S1C). Taken together, these findings suggest that KLF4 acts independently of cell survival to suppress axon and dendrite initiation and elongation by hippocampal neurons in vitro.

We next asked whether KLF4 regulates axon growth of RGCs. KLF4 expression increased postnatally, both by microarray analysis (*19*) (Fig. 2A) and by quantitative reverse transcriptase–polymerase chain reaction (qRT-PCR; Fig. 2B) of acutely purified RGCs. We purified RGCs from E20 rats and transfected them with FLAG-tagged KLF4 (*24*) or a FLAG-only control. Overexpression of KLF4 in embryonic RGCs reduced the percentage of neurons extending neurites (Fig. 2E), reduced neurite branching (fig. S4), and reduced axon and, less so, dendrite lengths (Fig. 2, C and D). The average axon length of KLF4-transfected RGCs continued to increase over 3 days, but at a slower rate than control-transfected neurons (fig. S5), suggesting that KLF4 overexpression decreases elongation rate. Furthermore, truncated KLF4 that lacked a C-terminal DNA binding domain (fig. S2A) (*24*) had no effect on axon growth (Fig. 2, C and D). Thus, KLF4 suppresses axon growth in embryonic RGCs, and KLF4's DNA binding domain is required for its growth-suppressive activity.

We next tested whether knocking out KLF4 in developing RGCs enhances axon growth ability. Because KLF4-null mice die perinatally (*25*), we used a Cre/lox strategy to target KLF4 knockout to RGCs. Floxed-KLF4 mice (*26*) were crossed to ROSA-EYFP (enhanced yellow fluorescent protein) reporter mice and Thy-1–promoter Cre recombinase mice. About 50% of RGCs purified from Thy-1-cre/ROSA-EYFP mice were EYFP+ (fig. S6). There was no effect of transgenic Cre expression on RGC neurite growth, neurite initiation, or survival in vitro (figs. S7 and S8). To examine axon growth from KLF4-deficient RGCs in vitro, we purified RGCs from P12 Thy1-cre$^{+/-}$/KLF4$^{fl/fl}$/ROSA-EYFP^{+} ("KO") or Thy1-cre$^{-/-}$/KLF4$^{fl/fl}$/ROSA-EYFP^{+} ("WT") littermate mice and cultured them for 3 days (Fig. 3A). No effect of KLF4-KO was seen on survival (fig. S8). P12 KLF4-KO RGCs showed a statistically significant increase in neurite initiation compared to controls (Fig. 3B), mirroring our previous finding that overexpression of KLF4 decreases neurite initiation (Fig. 2E). We also observed a significant increase in neurite lengths in KLF4-KO RGCs (Fig. 3C). These data demonstrate that knocking out KLF4 enhances axon growth ability in P12 RGCs in vitro.

We next asked if knocking out KLF4 during development enhances regeneration from adult RGCs in vivo. Thy1-cre^{+}/KLF4$^{fl/fl}$ (KO), Thy1-cre^{+}/KLF4$^{fl/+}$ (Het), or Thy1-cre^{+}/KLF4$^{+/+}$ (WT) littermate mice were subjected to optic nerve crush, and after 2 weeks we assessed regeneration of RGC axons in the optic nerve. By adulthood, there were no differences in RGC number between KO, Het, and WT animals (fig. S9A). Compared to controls, however, KLF4 KO mice showed an increased number of regenerating axons at multiple distances from the injury site (Fig. 3, D and E). KLF4 KO did not affect RGC survival after injury (fig. S9B), showing that this increase in regenerating axons was not secondary to an increased RGC number. Thus, knocking out KLF4 expression during development increases the regenerative potential of adult RGCs.

Although knocking out KLF4 enhanced axon growth and regeneration, the size of the effect led us to speculate that other KLF family members might compensate for the loss of KLF4. The KLF family comprises 17 related transcription factors with homologous DNA binding domains and divergent activation and repression domains (*27*). KLFs often regulate gene expression interactively, with both cooperative and competitive relationships among family members (*28*–*30*). Our microarray data suggested that many KLFs are expressed by RGCs (*19*) and that some are developmentally regulated (fig. S10). We reprofiled the expression of all 17 KLF family members in developing RGCs by RT-PCR and detected transcripts for 15 (Fig. 4E). Furthermore, qRT-PCR revealed that KLF6 and KLF7 transcripts decrease more than 10-fold, whereas KLF9 increases more than 250-fold (Fig. 4, A to C). Thus, expression of multiple KLFs is regulated in developing RGCs.

Do other KLF family members also regulate neurite growth? Other KLFs can affect neurite branching in response to thyroid hormone (KLF9) (*31*) or neurite outgrowth in zebrafish retinal explants (KLF6 and -7) (*32*). In RGCs, overexpression of KLF9 significantly decreased growth, similar to KLF4, and KLF6 and -7 increased neurite growth 13 and 23%, respectively (Fig. 4D). We comprehensively surveyed all 17 KLF family members' effects on neurite growth in cortical neurons in vitro, and found that although no KLFs affected cell survival (fig. S11), eight KLFs, including KLF4 and -9, suppressed neurite growth, and KLF6 and -7 again significantly increased neurite growth, 35 and 60%, respectively (Fig. 4E). As with KLF4, effects on neurite growth depended on the DNA binding domain (figs. S12 and S13). Clustering KLFs by sequence similarity revealed an association between functional domains (*27*) and effects on neurite outgrowth (Fig. 4E). For instance, overexpression of the BTEB cluster and the cluster containing KLF4 (orange and pink bars, respectively, Fig. 4E) decreased neurite growth. The TIEG and PVALS/T (*33*)–containing clusters (blue and green bars, Fig. 4E) had no effect on neurite length. KLF6 and KLF7, with 85% homologous activation domains, both increased neurite length (yellow bars, Fig. 4E). To explore coordinate regulation of neurite growth by KLFs, we coexpressed all two-way combinations of KLFs -4, -6, -7, and -9 in cortical neurons. The negative effects of KLF4 on neurite growth were dominant over the otherwise positive effects of KLF6 or -7; the negative effects of KLF9 summed with those of KLF6 or -7 to no net effect (Fig. 4F), suggesting a complexity to KLF-KLF interactions in regulating neurite growth. Thus, during development, RGCs down-regulate at least two growth-enhancing KLFs (KLF6 and -7), and up-regulate at least two growth-suppressive KLFs (KLF4 and -9), which may be dominant in their effect over KLF6 and -7.

These findings that the KLF family of transcription factors regulates axon growth in a number of CNS neurons have important implications. First, although KLF4 has been implicated in a wide variety of cellular events including differentiation (*34*, *35*), cancer progression (*36*–*38*), and stem cell reprogramming (*39*), this function for KLF4 in postmitotic neurons advances our knowledge of the transcriptional regulation of axon regeneration. KLF4 targets relevant for regeneration may include genes selectively expressed in neurons or important in growth cone function. Second, the clustering of KLF gene function according to domain homology may provide a key for understanding how KLFs cooperate and compete to determine cellular phenotype, whether for axon regeneration or for other systems (*27*). Third, the decrease in RGCs' intrinsic axon growth ability (*6*) parallels changes in expression within the KLF family: Postnatal RGCs express higher levels of axon growth-suppressing KLFs and lower levels of axon growth-enhancing KLFs; similar changes can be found in published corticospinal motor neuron data (*40*). Thus, manipulating multiple KLF genes may be a useful strategy to add to existing approaches to increase the intrinsic regenerative capacity of mature CNS neurons damaged by injury or disease.

References and Notes

1. J. Nicholls, N. Saunders, *Trends Neurosci.* **19**, 229 (1996).
2. D. F. Chen, S. Jhaveri, G. E. Schneider, *Proc. Natl. Acad. Sci. U.S.A.* **92**, 7287 (1995).
3. B. S. Bregman, E. Kunkel-Bagden, M. McAtee, A. O'Neill, *J. Comp. Neurol.* **282**, 355 (1989).
4. G. Yiu, Z. He, *Nat. Rev. Neurosci.* **7**, 617 (2006).
5. L. C. Case, M. Tessier-Lavigne, *Curr. Biol.* **15**, R749 (2005).
6. J. L. Goldberg, M. P. Klassen, Y. Hua, B. A. Barres, *Science* **296**, 1860 (2002).
7. M. Blackmore, P. C. Letourneau, *J. Neurobiol.* **66**, 348 (2006).
8. I. Dusart, M. S. Airaksinen, C. Sotelo, *J. Neurosci.* **17**, 3710 (1997).
9. L. Bouslama-Oueghlani, R. Wehrle, C. Sotelo, I. Dusart, *J. Neurosci.* **23**, 8318 (2003).
10. D. Li, P. M. Field, G. Raisman, *Eur. J. Neurosci.* **7**, 1164 (1995).
11. D. Cai *et al.*, *J. Neurosci.* **21**, 4731 (2001).
12. Y. Gao *et al.*, *Neuron* **44**, 609 (2004).
13. D. F. Chen, G. E. Schneider, J. C. Martinou, S. Tonegawa, *Nature* **385**, 434 (1997).
14. K. S. Cho *et al.*, *J. Cell Sci.* **118**, 863 (2005).
15. M. Lehmann *et al.*, *J. Neurosci.* **19**, 7537 (1999).
16. Y. Konishi, J. Stegmuller, T. Matsuda, S. Bonni, A. Bonni, *Science* **303**, 1026 (2004).
17. A. Lasorella *et al.*, *Nature* **442**, 471 (2006).
18. K. K. Park *et al.*, *Science* **322**, 963 (2008).
19. J. T. Wang *et al.*, *J. Neurosci.* **27**, 8593 (2007).
20. W. J. Buchser, J. R. Pardinas, Y. Shi, J. L. Bixby, V. P. Lemmon, *Biotechniques* **41**, 619 (2006).
21. S. Zhu, C. Tai, B. A. MacVicar, W. Jia, M. S. Cynader, *Brain Res.* **1250**, 49 (2009).
22. A. M. Ghaleb, J. P. Katz, K. H. Kaestner, J. X. Du, V. W. Yang, *Oncogene* **26**, 2365 (2007).
23. E. G. Hagos, A. M. Ghaleb, W. B. Dalton, A. B. Bialkowska, V. W. Yang, *Oncogene* **28**, 1197 (2009).
24. W. Zhang *et al.*, *Mol. Cell. Biol.* **26**, 2055 (2006).
25. J. A. Segre, C. Bauer, E. Fuchs, *Nat. Genet.* **22**, 356 (1999).
26. J. P. Katz *et al.*, *Development* **129**, 2619 (2002).
27. J. Kaczynski, T. Cook, R. Urrutia, *Genome Biol.* **4**, 206 (2003).
28. J. Jiang *et al.*, *Nat. Cell Biol.* **10**, 353 (2008).
29. S. A. Eaton *et al.*, *J. Biol. Chem.* **283**, 26937 (2008).
30. D. T. Dang, W. Zhao, C. S. Mahatan, D. E. Geiman, V. W. Yang, *Nucleic Acids Res.* **30**, 2736 (2002).
31. C. Cayrou, R. J. Denver, J. Puymirat, *Endocrinology* **143**, 2242 (2002).
32. M. B. Veldman, M. A. Bemben, R. C. Thompson, D. Goldman, *Dev. Biol.* **312**, 596 (2007).
33. Abbreviations for the amino acid residues are as follows: A, Ala; E, Glu; G, Gly; I, Ile; L, Leu; P, Pro; S, Ser; T, Thr; and V, Val.
34. A. M. Ghaleb *et al.*, *Cell Res.* **15**, 92 (2005).
35. X. Dai, J. A. Segre, *Curr. Opin. Genet. Dev.* **14**, 485 (2004).
36. B. D. Rowland, D. S. Peeper, *Nat. Rev. Cancer* **6**, 11 (2006).
37. S. Safe, M. Abdelrahim, *Eur. J. Cancer* **41**, 2438 (2005).
38. A. R. Black, J. D. Black, J. Azizkhan-Clifford, *J. Cell. Physiol.* **188**, 143 (2001).
39. R. Zhao, G. Q. Daley, *J. Cell. Biochem.* **105**, 949 (2008).
40. P. Arlotta *et al.*, *Neuron* **45**, 207 (2005).

41. This work was funded by a National Eye Institute (NEI) R03 grant (EY016790, J.L.G.) and subsequently by a National Institute of Neurological Disorders and Stroke (NINDS) R01 grant (NS061348, J.L.G.) and critical funding from The Glaucoma Foundation and the Seigal Foundation (J.L.G.), the C. H. Neilsen Foundation (V.P.L. and J.L.G.), the Ralph Wilson Medical Research Foundation and the W.G. Ross Foundation (V.P.L.), The Buoniconti Fund to Cure Paralysis (V.P.L. and J.L.B.), an NEI P30 grant (EY014801), and an unrestricted grant from Research to Prevent Blindness to the University of Miami. D.L.M. is a Lois Pope LIFE Fellow, with support from NINDS training grants T32 NS07492 and T32 NS007459. We are indebted for generous gifts of FLAG-tagged KLF4 (C. Liu, University of Texas), mCherry (R. Tsien, University of California, San Diego), and KLF2 constructs (J. Lingrel, University of Cincinnati). We are grateful to W. Feuer (University of Miami) for statistical contributions and to R. Corredor (University of Miami) for optimizing RGC electroporation. We thank the following lab members and collaborators for their meaningful contributions: Ne. Patel, Ni. Patel, J. Gallardo, N. Sharifai, E. Walford, M. Velarde, A. Sloan, M. Benny, A. Oliva, Y. Shi, E. Hernandez, G. Lambert, and G. Gaidosh. The authors declare they have no conflicts of interest.

Supporting Online Material

www.sciencemag.org/cgi/content/full/326/5950/298/DC1
Materials and Methods
Figs. S1 to S13
References

1 May 2009; accepted 10 August 2009
10.1126/science.1175737

CUTTING EDGE CANCER SCIENCE

An AACR Special Conference on

CANCER EPIGENETICS

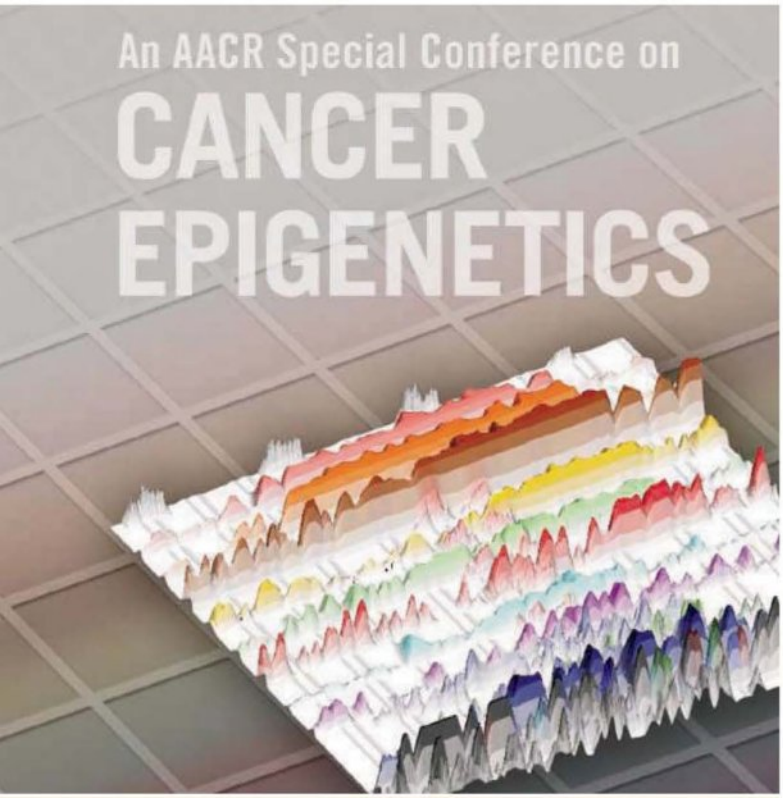

January 20-23, 2010
Caribe Hilton • San Juan, Puerto Rico

Conference Chairpersons:
Jean-Pierre J. Issa, UT M. D. Anderson Cancer Center, Houston, TX
Peter W. Laird, USC/Norris Comprehensive Cancer Center, Los Angeles, CA
Kornelia Polyak, Dana-Farber Cancer Institute, Boston, MA

ABOUT THE CONFERENCE:

This Special Conference will focus on the research being done at the interface of cancer epigenetics and cancer stem cells.

Topics will include:
- Epigenetics of Stemness and Differentiation
- Cancer Epigenomes
- Clinical Implications
- Epigenetic Therapies
- Environmental Effects on the Epigenome
- Interactive Workshop on Bioinformatics

Abstract Submission and Award Application Deadline: **Nov. 16**
Early Registration Deadline: **Nov. 2**

AACR American Association for Cancer Research

101st ANNUAL MEETING 2010

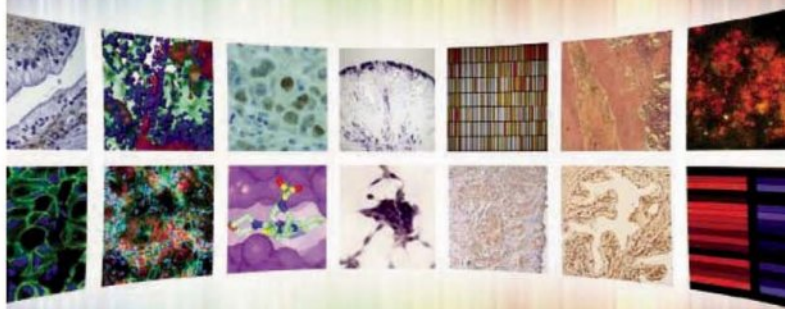

April 17-21, 2010
Walter E. Washington Convention Center
Washington, DC

Program Chairperson:
Frank McCormick, Director, UCSF Cancer Center

Abstract Deadline: December 1, 2009

Become an AACR Member and save on registration and other exclusive benefits!

For more information on these and other AACR meetings, visit www.aacr.org/meetingcalendar

AACR American Association for Cancer Research

EPIGENETICS:

THE FINAL FRONTIER?

Epigenetics is hot. In recent years, researchers in fields as diverse as cell biology, development, and even microbial pathogenesis have become very interested in heritable traits that don't rely on DNA. The idea itself is not new—cancer biologists have known for decades that mechanisms such as DNA methylation and chromatin modification can transmit changes to subsequent generations of cells without changing DNA sequences—but studying these phenomena has recently been increasing in popularity, aided by new technological innovations. **By Alan Dove**

Scientists who had never pondered epigenetics are now anxious to understand how it affects their favorite processes. Ironically, one of the major drivers of this newfound interest in non-DNA mechanisms was the complete sequencing of human DNA.

"It became clear from the human genome project that humans have about 25,000 or 26,000 genes, and that clearly didn't account for all the complexity that was present; they expected maybe 100,000 genes based on different types of proteins," says John Archdeacon, director of research and development for antibodies and amino acids at **Millipore** in Billerica, Massachusetts. Epigenetics is one way biology generates so many outcomes with so few genes.

Researchers have discovered three major ways organisms alter their DNA's inherited messages: small RNAs can modify the expression of specific genes, enzymes can methylate DNA to modulate transcription, and histone modification can induce or repress target sequences.

Small RNAs spawned an entire industry of user-friendly assays almost immediately after their discovery, but understanding DNA methylation or protein-DNA interactions requires more specialized techniques that can be tricky for the uninitiated. As a small sampling of tool makers reveals, companies are now trying to address these problems with a new generation of kits, reagents, and equipment to simplify epigenetic assays.

Challenges and Solutions

One way or another, researchers who want to study DNA methylation patterns must confront a technique called bisulfite conversion. Bisulfite treatment of DNA changes unmethylated cytosine residues to uracil, but leaves methylated cytosines unchanged. Assays such as sequencing, quantitative PCR, and microarrays can then compare the sequences of treated and untreated DNA to determine which bases were methylated.

Though conceptually simple, bisulfite treatment has a reputation for difficulty. "If you interview everyone who has done it, they all say it's not easy to do," says Xiao Zeng, director of R&D at **SA Biosciences** in Frederick, Maryland. He adds that "part of the problem we have encountered is the recovery; essentially you're going to lose about 50 percent of your input DNA after bisulfite treatment."

The DNA that remains after the procedure isn't in great shape, either. "Another problem that goes along with bisulfite conversion is the degradation of DNA due to the harsh conditions during the bisulfite treatment. Fragmentation of DNA lowers the sensitivity in PCR and subsequent analytical techniques," says Gerald Schock, senior global product manager for epigenetics and whole genome amplification at **Qiagen** in Hilden, Germany. Schock adds that incomplete removal of continued >

"Epigenetics is one way biology generates so many outcomes with so few genes."

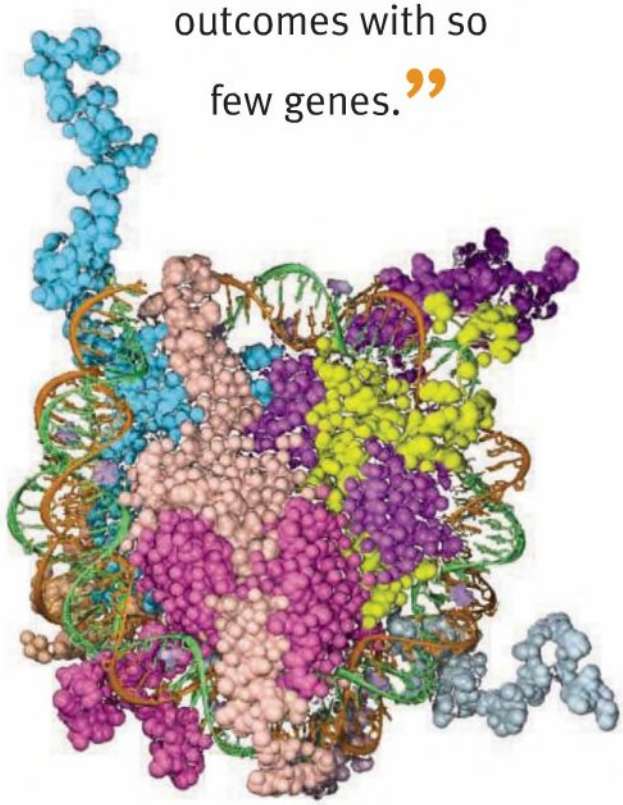

CREDIT: ISTOCKPHOTO.COM/THEASIS

Look for these **Upcoming** Articles

RNAi — October 16

Genomics 2: Microarrays — November 27

High Content Screening — February 19

Inclusion of companies in this article does not indicate endorsement by either AAAS or Science, *nor is it meant to imply that their products or services are superior to those of other companies.*

> "One way or another, researchers who want to study DNA methylation patterns must confront a technique called bisulfite conversion."

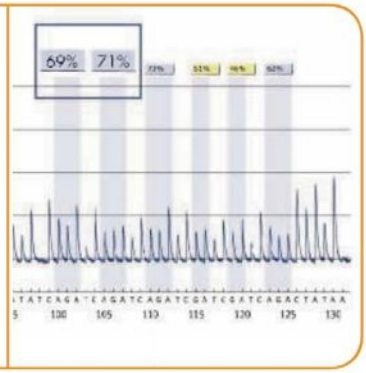

the reagents after conversion makes things even worse, as the DNA continues to break down during storage.

Unsurprisingly, Qiagen is one of the companies trying to address these problems. The company now offers a series of kits and reagents under the EpiTect name, covering every step of the bisulfite conversion process. The product line also includes important controls. "For example, when performing methylation-specific PCR, one must ensure that the PCR primers are specific for the detection of bisulfite-converted methylated or unmethylated DNA only," says Schock, adding that "EpiTect Control DNAs offer quality controlled pre-bisulfite-converted DNA derived from completely unmethylated or completely methylated DNA, which is suited for the analysis of any gene."

While every manufacturer claims its own bisulfite-conversion products are the best, Schock recommends asking pointed questions when shopping. For example, efficient bisulfite conversion is crucial. "Reliable results can only be achieved if complete conversion of all unmethylated CpG sites is ensured. One should ask for data on the conversion efficiency to be sure that the method chosen can accomplish that," says Schock.

Besides efficient CpG conversion, investigators may want to aim for efficient time management. Traditional bisulfite conversion involves overnight incubations, which add days to the already time-intensive procedure. Some reagent kits, such as the Methylcode product from **Life Technologies** (previously Invitrogen) in Carlsbad, California, can shorten these long incubations and speed the procedure considerably.

Newcomers to bisulfite conversion may also want to limit the number of variables by buying the key reagents rather than homebrewing them. "I would encourage customers to start with kits as much as possible for sample preparation as well as for sample analysis. The value to a customer in doing that is that they will be using validated reagents that have been optimized for these protocols and will have more consistent results," says Sallie Cassel, director of marketing for antibodies and immunoassays at Millipore.

Cassel also reiterates a simple but often ignored bit of laboratory wisdom: "Use controls." She adds that "a lot of times people think that they don't need them, but they can be very helpful."

Evasive Maneuvers

Given the inconvenience of bisulfite conversion, it's not surprising that many groups have developed ways to reduce or eliminate the need for it. At Life Technologies, for example, product developers have focused on simplifying the population of DNA in a sample to improve bisulfite conversion efficiency. The approach is especially useful for researchers doing genomewide methylation profiling.

"For these genomewide studies, you can actually pare down the number of sequences you need to look at—we've taken an approach of using a methyl binding domain protein," says Amy Cuneo, product manager for epigenetics at Life Technologies. The protein specifically binds methylated double-stranded DNA, separating it from the rest of the sample so it can be bisulfite-treated more efficiently.

Life Technologies' Carlsbad neighbor, **Active Motif**, takes the concept a step further. The company's MethylCollector Ultra kit uses two different methyl binding domain proteins to enrich for methylated DNA from samples, while its UnMethylCollector kit uses another isoform to pull out DNA with unmethylated CpG islands.

Active Motif says that the efficiency of the two kits is enough to get detailed methylation profiles from samples as small as 1,600 cells. Even better, researchers can perform PCR directly on the enriched samples to determine which sites are methlyated, without bisulfite conversion. Bart Challis, Active Motif's director of operations says, "Because of their ease of use and high specificities for methylated and unmethylated DNA, these complementary technologies can be used in combination to quickly and accurately perform DNA methylation analysis before proceeding with other, more costly downstream techniques."

Others are also keen to drive around the bisulfite problem. "We started with the pain," says SA Biosciences' Zeng. He explains that "we ourselves tried bisulfite treatment of DNA, and we realized it was very difficult, so then we looked at other technologies, such as enzymes."

In SA Biosciences' Methyl Profiler PCR system, the first step is not bisulfite conversion, but enzyme digestion. Splitting a DNA sample into two batches, then treating one with methylation-sensitive enzymes and the other with methylation-resistant enzymes, yields different fragment profiles that identify the methylation pattern in the original sample. "So essentially those two enzymes can recognize similar restriction sites, for example CGCG, but one of the enzymes will not cut if the C is methylated, but the other will," Zeng explains.

The Methyl Profiler system is designed for medium throughput, not whole-genome assays. Researchers who want to study the methylation status of specific subsets of promoters are the target market. "If they know their biology and they know there's a certain biological pathway involved in whatever system they study, they can do a panel of 24 genes or 96 genes in one shot," says Zeng, adding that "we want our customers to focus on their biology instead of the technology itself."

Not everyone is convinced that bisulfite conversion is so tough, though. "Just like swimming or bicycling, if you know how to do that, it's very normal, but if you're new, you need to learn. It's like this in epigenetics," says Larry Jia, founder and director of research and development at **Zymo Research** in Orange, California. He adds, "If you get into it and use it, it's pretty robust actually, so it depends on who defines whether it's easy or hard. Once you pick it up, it's not that bad at all."

Jia advocates starting with a kit and plenty of practice to learn traditional bisulfite conversion, rather than trying to work around it. "Antibodies, enzymes, other things—you can use them, but it's only indirect," he says.

continued >

CREDIT: © QIAGEN

Regardless of whether they choose practice or avoidance, researchers should plan their methylation studies with the entire procedure in mind, including the final assay. "There [are] performance differences and protocol differences, but you know looking at an entire workflow is probably one of the biggest questions that researchers would have when they're starting out. How are they going to read out their information and [make] sure that the tools work with their workflow?" says Cuneo.

> "For genomewide studies, you can actually pare down the number of sequences you need to look at—we've taken an approach of using methyl binding domain protein."

Application of ChIP

While methylation is an important component of epigenetic regulation, it certainly isn't the only way genomic information gets modified. To probe one of the other major epigenetic mechanisms, histone modification, researchers often turn to chromatin immunoprecipitation, or ChIP.

In a typical ChIP experiment, an investigator uses antibodies to precipitate modified and unmodified histones, along with all of the chromatin pieces that associate with them. Gene chips or PCR can then reveal the sequences in the precipitate, identifying the target histone modification sites in the genome. The technique can also coprecipitate histone-modifying enzymes for further analysis.

ChIP is relatively straightforward, but it has a few pitfalls. In particular, precipitating enough DNA for detection often means using a lot of cells, which may not be possible for some studies. For example, investigators working with difficult-to-culture stem cells or precious human biopsy samples may not be able to spare enough to perform a ChIP assay.

In response, companies have developed reagents for ChIP on smaller samples. Life Technologies, for example, recently introduced the MAGnify kit, which uses a version of the popular Dynabead magnetic precipitation system. "What we've done is to take one of the most widely published products, the Dynabeads protein A/G that are used in ChIP, and really optimized a kit that includes all the buffers and other reagents that are needed," Cuneo explains.

Instead of requiring a million cells, MAGnify kits can produce useful results from as few as 10,000 cells. The protocol also shortens the ChIP procedure by a day, and eliminates the use of blocking DNA that can contaminate the sample. "Using the Dynabeads eliminates any need for blockers that contain, for example, salmon sperm DNA [for assays where] you really need to avoid background at all cost," says Cuneo.

Other manufacturers also cater to the burgeoning ChIP market, of course, but nearly everyone cautions that no kit is foolproof. In particular, researchers need to be sure that they use suitable antibodies. Even a highly specific antibody may not be enough, if it hasn't been validated specifically for ChIP. Antibodies that work well on a denatured protein in a Western blot may not recognize their target at all in its native chromatin-binding conformation.

Worse, not every antibody that has been tested in one lab's ChIP assay will work in another lab. "Oftentimes [researchers] may have an antibody and somewhere in some paper somebody said that it works in ChIP," says Millipore's Cassel, adding that "that antibody, that lot, that vial that a customer gets may be very remotely related at best to that paper, and so the results may not be directly correlative." In response, companies such as Millipore now validate every lot of ChIP antibodies before selling it.

With a proven protocol and a validated antibody in hand, the next challenge is to figure out whether a target protein is abundant enough to precipitate. According to Millipore's Archdeacon, unmodified histones or those with common modifications may be easy to detect, but rarer proteins might not produce enough material to detect, even with a good antibody.

After the ChIP procedure, investigators need to identify the precipitated sequences, which usually means analyzing the sample with either a DNA microarray or quantitative PCR. Each approach has its adherents.

At Millipore, which recently announced a collaboration with chip maker Agilent, the emphasis is now on ChIP followed by DNA microarray analysis, or ChIP-chip. "We will have products in which we have partnered with Agilent to provide Agilent arrays and reagents in the kit for a total solution," says Cassel, adding that the new Millipore/Agilent kits should be on the market by late 2009.

For researchers who don't need a whole-genome view of a microarray, ChIP-qPCR may make more sense, especially for studying rare binding proteins. "The dynamic linear range for [microarrays] is about 5 logs less than real time PCR," says Jeffrey Hung, director of marketing at SA Biosciences, adding that "you can imagine that if you have a low abundance transcript, the real-time PCR-based technology can detect both the low abundance and the high abundance DNA fragments that associate with certain ChIP samples."

Regardless of the specific techniques they choose, researchers will find plenty of interesting questions to answer in epigenetics. "I think it might be the last great frontier in biology," says Zymo's Jia. He adds, "We understand genes and proteins and we can sequence genomes. The next thing in biology we ask is how do genomes organize. How is it working?"

Featured Participants

Active Motif
www.activemotif.com

Life Technologies
www.lifetechnologies.com

Millipore
www.millipore.com

Qiagen
www.qiagen.com

SA Biosciences
www.sabiosciences.com

Zymo Research
www.zymoresearch.com

Alan Dove is a science writer and editor based in Massachusetts.

DOI: 10.1126/science.opms.p0900038

New Products

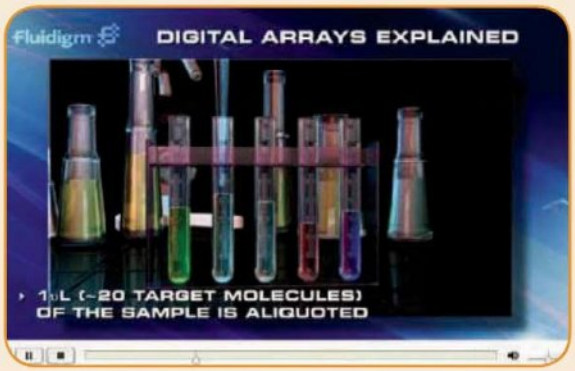

Digital PCR Array

The 48.77 Digital Array chip is an integrated fluidic circuit (IFC) capable of testing up to 48 samples at a time and automatically partitioning each of the samples into separate sets of 770 reaction chambers—delivering a total of 36,960 simultaneous digital polymerase chain reaction (PCR) reactions. Digital PCR is a technique to quantify the amount of nucleic acid in a sample, typically by counting amplifications from single molecules. Digital PCR offers high resolution for copy number variation experiments, improved selectivity to enhance mutation detection, and absolute molecule quantification.

Fluidigm Europe
For information +33-44-259-3861
www.fluidigm.com

DNA Methylation Assays

MethylCollector Ultra is a DNA methylation assay for the enrichment of CpG-methylated DNA. The kit makes use of a combination of methyl-binding protein MBD2b with its binding partner MBD3L1 to generate higher affinity for CpG-methylated DNA than antibody-based immunoprecipitation methods. The UnMethylCollector Kit is a novel DNA methylation assay for the specific isolation and enrichment of unmethylated CpG islands. UnMethylCollector makes it possible to identify hypomethylated promoters or to study the effects of compounds that inhibit methylation. Both assays make use of a fast, magnetic bead–based protocol that r equires minimal starting material and can be completed in less than three hours.

Active Motif
For information 877-222-9543
www.activemotif.com

Cell Dissociation

FACSmax is a gentle and effective cell dissociation solution. A proprietary formulation of proteolytic, collagenolytic, and deoxyribonuclease enzymes, it is effective in creating single-cell suspensions from clumped cell cultures, which enables accurate, reproducible cell counting, flow cytometry, viral transfection assays, cell sorting, and bioreactor scale-up. FACSmax solution gently dissociates clumped cells in minutes, resulting in homogeneous single-cell suspensions with maximum cell viability. It eliminates the need for extra washing steps.

AMS Biotechnology
For information +44-1235-828200
www.amsbio.com

DNA Shearing

SonicMan is a high throughput, multiprobe sonication instrument that is configurable in 96-well, 384-well, and 1,536-well formats. SonicMan makes use of disposable pin lids to transfer sonic energy to each individual well and to prevent well-to-well cross-contamination. The sonicator can shear 96 samples to smears with nothing above 250 base pairs in four hours. Fragment size is correlated with sonication settings of power and time, which can be controlled by the user. Fragments centered around a desired length can be repeatedly generated in seconds. Samples can be sonicated in volumes ranging from 25 µl to 1.5 ml per well. Unlike fragments produced by enzyme-based digestion, the random fragments generated are suitable for the sequencing of large genomes.

Process Analysis and Automation
For information +44-1252-373000
www.paa.co.uk

Cellular Assays

The BioFlux 1000 Workstation is a cell analysis system that integrates Well Plate Microfluidic technology with automated microscopy for high throughput shear flow assays. The workstation provides unattended operation with integrated microscopy and an automated stage that enables fast scanning of the BioFlux plates. BioFlux systems are designed to bridge the gap between in vitro and in vivo experiments by enabling physiologically relevant shear flow assays in a standard well-plate format under conditions that mimic those in the human body. This approach delivers a high content data set to ensure that only the most promising compounds move forward into animal and clinical trials. The BioFlux Controller delivers programmable shear flow to the plates while the Fluxion Montage software provides analysis and single-point control of all system components. Applications include research in cell and platelet adhesion, cancer biology, microbiology, and biofilms.

Fluxion
For information 650-241-4740
www.fluxionbio.com

RNA Extraction

A new kit for the extraction of high-quality RNA from formalin-fixed, paraffin-embedded (FFPE) tissues can be applied not only to polymerase chain reaction but also microarray applications. Traditional methods of formalin-fixation of tissues often result in severe RNA fragmentation and cross-linking, which impairs RNA solubilization and template activity in reverse transcription and subsequent downstream analysis. The new ExpressArt FFPE RNA-ready kit is optimized for isolation of total RNA from archival, formalin, or FFPE tissues and results in a concentrated, ready-to-use RNA product. Through special lysis and incubation conditions, the kit's technology is able to extract high-quality RNA and amplify very small amounts and degraded RNA.

AMS Biotechnology
For information +44-1235-828200
www.amsbio.com

Electronically submit your new product description or product literature information! Go to **www.sciencemag.org/products/newproducts.dtl** for more information.

Newly offered instrumentation, apparatus, and laboratory materials of interest to researchers in all disciplines in academic, industrial, and governmental organizations are featured in this space. Emphasis is given to purpose, chief characteristics, and availabilty of products and materials. Endorsement by *Science* or AAAS of any products or materials mentioned is not implied. Additional information may be obtained from the manufacturer or supplier.

POSITIONS OPEN

MICHIGAN STATE UNIVERSITY

TENURE-TRACK FACULTY POSITION in "Biochemistry of Photosynthetic Organisms" Department of Biochemistry and Molecular Biology

The Department of Biochemistry and Molecular Biology at Michigan State University seeks to recruit an **ASSISTANT PROFESSOR** to study any aspect of primary or secondary metabolism in photosynthetic model organisms, including plants, algae, or photosynthetic bacteria. Applications from individuals whose work integrates biochemical, genetic, physiological, genomic, or systems biological approaches are especially encouraged. A broad range of specific topics will be considered that enhance MSU's excellence in plant biochemistry (**website: http://www.bch.msu.edu/research/plant/plant.htm**) and complement our parallel search for a senior professor in the area of photosynthetic energy capture. The successful candidate will be expected to develop a vigorous, independent research program supported by extramural funding and contribute to undergraduate and graduate teaching. Michigan State University has a large and vibrant community of plant biologists, has state-of-the-art analytical core facilities, and co-leads the Great Lakes Bioenergy Research Center. Applications should include: cover letter, curriculum vitae, statement of research interests and future directions, and three or more letters of reference. Application materials should be sent electronically to **e-mail: plantbiochem@cns.msu.edu.**

Review of application materials will begin on December 1, 2009, and continue until a suitable applicant is identified. Questions regarding this position may be sent to **Christoph Benning, Chair, Search Committee, e-mail: benning@msu.edu.**

Michigan State University is an Affirmative Action, Equal Opportunity Employer. MSU is committed to achieving excellence through cultural diversity. The University actively encourages applications and/or nominations of women, persons of color, veterans, and persons with disabilities.

ASSISTANT PROFESSOR OF CHEMISTRY University of Wisconsin–Madison

The Department of Chemistry of the University of Wisconsin–Madison anticipates an opening for a faculty position to begin in August 2010. We seek outstanding candidates at the Assistant Professor level (tenure track) in all areas of chemistry including chemical education. Candidates must have a Ph.D. in chemistry or a related field; postdoctoral experience is desirable. The position requires development of an internationally recognized program of scholarly research as well as excellent teaching at both the undergraduate and graduate levels. Please submit curriculum vitae and concise description of research plans online at **website: http://www.facrecruit.chem.wisc.edu.** Three letters of recommendation will also be required through the online service directed to: **Chair, Faculty Search Committee, Department of Chemistry, University of Wisconsin–Madison, 1101 University Avenue, Madison, WI 53706-1322.** To guarantee full consideration, all materials must be received by November 25, 2009.

The University of Wisconsin is an Equal Opportunity Affirmative Action Employer; applications from qualified women and minority candidates are encouraged. Unless confidentiality is requested in writing, information regarding the identity of the applicant must be released on request. Finalists cannot be guaranteed confidentiality. A background check may be required prior to employment.

HUMBOLDT STATE UNIVERSITY Department of Fisheries Biology

Tenure-track **FACULTY POSITION** in freshwater fish ecology/salmonid biology. Ph.D. in fisheries biology or related discipline and expertise in freshwater fish ecology required. Fifty percent funded by National Marine Fisheries Service. Review: November 13, 2009. For more information, visit **website: http://apptrkr.com/127692.** *HSU is an Equal Opportunity/Title IX/ADA Employer.*

POSITIONS OPEN

CELLULAR ELECTROPHYSIOLOGY RESEARCH ASSOCIATE, Yale University.

Position available at Yale University School of Medicine, within multidisciplinary research group (molecular and cell biologists, biophysicists, physiologists, pharmacologists, pain physiologists) for a Cellular Electrophysiologist, at **POSTDOCTORAL** or **ASSOCIATE RESEARCH SCIENTIST** level. Incumbent will be expected to play a significant role in analysis of roles of ion channels in electrogenesis in normal and injured neurons. Ph.D. and/or M.D. degree and substantial experience with patch clamp, in voltage clamp and/or current clamp modes, is essential. Experience with cell transfections is desirable. Send statement of interest, curriculum vitae, and three letters of reference to: **Stephen G. Waxman, M.D., Ph.D., Director, Neuroscience and Regeneration Research Center, VA Connecticut (127A), 950 Campbell Avenue, West Haven, CT 06516. E-mail: stephen.waxman@yale.edu.** *Women and members of underrepresented minority groups are encouraged to apply. Affirmative Action/Equal Opportunity Employer.*

FACULTY POSITION in Environmental Microbiology

The Department of Civil and Environmental Engineering at Northwestern University invites applications for a tenure-track position in environmental microbiology. We seek outstanding candidates working on genomic approaches to complex microbial systems present in either the engineered or the natural environment. The successful candidate will be involved in cross-school initiatives between the Engineering, Science, and Medical Schools and should be eager to work in multidisciplinary collaborations.

Applicants should submit their application electronically as a single PDF document containing: a cover letter, curriculum vitae, a one-page summary of previous research contributions, a three-page description of plans for future work, a one- to two-page description of teaching interests, and a list of at least three persons who will write letters of recommendation. Application materials should be submitted to the Search Committee Chair via the **website: http://www.civil.northwestern.edu/employment/microbiology.html** or via **e-mail: a-levy@northwestern.edu.**

It is anticipated that this position will be filled at the junior level, but outstanding senior candidates with exceptional records are encouraged to apply. The Search Committee will start reviewing applications on November 15, 2009.

Northwestern University is an Affirmative Action Equal Opportunity Employer. Women and individuals in underrepresented groups are encouraged to apply. Hiring is contingent upon eligibility to work in the United States.

ASSISTANT, ASSOCIATE, FULL PROFESSOR Computational Biology and Bioinformatics

Applications are invited for a tenure-track position in computational biology in Cornell University's Computer Science Department. The position could be at the Assistant, Associate, or Full Professor level, depending on experience. Applicants must possess a Ph.D. in computer science, or a Ph.D. in a related field and sufficient expertise in computer science to fit within a computer science department. Outstanding applicants in all areas of computational biology will be considered, but research areas of special interest include evolutionary, comparative, and population genomics; applications of new high-throughput genomic or proteomic technologies; dynamical behavior at the subcellular and cellular levels; networks in biological systems; and applications of machine learning to biological problems. To ensure full consideration, applications should be received by December 15, 2009, but they will be accepted until the position is filled. Applicants should submit curriculum vitae and a research statement and should arrange to have three reference letters submitted, all at **website: http://www.cs.cornell.edu/apply.**

Positions @ NIH

THE NATIONAL INSTITUTES OF HEALTH

Department of Health and Human Services
National Institutes of Health
Intramural Research Programs
NCI, NEI, NHLBI, NIAID, NIDDK, NIMH, NINDS and CIT
Bethesda, MD

Tenure Track/Tenured Positions In Systems Biology

The NIH Intramural Research Program (IRP) is recruiting outstanding systems biologists at the tenure-track or tenured levels. These individuals will direct independent research programs on the NIH campus in Bethesda, MD and participate in a Trans-NIH Initiative in Systems Biology promoting interaction between experimentalists, theoreticians and computational investigators. Candidates will have demonstrated an ability to conduct outstanding independent biomedical research on key topics in systems biology such as computational modeling of biological processes at various scales, analysis ofglobal datasets, construction and analysis of biological networks, and 'omic' scale interrogation of biological systems. The internationally recognized NIH faculty covers a wide range of basic and clinical research topics with a growing strength, support and emphasis on systems biology and informatic approaches to biomedicine.

The NIH IRP promotes creative and innovative science unconstrained by the conventional support mechanisms demanded at academic or private research institutes. Investigators have ready access to and support from state-of-the art experimental and computational cores and facilities, and a variety of programs to recruit graduate students and post-doctoral fellows.

Candidates must have an M.D. and/or Ph.D., or equivalent doctoral degree, and an outstanding record of research accomplishment and peer-reviewed publications. Recruits will be provided a competitive salary commensurate with experience and qualifications, and will be assigned ample research space, supported positions, operating budget, and start-up funds. Appointees may be US citizens, resident aliens, or eligible foreign nationals. Review of applications will commence on Nov.1, 2009 and continue until the positions are filled. Please submit a curriculum vitae, brief (not to exceed 3 pages) statement of research interests that includes how you see your research group helping to create a world-class, integrated systems biology effort at NIH, and three letters of reference in .pdf or MS word format only (no paper applications will be accepted) to: **http://tenuretrack.nih.gov/apply/**

National Institutes of Health
National Institute of Arthritis and Musculoskeletal and Skin Diseases, Intramural Research Program

Tenured/Tenure-Track Investigator(s)

The Intramural Research Program of the National Institute of Arthritis and Musculoskeletal and Skin Diseases (NIAMS) of the National Institutes of Health (NIH) in the Department of Health and Human Services (DHHS) is recruiting outstanding tenure-track and/or senior (tenured) scientists (M.D., Ph.D, or M.D./Ph.D) active in any of the following areas relevant to musculoskeletal biology or diseases:

- Basic, Translational and Clinical Research in Orthopaedics, Bone, Cartilage, or Muscle
- Nanotechnology related to Bone, Cartilage, Tendon/Ligaments, or Muscle
- Biology of inducible pluripotent stem (iPS) and mesenchymal stem cells for the study of human disorders
- Biological/Tissue Engineering
- Regenerative Medicine

Emphasis will be placed on the applicants' demonstrated track record of high-quality research and the originality and promise of their future plans. Successful applicants will be expected to develop energetic, creative, independent research programs within an existing highly interactive scientific environment. The ideal candidate would benefit from pre-existing expertise within NIAMS.

This position(s) is located on the NIH campus in Bethesda, Maryland, a suburb of Washington, D.C. NIAMS and the NIH offer tremendous depth and breadth of intellectual and technological resources, as well as opportunities for collaboration with investigators both within and outside of the NIH. NIAMS is also a major user of the NIH Clinical Research Center, a state-of-the-art research hospital on the campus of the NIH in Bethesda, Maryland. The research environment is highly conducive to advancing basic and translational research and highly collaborative, encouraging multidisciplinary and interdisciplinary team science.

The mission of NIAMS is to support research into the causes, treatment, and prevention of arthritis and musculoskeletal and skin diseases, the training of basic and clinical scientists to carry out this research, and the dissemination of information on research progress in these diseases.

Applicants should submit a cover letter that includes a short research interest statement (two page maximum), a curriculum vitae and complete bibliography, along with complete contact information of three referees. Applications should be submitted by **February 1, 2010**.

Applications should be submitted to: **Mrs. Wanda White – RE: Musculoskeletal Initiative, Building 31 Room 4C-12, 9000 Rockville Pike, Bethesda MD 20892, Email: whitewan@mail.nih.gov**

THE NIH IS DEDICATED TO BUILDING A DIVERSE COMMUNITY IN ITS TRAINING AND EMPLOYMENT PROGRAMS

WWW.NIH.GOV

Tenure-Track/Tenured Investigator Laboratory of Immunology

The Laboratory of Immunology (LI), Division of Intramural Research, National Institute of Allergy and Infectious Diseases, National Institutes of Health (NIH) invites applications for a tenure-track/tenured investigator position in immunology. Applicants should have a Ph.D., M.D., or equivalent degree; an outstanding record of postdoctoral accomplishment; and an interest in any area of biomedical research related to immunology.

Specifically, we seek a highly creative individual who will establish an independent, world-class research program that takes full advantage of the special opportunities afforded by the stable, long-term funding of the intramural research program at NIH. She or he should be interested in developing and applying novel approaches to the study of problems of major biological and/or medical importance, which could include a significant clinical or translational effort in addition to bench research. In the former case, the successful candidate would have access to the NIH Clinical Center, a state-of-the-art research hospital on the NIH campus in Bethesda, MD, and ample opportunity to participate in the activities of theTrans-NIH Center for Human Immunology.

Generous ongoing support for salary, technical personnel, postdoctoral fellows, equipment, and research supplies will be provided. Available core or collaborative facilities include flow cytometry, advanced optical imaging, microarray generation and analysis, high throughput sequencing, computational biology, production of transgenic and gene-manipulated mice, biosafety level (BSL)-3 facilities, chemical genomics, and support for projects involving RNAi screening. The successful applicant will also have access to Trans-NIH initiatives involving technology development, translational investigation, and multidisciplinary science. In addition to an outstanding international postdoctoral community, a superior pool of graduate and undergraduate students is available to the successful applicant.

LI has a distinguished history of accomplishment in immunology. We strongly encourage application by outstanding investigators who can continue and enhance this record of achievement. Current LI investigators are Ronald Germain, Michael Lenardo, David Margulies, Stefan Muljo, William Paul, Ethan Shevach, and Tsan Xiao.

To apply, e-mail curriculum vitae, bibliography, and outline of a proposed research program (no more than two pages) to Ms. Yushekia Hill at NIAID.DIR.Search@niaid.nih.gov. In addition, three letters of reference must be sent directly from the referee to Drs. Giorgio Trinchieri and Dan Kastner, Co-Chairs, NIAID Search Committee, c/o Ms. Yushekia Hill, at NIAID.DIR.Search@niaid.nih.gov or 10 Center Drive, MSC 1356, Building 10, Room 4A22, Bethesda, MD 20892-1356. E-mail is preferred. Applications will be reviewed starting **11/16/09** and will be accepted until the position is filled. Please refer to ad #028 on all communications. For further information about this position, contact Dr. William Paul at 301-496-5046 or wpaul@niaid.nih.gov.

A full package of benefits (including retirement and health, life, and long-term care insurance) is available. Women and minorities are especially encouraged to apply. U.S. citizenship is not required.

NIAID

National Institute of Allergy and Infectious Diseases

To learn more about NIAID and how you can work in this exciting research organization, please visit us on the web at **www.niaid.nih.gov/careers/sti**.

U.S. DEPARTMENT OF HEALTH AND HUMAN SERVICES
National Institutes of Health

National Institute of Allergy and Infectious Diseases

Proud to be Equal Opportunity Employers

Kumamoto University

Location: Kumamoto, Japan

Open Recruitment of a Tenure-Track Assistant Professor

Kumamoto University is seeking for an outstanding young researcher as a specially appointed assistant professor. Sufficient research space in a fully equipped new building, research funds (¥ 2 million per year), start-up funds (¥ 5 million), as well as his/her own office, will be provided. A research assistant may also be assigned. After 4 years employment until March 2014, it will be evaluated whether he/she will be promoted to "Associate Professor", in addition to annual assessments.

Candidates with outstanding CVs and research interest in the following research fields will be considered: **Developmental and regenerative medicine, Translational research, Bioimaging, Systems biology, Stem cells, Cell differentiation, and Organogenesis**. The selected researcher can pursue his/her own research independently, while interacting with the closely located Institute of Molecular Embryology and Genetics (IMEG), and the global Center for Excellence (COE). Detailed information on the Institute and its activities can be found at: **http://www.imeg.kumamoto-u.ac.jp/en/index.html** and **http://www.g-coe.org/**

Application Deadline: October 30, 2009 (Friday).
Arrival: Between December 2009 and February 2010.
Employment: through March 2014.
Salary: Approximately ¥ 7 million per year
Applications: Applications should include curriculum vitae, academic achievements, 5 copies of main research papers, outline of the research and three references. Submit applications by mailing to: Research Cooperation Section, Kumamoto University, Kurokami 2-39-1, Kumamoto City, Kumamoto Prefecture, 860-8555 (Application is not acceptable through our web site)
Inquiries: **k-senryaku@jimu.kumamoto-u.ac.jp**
Detailed information: **http://sendou.kuma-u.jp/en/recruitment/index.html**

MAX-PLANCK-INSTITUT FÜR BIOPHYSIKALISCHE CHEMIE
KARL-FRIEDRICH-BONHOEFFER-INSTITUT
GÖTTINGEN

The Research Group "Sleep and Waking" at the Max Planck Institute for Biophysical Chemistry invites applications of prospective

Graduate/PhD Students and Postdoc Positions
(Code Number 29-09)

Ultimate goal of the lab is to understand how a nervous system sleeps and why we need to sleep. The group is trying to understand the molecular, cellular and circuit principles of sleep. The lab has started investigating sleep in the nematode *C. elegans* and is interested in expanding the research onto other model organisms. The group is using behavioral assays combining genetics, microscopy of neural function and micromanipulation.

Candidates should be exceptionally talented and motivated and should have a strong scientific background. PhD students and Postdocs can be awarded a Max Planck Fellowship.

Applications should include a CV, a list of publications (if applicable) and letters of one to three references familiar with the work of the candidate. Please submit all materials in electronic form (preferably as one single PDF-file) **with reference to the code number via email to Henrik.Bringmann@mpibpc.mpg.de.**

Max Planck Institute for Biophysical Chemistry
RG „Sleep and Waking"
Dr. Henrik Bringmann
Code Number 29-09
Am Fassberg 11
37077 Göttingen
Germany

MAX PLANCK INSTITUTE FOR **HUMAN COGNITIVE AND BRAIN SCIENCES** LEIPZIG

The Max Planck Institute for Human Cognitive and Brain Sciences in Leipzig, Germany, Department of Cognitive Neurology (Head of Department: Prof. Dr. Arno Villringer) invites you to apply for

1 PostDoctoral position and 1 PhD position

The focus of these positions is on somatosensory plasticity in stroke rehabilitation in humans. You are part of multi-disciplinary group that aims to merge stimulation protocols (e.g., TMS, tDCS), cognitive tasks and drug administration to induce neuroplasticity as observed by electro-physiological methods and functional magnetic resonance imaging (alone AND in combination, e.g. fMRI-EEG). Candidates interested in clinical neuroscience, neuroplasticity, as well as in higher cognitive function and brain imaging are invited to apply. The successful candidates should be enthusiastic and will have a strong interest in this exciting research area.

A background in EEG, TMS or fMRI acquisition and analysis techniques (SPM, FSL, Matlab, BESA etc.) would be of advantage. The Max Planck Institute in Leipzig offers an excellent multi-disciplinary and interactive research environment with access to excellent research facilities (3T and 7T research MRI scanners, MEG, EEG and TMS/tDCS devices). The PostDoctoral position is funded for maximally 5 years and the PhD position for 3 years from now and will be held open until suitable candidates have been found.

For further details please contact Dr. Burkhard Pleger by email: bpleger@cbs.mpg.de or phone: +49 (0) 341-9940-135.

In order to increase the proportion of female staff members, female scientists are particularly encouraged. Disabled applicants are preferred if qualification is equal.

The closing date for applications is **31.10.2009.**

Please send your application including the name of referees by email (preferred) or post, citing the **code number "D3-09"** to:

Max-Planck-Institut für
Kognitions- und Neurowissenschaften
- Verwaltung -
Stephanstraße 1a, D-04103 Leipzig
www.cbs.mpg.de

MAX-PLANCK-GESELLSCHAFT

Human Genetics Professor

The NIH-supported Institute for Clinical & Translational Research (ICTR) – a partnership among the Schools of Medicine & Public Health, Pharmacy, Veterinary Medicine, Nursing, and the College of Engineering – invites applications from a PhD and/or MD with a proven record in research and extramural funding. This recruitment is the anchor for a Cluster Hire dedicated to human genetics research and its application to human disease.

This tenured genetics leader will develop a well-funded research program, working closely with ICTR on the rapid translation of genetics and genomics-based findings to advance early detection, diagnosis, and treatment of complex diseases. We welcome candidates with expertise in human genetics, genetic epidemiology, computational biology, and related fields. See complete details at **www.ictr.wisc.edu/employment**.

Send application materials, noting **PVL # 62591**, to:
Paulette Sacksteder, Administrative Director
UW-Madison ICTR, 4248 HSLC
750 Highland Avenue, Madison, WI 53705

The UW-Madison is an AA/EEO employer; Wisconsin open records and caregiver laws apply. A criminal background check will be conducted prior to an offer of employment.

UNIVERSITY OF WISCONSIN-MADISON

PICTURE YOURSELF AS A AAAS SCIENCE & TECHNOLOGY POLICY FELLOW

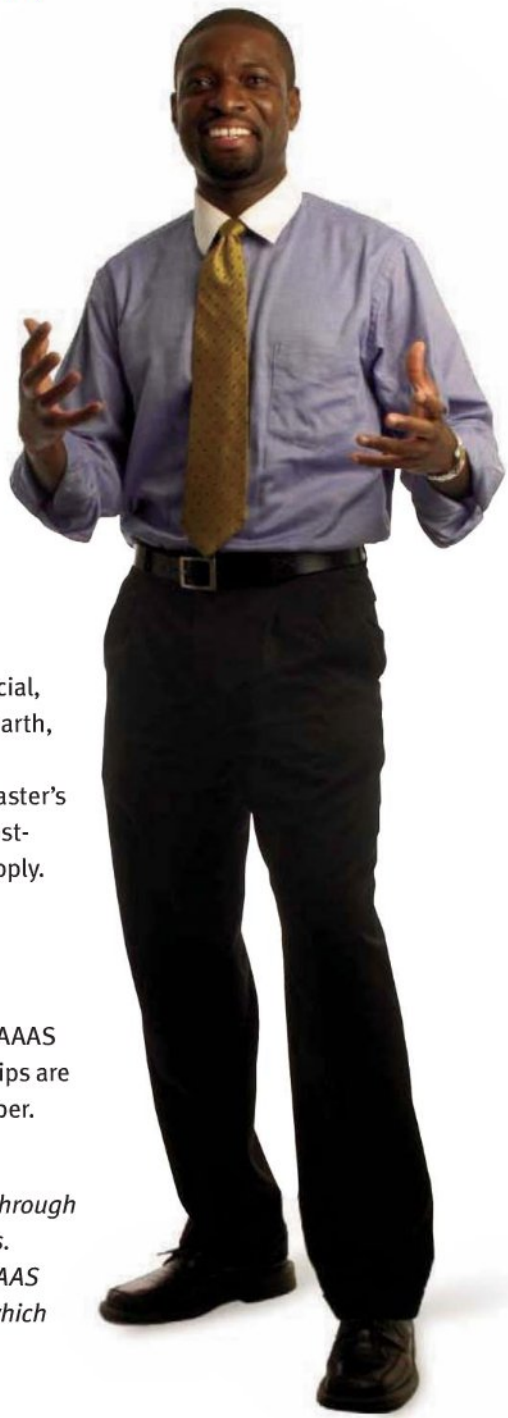

Make a Difference.
Help give science a greater voice in Washington, DC! Since 1973, AAAS Fellows have applied their skills to federal decision-making processes that affect people in the U.S. and around the world, while learning first-hand about the government and policymaking.

Join the Network.
Year-long fellowships are available in the U.S. Congress and federal agencies. Applicants must hold a PhD or equivalent doctoral-level degree in any behavioral/ social, biological, computational/ mathematical, earth, medical/health, or physical science, or any engineering discipline. Individuals with a master's degree in engineering and three years of post-degree professional experience also may apply. Federal employees are not eligible and U.S. citizenship is required.

Apply.
The application deadline for the 2010-2011 AAAS Fellowships is 15 December 2009. Fellowships are awarded in the spring and begin in September. Stipends range from $73,000 to $95,000.

Note: Additional fellowships are available through approximately 30 scientific society partners. Individuals are encouraged to apply with AAAS as well as with any scientific societies for which they qualify.

Full details at: **fellowships.aaas.org**

Enhancing Public Policy, Advancing Science Careers

Kwabena Yiadom, PhD

Chemistry, Georgetown University

2004-05 AAAS Fellow at the U.S. Department of Defense, International Technology Programs Office

Now an operational research analyst at the U.S. Department of Defense, Office of the Secretary of Defense

AAAS
ADVANCING SCIENCE, SERVING SOCIETY

UNIVERSITÉ DE SHERBROOKE

Professor in plant ecology

Faculté des sciences, Département de biologie
Offer no. 00473

FUNCTIONS

- Teaching at the undergraduate and graduate levels
- Research
- Graduate student supervision

REQUIREMENTS

- Doctoral degree and postdoctoral experience in plant ecology
- The ability to carry out a strong independent research program financed by external sources
- The ability to teach in French or to rapidly acquire this ability

Deadline is 5 PM on November 30th 2009.

Université de Sherbrooke values employment diversity, equality and equity within its community, and welcomes applications from any qualified persons, in particular women, members of visible and ethnic minorities, aboriginals and disabled persons.

Check our website for the full description of all our job opportunities, then submit your application online.

www.USherbrooke.ca/emplois

NDSU

Assistant/Associate Professor in Pharmacology

The Department of Pharmaceutical Sciences at North Dakota State University invites applications for a tenure-track faculty position at the rank of Assistant/Associate Professor, with appointment beginning on or after August 15, 2010. Candidates must hold a doctoral degree in pharmacology, physiology, or closely related field, have at least two years of postdoctoral experience with a strong record of scholarship, and possess good interpersonal skills and effective written and oral communication skills. Preference will be given to applicants with training and research expertise in areas that complement existing departmental strengths in cancer, cardiovascular, and vaccine research. The successful candidate will be expected to establish an externally funded research program, teach and mentor graduate students, and participate in team-taught pharmacology courses offered to pharmacy students. A highly competitive salary and a start-up package commensurate with qualifications and experience are available. Currently, the fast growing department has 12 faculty members, 30 doctoral students and 8 post-doctoral fellows/research associates, has a Center of Excellence, Center of Biopharmaceutical Research and Production (CBRP), and participates in a NIH-funded ($10.5 million) Center of Biomedical Research Excellence. Additional information about the Department and University can be obtained at **www.ndsu.edu/pharmsci/**.

Application deadline is **December 31, 2009**, or thereafter until the position is filled. The application portfolio containing the curriculum vitae, statement of teaching philosophy, description of research interests and future plans, and three letters of reference must be submitted electronically: **jobs.ndsu.edu/applicants/Central?quickFind=51125**. For more information, please contact **Dr. Stephen O'Rourke (e-mail: stephen.orourke@ndsu.edu), North Dakota State University College of Pharmacy, Nursing and Allied Sciences, Fargo, ND 58105**.

NDSU is an Equal Opportunity Institution. Women and traditionally underrepresented groups are encouraged to apply.

FACULTY POSITIONS

Penn Medicine

University of Pennsylvania School of Medicine seeks candidates for several Assistant or Associate Professor positions in the tenure track. Rank will be commensurate with experience. The successful applicant will have experience in the field of chromatin biology with a focus on epigenetics. Responsibilities include research addressing outstanding questions in chromatin biology and epigenetics, using genomic, genetic, structural, biochemical or systems approaches. It is anticipated that successful candidates will develop independent, interactive research groups and excel in interdisciplinary training. Applicants must have an M.D. or Ph.D. or M.D./Ph.D. degree and have demonstrated excellent qualifications in Research.

The Penn Epigenetics Program encompasses a broad range of research groups at the University of Pennsylvania and within the Philadelphia region. State-of-the-art laboratory space, including shared computational and experimental core facilities, will be available in the Fisher Translational Research Building, to be completed in the fall of 2010.

The University of Pennsylvania is an equal opportunity, affirmative action employer. Women and minority candidates are strongly encouraged to apply.

Apply for this position online at:

http://www.med.upenn.edu/apps/faculty_ad/index.php/g305/d2104

UNIVERSITY OF WASHINGTON

FACULTY POSITION in CARDIOVASCULAR PHYSIOLOGY

The **Department of Physiology & Biophysics** at the University of Washington announces a search for a tenure-track faculty member. Appointment at the assistant professor level is preferred but associate professor will also be considered, if appropriate. We seek an individual (PhD and/or MD) with research interests and demonstrated scholarly achievements in the field of cardiovascular physiology. The new faculty member will be expected to establish a vigorous research program and participate in teaching of graduate and professional students. For information about the Department, see our website at **http://depts.washington.edu/pbiopage**.

Application packages should be submitted electronically to **pbsearch@uw.edu**. Applicants should submit a curriculum vitae and a description of research accomplishments and plans and have three letters of reference sent to: **Cardiovascular Search Committee, Department of Physiology & Biophysics, Box 357290, University of Washington, Seattle, WA 98195-7290**. Review of applications will begin on **October 1, 2009**, and continue until the position is filled.

The University of Washington is building a culturally diverse faculty and strongly encourages applications from women and minority candidates. The University of Washington is an Affirmative Action/Equal Opportunity Employer.

Open Faculty positions
The Department of Biotechnology and Food Engineering, Technion, Haifa, Israel. Website: http://biotech.technion.ac.il/)

The Department of Biotechnology and Food Engineering is actively seeking for **two tenure track Faculty members** at the level of senior lecturer\associate professor.

We are mainly interested in the following areas: Synthetic Biology, System Biology, Metabolic Engineering, Controlled Drug Release, Protein Engineering and any related areas in Biotechnology Engineering (not Biology).

Candidates should hold a PhD degree and post-doctoral training in the relevant areas. Candidates are expected to carry first rate independent research program, lead a research group, and mentor graduate students. Candidates are expected to teach courses aimed for undergraduate and graduate students. Proficiency in Hebrew for teaching is necessary.

Applicant should send curriculum vitae with list of publications and a summary of current and proposed research program and arrange for three letters of recommendations to be sent by e-mail to:

Professor Ben-Zion Levi, Dean, Department of Biotechnology and Food Engineering, E-mail: **deanbfe@technion.ac.il**

Max Planck Institute for the Physics of Complex Systems

The Max Planck Institute for the Physics of Complex Systems in Dresden announces the opening of a

Postdoctoral position

in condensed matter theory, to be filled in 2010.The areas of interest include strongly correlated electron systems, quantum phase transitions, frustrated quantum spin systems, non-equilibrium dynamics and transport in correlated systems, exotic ground states in quantum impurity systems, statistical mechanics and dynamics of cold atoms, quantum information theory and computational many-body physics. The successful candidate(s) will be able to interact with Roderich Moessner, Andreas Läuchli and Stefan Kirchner of the Condensed Matter Division, as well as with members of the Institute's other divisions and research groups, which make for a lively and interdisciplinary research atmosphere.

The Institute provides a particularly stimulating environment due to the in-house workshop program and the close links to the nearby Max Planck Institute for Chemical Physics of Solids, the Technical University, the Institute for Solid State and Materials Research and the Forschungszentrum Dresden-Rossendorf with its high magnetic field laboratory. The computational support is excellent based on local clusters, facilities at the TU Dresden and the Max Planck computing centre in Garching. For details of the application procedure please visit the webpage at
http://www.pks.mpg.de/~aml/openings.html

The Max Planck Institute aims to increase the number of women in scientists positions. Female candidates are therefore particularly encouraged to apply. In case of equal qualifications, candidates with disabilities will take precedence.

GEORGE MASON UNIVERSITY — BIOENGINEERING FACULTY

The George Mason University, Volgenau School of Information Technology & Engineering is seeking faculty to assist in the building of a new program in bioengineering. Each successful applicant will receive a tenure-track appointment as assistant or associate professor in one of the six Volgenau School departments (http://ite.gmu.edu). Candidates are expected to shape bioengineering at Mason by maintaining an active research program, and by teaching at both undergraduate and graduate levels.

Required: Earned doctorate in bioengineering, biomedical engineering, computer science, computer engineering, electrical engineering, operations research, systems engineering, statistics or other closely related fields. Preference will be given to candidates with a strong potential for interaction with current faculty members, especially in integrating measurement and computational approaches. Neuroengineering, neuroinformatics, rehabilitation engineering, biosensors and computational bioengineering are of special interest. See http://bioengineering.gmu.edu for an overview of Bioengineering at Mason. Questions should be directed to Prof. Peter Katona (pkatona@gmu.edu), or to the chair of any of the Volgenau School departments.

Applicants should submit a cover letter, CV, and a statement of research and teaching interests for **position F9305z at http://jobs.gmu.edu/**. The material should include contact information for three references. Review of applications will begin on November 1, 2009, and continue until the positions are filled. George Mason University is an innovative, entrepreneurial institution with four campuses in the greater Washington, D.C. area. Potential interactions with government agencies and medical institutions abound.

AA/EOE

MRC Laboratory of Molecular Biology

Cambridge

Group Leaders in Neurobiology

£37,000 - £47,000 per annum

The Division of Neurobiology at the MRC Laboratory of Molecular Biology (LMB) wishes to recruit talented scientists interested in developing an independent programme of research. We are particularly interested in individuals working on the function of neural circuits using electrophysiological or imaging techniques, and we envisage that such work would make use of organisms open to genetic manipulation. Current interests in the Division include visual and olfactory processing, circadian rhythms, mechanisms of synaptic transmission, and protein misfolding in relation to neurodegenerative diseases (www2.mrc-lmb.cam.ac.uk/NB/).

The LMB provides an excellent environment for hands-on research. Core funding by the Medical Research Council provides long-term support for ambitious projects, while administrative duties are minimal and no teaching is required. Interactions across the four Divisions of the Laboratory are encouraged and construction has begun on a new state-of-the-art research building (www2.mrc-lmb.cam.ac.uk/newlmb.html). There is extensive central support, including electronic and instrumentation workshops, imaging and transgenic mouse facilities. The University of Cambridge and affiliated institutions form a vibrant neuroscience community (http://www.neuroscience.cam.ac.uk/).

Candidates should have an MD and/or PhD and will have completed a period of postdoctoral training or equivalent, with an excellent track record, and show outstanding potential for independent research. You will lead a small team and substantial funding will be available.

This appointment will be made at either Programme Leader or Programme Leader-track level, depending on achievements and experience.

Further information can be obtained from Dr. Michel Goedert (email: mg@mrc-lmb.cam.ac.uk).

Your salary will be supported by a flexible pay and reward policy, 30 days' annual leave entitlement, an optional MRC final salary pension scheme and excellent on-site sports and social facilities.

This position is subject to pre-employment screening.

If you would like to receive this advert in large print, Braille, audio, or electronic format/hard copy, please contact the Recruitment team at the MRC Shared Service Centre on the telephone number below or recruitment@ssc.mrc.ac.uk

Applications for this role must now be made online at http://jobs.mrc.ac.uk inputting reference LMB09/503. Applicants should include a full CV, an outline of current and future research interests and the names and addresses of three professional referees who have agreed to be contacted. If you do not have internet access or experience technical difficulties please call 01793 301280.

Closing date: 13 November 2009.

For further information about the MRC please visit www.mrc.ac.uk

The Medical Research Council is an Equal Opportunities Employer

MichiganTech

Endowed Professorships and Faculty positions in Health

Michigan Technological University invites applicants for new tenure-track positions at any rank in the broad areas of health sciences and engineering. This campus-wide Strategic Faculty Hiring Initiative (SFHI) is projected to bring up to ten new faculty members, including possible endowed positions, to campus over the next two years to strengthen the key focus areas of biochemistry, bioengineering, bioethics, biomaterials, biomechanics, human factors, medical informatics, cell biology, physiology, and statistical genetics.

Faculty hired through this initiative are expected to establish a vigorous, nationally competitive research program and to be committed to excellence in both undergraduate and graduate education. The application review process will begin on **November 15, 2009**. Details on the SFHI and application instructions are available at **www.mtu.edu/sfhi**.

Michigan Tech is an internationally renowned doctoral research university located in Michigan's scenic Upper Peninsula, on the south shore of Lake Superior. Houghton provides a unique setting where natural beauty and exceptional year-round outdoor activities, culture, education, and a diversity of residents from around the world come together to share a superb living and learning experience. As part of its strategic focus, Michigan Tech is experiencing remarkable growth in research. In the last five years, research expenditures have doubled, up to $60M in 2008. The university has also recently initiated efforts to advance health-related research capabilities with the establishment of animal facilities and the formation of the Departments of Biomedical Engineering and Exercise Science, Health and Physical Education. Michigan Tech is an ADVANCE institution, one of a limited number of universities in receipt of NSF funds in support of our commitment to increase diversity and the participation and advancement of women in STEM.

Michigan Technological University is an Equal Opportunity, Affirmative Action Employer/Educational Institution. Applications from women and minorities are encouraged.

Director, Richard King Mellon Foundation Institute for Pediatric Research
University of Pittsburgh School of Medicine
Children's Hospital of Pittsburgh of UPMC

The Department of Pediatrics of the University of Pittsburgh School of Medicine and Children's Hospital of Pittsburgh of UPMC is seeking an internationally renowned scientist to lead this new institute dedicated to basic research on diseases and disorders prevalent in the young, and to advancing the careers of junior investigators with this interest. The Richard King Mellon Foundation has provided $23 million to start the institute, which will be housed in 10,000 square feet in the new Rangos Research Centre of Children's Hospital of Pittsburgh (total 300,000 square feet). We are anticipating that the Institute Director will expand his/her own active laboratory program as well as provide mentoring and administrative oversight for five Scholars who will be recruited from top programs around the country. These Scholars will be Assistant Professors who may not yet have their own R01 funding but are ready to begin their own laboratories. Scholars will receive start-up and continuous funding as well as access to state-of-the-art core facilities and dedicated administrative support. The Director will hold the Richard King Mellon Foundation Professor of Pediatrics endowed chair and will be provided with extensive funding for his/her own laboratory program.

The University of Pittsburgh School of Medicine is enjoying unparalleled growth in its research, clinical and academic missions. Of more than 3,000 institutions nationwide, the University is currently ranked 5th in NIH funding. The Department of Pediatrics/Children's Hospital of Pittsburgh is ranked 7th in NIH funding among all children's hospitals and pediatric research programs.

Academic credentials should qualify the candidate for faculty appointment at the level of Professor. Applicants should submit a CV by e-mail in MS-Word format before **November 15, 2009** to: **David H. Perlmutter M.D., Vira I. Heinz Professor and Chair, Department of Pediatrics; Margaret.lyle@chp.edu.**

The University of Pittsburgh is an Equal Opportunity, Affirmative Action Employer.

Penn State University Department of Biology

Faculty Position in Evolutionary Genomics and Bioinformatics

The Department of Biology at Penn State University invites applications for **faculty position** open at all professorial ranks in evolutionary genomics and bioinformatics. Penn State is home to a highly successful and interactive research community in evolutionary genetics, genomics, and bioinformatics. Among the institutes and centers supporting research are the Institute of Molecular Evolutionary Genetics, the Center for Comparative Genomics and Bioinformatics, and the Institute for Genomics, Proteomics and Bioinformatics. Prospective candidates should have a strong record of research accomplishments, ability to secure extramural grants, and a commitment for teaching.

Candidates should email a letter of application, curriculum vitae, research prospectus, statement of teaching interests, and names and contact information of at least three references, all as a single PDF document to **egb2@bio.psu.edu**. Publications and manuscripts (not more than three) may be submitted as separate PDF documents along with the application. Review of completed applications will begin **October 15, 2009**.

Penn State is committed to Affirmative Action, Equal Opportunity and the diversity of its workforce.

FACULTY POSITIONS

Penn Medicine

The Department of Cancer Biology at the University of Pennsylvania's School of Medicine seeks candidates for an Assistant, Associate, or Full Professor position in the tenure track. Rank will be commensurate with experience. Applicants must have an M.D. and/or Ph.D degree and have demonstrated excellence in education and research.

The Department of Cancer Biology is a partner with the Abramson Cancer Center at the University of Pennsylvania and the Abramson Family Cancer Research Institute. Qualified applicants may have scientific interests and experience in any field of cancer biology, including but not limited to cancer genetics and genomics, tumor microenvironment, epigenetics, angiogenesis, cancer cell metabolism, and oncogenic signaling.

Responsibilities will include the development of an independent research program. Qualifications and experience in teaching are required.

The University of Pennsylvania is an equal opportunity, affirmative action employer. Women and minority candidates are strongly encouraged to apply.

Please upload CV, cover letter, 3 references letters, and a statement of research interests at:

http://www.med.upenn.edu/apps/faculty_ad/index.php/g304/a2077

Lewis A. Chodosh, M.D., Ph.D.
Professor and Chair, Dept of Cancer Biology
612 BRB II/III, 421 Curie Blvd, Phila, PA 19104
cbiorecr@mail.med.upenn.edu

GIScCE SDSU

Associate Professor or Full Professor, Geographic Information Science Center of Excellence, South Dakota State University

The Geographic Information Science Center of Excellence (GIScCE) invites faculty applications from scientists with research interests in quantitative remote sensing, large-area terrestrial monitoring and/or modeling. Specialization in one of the following areas is preferred: (1) land/atmosphere interactions and climate modeling, (2) active sensors (radar and/or lidar) for vegetation characterization, (3) modeling the dynamics of coupled human-environmental systems. We seek motivated, broad-thinking scientist-educators to establish vigorous research programs and provide intellectual leadership in their field. GIScCE faculty have 80% research, 10% service and 10% teaching loads. The GIScCE is a collaboration with the USGS Center for Earth Resource Observations and Science (EROS). For more information, visit (**http://globalmonitoring.sdstate.edu**); for a list of required qualifications and directions for online application, visit **http://jobs.sdstate.edu**. For questions on the electronic employment process, contact **SDSU Human Resources** at **(605) 688-4128**. Application deadline is **December 21, 2009**.

SDSU is an AA/EEO Employer and encourages applications from women and minorities. ADA Accommodations: (605) 688-4394.

The University of Texas at Austin

Endowed Chair Position

The Institute for Cellular and Molecular Biology

The Institute for Cellular and Molecular Biology invites applications for an Endowed Chair Position. An academic appointment at the level of tenured Professor will be held in an appropriate academic unit in the College of Natural Sciences. Candidates should have an outstanding research program that applies molecular biological and/or biochemical approaches to important biological problems. Areas of interest include, but are not limited to, Biochemistry, Cancer Biology, and Human Genetics. The position carries an exceptional salary and start-up package.

Building on a strong existing faculty, the Institute has recruited more than 60 new faculty members in the past ten years. Faculty roster can be reviewed at http://www.icmb.utexas.edu. In addition to its highly interactive and interdisciplinary research environment, The Institute is the home base for the University-wide Graduate Program in Cell and Molecular Biology and supports the state-of-the-art core facilities for DNA and protein analysis, mass spectrometry, electron and confocal microscopy, DNA microarrays, robotics, X-ray crystallography, mouse genetic engineering, and NexGen genomic sequencing. An MD-PhD program with the UT Medical Branch and the new Dell Pediatrics Research Institute in Austin further enhance the environment for Biomedical Research.

Austin is located in the Texas hill country and is widely recognized as one of America's most beautiful and livable cities.

Please send curriculum vitae, summary of research interests, and names of five references to:

Dr. Alan M. Lambowitz, Director
The Institute for Cellular and Molecular Biology
The University of Texas at Austin
1 University Station A4800
Austin TX 78712-0159

The University of Texas at Austin is an Equal Opportunity Employer. Qualified women and minorities are encouraged to apply; a background check will be conducted on applicant selected.

PENNSTATE

Tenure-track Positions in Energy Science, Engineering, and Policy

The Pennsylvania State University invites applications from outstanding individuals for the following eight faculty positions:

1. Solar Energy to Electric Conversion
2. Quantitative Analysis of Energy Risk
3. Membranes for Energy Production
4. Wind Energy
5. Landscape Ecology
6. Molecular Energy Conversion Processes
7. Integrated Assessment of Energy Systems and Policy
8. Plant Biology Energy Storage

Plant Biology Energy Storage

The Department of Biology (www.bio.psu.edu) invites applications for a faculty position in Plant Biology related to energy storage in plants. Penn State is an international center for plant biology research, with emphases in cell biology, development, genomics, ecology, and evolution. The successful candidate will use a combination of approaches, such as genomics, systems biology, genetics, cell biology or biochemistry, to elucidate the molecular control of the formation and accumulation of lignocellulose, starch, oils or sucrose in plants. Candidates should have a strong research record and a commitment to teaching.

For more details please see www.psiee.psu.edu/open_positions.asp.

Penn State is committed to affirmative action, equal opportunity and the diversity of its workforce.

DEPARTMENT OF BIOTECHNOLOGY
Ministry of Science & Technology
Govt. of India
TRANSLATIONAL HEALTH SCIENCE AND TECHNOLOGY INSTITUTE (THSTI)

(Autonomous Institute and Part of NCR Bio-medical Science Cluster)
Present location at the National Institute of Immunology
JNU Complex, Aruna Asaf Ali Marg, New Delhi -110067

EXECUTIVE DIRECTOR AND DEANS

The Department of Biotechnology, Ministry of Science & Technology (Government of India) has established the Translational Health Science and Technology Institute (THSTI), an autonomous institution, as a part of the interdisciplinary Health Biotech Science cluster, located in Faridabad, Haryana, in the National Capital Region. Major Indian and overseas institutions are mentoring the development of the THSTI. The THSTI is designed to be a dynamic and interactive organization with a mission to conduct innovative, interdisciplinary and translational research and develop research collaborations across disciplines and professions to accelerate the extension of concepts to the improvement of human health. The other members of the cluster include the Regional Center for Biotechnology (RCB) under the aegis of UNESCO, with which THSTI will have seamless scientific collaboration to achieve interdisciplinary expertise. The cluster institutions will have access to state of the art experimental animal facility, platform technology resources and incubation facilities.

THSTI is looking for exceptional candidates for the post of Executive Director (ED) and Deans to spearhead the establishment of this institute. The position of ED offers a unique opportunity for the right individual in providing strong and visionary leadership to the new institution.

The Institute will engage in a unique inter-disciplinary translational research programme to bring science from bench to bedside. The key feature of this institute will be a dynamic inter-relationship of basic science, engineering, health research and biotech industry to produce translational knowledge and innovation technologies through group excellence.

The permanent laboratories of THSTI will come up at Faridabad over the next three years. Interim laboratories will function from Gurgaon in the South Delhi area with adequate housing, transportation and schooling facilities. Campus housing may be made available when the institution moves to the Faridabad campus.

The core Health Science Technology (HST) Centre of THSTI is modeled on the Harvard-MIT Health Sciences and Technology Division, THSTI will provide multidisciplinary, multi-professional, research and education, will be highly interconnected with regional centers of excellence, and will promote the translation of discoveries and inventions to societal use for the benefit of human health. The new organization will include faculty from multiple disciplines and professions, offer degrees through multidisciplinary programs, and develop strong ties with other institutions in the public and private sectors. The underlying premise is two fold: no one discipline or profession alone offers the potential to make transformative advances in medicine; and the potential for students and faculty to innovate is unleashed as they reach far beyond their core disciplines and professions to gain experience and understanding of other disciplines and professions. The other components of THSTI will be a series of integrated programme oriented centres such as for Vaccine and Infectious Disease, Child Biology, Chronic Disease etc. These will be developed in a planned manner.

The candidates must have an MD, Ph.D or equivalent degree in biomedical sciences and have knowledge of molecular paradigms of disease. He/She must have at least 15 years research experience, be able to interact nationally and internationally, create an inter-disciplinary team and have aptitude for translational research and interaction with industry.

The responsibilities of the Executive Director include (1) leading and nurturing the core multi-disciplinary research facility; (2) developing policies and fostering collaboration with scientific, medical and engineering partner institutions; (3) developing mechanism for collaboration with industry; (4) recruitment of appropriate faculty; (5) management of the extramural activities including supporting research resource units in other institutes. The Deans will support the Executive Director in establishing and nurturing the institute and will lead major programme centres.

To apply submit a curriculum vitae and a two-three page write-up of your vision on how a Translational Health Science and Technology Institute should be developed to **Dr. T.S.Rao, Adviser, Department of Biotechnology, Ministry of Science and Technology, Room No.819, Block II, CGO Complex, Lodi Road, New Delhi -110003**. Tel.: 011-24364065 Fax : 011-24362884, E-mail : **tsrao@dbt.nic.in**, on or before **10th November 2009**.

POSITIONS OPEN

NICHOLAS SCHOOL OF THE ENVIRONMENT AND EARTH SCIENCES
DUKE UNIVERSITY

Cluster Hire in the Nicholas School of the Environment; Intersection between Ecology and Hydrology
October 2009

The Nicholas School of the Environment (NSOE) at Duke University (DU) will make four tenure-track appointments at junior or senior levels as part of a cluster hire in ecohydrology (see **website: http://nicholas.duke.edu/application**). This new initiative builds on DU's strengths in ecological and hydrological sciences and seeks to attract outstanding faculty who will engage in and facilitate multidisciplinary interactions across the NSOE and other units on campus, such as biology, civil and environmental engineering, and the Global Health Institute, on research at the interface between ecosystem function and hydrological processes. Candidates will contribute to the NSOE's curriculum at the undergraduate, professional Master's, and doctoral levels.

Consideration of applications will begin immediately and continue until all positions are filled. Applications should include a full curriculum vitae along with a statement of research and teaching goals and applicants should arrange for three letters of reference to be forwarded to **website: http://nicholas.duke.edu/application.**

The Nicholas School and Duke University are committed to Equal Opportunity in Employment. Applications are strongly encouraged from members of underrepresented populations.

POSTDOCTORAL POSITIONS (NIH-funded) are immediately available in the Department of Pathology and Laboratory Medicine at the Temple University School of Medicine. The fellows will join a highly interactive and collaborative research team that focuses on translational research on the function of blood-brain barrier (BBB), signaling events that contribute to brain endothelial formation, repair and response to inflammatory stimuli, drug delivery in the setting neuroinflammation, HIV-1 infection, and drug/alcohol abuse. These topics will be investigated using systems such as in vivo and in vitro models of BBB function, animal model of HIV-1, functional genomics including immunogenomics, multiparametric flow cytometery, immunochemistry, and state-of-the-art time lapse live cell imaging. Strong laboratory skills in a broad range of cellular and molecular immunological techniques or expertise in brain endothelial biology are preferred. Applicants are expected to have strong ability, be self-motivated, and be a major contributor to the research programs. Qualified candidates with a Ph.D. and/or M.D. with expertise in areas of immunology, cellular biology, biochemistry, or physiology are invited to apply. Applications should be sent electronically to **e-mail: patricia.harper@tuhs.temple.edu; attention: Dr. Yuri Persidsky, Professor and Chair, Department of Pathology and Laboratory Medicine, Temple University School of Medicine, 3401 North Broad Street, Philadelphia, PA 19140.**

Black Hills State University seeks to fill a **SYSTEMATIC BOTANIST** tenure-track, **ASSISTANT PROFESSOR** position starting August 2010. Ph.D. in botany or related field and advanced knowledge of plant systematics are required. Candidate will be expected to develop a research program involving students and teach general and advanced-level botany classes. For a full position description and to apply, go to **website: http://yourfuture.sdbor.edu.** Applicants should provide curriculum vitae, transcripts, a letter detailing research and teaching experience/philosophy, reprints of recent papers, and three letters of reference. Reprints and letters should be sent directly to: **Dr. Garth Spellman, 1200 University Street, Unit 9073, Spearfish, SD 57799. E-mail: garth.spellman@bhsu.edu.** Review of applications will begin November 13, 2009.

POSITIONS OPEN

UNIVERSITY OF MINNESOTA

FACULTY POSITION IN MICROBIOLOGY

The Department of Microbiology at the University of Minnesota Medical School invites applications for a faculty position to be filled at the tenure-track **ASSISTANT PROFESSOR** level in the area of bacterial pathogenesis. The successful applicant will be expected to establish a productive, independent research program and contribute to departmental teaching. The Department and affiliated units at the University have broad research strengths in microbiology and immunology, including immunity and host defense, microbial pathogenesis, virology, microbial physiology, genetics, genomics, environmental microbiology, and biotechnology. More information about the Department of Microbiology, with links to affiliated institutes and centers and the graduate training program, can be found on the department **website: http://www.microbiology.med.umn.edu.**

Minimum qualifications: Ph.D. in microbiology, M.D., or D.V.M. and applicable postdoctoral or faculty experience. Review of applications will continue until suitable candidates are identified. To apply, please submit curriculum vitae and concise summary of research interests and activities to **requisition number 154920** at **website: http://employment.umn.edu.** Please also arrange to have three letters of recommendation sent electronically to **e-mail: microbiology@umn.edu** or mailed to: **Patrick M. Schlievert, Ph.D., Search Committee Chair, Department of Microbiology, University of Minnesota, MMC 196, 420 Delaware Street S.E., Minneapolis, MN 55455.** Top candidates will be invited for a seminar/interview as a component of the selection process.

The University of Minnesota shall provide equal access to and opportunity in its programs, facilities, and employment without regard to race, color, creed, religion, national origin, gender, age, marital status, disability, public assistance status, veteran status, sexual orientation, gender identity, or gender expression.

DEPARTMENT HEAD AND PROFESSOR
Department of Animal and Range Sciences

The Department of Animal and Range Sciences (A&RS) at Montana State University in Bozeman, Montana, is seeking applications and nominations for the position of Department Head and Professor.

Founded in 1893 in the scenic Gallatin Valley just north of Yellowstone National Park, Montana State University (MSU) is a land grant university with total enrollment of 12,000 students. Departmental teaching programs from B.S. to Ph.D. levels serve 230 students. Research programs focus on cattle, sheep, equine, and range ecology and an outreach focus on livestock production and range management. The Department will be housed in a new state-of-the-art building that substantially expands the Department's research and teaching opportunities. The new Department Head in conjunction with faculty and constituents will have an unusual opportunity to shape and expand the Department including new faculty hires. Montana and the surrounding region provide exceptional opportunities for multiple discipline, multiple-scale, from the laboratory to landscape, research and instruction.

For a vacancy announcement, including a listing of required and preferred qualifications and application procedures, visit **website: http://ag.montana.edu; e-mail: lduffey@montana.edu; or telephone: 406-994-3681.** Screening will begin December 18, 2009, and continue until a suitable candidate is hired.

ADA/Equal Opportunity/Affirmative Action/Veteran's Preference Employer.

The Chicago State University Department of Biological Sciences is seeking to fill one tenure-track faculty position at the **ASSISTANT PROFESSOR** level in the area of genetics and bioinformatics. Please see the online ad at **website: http://www.csu.edu** to apply.

Dr. Juanita C. Sharpe
Department of Biological Sciences
Chicago State University
9501 South King Drive/SCI-310
Chicago, IL 60628-1598

Chicago State University is an Equal Opportunity Employer.

POSITIONS OPEN

UNIVERSITY OF NOTRE DAME

CHEMICAL & BIOMOLECULAR ENGINEERING FACULTY OPENINGS
University of Notre Dame

The Department of Chemical & Biomolecular Engineering at the University of Notre Dame is pleased to announce openings for tenured or tenure-track faculty at any rank.

A Ph.D. or equivalent degree is required. All research fields are welcome. Applicants should have developed, or show potential for development of, an outstanding research program and should possess a strong commitment to graduate and undergraduate education.

Applicants should send a PDF file of their curriculum vitae, statement of teaching and research interests, and the names and complete addresses of at least four references to **e-mail: cbeopen@nd.edu.**

Please direct any questions to **e-mail: mjm@nd.edu.** *Notre Dame is an Equal Opportunity/Affirmative Action Employer.*

LECTURER POSITION
in Environmental Technology
School of Public and Environmental Affairs
Indiana University–Bloomington Campus

The School of Public and Environmental Affairs (SPEA) at Indiana University seeks to appoint a Lecturer or Senior Lecturer on the Bloomington campus. This is a nontenure-track, full-time, permanent faculty position with primary responsibility in teaching. SPEA is interested in candidates with strong teaching interests in sustainability-related topics, including, but not limited to, life cycle analysis, alternative energy development, waste management, and pollution prevention. Preference will be given to candidates with a Ph.D. in a related field (e.g., civil, environmental, or mechanical engineering) or a related professional degree combined with substantial practical and/or teaching experiences.

Review of applications will begin October 8, 2009, and continue until the position is filled. Please submit a letter of application, current vita, supporting documentation of outstanding instructional abilities, complete contact information, and three letters of recommendation electronically to **e-mail: speahr@indiana.edu** or a hard copy to:

Dr. David Reingold
Associate Dean for Bloomington
SPEA, Room 300
1315 E. Tenth Street
Indiana University
Bloomington, IN 47405-1701

For more information see **website: http://www.indiana.edu/~spea.** *Indiana University is an Equal Opportunity/Affirmative Action Employer, Educator and Contractor, Minorities/Females/Persons with Disabilities and strongly committed to achieving excellence through cultural diversity. The University actively encourages applications and nominations of women, persons of color, applicants with disabilities, and members of other underrepresented groups.*

POSTDOCTORAL POSITIONS
Infectious Disease Pathogenesis/Immunology
Yale University School of Medicine

Positions available to study the interactions between pathogens, arthropod vectors, and the mammalian host. *Borrelia burgdorferi*, *Anaplasma phagocytophilum*, West Nile virus, and *Plasmodium falciparum* are among the model organisms. Experience in microbial pathogenesis, immunobiology, cell biology or molecular biology necessary.

Send curriculum vitae and recent publications to: **Erol Fikrig, M.D., Investigator, Howard Hughes Medical Institute, Yale University School of Medicine, Section of Infectious Diseases, P.O. Box 208022, New Haven, CT 06520-8022.** Or **e-mail: erol.fikrig@yale.edu.** *Yale University is an Affirmative Action, Equal Opportunity Employer. Applications from women and minorities are encouraged.*

The **University of Washington School of Medicine** requests applications for a **tenure-track Assistant Professor of Pharmacology** from individuals with a Ph.D. or M.D. currently holding postdoctoral or non-tenure track faculty appointments and having strong training and research productivity using functional proteomic methods to probe the composition and regulation of molecular signaling complexes in neural signaling and drug addiction. Adjunct appointments in Genome Sciences or Psychiatry & Behavioral Sciences and membership in the University of Washington Proteomics Resource may also be possible. The successful candidate will initially be supported by a program grant (ARRA-P30) from the National Institute on Drug Abuse and will also receive a generous start up package from the university. University of Washington faculty engage in teaching, research and service, and the successful candidate will participate in outstanding graduate training programs in Pharmacology and Genome Sciences, as well as interdisciplinary graduate programs in Neurobiology & Behavior, Molecular & Cellular Biology, and Molecular Medicine.

For full consideration, applicants should submit applications electronically as a single PDF containing a cover letter describing accomplishments and future research plans, a complete CV, and a representative research publication to **p30nida@uw.edu** and should arrange to have three confidential letters of reference electronically forwarded before November 15, 2009. More description of the new position and the departmental programs can be found at **http://depts.washington.edu/phcol/**. Additional information may also be obtained by contacting **Dr. Charles Chavkin, Search Committee Chair, Department of Pharmacology, University of Washington, Box 357280, Seattle, WA 98195-7280**.

The University of Washington is an Affirmative Action/Equal Opportunity Employer. Women and under-represented minority individuals are strongly encouraged to apply.

University of Massachusetts
UMASS Medical School

Department of Obstetrics and Gynecology
Basic Scientist Faculty Positions

We are seeking 2-3 basic science research faculty (Ph.D., M.D., M.D./Ph.D. or equivalent) at the Assistant, Associate or Full Professor levels who will conduct innovative research and provide strong scientific leadership while interfacing with clinical faculty to foster collaborations. Our primary goal is to recruit exceptional scientists whose work is directly influenced by or has the potential to impact women's reproductive health. Scientists working with mammalian systems will be favored. Current departmental expertise and associated interests include but are not limited to pregnancy, maternal-fetal interface and obstetric outcomes, reproductive endocrinology and infertility, gynecologic oncology, female pelvic floor dysfunction and reconstructive surgery, stem cell biology and women's mental health as it relates to reproduction. A strong record of scholarly contributions, publications and funding is desirable. For mid-career and senior-level appointments, preference will be given to those with demonstrated excellence in mentorship and teaching as well as proven record of continuous funding. A desire to work in a collaborative environment is important as interdisciplinary research efforts are highly encouraged at UMMS. Appropriate lab space and resources are available to support successful candidates. Joint appointments would be in the Department of Obstetrics and Gynecology and an appropriate basic science department.

Please submit curriculum vitae, statement outlining research interests and the names and contact information for three or more references by email to **Tiffany A. Moore Simas, MD, MPH, MEd (TiffanyA.MooreSimas@UMassMemorial.org), Director, Research Division, Department of Obstetrics and Gynecology, UMMS/UMMHC – Memorial Campus, 119 Belmont Street, Worcester, MA 01605**. Additional information about the University of Massachusetts Medical School, its research mission and the Department of Obstetrics and Gynecology is available at **http://www.umassmed.edu/index.aspx**. The positions will remain open until filled. To be assured full consideration, applications should be submitted by **December 15, 2009**.

The University of Massachusetts and its clinical partner, UMass Memorial Medical Center, are Equal Opportunity Employers building strength through diversity. We welcome all applicants.

MATERIALS ENGINEER
U.S. ARMY RESEARCH OFFICE

Applications are being solicited for a Materials Engineer, DB-0806-03 (equivalent to the GS-12/13 grade levels), $69,704 - $107,756 per annum, or a Materials Engineer, DB-0806-04 (equivalent to the GS-14/15 grade levels), $97,948 - $149,782 per annum. Salary within the ranges above includes a locality adjustment and depends upon individual qualifications and salary history. The position is located at the U.S. Army Research Office in Research Triangle Park, N.C.

The incumbent develops, manages, and oversees the Army's extramural research program in materials science, focusing on synthesis and processing of materials (both experiment and theory), and identifying and fostering scientific achievements with application to Army materiel systems. Expertise is required in the areas of fabrication, synthesis, and processing of advanced materials.

Duties include: Initiating new research projects to advance the frontiers of materials science. Stimulating proposals to create unprecedented scientific opportunities relevant to Army needs. Analyzing and evaluating proposals. Communicating with grantees and contractors. Reviewing and analyzing research reports, and ensuring their effective distribution. Stimulating technology transfer to both Army and civilian users. Evaluating grantee and contractor performance. Disseminating program policies and research results. Maintaining awareness of Army in-house R&D programs. Developing and presenting briefings and research summaries that highlight projects, objectives, progress, accomplishments and emerging opportunity areas within materials science to Army leadership and the scientific community. Initiating and carrying out workshops, conferences, and symposia addressing emerging materials research initiatives. Serving as the principal Army advocate and representative for basic research activities and needs in synthesis and processing of materials.

In order to maintain scientific acumen, the incumbent may perform research at a local university for up to one day per week. Travel up to 25% of the time may be required. Outstanding verbal and written skills are required. Applicants must show successful completion of a full 4-year course of study in an accredited college or university leading to a bachelor's or higher degree in materials science, or a combination of education and experience equal to a GS-12/13 level position in the Federal government for DB-03 or GS-14/15 for DB-04. An advanced degree at the PhD level preferred. Experience must have been in or related to the work of the position and have equipped the applicant with the knowledge, skills, and abilities to successfully perform the duties of the position.

Applicants must be U.S. citizens, be able to obtain a secret clearance, and comply with provisions of the Ethics in Government Act. Interested individuals must apply electronically following instructions at **www.usajobs.opm.gov** or at **www.cpol.army.mil**. Vacancy Announcement numbers are **NEAC09559221D/NEAC09559221** for the **DB-04** and **NEAC09560030D/NEAC09560030** for the **DB-03**. Opening date for this position is **October 5, 2009** and closing date will be **December 4, 2009**. If you have questions, please contact **Mrs. Paula Valdez, 301-394-2109, e-mail: paula.geny.valdez@us.army.mil** or **Wanda Wilson, Administrative Officer, Army Research Office at (919) 549-4296, e-mail: wanda.wilson@us.army.mil**.

POSITIONS OPEN

PURDUE UNIVERSITY

ASSISTANT PROFESSOR
Molecular Pharmacology

The Department of Medicinal Chemistry and Molecular Pharmacology, Purdue University School of Pharmacy and Pharmaceutical Sciences, invites applications for a tenure-track faculty position at the level of Assistant Professor. Research in the Department is highly interdisciplinary with strengths in molecular pharmacology, cancer biology, neuroscience, chemical biology, drug design, systems biology, and computational chemistry (**website: http://www.mcmp.purdue.edu/research/**).

The successful candidate will have a Ph.D. in pharmacology or a related field, appropriate postdoctoral experience, and the potential to establish a vigorous research program and will participate in undergraduate, pharmacy, and graduate education.

Applicants are sought with research interests in any area of molecular pharmacology including, but not limited to, signal transduction, protein structure and function, drug-receptor interactions, drug discovery, and pharmacogenomics.

For full consideration, please submit a single PDF file to **Ms. Angie Schutz, e-mail: arschutz@purdue.edu** containing the following items: a cover letter, a full curriculum vitae (including publications and research and teaching experience) and a statement of research plans (not to exceed two pages). Applicants should arrange to have three letters of reference sent directly to the same e-mail address. Please direct any questions regarding this position or application requirements to the Chair of the Search Committee, **Dr. Gregory Hockerman, e-mail: gregh@purdue.edu.**

Purdue University is an Equal Opportunity/Equal Access/Affirmative Action Employer fully committed to achieving a diverse work force.

ASSISTANT PROFESSOR
Tenure Track – Biology

The Biology Department of the College of Saint Benedict and Saint John's University is seeking to fill a full-time, tenure-track position starting August 2010 for a **VERTEBRATE BIOLOGIST** to teach a one-semester course in human anatomy and physiology for students pursuing careers in allied health. We seek a dynamic teacher-scholar with a strong commitment to teaching and research in an undergraduate liberal arts environment. The successful candidate should hold a Ph.D. and, in addition to the anatomy and physiology course, be able to offer an upper-division course in endocrinology or neurobiology, develop a research program involving undergraduates, and compete for extramural funding.

St. John's University, a liberal arts college for men, and the College of St. Benedict, a liberal arts college for women, are located four miles apart in Central Minnesota just outside metropolitan St. Cloud and 70 miles from Minneapolis. Both are Catholic colleges in the Benedictine tradition, which emphasize quality teaching and a commitment to intercultural learning. For further information visit **website: http://www.csbsju.edu.**

Send letter of interest, curriculum vitae, three letters of reference, copies of transcripts (official transcripts required for interview), statement of teaching and research interests, and evidence of teaching effectiveness to:

College of Saint Benedict/Saint John's University
Human Resources–Position #HRW2009045
37 South College Avenue
St. Joseph, MN 56374
E-mail: employment@csbsju.edu

Applications received after November 4, 2009, cannot be guaranteed full consideration.

Women and people of diverse racial, ethnic, and cultural backgrounds are encouraged to apply. The College of Saint Benedict/Saint John's University are Equal Employment Opportunity/Affirmative Action Employers.

POSITIONS OPEN

UT SOUTHWESTERN MEDICAL CENTER

THE UNIVERSITY OF TEXAS
SOUTHWESTERN MEDICAL CENTER

ASSISTANT PROFESSORS. The Department of Physiology invites outstanding scientists with Ph.D., M.D., or equivalent degrees to apply for tenure-track Assistant Professor positions. Candidates who use innovative optical, mechanical, electrical, molecular biological, or computational methods with important applications to physiological systems, ranging from individual genes and proteins to cells and organs, are encouraged to apply. However, the scientific excellence of the candidates is more important than the specific area of research.

These positions are part of the continuing growth of the Department at one of the country's leading academic medical centers and will be supported by significant laboratory space on our new campus, competitive salaries, and exceptional startup packages. The University of Texas Southwestern Medical Center is the scientific home to four Nobel Prize laureates, 17 members of the National Academy of Sciences, and 17 members of the Institute of Medicine. UT Southwestern conducts more than 3,500 research projects annually totaling more than $400 million.

Applicants should submit curriculum vitae along with a brief statement of research plans and should arrange to have three letters of reference sent to: **James Stull, Ph.D., c/o Ronald Doris, Department of Physiology, The University of Texas Southwestern Medical Center, 5323 Harry Hines Boulevard, Dallas, TX 75390-9040.** *UT Southwestern strongly encourages applications from women, minorities, and people with physical challenges. An Equal Opportunity Employer.*

RESEARCH ASSOCIATE

NIH-funded **POSTDOCTORAL POSITION** available immediately in the Department of Chemistry and Biochemistry of the University of Maryland, Baltimore County, located in suburban Maryland. This position will focus on the structural determination of RNA and protein-RNA complexes involved in the HIV-1 lifecycle, using novel in vivo approaches developed in the laboratory. The ideal candidate should have experience in recombinant techniques and structural biology. Candidates with a background in nucleic acids biochemistry will also receive strong consideration. Send your curriculum vitae and the names of two professional references to:

Dr. Dan Fabris
Department of Chemistry and Biochemistry
University of Maryland, Baltimore County
1000 Hilltop Circle
Baltimore, MD 21250
E-mail: fabris@umbc.edu

UMBC is an Equal Opportunity/Affirmative Action Employer and applications from women, minorities, and individuals with disabilities are especially encouraged. Applications will be received until a suitable candidate is found.

THE UNIVERSITY OF CHICAGO
Department of Radiation and Cellular Oncology

The University of Chicago, Department of Radiation and Cellular Oncology, is seeking applicants for a full-time **RESEARCH ASSOCIATE (ASSISTANT PROFESSOR)** position, under the general direction of **Professor Douglas K. Bishop.** The primary activity of a Research Associate (Assistant Professor) is academic research in association with a faculty member or team. Candidates are required to possess a Doctorate with experience in protein biochemistry. Candidates with experience in protein crystallography and enzymology will be favored.

For consideration please submit online a current curriculum vitae and contact information for three references at **website: http://tinyurl.com/UC-Rad-Onc-RA50661.** Statement of research interests is preferred.

The University of Chicago is an Affirmative Action/Equal Opportunity Employer.

POSITIONS OPEN

UAB THE UNIVERSITY OF ALABAMA AT BIRMINGHAM

The Department of Physiology and Biophysics at the University of Alabama at Birmingham (UAB) invites applications for two tenure-track **ASSISTANT PROFESSOR** positions. UAB is a leading research university ranked among the top public universities in NIH funding. We are seeking dynamic investigators/educators to complement the existing strengths of our Department (see our **website: http://www.medicine.uab.edu/physiology**). Applicants with expertise in cell signaling and/or cancer biology are especially encouraged to apply. The successful candidates will have an M.D. or Ph.D. in a biomedical science, a strong publication record, a commitment to teaching, and excellent funding potential. Salary will be commensurate with experience. Competitive startup funds and generous laboratory space will be offered. Please send curriculum vitae, statement of research plans, and three references to: **Dr. Kevin L. Kirk, Department of Physiology and Biophysics, University of Alabama at Birmingham, 1918 University Boulevard, MCLM 982, Birmingham, AL 35294-0005** or electronically to **e-mail: klkirk@uab.edu.** *The University of Alabama at Birmingham is an Affirmative Action/Equal Opportunity Employer.*

BIOLOGY TENURE-TRACK POSITIONS
Department of Biology
Georgia Southern University

The Department of Biology invites applications for two tenure-track positions at the **ASSISTANT PROFESSOR** rank to begin August 2010. The successful applicants will be expected to develop externally funded research programs and to contribute to excellence in teaching at the undergraduate and Master's levels. Screening of completed applications will begin November 1, 2009, and continue until the positions are filled. Applicants must have a Ph.D. in the biological sciences by December 31, 2009.

ASSISTANT PROFESSOR in animal physiology. Teaching requirements will include comparative animal physiology. Preference will be given to applicants whose research focuses on integrative/organismal physiology.

ASSISTANT PROFESSOR in aquatic ecology. This position is part of the Allen E. Paulson College of Science and Technology's initiative to create an interdisciplinary research program on the science of the Southeastern Coastal Plain. Preference will be given to applicants working on freshwater systems who can develop an interdisciplinary research program in the coastal plain involving collaborations with faculty in other departments of the College.

For full details and qualifications see **website: http://www.bio.georgiasouthern.edu/jobs/.** Candidates must send a letter of application indicating the position for which they are applying, curriculum vitae, statements of teaching and research interests, and three letters of reference to the appropriate Search Chair (see below). Letters of reference in PDF format may be sent via e-mail. Applications may also be sent electronically with the entire packet as a single PDF format attachment (include applicant name in filename).

Animal Physiology: Dr. James B. Claiborne, Chair, Animal Physiology Search Committee, e-mail: physiologysearch@georgiasouthern.edu.

Aquatic Ecology: Dr. Lorne Wolfe, Chair, Aquatic Ecology Search Committee, e-mail: aquaticsearch@georgiasouthern.edu.

Department of Biology, P.O. Box 8042, Georgia Southern University, Statesboro, GA 30460.

Georgia Southern University is an Affirmative Action/Equal Opportunity Institution, and the state is an Open Records state. Finalists will be required to submit to a background investigation. Individuals who need reasonable accommodations under the ADA to participate in the search process should contact the Associate Provost.

FELLOWSHIPS

POSITIONS OPEN

ASSISTANT/ASSOCIATE PROFESSOR
Chemical Biology/Biomedical Nanoscience/Drug Delivery/Drug Discovery
School of Pharmacy

The University of Southern California Department of Pharmacology and Pharmaceutical Sciences (**website: http://www.usc.edu/schools/pharmacy/departments**) invites applications for an Assistant/Associate Professor position, tenure-track or tenured, with research interests in chemical biology, biomedical nanoscience, drug delivery, or drug discovery. Of particular interest are candidates with research interest at the chemistry/biology interface and the capability of working in a multidisciplinary Department with chemists and biologists. Candidates should have a doctoral degree and postdoctoral experience in chemistry, pharmaceutical sciences, biochemistry, engineering, or a related discipline. The successful candidate is expected to develop a strong multidisciplinary research program with extramural funding.

Candidates should send the names of three references, curriculum vitae, and a summary of research accomplishments and future research and educational goals to: **Professor Clay Wang, Ph.D., Chair, Chemical Biology/Drug Discovery Search Committee, University of Southern California School of Pharmacy, 1985 Zonal Avenue, Los Angeles, CA 90089-9121.** Or **e-mail: clayw@usc.edu.** Review of completed applications will begin on November 1, 2009, and will continue until the position is filled. *The University of Southern California values diversity and is committed to equal opportunity in employment.*

Georgetown University wishes to recruit a tenure-track **ASSISTANT PROFESSOR** in physical chemistry to begin fall 2010. Areas of research are open, but proposals related to sustainable energy or environmental chemistry are preferred. Candidates must have a Ph.D. degree in chemistry or a closely related field and significant postdoctoral training or equivalent. Development of an internationally recognized research program and teaching at the undergraduate and graduate levels are expected. Please send curriculum vitae, description of research plans, and statement of teaching philosophy, and arrange for three letters of recommendation to be sent to: **Faculty Search Committee, Department of Chemistry, Georgetown University, Box 571227, Washington, DC 20057-1227.** For full consideration, complete applications should arrive before November 23, 2009. *Georgetown University is an Affirmative Action/Equal Opportunity Employer; applications from qualified women and minority candidates are encouraged.*

CARDIO/PULMONARY MEDICAL WRITER

The Prescott Medical Communications Group, a consulting firm serving the pharmaceutical and biotechnology industries, has an immediate opening for a medical science writer/editor. Candidates must possess an advanced biomedical science degree (M.S., Ph.D., Pharm.D., M.D.) and a minimum of three to five years of academic, industry, or agency (or similar) experience.

This full-time, in-house position will require residing in the Chicago area and occasional domestic/international travel. Please send employment history and three writing samples (scientific poster, manuscript, presentation deck) to: **Jim Bachleda, Prescott Medical Communications Group, 205 N. Michigan Avenue, Suite 3400, Chicago, IL. Fax: 312-529-3901; e-mail: jim.bachleda@prescottmed.com.**

FACULTY POSITION
Department of Biochemical Science and Technology, National Taiwan University, Taipei, Taiwan

The Department of Biochemical Science and Technology at National Taiwan University, Taipei, Taiwan, invites applications for three **ASSISTANT** or **ASSOCIATE PROFESSOR** positions beginning from 1 August 2010. For details, please visit **website: http://www.bst.ntu.edu.tw/.** Thank you.

POSITIONS OPEN

POSTDOCTORAL POSITION

The Biomedical Engineering Department of Northwestern University is seeking a highly motivated and qualified individual to perform research in biomaterials for vascular tissue engineering applications. The project will involve the synthesis of biomaterials for in vivo polymerization to address problems associated with vascular surgery. The qualified person should have experience with standard polymer synthesis (in particular radical polymerization) and characterization techniques, cell and tissue culture techniques (a plus), and basic methods for polymer-based drug delivery. The successful candidate is expected to begin the position on October 1, 2009. For information about the research group, you may visit the **website: http://www.ameerlab.northwestern.edu.**

Please send your curriculum vitae to: **Prof. Guillermo Ameer, e-mail: g-ameer@northwestern.edu.**

Northwestern University is an Equal Opportunity Employer.

ANNOUNCEMENT

U.S. POSTAL SERVICE

Statement required by the Act of 12 August 1970, Section 3685, Title 39, United States Code, showing the ownership, management, and circulation of:

1-9. *Science,* Publication No. 0036-8075, is published weekly on Friday, except the last week in December, at 1200 New York Avenue, N.W., Washington, DC 20005. Date of filing: 25 September 2009. This is also the address of the publisher, the editor, and the managing editor, who are, respectively, Beth Rosner, Bruce Alberts, and Monica M. Bradford.

10. The owner is the American Association for the Advancement of Science, 1200 New York Avenue, N.W., Washington, DC 20005. Stockholders: None.

11. Known bondholders, mortgages, and other security holders owning or holding 1 percent or more of total amount of bonds, mortgages, or other securities: None.

12. The purpose, function, and nonprofit status of this organization and the exempt status for federal income tax purposes have not changed during the preceding 12 months.

13-15. The average number of copies of each issue during the preceding 12 months is (A) Total number of copies printed: 127,868; (B) Paid circulation: 116,262; (1) Paid/Requested outside-county mail subscriptions stated on form 3541: 96,995; (2) Paid/Requested in-county subscriptions stated on form 3541: 0; (3) Sales through dealers and carriers, street vendors, counter sales: 19,249; (4) Other classes mailed through USPS: 17; (C) Total paid circulation: 116,262; (D) Free distribution: samples, complimentary, and other free copies: 10,851; (1) Outside-county as stated on form 3541: 2,154; (2) In-county as stated on form 3541: 0; (3) Other classes mailed through the USPS: 4; (E) Free distribution outside of mail: Carrier or other means: 8,693; (F) Total free distribution: 10,851; (G) Total distribution: 127,113; (H) Copies not distributed: 755; (I) Total: 127,868; (J) Percent paid and/or Requested Circulation: 91.5%.

Actual number of copies of single issue (9/18/2009) published nearest to filing date are (A) Total number of copies printed: 115,200; (B) Paid circulation: 110,281; (1) Paid/Requested outside-county mail subscriptions stated on form 3541: 92,282; (2) Paid/Requested in-county subscriptions stated on form 3541: 0; (3) Sales through dealers and carriers, street vendors, counter sales: 17,981; (4) Other classes mailed through USPS: 18; (C) Total paid circulation: 110,281; (D) Free distribution: Samples, complimentary, and other free copies: 4,218; (1) Outside-county as stated on form 3541: 1,949; (2) In-county as stated on form 3541: 0; (3) Other classes mailed through the USPS: 4; (E) Free distribution outside of mail: Carrier or other means: 2,265; (F) Total free distribution: 4,218; (G) Total distribution: 114,499; (H) Copies not distributed: 701; (I) Total: 115,200; (J) Percent paid and/or Requested Circulation: 96.3%.

I certify that the statements made above are correct and complete. (signed) Beth Rosner, Publisher.

POSITIONS OPEN

POSTDOCTORAL POSITION (100 percent, multiyear) in mouse genetics and neurodegenerative disease available immediately at University of California, Davis to use mouse models to study the genetic, cellular, molecular, and mitochondrial mechanisms of neurodegenerative disease. Expertise in cloning, conditional knockouts, and overexpression of genes required. Salary depends upon experience (NIH scale). Send curriculum vitae to **e-mail: gcortopassi@ucdavis.edu. Website: http://cortopassilab.ucdavis.edu.**

UCD is an Affirmative Action/Equal Opportunity Employer.

POSTDOCTORAL RESEARCH ASSOCIATE
Neurotoxicology of Insecticides

A Postdoctoral Research Associate position is available on or after November 1, 2009, in the Insecticide Toxicology Research Laboratory at Cornell University's New York State Agricultural Experiment Station campus in Geneva, New York. The successful applicant will participate in NIEHS-funded research to define the mechanisms of insecticide action on rat and human voltage-sensitive sodium channels, to map the binding sites for insecticides in relation to sites of action of other toxicants and drugs, and to identify the molecular basis of the differences in sensitivity to insecticides between mammalian sodium channel isoforms and between mammalian and insect sodium channels.

A Ph.D. degree in an appropriate biological discipline and experience in the patch clamp analysis of ion currents are required. Salary will be based on NIH postdoctoral compensation guidelines; an attractive fringe benefits package is included.

Send a letter of application, curriculum vitae, and names of three professional references to: **Prof. David M. Soderlund, Department of Entomology, New York State Agricultural Experiment Station, Cornell University, 630 West North Street, Geneva, NY 14456. E-mail: dms6@cornell.edu.**

Cornell University is an inclusive, dynamic, and innovative Ivy League university and New York's landgrant institution. Its staff, faculty, and students impart an uncommon sense of larger purpose and contribute creative ideas and best practices to further the university's mission of teaching, research, and outreach.

Cornell University is an Equal Opportunity, Affirmative Action Educator and Employer.

MARKETPLACE

Prestige Antibodies®

Powered by ATLAS ANTIBODIES

SIGMA Life Science

Turn your research into a masterpiece with Prestige Antibodies®

The most highly characterized antibodies in the industry — powered by Atlas Antibodies.

- Now over 6,100 antibodies, covering 5,300 protein targets
- Validated by the Human Proteome Resource (HPR)
- Standardized in universal protocols
- Over 700 IF, IHC and WB images per antibody
- All data conveniently searchable online

Visit *sigma.com/prestige* for more information.

Our Innovation, Your Research — Shaping the Future of Life Science

Now Available!
New 2009
Antibodies Catalog

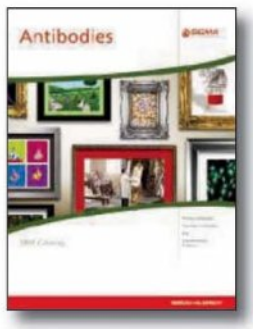

Request your copy at
sigma.com/reserve

R&D Systems
Antibodies for Neuroscience Research

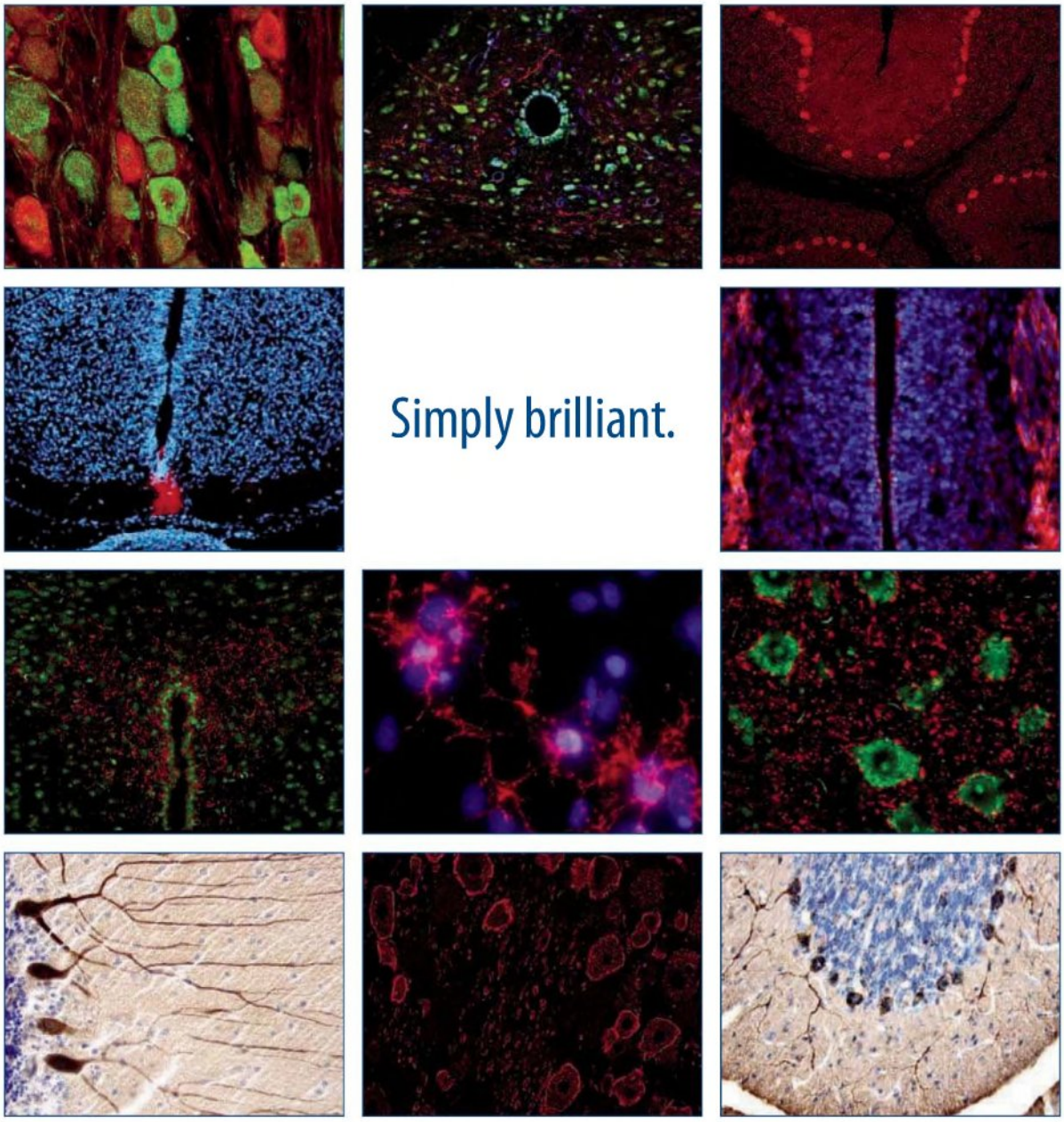

Simply brilliant.

For research use only. Not for use in diagnostic procedures.

For more information visit our website at **www.RnDSystems.com/go/Neuroscience**

R&D Systems Tools for Cell Biology Research™

USA & Canada **R&D Systems, Inc.** Tel: (800) 343-7475 info@RnDSystems.com

Europe **R&D Systems Europe, Ltd.** Tel: +44 (0)1235 529449 info@RnDSystems.co.uk

Selection expanding weekly—visit **www.RnDSystems.com/go/request** to sign up for weekly new product updates.

R&D SYSTEMS®